CONFORMATIONAL DYNAMICS AND ALLOSTERY IN SIGNALING PROTEINS: MONITORING TRANSIENT STATES BY STRUCTURAL MASS SPECTROMETRY

SRINATH KRISHNAMURTHY

(B.Tech in Industrial Biotechnology)

A THESIS SUBMITTED FOR THE DEGREE OF

DOCTOR OF PHILOSOPHY

DEPARTMENT OF BIOLOGICAL SCIENCES

NATIONAL UNIVERSITY OF SINGAPORE

2014

Declaration

I hereby declare that this thesis is my original work and it has been written by me in its entirety. I have duly acknowledged all the sources of information which have been used in the thesis.

This thesis has also not been submitted for any degree in any university previously

---

Srinath Krishnamurthy

23/01/2014

Acknowledgements

Through the course of this PhD, I have gained a wealth of experience and knowledge, learnt what it means to do scientific research, begun to understand the ways of the academic world and in a small way was even able to contribute to existing scientific knowledge. As I stand at the doorstep to the world of science, I hope I prove myself worthy to be called a scientist.

Earning a PhD may seem like an individual milestone, but only after going through the entire process do I understand that a PhD is not possible without the constant support and guidance of many people along the way. First and foremost I express my sincere gratitude to my Doctoral Advisor, A/Prof Ganesh Anand. When I joined his lab my assumptions of science were that of a serious endeavor. My advisor taught me otherwise, he taught me first and foremost science and research is fun and interesting. He has always been a constant source of ideas, guidance and support. Importantly, he has taught me the mental tools to think like a scientist and provided the freedom to use those tools to carry out interesting research.

I would like to thank my qualifying exam panel members, Prof. Paul Matsudaira, Prof. Sivaraman and Prof. Patrice Koehl for giving me a fair critique of my work. The constructive criticism and discussions inspired me to strive harder and work better towards my goals.

I would also like to extend my gratitude to my collaborators, Prof. John E Johnson, Dr. Ivana Mihalek, Dr. Anna Jansson and Mr. Mark Ritchie for the fruitful exchange of data and ideas. I am greatly indebted to my seniors, Dr. B.S Moorthy, Dr. Suguna Badireddy, Dr. Priya Jayaraman and Roopsha Brahma for taking me under their wing and guiding me during my PhD. I thank my current lab mates Jeremy Wang, Madhubrata Ghosh, Nikhil Tulsian, Xin Xiang Lim and Xin Shan Lim, with whom I have had many interesting discussions on science and beyond.

My time in Singapore has been a joyous experience and for that I have to thank all my friends. I will cherish the times I spent amongst them. Last but not least I would like to thank my family for the constant support and belief they have placed in me.

Table of Contents

Summary

A commonly quoted axiom in protein biochemistry dictates that a protein's primary amino acid sequence defines the structure of the protein and the structure consequently defines the function of a protein.

Sequence ⟶ Structure ⟶ Function

Years of research in protein biochemistry and structure-function relationships have revealed that proteins populate various alternate and interchanging structures or conformations which are critical for their function. Protein dynamics describes the conformational switching in proteins with respect to time. A true understanding of the link coupling a protein's average structure with its function can only be obtained by describing its dynamics in solution.

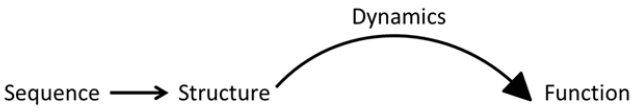

In this dissertation, I have primarily used structural mass spectrometry, in particular Amide Hydrogen/Deuterium Exchange Mass Spectrometry (HDXMS), to probe the conformational dynamics and allosteric effects of signaling proteins largely in the cAMP pathway. One of the main goals of my research is to understand how the cAMP pathway is regulated and terminated from a conformational dynamics perspective. Of primary interest is to define models on how allosteric effects on proteins correlate with protein function.

cAMP (3' 5'- cyclic adenosine monophosphate) is an important second messenger molecule that is involved in the regulation of a wide range of metabolic processes. The main receptor for the cAMP molecule in cells is the regulatory subunit of Protein Kinase A (PKAR). Inactive PKA in the absence of cAMP exists as a heterotetramer of two PKAR molecules each bound to an inactive catalytic kinase

subunit (PKAC) collectively termed as PKA holoenzyme. cAMP binding to PKAR causes an allosteric chain reaction which results in the PKAC molecule being released from the regulatory subunit. The PKAC enzyme once released is activated to carry out its role in phosphorylating numerous targets. Signal termination occurs only when the cAMP levels in the cell are depleted by the enzymatic activity of Phosphodiesterases (PDEs), which convert cAMP to AMP. Once cAMP levels are depleted the *apo* PKAR molecule binds the PKAC molecule and inactivates it. Though the cAMP pathway is a well-studied pathway with crystallographic structures available for all end point states, the nature and dynamics of transition states are relatively unknown.

In the first part of this study (**Chapter 1**), we were interested in probing the dynamics of the activation phase transition state complex. This transition state is a state where cAMP binds to the regulatory PKAR subunit while the PKAC molecule is simultaneously bound to it, in a transient ternary complex. To capture the ternary complex, a Thio-substituted cAMP analog, Rp-cAMPS, was used as a ligand. The Rp-cAMPS molecule acts as an inverse agonist to cAMP and maintains the PKAR in the Holoenzyme conformation, thus a ternary complex of cAMP-PKAR-PKAC can be studied. Time dependent HDXMS was used to monitor the allosteric effects of ligand binding on PKA holoenzyme. Most allosteric events were observed on the PKAR molecule, but it was also observed that certain regions of the PKAC molecule also showed significant increases in conformational dynamics. Thus allosteric effects caused by ligand binding on one protein can propagate across the interaction interface to cause conformational changes in an interacting protein.

The previous study provided insights into the conformational dynamics of the activation phase of the cAMP pathway. In the next part of this dissertation; I focus on the termination phase of the cAMP pathway. Most studies on the termination phase of the cAMP pathway assumed a passive role for Phosphodiesterases (PDEs), wherein PDEs deplete levels of free cAMP in the cell, but this model though did not adequately explain how cAMP that is bound to PKAR, dissociates from the ligand binding pocket. Recent studies with a PDE from *Dictyostelium discoideum,* RegA, revealed that cAMP signal termination

is initiated by direct interactions between RegA and PKAR. RegA binds to the cAMP binding pocket of PKAR and in a two-step process catalyzes the dissociation and hydrolysis of bound cAMP. In this study (**Chapter 2**) we set out to monitor complex formation and cAMP dissociation, using a PDE-resistant sulphur substituted cAMP analog, Sp-cAMPS. Reaction monitoring of the PKAR-RegA interaction revealed that at high/saturating concentrations, a ternary complex of PKAR-SpcAMPS-RegA exists. When diluted, SpcAMPS dissociation from the complex was observed in a time dependent manner.

While the previous studies on PDE-PKAR interactions were carried out using a mammalian PKAR and *Dictyostelium* PDE, RegA, the aim of this study (**Chapter 3**) was to ascertain whether PDE-PKAR interactions are conserved in mammalian systems, and to determine the mammalian homolog of RegA that interacts with PKAR. HDXMS and peptide array analysis were carried out on the PKAR-RegA interaction, to probe for the PKAR interacting interface on RegA. Positive 'hits' obtained from peptide array and regions that showed decreases in deuterium exchange from HDXMS were correlated to obtain a map of the binding region. Interestingly the regions that were involved in the interaction interface were regions around the catalytic pocket of RegA, particularly the M-loop which is involved in anchoring cAMP. Regions that show decreases in deuterium exchange in HDXMS but do not show hits in peptide array, are by direct inference, regions which show allosteric effects on PKAR binding. Such allosteric effects were observed at both the N and C termini, indicating that PKAR interaction may trigger allosteric effects of a regulatory nature. Bioinformatics analysis of the binding interface was carried out to identify the closest mammalian homolog. The catalytic pocket and the binding interface is highly conserved across all PDEs from all organisms, hence it is likely that all PDEs may undergo interactions with PKAR subunits. The closest mammalian homologs to RegA, based on primary sequence are PDE8 and PDE9. Of these PDE8 is a cAMP PDE similar to RegA and hence was chosen for further studies. Kinetic assays and HDXMS studies of PDE8-PKAR interactions revealed that the catalytic domain of PDE8A binds to PKAR and hydrolyzes cAMP bound to PKAR. The interaction interface on both PDE8A and PKAR is comprised of the active site of PDE8 interacting with the cAMP binding pocket of PKAR. The PKAR

used in this study contains two tandem cAMP binding domains, and it was seen that both domains showed significant decreases in deuterium exchange upon PDE8 binding. Computational docking was carried out based on HDXMS experimental data, and a model was obtained which showed active site coupling between a PDE8 dimer and the two tandem cAMP binding domains of PKAR. Active site coupling between PDE and PKAR provides a model to explain the cAMP pathway termination phase.

In the fourth part (**Chapter** 4) of this study, we have aimed to apply knowledge gained from protein-ligand interactions to develop a novel application for HDXMS in Fragment Based Drug Discovery. In this study, HDXMS was used to screen for weak affinity inhibitors and capture the allosteric effects that fragments molecules have on the target protein, HSP90. It was found that fragment molecules which have ~10000 fold lower affinities than the natural ligands/inhibitors allosterically affect the same regions as that of the natural ligands. It was also seen that by using time series deuterium labeling, direct interaction effects can be clearly segregated from conformational stabilization effects. Since direct binding effects of small ligands are diffusion dependent, they are easily visualized in earlier deuterium exchange time points. Conformational stabilization effects are a product of ligand binding and are an accumulated effect; hence they occur at a slower rate than direct binding effects.

In the final part (**Chapter** 5) of this study, we push the boundaries of HDXMS technology by applying it to biologically complex systems. The main aim of this final study was to derive biologically relevant conclusions, by probing the dynamics of complex systems by HDXMS. To this end two test systems were studies, 1) Allosteric effects in partially disordered proteins binding to DNA and 2) Capsid protein dynamics in viral maturation pathway. In the first example, we propose a model to describe the function of the partially disordered protein, H-NS (Heat stable nucleoid protein) based on its dynamic nature. H-NS is a DNA binding protein which serves two functions in bacterial cells, it is involved in DNA packaging and also gene silencing, depending on the type of DNA it is binding and on the concentration of Mg^{2+} ions in the environment. It was found that H-NS exists in an ensemble of conformations, in the presence of high Mg^{2+} concentration or when it binds to a specific recognition motif; H-NS adopts a

single conformation and is stabilized. When it binds to a DNA fragment chosen at random, it adopts multiple conformations. Thus a model was derived where H-NS undergoes conformational selection, and Mg^{2+} and specific recognition motif select for a stable conformation, while other DNA stretches do no stabilize a single conformation.

In the second example we have aimed to understand conformational dynamics of proteins in macromolecular complexes. In this example, we have looked at a key step in the maturation pathway of the bacteriophage HK97. In the first step of HK97 maturation, free capsid proteins spontaneously assemble through N terminal scaffolding domains. In the next step, a protease cleaves the scaffolding domains of the viral coat capsid proteins thereby ensuring the maturation pathway is irreversible. In this study, HDXMS is used to probe the dynamics and map the interactions of an inert protease to the capsid proteins. It is seen that the protease binds to the N terminal region of the capsid protein and stabilizes the capsid proteins and thereby the entire viral capsid. Conformational stabilization effects are observed from the N to C terminus of the capsid protein thus indicating that capsid protein stabilizing is an essential step in the maturation pathway

Commonalities in the way allosteric effects propagate can be drawn from globular signaling proteins to highly dynamic proteins to macromolecular complexes, but a common underlying theme is that conformational dynamics and allostery are important parameters to understand the relationship between a protein's structure and function.

List of Tables

List of Figures

List of Abbreviations

AKAP- A-Kinase anchoring protein

AC- Adenylyl Cyclase

βME- β- Mercaptoethanol

PKA C- Catalytic subunit of Protein Kinase A

cAMP- Cyclic adenosine 3', 5' monophosphate

CIAP/ SAP- Alkaline phosphatase

DTT- Dithiothreitol

E.coli- Escherichia coli

EDTA- Ethylene diamine tetraacetic acid

FBLD- Fragment based ligand discovery

FM- Fluorescein Maleimide

GST- Glutathione- S- Transferase

H-NS- Heat stable nucleoid protein

Hsp90- Heat shock protein 90

HDXMS- Amide hydrogen/ deuterium exchange mass spectrometry

FP- Fluorescence Polarization

LB- Luria-Bertoni

LC-ESI QTOF- Liquid chromatography- electrospray ionization quadrupole time of flight

MES- 2-(N-morpholino) ethanesulfonic acid

MOPS- 3- (N-morpholino) propanesulfonic acid

MS- Mass spectrometry

MW- Molecular weight

NMR- Nuclear Magnetic resonance

PBC- Phosphate binding cassete

PCR- Polymerase chain reaction

PDE- Cyclic nucleotide PDE

PDE8A- Full length PDE8A isoform

$PDE8A_C$- Catalytic doman of PDE8A spanning residues 472-829

PKA- Protein Kinase A

RegA- Phosphodiesterase from *Dictyostelium discoideum*

RIα- Iα isoform of the regulatory subunit of PKA

$RI\alpha_A$- Deletion mutant of RIα spanning residues 91-244

$RI\alpha_{AB}$- Deletion mutant of RIα spanning residues 75-379

Rp-cAMPS- Thiol substituted cAMP with the thiol substitution at the equatorial oxygen position

Rpm- revolutions per minute

SAR- Structure-Activity relationships

Sp-cAMPS- Thiol substituted cAMP with the thiol substitution at the axial oxygen position

TFA- Trichloroacetic acid

WT- Wild type

List of Publications

- Anand, G. S., **S. Krishnamurthy**, T. Bishnoi, A. Kornev, S. S. Taylor and D. A. Johnson (2010). "Cyclic AMP- and (Rp)-cAMPS-induced conformational changes in a complex of the catalytic and regulatory (RI{alpha}) subunits of cyclic AMP-dependent protein kinase." Mol Cell Proteomics **9**(10): 2225-2237.
- **Krishnamurthy, S**., B. S. Moorthy, L. Liqin and G. S. Anand (2013). "Dynamics of phosphodiesterase-induced cAMP dissociation from protein kinase A: capturing transient ternary complexes by HDXMS." Biochim Biophys Acta **1834**(6): 1215-1221.
- Veesler, D., R. Khayat, **S. Krishnamurthy**, J. Snijder, R. K. Huang, A. J. Heck, G. S. Anand and J. E. Johnson (2013). "Architecture of a dsDNA Viral Capsid in Complex with Its Maturation Protease." Structure.
- **Krishnamurthy, S.**, B.S Moorthy, Xin Xiang, L., Xin Shan, L., Bharatham, K., Tulsian, N.K, Mihalek, I., and Anand,G.S.

  Active site coupling in PDE-PKA Complexes Promotes cAMP Signal Termination

  the Biophysical Journal, (2014)

Introduction

I. Conformational dynamics in proteins

The field of study known today as structural biology, for most of its nascent years, concentrated on a static view of the protein molecules that make up most of the biological world. This static view was perpetuated by high resolution structural information obtained from X-ray crystallography studies. X-ray crystallography is an invaluable technique in structural biology as it provides atomic resolution level structural information. But the resulting structural model represents the average structure of many molecules in a crystal lattice over long time scales. While it provides structures for end point states, and a limited overview of protein dynamics, it does not provide information on conformational changes that proteins undergo over time (Figure 1)(Henzler-Wildman and Kern 2007).

Seminal early work by Anfinsen and colleagues lead to the idea which is now widely proven that the primary sequence of the protein defines its tertiary structure and its fully formed tertiary structure defines the function of the protein (Anfinsen, Steinberg et al. 1956, Anfinsen 1973). In recent times it has been seen that, in many cases the structure of the protein does not readily present direct information on its function, especially in the case of disordered proteins. There is a growing number of cases where deciphering the conformational dynamics of a protein leads to a better understanding of its function (Berendsen and Hayward 2000).

Protein dynamics is the study of time dependent changes in the conformations of proteins. Early work in the field of protein biochemistry (Koshland 1958, Benson and Linderstrom-Lang 1959, Monod, Wyman et al. 1965), introduced the concept that proteins are labile molecules that undergo conformational changes. In later work it was seen that protein motions are governed by an energy landscape where molecules attempt to move from a high energy conformation to a low energy conformation (Frauenfelder, Sligar et al. 1991). This study also introduced the concept of multiple meta-stable conformational sub-states that a protein can populate (Figure 1a) and thereby paved the

way for the study of protein dynamics. All proteins can theoretically exist in multiple conformations; the variations between these multiple conformations define whether a protein is rigid or labile.

Protein conformational changes are triggered by a wide range of perturbations. These perturbations can range from environmental factors such as pH and temperature to molecular factors like phosphorylation, protein-ligand, protein-DNA interactions and protein-protein interactions. Deciphering how proteins sense these perturbations and react to them has been the subject of intense study for past 50 years. In this dissertation I focus here primarily on three types of perturbations, protein-ligand, protein-protein and protein-DNA.

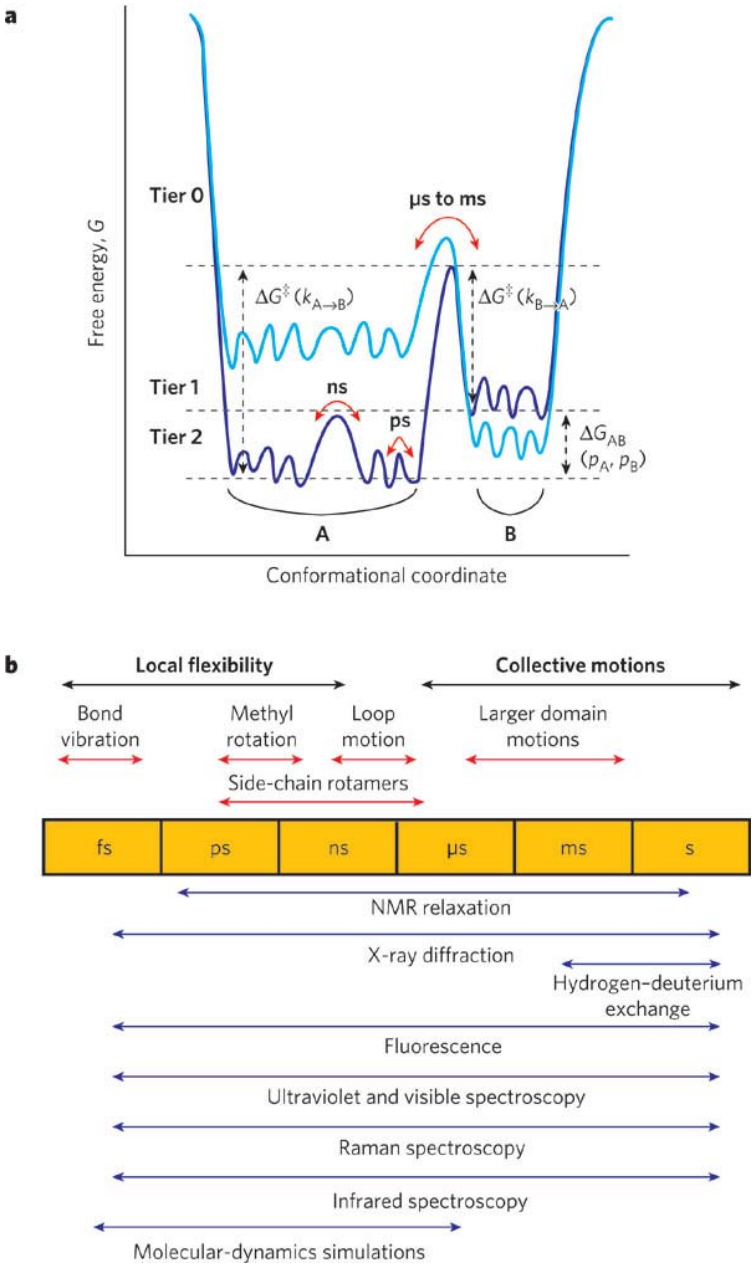

Figure 1: Overview of Protein dynamics A) Proteins exist in multiple meta-stable substates that have very similar free energy values (conformation A). The protein can freely change between conformations in this substate. All motions in this substate are in picosecond to nanosecond regime. Free energy is required for the protein to change from Conformation A to conformation B. These changes occur in the microsecond to millisecond regime. B) The various techniques used in structural characterization of proteins are plotted on the timescale regime that they probe. Hydrogen-deuterium exchange, the technique primarily used in this body of work, is unique in that it probes protein motions only in the millisecond to second regime thereby capturing larger domain motions and ignoring more short lived conformational changes.

Figure adapted with permissions from (Henzler-Wildman and Kern 2007)

In a cellular context, a protein may be subjected to more than one perturbation at any given point in time leading to a ternary complex where more than 2 perturbants influence a protein's function. In these cases, it is essential to decipher the mode in which these perturbations affect the proteins conformation and dynamics. While the rules for protein dynamics can apply to any perturbant, I shall focus mainly on protein-ligand interactions in this discussion.

There are two widely accepted models for protein-ligand interactions, 1) the induced fit model proposed by (Koshland 1958) and 2) conformational selection model proposed by (Monod, Wyman et al. 1965). In the induced fit model, the assumption is that ligand binding to protein provides the free energy to the protein to undergo a conformational change to a lower energy conformation. In the conformational selection model, the protein is constantly sampling an ensemble of conformations. In this ensemble of conformations, the conformation the protein attains on ligand binding is also briefly populated. The presence of the ligand stabilizes the protein in the ligand bound populations. The population equilibrium shifts towards the ligand bound form over time (Boehr, Nussinov et al. 2009, Changeux and Edelstein 2011) (Figure 2).

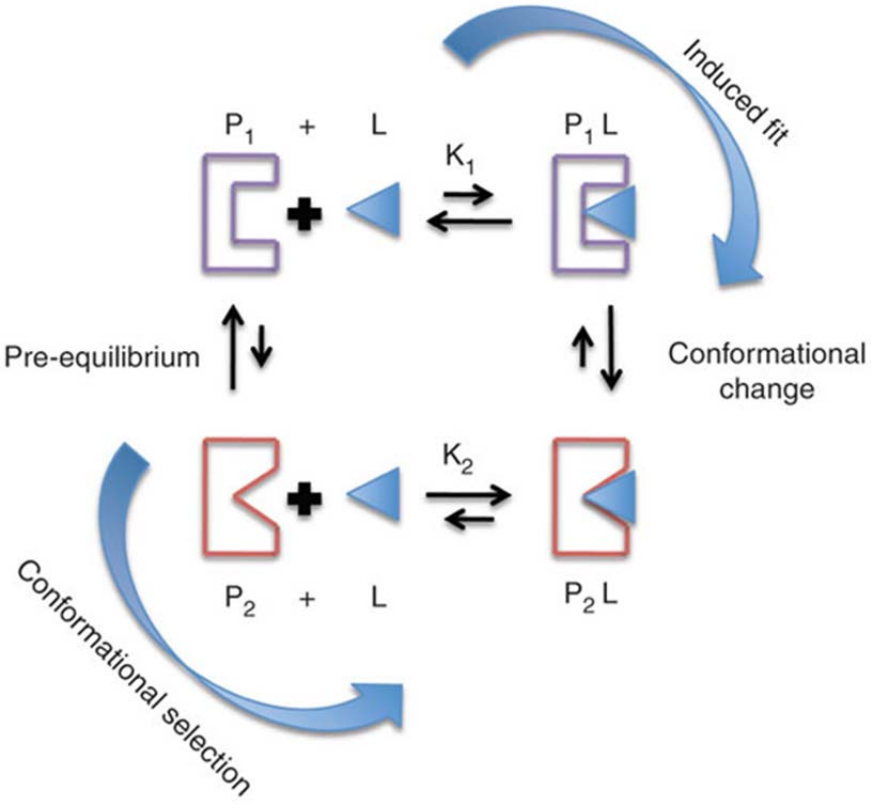

Figure 2: Induced fit vs conformational selection: In the induced fit regime, P_1 binds to the ligand resulting in a conformational change to the P_2L state. In the conformational selection regime, P_1 and P_2 are in a rapid interchanging equilibrium with the P_1 state being the predominant state. Ligand binding selects sparsely populated P_2 state resulting in the P_2L state. *Figure adapted with permissions from (Boehr, Nussinov et al. 2009)*

It is generally believed that highly dynamic proteins bind ligands in the conformational selection regime and more rigid proteins bind in the induced fit regime. This axiom is currently being contested by newer results from single molecule FRET experiments (Kim, Lee et al. 2013). It is generally assumed that induced fit and conformational selection are mutually exclusive binding regimes, but recently postulated theories are beginning to show that they do not need to be mutually exclusive. There are many instances of a protein binding a ligand in the conformational selection regime followed by structural adjustments which constitute induced fit mode of binding (Csermely, Palotai et al. 2010).

Differences between induced fit and conformational selection regimes, might appear subtle, but are extremely important for recognition and sensing in a cellular and signaling context as it can define the sequence of events that govern protein mediated cellular processes.

II. 3' 5'-cAMP dependent Protein Kinase pathway

Cells respond to external hormonal stimuli through membrane bound receptors proteins. There are various classes of membrane bound receptor proteins, of which the most well studied class are the G protein coupled receptors (GPCRs). They constitute one of the largest families of membrane proteins and typically have seven transmembrane helices that anchor the protein to the membrane (Wess 1997). GPCRs respond to a wide variety of molecular stimuli including hormones, neurotransmitters, lipids and nucleotides, and regulate a wide range of physiological functions (Gurrath 2001). GPCRs are associated with 3 domains namely G_α, G_β and G_γ in their cytosolic side. The G_α domain is a domain which exhibits GTPase activity.

3' 5' cyclic adenosine monophosphate (cAMP) is an important second messenger molecule in the cell which regulates a wide range of cellular functions. In the cAMP dependent protein kinase pathway, an external stimulus binds to the extracellular domain of a GPCR causing a conformational change across the entire protein. The signal then transduces across the membrane to the cytosolic domain of the GPCR. The activated GPCR induces the G_α domain to bind GTP and leading to the activation of the G_α subunit. The activated G_α subunit dissociates from the GPCR and causes the downstream

activation of adenylyl cyclases (ACs). Once activated, adenylyl cyclases synthesize 3' 5'- cyclic adenosine monophosphate (cAMP) from ATP. The main target of cAMP in cells is the cAMP-dependent protein kinase, or protein kinase A (PKA) (Berman, Ten Eyck et al. 2005). In its inactive form, PKA exists as a hetero tetramer composed of a dimer of regulatory subunits each bound to a catalytic kinase subunit (Francis and Corbin 1994). In the activation phase of the cAMP signaling pathway, high levels of cAMP is produced by adenylyl cyclases and released into the cytosol. The free cAMP binds to the inactive PKA holoenzyme, causing the dissociation of the regulatory and catalytic subunits. The catalytic kinase once released from the holoenzyme is free to phosphorylate its target proteins in its downstream role in regulating myriad cellular functions. Signal termination is achieved by a class of enzymes called cyclic nucleotide phosphodiesterases (PDEs). In mammalian cells there are 11 families of phosphodiesterases, each with its own substrate specificity, subcellular localization and tissue specificity. Phosphodiesterases catalyze the conversion of 3' 5' cAMP to AMP by hydrolyzing the phosphodiester bond (Beebe 1994). This pathway is summarized in Figure 3.

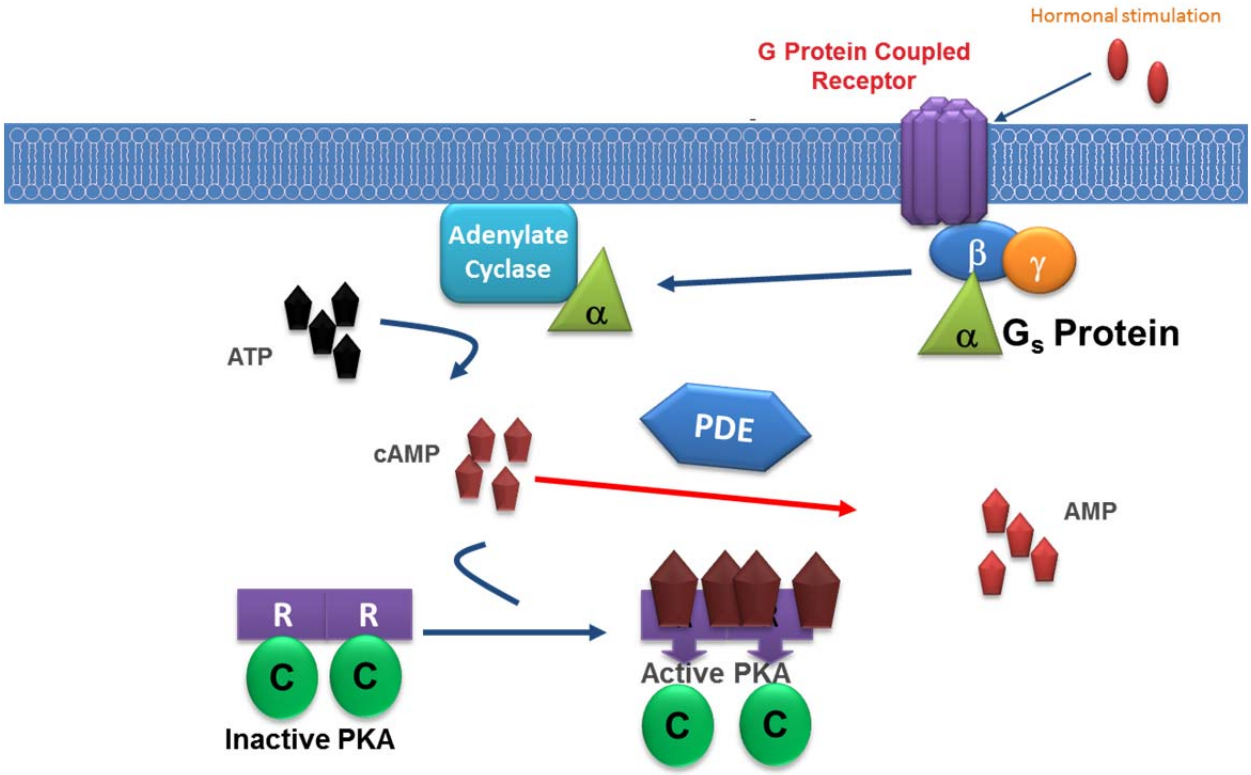

Figure 3: Overview of the 3' 5' cAMP signaling pathway: Hormonal stimulation of membrane-anchored GPCRs results in the activation of G_α (α) subunit. This in turn activates the adenylyl cyclases to catalyze conversion of ATP to cAMP. The heterotetrameric PKA molecule has 2 cAMP binding sites in each regulatory subunit (R) monomer (4 in the stable dimer). Binding of cAMP induces conformational changes releasing the activated Catalytic kinase subunit (C). Phosphodiesterases (PDEs) catalyze the hydrolysis of the cAMP to AMP.

III. Regulatory subunit of PKA acts as a conformational switch

The most prevalent isoform of the regulatory subunit of PKA is the isoform RIα. It is also the most well studied isoform of PKA and knockdown studies with RIα show that it was embryonically lethal (Amieux and McKnight 2002). RIα was shown to be a highly dynamic protein which exists in an ensemble of conformations (Badireddy, Yunfeng et al. 2011, Akimoto, Selvaratnam et al. 2013). It has two main end point states, one is the holoenzyme bound state (H form) (Kim, Cheng et al. 2007) where it is bound to the Catalytic kinase subunit, and the other is the cAMP bound (B form) state. Crystal structures are available for both these states and show the protein has to undergo vast conformational changes to transition from one conformation to the other. Conformational switching of RIα is depicted in figure 4.

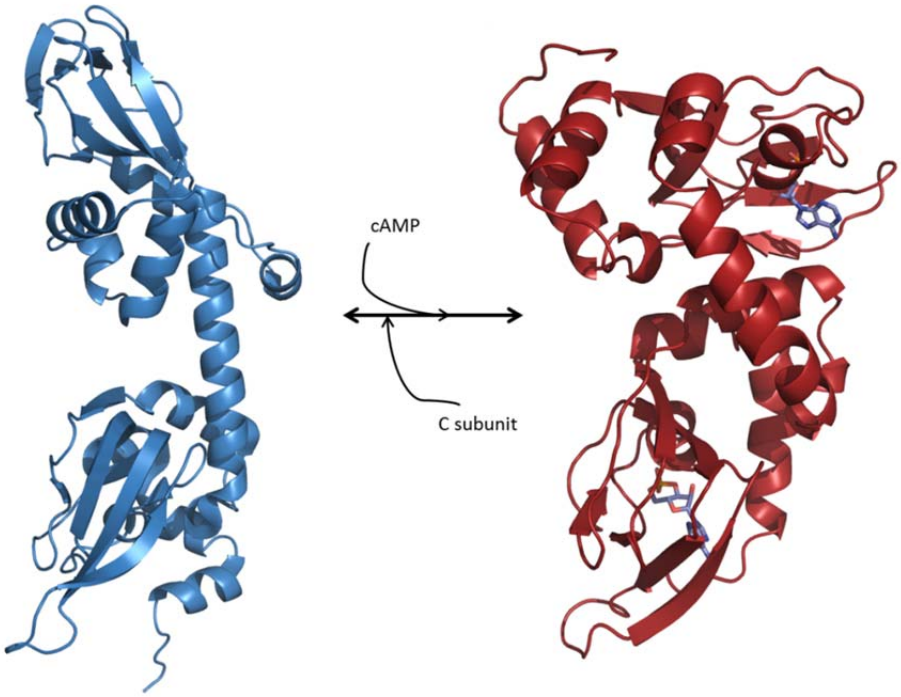

Figure 4: PKA RIα is a conformational switch: The 'H' inactive form structure in blue, is an extended structure (PDB ID: 2QCS) while the 'B' active form structure is a compact structure (PDB ID: 1RGS). cAMP bound to the pocket is in blue sticks. The 'H' form represents the conformation when bound to the C-subunit and the 'B' form represents the cAMP-bound conformation.

IV. Cyclic Nucleotide Phosphodiesterases

Cyclic nucleotide phosphodiesterases are large group of enzymes, which are classified into 11 families based on their amino acid sequence, substrate specificity, regulatory domains and tissue distribution (Jeon, Heo et al. 2005, Francis, Blount et al. 2011). All PDEs have a highly conserved catalytic domain, but show great variability in the regulatory domain (Figure 5). PDEs are mainly classified based on their specificity towards cyclic nucleotides, cAMP specific PDES (PDE4, 7, 8), cGMP specific PDES (PDE5,6 and 9) and dual specific PDEs (PDEs 1, 2, 3, 10 and 11). While crystal structures are available for the catalytic domain of PDEs, full length crystal structures are proving more difficult (Conti and Beavo 2007).

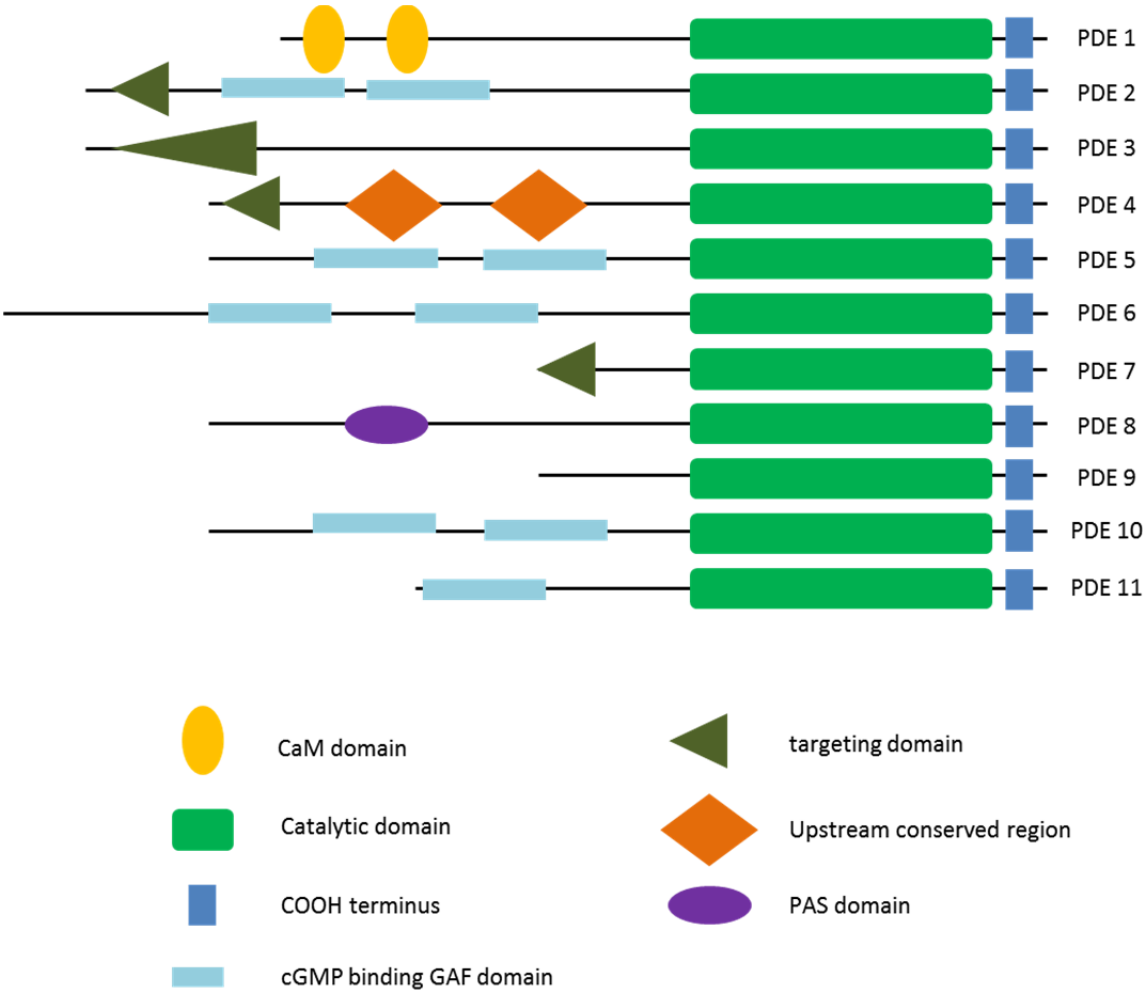

Figure 5: Domain organization of the 11 PDE families. Each domain is represented as a block figure and shows the diversity of the varied regulatory domains along with the conserved catalytic domain. *(adapted from Conti and Beavo, 2007)*

In recent times, a structure of PDE4 with its regulatory domains has shown that the upstream conserved regions (UCRs) of PDE4 serve to regulate the activity of the catalytic domain by capping the active site. These conserved regions are activated by PKA and ERK phosphorylation in PDE4 (Burgin, Magnusson et al. 2010).

PDEs are generally perceived to act on free cAMP in the cytosol, but it is recently becoming evident that cAMP concentrations in the cell are not uniform and point towards the presence of microdomains inside the cell (Davare, Avdonin et al. 2001, Zaccolo 2006). I discuss how PDEs are involved in direct interactions with the regulatory subunit of PKA, lending further evidence for the presence of microdomains of sequestered cAMP.

V. Amide hydrogen deuterium exchange mass spectrometry (HDXMS)

Early work carried out Linderstrom-Lang on deuterium exchange in myoglobin (Benson and Linderstrom-Lang 1959) has paved the way in monitoring hydrogen/deuterium exchange. In recent years, the availability of high end mass spectrometry coupled to ultra-high performance liquid chromatograph has greatly advanced the field of HDXMS, and has established HDXMS in the forefront of structural biology (Katta and Chait 1991, Hoofnagle, Resing et al. 2003).

Hydrogen/deuterium exchange is based on the theory that hydrogens in O-H, N-H or S-H groups are labile and exchange with OH^- groups from the solvent. This can be an acid or base catalyzed reaction depending on the pH. In the context of the protein backbone, the labile groups on the sidechains exchange too rapidly with solvent to be detectable, while the amides on the peptide bond exchange at a slower time scale and can be monitored (Figure 6). This proves as a convenient probe, as mainly the amide hydrogens and hence backbone motions can be effectively monitored.

The hydrogen deuterium exchange reaction is carried out by diluting the protein in a buffer reconstituted in deuterium oxide.

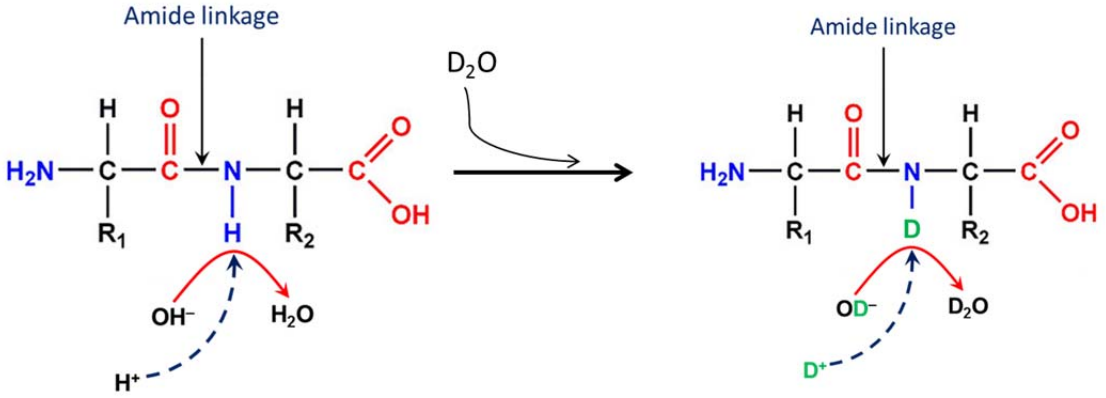

Figure 6: Hydrogen/Deuterium exchange at amide positions in proteins: The amide hydrogen exchanges freely with the water in the solvent. When water is replaced by deuterium oxide, the deuterium also exchanges freely with the amide proton.

The deuterium gets incorporated onto the protein backbone thereby increasing the mass of the peptide by ~ 1 Dalton for every deuterium ion incorporated. Mass spectrometry is then carried out to determine the average increase in mass for the population of proteins in the reaction mixture. This average mass is determined by calculating the centroid of mass spectra (Figure 7). Perturbations are introduced to monitor the changes in deuterium exchange caused by the perturbations.

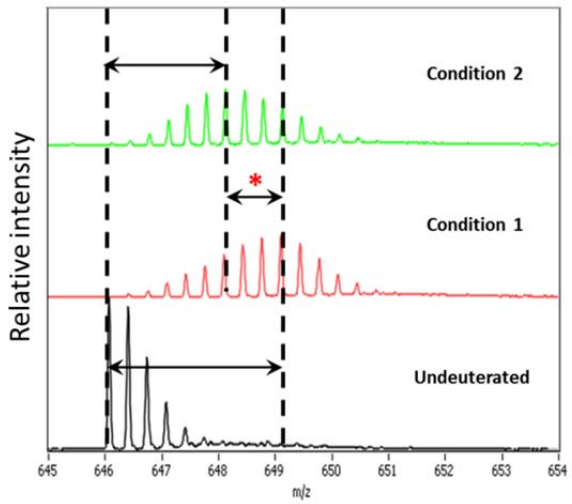

Figure 7: Effect of H/D exchange on mass spectral envelope of peptides: In the undeuterated state, the characteristic isotopic distribution for a peptide is observed. In the deuterated state, the peptide increases in mass. The amount of deuteration can be quantified by calculating the centroid of the mass spectra. Perturbations can change the deuterium exchange rates and the effect of these perturbations can be calculated by the difference in the centroids of the two conditions (represented by the bifunctional arrows between the two dashed lines. Condition 1- represents the results of exchange at time t1 and condition 2 displays the results at time t2, where t1>t2. The results shown here are for a representative peptide (m/z= 646.086).

The deuterium exchange reaction is governed mainly by two factors, the solvent accessibility of the amide and the strength of hydrogen bonding. Other effects including neighborhood effects and amino acid side chain moieties also have an effect on exchange rates. It is believed that the hydrogen bonding status of the amide has a greater influence on its deuterium exchange rate than the solvent accessibility (Englander and Kallenbach 1983) .

The HDX reaction occurs according to the following equation

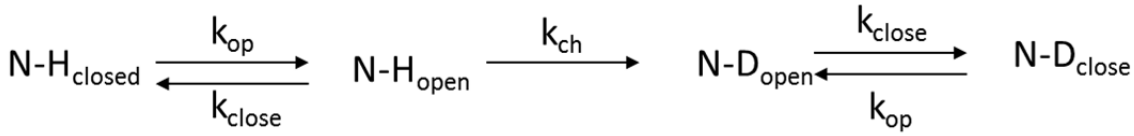

The proteins opening and closing rate constants are k_{op} and k_{close}. There are two kinetic regimes for deuterium exchange that a region of the protein can undergo and it is dependent on the opening and closing rate of the protein backbone. The two modes are EX1 and EX2 (Weis, Wales et al. 2006).

In the EX1 regime, the rate of exchange $k_{ch} >> k_{close}$, thus this leads to multiple deuterium exchange events every instance the structure opens. And

$$k_{HDX}=k_{op}$$

Since the HDX rate at the amide is governed only by its closing rate, this leads to a bimodal distribution. In the population of proteins in the mixture, some proteins may have undergone the opening motions while other might not yet have undergone structural opening. This leads to the perception of two populations in the mixture indicated by the bimodal distribution.

In the case of EX2 regime, $k_{cl} >> k_{ch}$, thus

$$k_{HDX}=K_{opkch}$$

Where $K_{op}=k_{op}/k_{cl}$ is the opening reaction equilibrium constant. In EX2, every opening reaction does not lead to a deuteration event, and deuteration incrementally adds over time depending on the amide opening/closing cycles. Most folded proteins exchange in the EX2 regime.

The deuterium exchange reaction is started by diluting the protein in deuterium oxide buffer at the physiological pH of the protein. Once the reaction has progressed for a certain time period, the reaction is quenched by reducing the pH to 2.5 and 0 °C temperature. The deuterium exchange reaction is slowed by several orders of magnitude in the low temperature and pH=2.5 quench conditions. The protein is subsequently cleaved by acid stable pepsin protease and subjected to reverse phase HPLC separation and analyzed by mass spectrometry. The centroids of the resulting mass spectra are quantified and percentage deuterium uptake for a particular peptide is calculated by the following formula

$$D = \frac{m - m_{0\%}}{m_{100\%} - m_{0\%}} \times N_{max}$$

Where m= mass of deuterated peptide, $m_{0\%}$=mass of non-deuterated peptide, $m_{100\%}$= mass of fully deuterated peptide and N_{max}= maximum possible number deuterium ions incorporated in a given peptide.

VI. Objectives

In this dissertation, I have chosen to focus on the following objectives for my graduate research

1. Monitor conformational dynamics and allostery in the activation phase of cAMP pathway by capturing a transient ternary complex composed of PKA holoenzyme and a cAMP analog.
2. Probe dynamics in a transient ternary complex of PKA-PDE and a cAMP analog and monitor ligand release from the regulatory subunit of PKA
3. Discover a mammalian PKA-PDE interaction and map the interaction interface.
4. Using the knowledge gained from protein ligand interactions, test the viability of HDXMS as a fragment screening tool in a fragment based ligand discovery pipeline
5. By studying the dynamics of the partially disordered protein H-NS, decipher its DNA-binding function
6. Decipher protein dynamics in the macromolecular viral capsid of HK97, and in particular map the interaction interface of the viral capsid protein with its maturation protease.

Chapter 1

Conformational Dynamics in Molecular Signaling I: Describing allosteric relays in transient complexes in the activation phase of cAMP signaling pathway

1 Conformational Dynamics in Molecular Signaling I: Describing allosteric relays in transient complexes in the activation phase of cAMP signaling pathway

1.1 Introduction

The Cyclic AMP signaling pathway is an important pathway which regulates a wide range of cellular functions. Cyclic AMP-dependent protein kinase (PKA) is an important molecule in the cAMP signaling pathway. All isoforms of PKA are composed of two catalytic (C) subunits and homodimeric regulatory (R) subunits (Beebe 1986, Johnson, Akamine et al. 2001, Shabb 2001). Of the many isoforms of PKA, Cα and RIα are the most widely distributed across all mammalian tissue and also the best studied isoforms (Amieux and McKnight 2002). The cAMP pathway is activated by the binding of cAMP to the regulatory subunit of PKA. This triggers large conformational changes that result in the dissociation of the PKA holoenzyme into the component Regulatory and Catalytic kinase domains. The binding of PKAC to its substrate has also been implicated in facilitating the dissociation of the PKA holoenzyme (Viste, Kopperud et al. 2005).

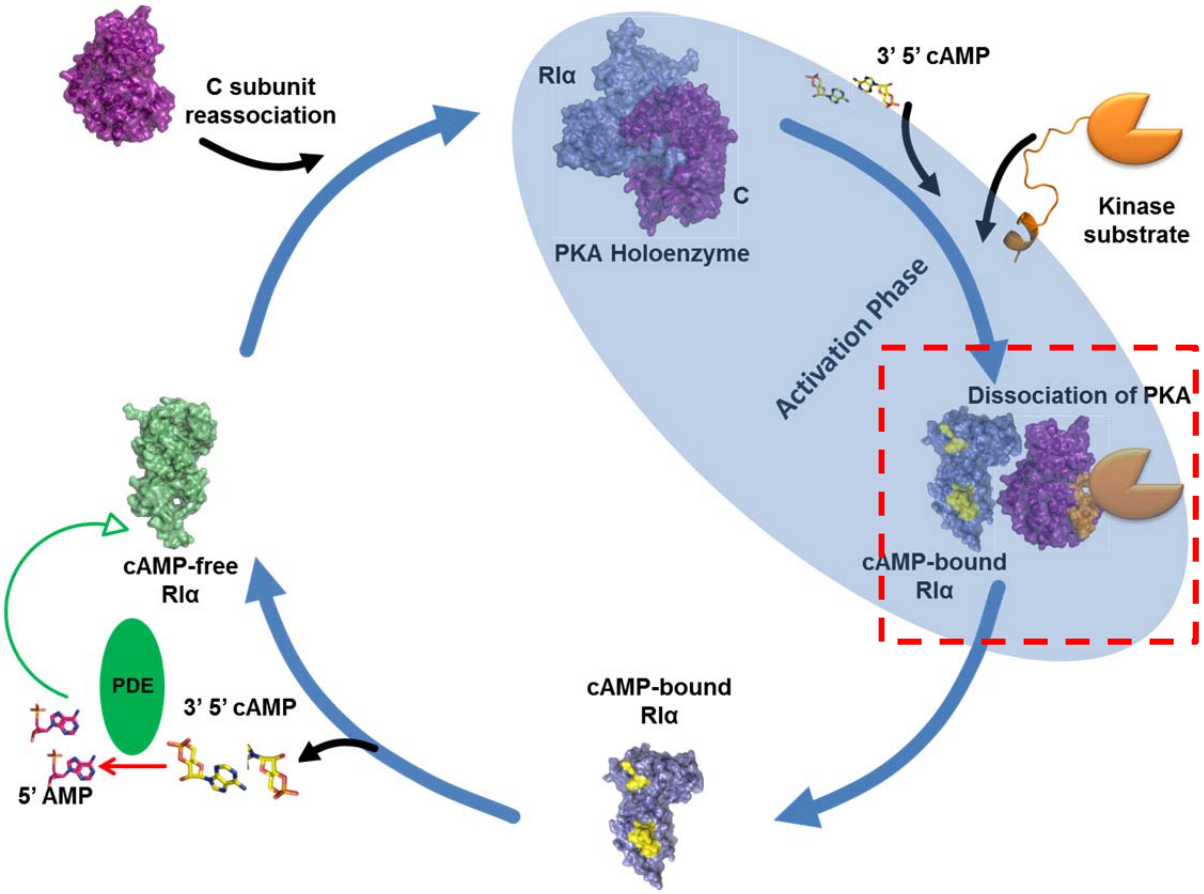

Figure 1.1: The activation phase of cAMP pathway: The cAMP signaling pathway is activated by cAMP (yellow sticks) binding to the PKA holoenzyme composed of the Regulatory subunit (Blue) and Catalytic subunit (Purple). The catalytic subunit binds to a kinase substrate (orange) and dissociates from the PKA holoenzyme complex. The red box indicates the transient Ternary complex of cAMP: PKAR: PKAC which is the focus of this study. The termination phase of the cAMP signaling pathway is the process by which the cAMP dissociates from the Regulatory subunit, thereby allowing it reassociate with the Catalytic subunit. cAMP dissociation and hydrolysis to AMP (magenta sticks) is carried out by enzymes called cyclic nucleotide phosphodiesterases (PDEs) (green).

The Catalytic domain once released from the Regulatory domain, is activated to carry out its downstream effects (Figure 1.1) (Corbin, Cobb et al. 1988).

Much progress has been made in the last decade in delineating the molecular basis of action of cAMP. An important tactic in this endeavor has been through the comparison of the effects of cAMP with those of two phosphorothioate cAMP analogs: (Sp)-cAMPS (a cAMP mimic) and (Rp)-cAMPS (an antagonist and a diastereoisomer of (Sp)-cAMPS) (Figure 1.2).

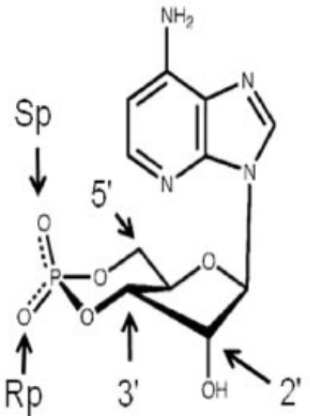

Figure 1.2: Thiol substituted analogs of cAMP: This figure depicts Thiol-substituted analogs of cAMP. Sulfur substitution at the axial position results in the Sp-cAMPS analog which is an agonist to cAMP. A sulfur substitution at the equatorial oxygen results in the Rp-cAMPS analog, which acts as an antagonist to cAMP.

Although the importance of geometry of the sulfur substitution is critical in determining the pharmacological properties of the two phosphorothioate cAMP analogs, the molecular basis for this behavior is not fully understood. To date, these comparisons have only been made using either wild-type or truncated mutants of the type Iα regulatory subunit (RIα) that are free in solution, not complexed to the C-subunit. X-ray crystallographic examination of ligand-bound RIα(92–379) complexes reveals few differences between ligand- bound complexes, but the (Rp)-cAMPS complex is structurally "looser" with higher thermal factors than complexes formed with either cAMP or (Sp)-cAMPS (Wu, Brown et al. 2004, Badireddy, Yunfeng et al. 2011). This is consistent with the observation that both cAMP and (Sp)-cAMPS, but not (Rp)-cAMPS, raise the urea concentration

required for wild-type RIα unfolding (Dostmann 1995). Further insight into the structural basis of cAMP action stems from NMR spectroscopic comparison of the effects of (Rp)-cAMPS, cAMP, and (Sp)-cAMPS on chemical shifts and ^{15}N relaxation of the RIα (119–244) mutant (Das and Melacini 2007). In addition to producing fewer significant chemical shift changes than either cAMP or (Sp)-cAMPS, (Rp)-cAMPS binding is associated with enhanced millisecond to microsecond time scale backbone motions of a β-turn (β2,β3 loop) and around the phosphate-binding cassette (PBC) (Das and Melacini 2007). It was previously reported that (Rp)-cAMPS increased the affinity of RIα toward C-subunit using a non-quantitative bioluminescence resonance energy transfer assay (Gesellchen, Prinz et al. 2006).

Further insight into the molecular basis of actions of cAMP and its analogs should come from the analysis of ligand bound R:C complexes. Unfortunately, the large size of even the heterodimeric R:C complex (~95 kDa) and the difficulty of generating (Rp)-cAMPS: R: C-subunit crystals currently preclude the use of both NMR spectroscopy and X-ray crystallography. Site-directed labeling combined with fluorescence spectroscopy was used to examine both the effects of cAMP and its analogs on R: C subunit binding kinetics and on the conformational dynamics of RIα (91–244) (Anand, Krishnamurthy et al. 2010). RIα (91–244) includes the "A" cyclic nucleotide binding (CNB) domain, the pseudosubstrate, and linker domains and represents the minimal segments necessary for high affinity C-subunit binding (Huang and Taylor 1998). For fluorescence stop-flow kinetics and fluorescence anisotropy experiments, fluorescein maleimide (FM) was conjugated to three cysteine substitution mutants with the substitution sites located near or within the pseudosubstrate sequence, the linker domain, or αC (R92C, T104C, and R239C, respectively) of RIα (91–244). Fluorescence stop flow experiments indicated that all three ligands tested (cAMP, Sp-cAMPS and Rp-cAMPS) had no effects on the PKA holoenzyme association rate. Monitoring dissociation rates revealed that, cAMP and Sp-cAMPS increased the dissociation rate 150-200 fold as compared to the basal rate. Rp-cAMPS on the other hand slowed the dissociation by 5 fold in comparison to the basal dissociation rate. The time-resolved fluorescence anisotropy results suggest that cAMP and (*S*p)-cAMPS reduce the interaction of the RIα linker domain and αC with the two peripheral R:C interaction sites on the C-

subunit (so-called Sites 2 and 3) without affecting the interaction of the pseudosubstrate sequence with the active site cleft (so-called Site 1) (Table 1.1).

Ligand	k_a $M^{-1}s^{-1}$	k_d s^{-1}
Control	$2.0 \pm 0.12 \times 10^7$	$3.8 \pm 0.1 \times 10^{-3}$
cAMP	$1.7 \pm 0.11 \times 10^7$	0.55 ± 0.05
(*Rp*)-cAMPS	$1.9 \pm 0.17 \times 10^7$	$7.5 \pm 0.3 \times 10^{-4}$
(*Sp*)-cAMPS	$1.9 \pm 0.16 \times 10^7$	0.75 ± 0.02

Table 1.1: Fluorescence stop flow kinetics based quantification of PKA holoenzyme interaction: cAMP, Sp-cAMPS and Rp-cAMPS have no discernible effect on the PKA holoenzyme association rates. Rp-cAMPS causes 5 fold slower dissociation rate of PKA holoenzyme while cAMP and Sp-cAMPS increase the dissociation rate. Figure adapted from the following article (Anand, Krishnamurthy et al. 2010).

In this study we have aimed to examine the effects of cAMP and its analogs on solvent exposure/conformational flexibility of RIα (91–244): C-subunit complex using H/D amide exchange measured with a combination of mass spectrometry (ESI-QTOF) and proteolytic fragmentation (HDXMS). Because of limitations of the amide H/D exchange experiments, only the effects of (Rp)-cAMPS on H/D amide exchange in RIα (91– 244): C-subunit complex could be investigated. The results showed that (Rp)-cAMPS induces a relatively widespread increase in amide exchange, indicating limited unfolding and/or enhanced conformational flexibility that is propagated almost globally through the C-subunit and, at least, part of RIα. These conformational changes were accompanied by a 5-fold increase in the affinity of RIα (91–244) toward C-subunit, suggesting that, at least, some of the (Rp)-cAMPS effects are mediated by an increase in internal entropy. Finally, the (Rp)-cAMPS induced increase in PKAR: PKAC affinity indicates that (Rp) cAMPS is better described as an inverse agonist because the basal activity of the PKA holoenzyme should be decreased by (Rp)-cAMPS. For ease of understanding RIα (91-244) fragment will henceforth be referred to as $RI\alpha_A$ and the PKA catalytic subunit shall be referred to as PKA C.

1.2 Materials and Methods

1.2.1 Reagents

ATP, cAMP, and MOPS were obtained from Sigma-Aldrich. (Sp)-cAMPS, (Rp)-cAMPS and 8-AEA-cAMP were obtained from Biolog (Bremen, Germany). NHS-activated sepharose 4 Fast Flow was obtained from GE (Chicago, IL). Talon Cobalt based metal affinity resin (Clontech laboratories, Mountain View, CA) was used for purification of hexahistidine-tagged PKA C-subunit following the manufacturer's specifications. BL21 (DE3) *E.coli* strains were from Novagen (Madison, WI). Immobilized pepsin cartridges (Poroszyme) were obtained from Applied Biosystems (Redwood City, CA). Deuterium oxide (99.9% deuterium) was obtained from Cambridge Isotopes (Andover, MA). Trifluoroacetic acid (TFA) and acetonitrile were from Fisher Scientific. PD10 columns were from GE Healthcare. All other chemicals were at least reagent grade.

1.2.2 Expression and Purification of PKA RIα_A

Recombinant PKA RIα_A was expressed and purified from bacterial cells using cAMP sepharose affinity resin as previously described (Diller, Xuong et al. 2000, Anand, Taylor et al. 2007). Plasmid containing PKA RIα_A from bovine source was transformed into *E.coli* [BL21 (DE3)] and grown in LB media at 37 ºC, till mid log phase growth with an OD of 0.7 was achieved. Cells were subsequently induced to express recombinant protein by the addition of 500 µM of IPTG and left to shake overnight at 18 ºC. Cells were harvested by centrifugation at 6000×g and 4 ºC (Beckman Coulter JA-10 rotor) for 20 min. The cell pellet was resuspended in lysis buffer (20 mM MES pH 6.5, 100 mM NaCl, 2 mM EDTA) and lysed by sonication for 15 min. Cell lysates were centrifuged at 17000 × g for 30 min at 4 ºC and the supernatant was precipitated using 45% ammonium sulphate. The ammonium sulphate precipitate was subjected to centrifugation at 6500 × g for 15 min to remove the supernatant. The precipitate was subsequently resuspended in lysis buffer followed by overnight incubation with cAMP sepharose resin at 4 ºC. cAMP sepharose resin was made by conjugating 8-AEA-cAMP with NHS activated sepharose beads using a manufacturer prescribed protocol. The resin was then transferred into columns and purified PKA RIα_A was eluted with 40 mM cGMP elution

buffer (50 mM MES pH 5.8, 200 mM NaCl, 2mM EDTA, 40 mM cGMP). The purified PKA $RI\alpha_A$ was further purified by size exclusion chromatography (S75 size exclusion AKTA column, GE healthcare) as a final purification step.

1.2.3 Expression and Purification of PKA C-subunit

The PKA C-subunit was expressed with an N-terminal hexahistidine tag in *E.coli* [BL21 (DE3)] cells and purified by Talon cobalt His-tag resin(Anand, Hughes et al. 2002). Cells expressing PKA-C were cultured at 37 ºC until mid-log phase growth with an OD of 0.7 was achieved. Protein expression was induced by the addition of 500 µM IPTG and shaken at 180 rpm overnight at 18 ºC. Cells were harvested by centrifugation at 6000 × g and 4 ºC (Beckman Coulter JA-10 rotor) for 20 min. The cell pellet was resuspended in lysis buffer (50 mM KH_2PO_4, 20 mM Tris-HCl pH 8.0, 100 mM NaCl, 5 mM β-mercaptoethanol (βME), 5 mM imidazole) and lysed by sonication for 15 min. Cell lysates were centrifuged at 17000 × g for 30 min at 4 ºC and the supernatant was incubated with Talon metal affinity resin for 1 hr at 4 ºC. The resin was then transferred into columns and washes thrice with Lysis buffer. PKA-C was eluted with elution buffer (Lysis buffer with 200 mM Imidazole, pH 7.0). The purified PKA-C was further purified by size exclusion chromatography (S200 size exclusion AKTA column, GE healthcare) as a final purification step.

1.2.4 Formation and Purification of PKA $RI\alpha_A$: C holoenzyme

The PKA holoenzyme is formed by combining PKA $RI\alpha_A$ with PKA-C subunit in a condition which favors dissociation of cGMP from the active site of PKA $RI\alpha_A$ and thereby allows PKA-C to bind to PKA $RI\alpha_A$. To this end PKA $RI\alpha_A$ (1 µM) and PKA-C were mixed in a 1:1.2 molar ratio in a buffer containing 50 mM MOPS, 50 mM NaCl, 1 mM DTT, 2 mM MgCl2, 0.2 mM ATP, pH 7.0 (Buffer A) using Spectra/por 30 kDa molecular weight cut off dialysis membrane. Dialysis was allowed to proceed for 16h at 4 ºC with constant mixing with 3×1 litre buffer changes. The holoenzyme was further purified by size exclusion chromatography (S200 size exclusion column, AKTA GE healthcare) to separate holoenzyme from the individual proteins.

1.2.5 Amide Hydrogen/ Deuterium Exchange Mass spectrometry (HDXMS) of PKA holoenzyme in complex with thiol substituted cAMP analog, Rp-cAMPS

The PKA RIα_A: C holoenzyme obtained from Size exclusion chromatography was concentrated to a final concentration of 109 µM using Vivaspin concentrators (Satrorius Stedim Biotech GmbH, Goettingen, Germany). For this experiment, deuterium exchange in PKA holoenzyme was measure in in the absence and presence of 1 mM (Rp)-cAMP. 1 µL of PKA holoenyzyme at 109 µM was incubated with 1 µL of 20 mM Rp-cAMPS for 30 min on ice. Deuterated buffer was obtained by drying Buffer A (50 mM MOPS, 50 mM NaCl, 1 mM DTT, 2 mM MgCl2, 0.2 mM ATP, pH 7.0) in a Centrivap vacuum dryer, the dried buffer was subsequently reconstituted in D_2O. The complex was allowed to exchange with deuterated buffer solutions by 10-fold dilutions of protein samples in deuterated Buffer A. The reactions were then quenched after timed intervals of 30 s, 1 min, 2 min, 5 min, and 10 min by chilling on ice and the addition of 30 µl of 0.2% trifluoroacetic acid, to obtain a final pH_{read} of 2.5. Undeuterated samples were included to serve as a template for peptide identification and also to provide a baseline value for deuterium exchange quantification. One sample was allowed to exchange with deuterated buffer A for 24 h to allow for complete deuteration of solvent-exposed regions of the protein. This was used to calculate back-exchange under our experimental conditions and is described in greater detail in subsequent sections. 50 µl of the reaction samples was washed through an on-line Poroszyme immobilized pepsin cartridge (Applied Biosystems) to digest proteins into peptides and trapped onto 2.1×5 mm C18 trap (ACQUITY BEH C18 Vanguard pre-column, 1.7 µM, Waters, Milford, MA). Higher resolution peptide separation was achieved by reverse phase HPLC through a C18 column (ACQUITY UPLC BEH 1.0 × 100 mm, 1.7 µM, Waters, Milford, MA) in a 10 min gradient with water as the polar phase and Acetonitrile as the organic phase. 0.1% TFA was added to all buffers to lower the pH to 2.5 and also to serve as an ion pairing agent to increase chromatographic resolution and greater detection in mass spectrometry. Peptides resolved by reverse phase HPLC were subsequently injected onto an ESI-QTOF Waters Synapt high definition mass spectrometry (HDMS) system (Waters) operating in positive ion mode.

The Mass spectrometer was operated in MS^E mode, where it simultaneously collects primary peptide mass spectra along with peptide fragmentation spectra. Both the pepsin cartridge and C18 column were housed in a refrigerated module at 2 °C to minimize deuterium back-exchange during analysis (Wu, Engen et al. 2006, Engen 2009).

1.2.6 Peptide Identification and HDXMS Data analysis

Mass spectra of peptides and peptide fragmentation data obtained from the undeuterated control were used for peptide identification by Protein Lynx Global Server (PLGS) (v2.4) search software (Waters). A database containing a primary sequence of PKA RIα and C-subunits was used as a template for peptide identification. A mass error tolerance of 10 ppm was used to sequence the peptides. Continuous instrument calibration was carried out with Glu-fibrinogen peptide at 100 fmol/µl. Deuterium exchange quantitation was carried out with HX-Express software (Weis, Engen et al. 2006)

1.2.7 Calculation of back exchange correction factor

Deuterium back exchange is the loss of deuterium ions from labeled peptides over time. Each experimental system has a different back exchange factor which is dependent on temperature, pH of buffers, time of experiment, length of tubing, etc. Though the back exchange rate is at its minimum at pH 2.5 and cold conditions, a significant amount of deuterium ions are lost during the course of the experiment. Deuterium back exchange loss for our experimental system was determined by calculating the deuterium loss from peptides that have undergone theoretically maximum deuterium exchange. To this end, ligand-free $RI\alpha_A$ was incubated with deuterated buffer A for 24 h at room temperature (20 °C). Certain regions of $RI\alpha_A$ get rapidly incorporated with deuterium ions while other regions are involved in rigid secondary structural elements and do not exchange even after 24 h of deuterium exchange. The regions which undergo rapid exchange were mainly considered for back exchange factor calculation; these regions are mainly found in the N-terminal region PKA $RI\alpha_A$. The region in $RI\alpha_A$ spanning residues 111–130 is a highly solvent-exchangeable region (Anand, Hughes et

al. 2002), and peptides used for calculations of back-exchange span this region and showed nearly complete exchange in ligand-free $RI\alpha_A$ following 10-min deuterium exchange and would represent fully deuterated samples following 24-h exchange. The average deuterium back-exchange loss of 32.8±1.6% was calculated from average back-exchange values for five peptides: RIα(111–123) (m/z 547.65) (back-exchange, 34.4%), RIα(111–119) (m/z 559.34) (back-exchange, 33.7%), RIα(111–126) (m/z 632.701) (back-exchange, 30.4%), RIα(111–119) (m/z 595.34) (back-exchange, 33.7%), and RIα (112–126) (m/z 578.35) (back-exchange, 32.0%) (Anand, Krishnamurthy et al. 2010, Badireddy, Yunfeng et al. 2011). All deuterium exchange values reported were corrected for a 32.7% back-exchange by multiplying the raw centroid values by a multiplication factor of 1.49. Deuterium exchange kinetic plots were obtained by plotting deuterium uptake values against labeling time and fitting the points to a one phase association curve to account for fast exchanging solvent accessible amides which exchange deuterium ions within 10 mins of deuterium labeling (Mandell, Falick et al. 1998).

1.3 Results and Discussion

The activation phase of the cAMP signaling pathway has two end state complexes, namely PKA $RI\alpha_A$: PKA C holoenzyme complex and the cAMP: PKA $RI\alpha_A$ end state complex (Figure 1.1). These are well studied stable complexes, with the availability of high resolution crystal structures (Su, Dostmann et al. 1995, Kim, Cheng et al. 2007). The transition state between these two end-states is a ternary complex of PKA $RI\alpha_A$: cAMP: PKA C which is a transient and dynamic complex. The goal of this study is to probe the dynamics of the ternary complex and understand the processes involved in cAMP mediated dissociation of PKA holoenzyme. To this end we captured the ternary complex in a meta-stable state by using a thiol substituted analog of cAMP, Rp-cAMPS. Rp-cAMPS is chemically similar to cAMP and differs by a single Sulfur substitution at the equatorial oxygen postion of cAMP. Though very similar to cAMP, Rp-cAMPS has been shown to act antagonistically to cAMP by capturing $RI\alpha_A$ in 'C' bound conformation (Badireddy, Yunfeng et al. 2011). HDXMS mass spectrometry was carried out to ascertain the nature of the holoenzyme interaction in the presence and absence of Rp-cAMPS and to come up with a model to explain the increased affinity of the complex

in the presence of Rp-cAMPS. The same experiment when repeated with cAMP or the agonist Sp-cAMPS lead to the dissociation of the PKA holoenzyme. The ultimate aim of this study was to capture the Rp-cAMPS bound ternary complex and map out the conformational dynamics and allosteric relays in cAMP mediated dissociation of PKA holoenzyme.

1.3.1 Pepsin digestion of PKA RIα$_A$ and PKA C

Undeuterated control of the PKA holoenzyme was carried out as described in Materials and Methods. Output from PLGS global server was subsequently analyzed and a list of peptides was generated. Only peptides with a high confidence and multiple fragment ions were considered. All peptides which were selected for subsequent deuterium exchange quantification had a signal to noise ratio (S/N) of atleast 6. In total, 22 peptide fragments were obtained for RIα$_A$, which accounted for 92% of the protein sequence with overlapping peptides available for almost all important regions of the protein. The presence of high number of overlapping peptides especially at the cAMP binding pocket, enabled higher resolution in probing for subtle changes in amide exchange rates. Coverage was not available mainly for the beginning 10 amino acids in the N-terminal and final 6 amino acids in the C-terminal of RIα$_A$. In PKA C, 50 peptide fragments were obtained which accounted for 85% of the sequence coverage. Numerous overlapping peptides were also obtained for PKA C thereby increasing the resolution of the study. The sequence coverage obtained from HDXMS experiment is mapped onto the crystal structure of PKA holoenzyme in Figure 1.3, regions showing coverage are in color while regions showing no coverage are in grey. All analyzed peptides are listed with the deuterium ions incorporated after 10 min of deuterium labeling and are summarized in Table 1.2 for PKA RIα$_A$ and Table 1.3 for PKA C. Regions which show significant differences upon Rp-cAMPS binding to PKA holoenzyme are highlighted in bold. A difference of a minimum of 0.5 Da was considered significant (Houde, Berkowitz et al. 2011).

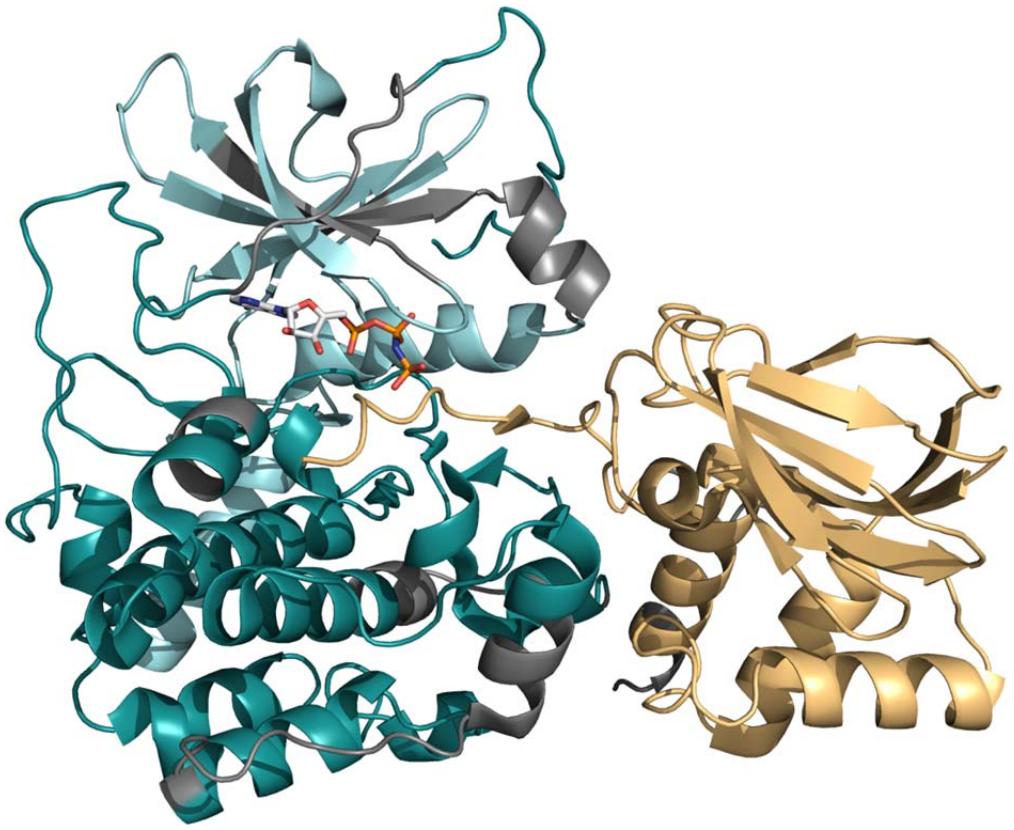

Figure 1.3: Sequence coverage map: Structure of PKA holoenzyme (PDB ID: 3FHI) with regions showing coverage in PKA RIα_A in light orange, and PKA-C N-lobe in Cyan and the C-lobe in Teal. Regions showing no coverage are in grey. AMP-PNP molecule bound to PKA C is represented in stick form.

Table 1.2: *Effects of Rp-cAMPS on H/D exchange of RIα_A in the PKA holoenzyme complex.*

			Maximum Amides Exchanged[a]	
Fragment of R-subunit (*m/z*)[region]	Number of Exchangeable amides	Charge (z)	Control (Mean ± S.E.)	Plus Rp-cAMPS (Mean ± S.E.)
92- 102(588.3)[pseudo substrate]	10	2	3.12 ± 0.04	3.27 ± 0.1
102-106(640.29)[linker]	4	1	3.0 ± 0.01	2.9 ± 0.07
111-126 (632.70)[linker]	14	3	8.7 ± 0.26	9.0 ± 0.34
112-119 (477.81)[linker]	6	2	4.2 ± 0.09	4.6 ± 0.13
126-134 (493.29)[αXn]	8	2	3.4 ± 0.05	3.6 ± 0.10

136-143 (976.40)[loop-αA]	**7**	**1**	**1.8 ± 0.12**	**2.4 ± 0.14**
136-148 (797.86)[loop-αA]	**12**	**2**	**1.3 ± 0.08**	**1.7 ± 0.10**
144-148 (637.34)[αA]	4	1	0.3 ± 0.24	0.1 ± 0.02
149-156 (913.42)[αA]	6	1	1.2 ± 0.03	1.2 ± 0.23
157-172 (846.89)[β2-β3]	**15**	**2**	**5.7 ± 0.18**	**4.8 ± 0.22**
161-172 (1322.58)[β2-β3]	**11**	**1**	**4.8 ± 0.17**	**3.9 ± 0.21**
162-172 (1225.54)[β2-β3]	**10**	**1**	**4.7 ± 0.16**	**3.9 ± 0.20**
172-180 (1101.49)[β4]	8	1	1.1 ± 0.02	1.1 ± 0.04
183-187 (638.28)[β4]	4	1	2.0 ± 0.02	2.0 ± 0.04
188-198 (1097.49)[β5-β6]	10	1	4.0 ± 0.10	4.0 ± 0.15
188-201(1396.64)[β5-β6-αB']	**13**	**1**	**6.4 ± 0.22**	**4.5 ± 0.16**
202-212 (567.32)[αB']	**9**	**2**	**3.7 ± 0.14**	**1.9 ± 0.18**
202-221 (705.76)[αB'-β7]	**18**	**3**	**4.1 ± 0.18**	**2.4 ± 0.14**
204-221(644.3)[αB'-β7]	**16**	**3**	**4.0 ± 0.13**	**2.0 ± 0.14**
213-221 (500.83)[β7]	**8**	**2**	**0.8 ± 0.01**	**1.0 ± 0.03**
222-229 (506.23)[β8-αB]	6	2	0.6 ± 0.05	0.6 ± 0.07
230-238 (523.81) [(αB-αC]	8	2	2.6 ± 0.05	2.6 ± 0.11

** Non-overlapping 95% confidence intervals relative to control values determined by Prizm™ computer program.*

[a] Average number of deuterons exchanged determined from fitting plots of the time course of deuteration during a 10-min exposure to deuterium oxide to a single -exponential equation. Values reported are the mean and standard error of the amplitude term of fits and results are from at least two independent experiments. Peptides showing significant differences upon Rp-cAMPS binding are in bold.

Table 1.3: *Effects of Rp-cAMPS on H/D exchange of PKA C in the PKA holoenzyme complex.*

			Maximum Amides Exchanged[a]	
Fragment of C-subunit (*m/z*)[region]	Number of Exchangeable amides	Charge (z)	Control (Mean ± S.E.)	Plus Rp-cAMPS (Mean ± S.E.)
7-18(700.32)[αA]	**11**	**2**	**8.2 ± 0.05**	**9.7 ± 0.19**
14-31 (732.72)[αA]	**17**	**3**	**4.3 ± 0.11**	**5.3 ± 0.11**
19-26 (461.25)[αA]	**7**	**2**	**4.2 ± 0.10**	**5.3 ± 0.37**
19-27 (534.79)[αA]	**8**	**2**	**4.4 ± 0.13**	**4.9 ± 0.18**
21-36 (953.5)[αA-β1]	**14**	**2**	**8.4 ± 0.19**	**9.5 ± 0.22**
27-40 (822.44)[αA-β1]	**12**	**2**	**7.7 ± 0.17**	**8.3 ± 0.20**
28-40 (765.90)[αA-β1]	**11**	**2**	**7.6 ± 0.12**	**8.2 ± 0.19**
42-55 (792.90)[β1]	13	2	1.9 ± 0.07	2.0 ± 0.13
45-55 (597.83)[β1]	10	2	3.0 ± 0.11	3.0 ± 0.14
60-71 (700.84)[β1-β2]	**11**	**2**	**0.4 ± 0.02**	**0.9 ± 0.04**
83-100 (727.74)[αB-αC]	17	3	3.3 ± 0.09	3.2 ± 0.13
92-100 (544.83)[αC]	8	2	1.7 ± 0.06	1.6 ± 0.09
98-103 (736.403)[αC]	4	1	0.9 ± 0.02	0.8 ± 0.04
98-104 (807.44)[αC]	5	1	1.6 ± 0.03	1.6 ± 0.09
104-108 (635.38)[β4]	4	1	Solvent inaccessible	Solvent inaccessible
104-110 (869.48)[β4]	6	1	1.0 ± 0.02	1.2 ± 0.07
105-110 (770.41)[β4]	5	1	1.0 ± 0.05	1.1 ± 0.08
106-115 (1200.55)[β4]	9	1	1.7 ± 0.06	1.7 ± 0.11
109-116 (924.44)[β4]	7	1	1.0 ± 0.02	1.1 ± 0.06

119-126 (825.38)[β5]	7	1	0.2 ± 0.02	0.4 ± 0.02
122-128 (726.32)[β5-αD]	6	1	1.0 ± 0.17	0.8 ± 0.08
122-129 (855.36) [β5-αD]	7	1	1.0 ± 0.14	1.0 ± 0.29
133-145 (570.29)[αD-αE]	12	3	1.2 ± 0.03	1.3 ± 0.01
144-151(470.26)[αE]	7	2	3.0 ± 0.10	2.9 ± 0.03
156-163 (989.49)[αE-β6]	7	1	0.3 ± 0.02	0.3 ± 0.01
162-173 (743.94)[β6-β7]	10	2	0.5 ± 0.04	0.3 ± 0.3
173-178 (673.35)[β7]	**5**	**1**	**1.3 ± 0.01**	**0.9 ± 0.05**
180-185 (722.36)[β8]	5	1	0.3 ± 0.24	0.2 ± 0.19
180-187 (926.46)[β8]	7	1	Solvent inaccessible	Solvent inaccessible
182-187 (685.32)[β8]	5	1	Solvent inaccessible	Solvent inaccessible
188-212(981.52)[β9-activation loop]	22	3	3.5 ± 0.08	3.5 ± 0.08
189-212(932.50)[β9-activation loop]	21	3	3.3 ± 0.08	3.2 ± 0.09
198-211(1418.73)[β9-activation loop]	10	1	Solvent inaccessible	Solvent inaccessible
205-211(768.49)	5	1	Solvent inaccessible	Solvent inaccessible
222-227 (658.40)[αF]	5	1	Solvent inaccessible	Solvent inaccessible
231-245 (826.90)[αF-αG]	11	2	5.3 ± 0.12	5.0 ± 0.19
232-239 (869.43)[αF]	5	1	1.1 ± 0.03	1.2 ± 0.02
241-247 (784.42)[αF-αG]	5	1	3.0 ± 0.10	2.9 ± 0.27
262-269 (890.48)[αH]	7	1	Solvent inaccessible	Solvent inaccessible
262-273 (693.90)[αH]	11	2	Solvent inaccessible	Solvent inaccessible
268-273 (741.50)[αH]	5	1	Solvent inaccessible	Solvent inaccessible
268-274 (869.56)[αH]	6	1	Solvent inaccessible	Solvent inaccessible
278-302(748.40)[αH-αI]	**24**	**4**	**7.0 ± 0.20**	**8.1 ± 0.20**
291-303 (831.41)[αH-αI]	12	2	3.1 ± 0.16	3.3 ± 0.22

298-303 (740.33)[αH-αI]	5	1	2.4 ± 0.08	2.6 ± 0.15
303-326(669.87)[C-terminal tail]	**19**	**4**	**9.5 ± 0.12**	**9.9 ± 0.20**
303-327(706.64)[C-terminal tail]	**20**	**4**	**9.0 ± 0.17**	**9.4 ± 0.17**
305-327(623.85)[C-terminal tail]	**18**	**4**	**10.0 ± 0.13**	**10.5 ± 0.25**
306-327 (632.34)[C-terminal tail]	**17**	**4**	**8.1 ± 0.06**	**8.5 ± 0.13**
336-347 (728.36)[C-terminal tail]	**11**	**2**	**7.0 ± 0.10**	**7.9 ± 0.11**

** Non-overlapping 95% confidence intervals relative to control values determined by PrizmTM computer program.*
[a] Average number of deuterons exchanged determined from fitting plots of the time course of deuteration during a 10-min exposure to deuterium oxide to a single -exponential equation. Values reported are the mean and standard error of the amplitude term of fits and results are from at least two independent experiments. Peptides showing significant differences upon Rp-cAMPS binding are in bold.

1.3.2 Rp-cAMPS binding does not lead to the dissociation of PKA holoenzyme

The primary goal of this study was to capture the ternary complex of Rp-cAMPS:PKA $RI\alpha_A$: PKA C, thus it was important to first determine that Rp-cAMPS, being almost identical to cAMP, does not cause dissociation of PKA holoenzyme. This was confirmed by quantifying deuterium exchange at the N-terminal pseudeosubstrate region of $RI\alpha_A$. This loop is involved in direct interactions with the substrate binding pocket of PKA C and shows decreased deuterium exchange in HDXMS experiments (Anand, Law et al. 2003, Kim, Cheng et al. 2007). Rp-cAMPS binding to the *apo* $RI\alpha_A$ CNB domain causes significant decreases in deuterium exchange across the entire protein but has no effects at the N- terminal pseudo substrate region (Badireddy, Yunfeng et al. 2011). $RI\alpha_A$ in the PKA holoenzyme state shows significant decreases in deuterium exchange at the pseudo substrate region when compared with the $RI\alpha_A$ in the ligand free State and Rp-cAMPS bound state. The ternary complex of Rp-cAMPS:PKA holoenzyme also shows significant protection at the pseudosubstrate region, equivalent to the free holoenzyme form (Figure 1.4). This shows that Rp-cAMPS does not cause the dissociation of the PKA holoenzyme. Subsequent sections will highlight Rp-cAMPS induced conformational changes in the PKA holoenzyme.

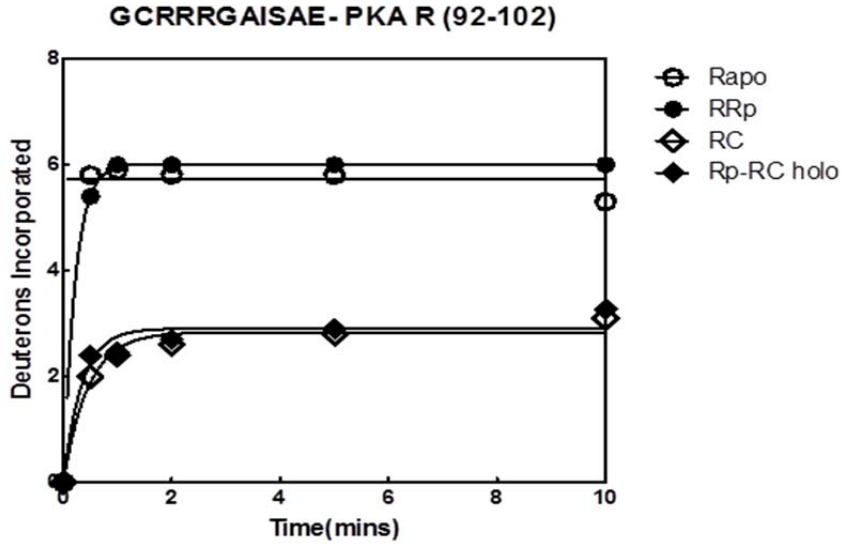

Figure 1.4: Time course of deuterium exchange for a peptide spanning the N-terminal pseudo substrate region. Open circle (○) denotes $RI\alpha_A$ in the *apo* state, filled circle (●) denotes $RI\alpha_A$ in the Rp-cAMPS bound state, open diamond (◊) indicates $RI\alpha_A$ in the PKA holoenzyme state and closed diamond (♦) indicates $RI\alpha_A$ in the ternary complex state of $RI\alpha_A$:Rp-cAMPS:PKAC. Deuterium labeling reaction was carried out for 0.5, 1, 2, 5 and 10 min and the data was plotted against time. Data was fit to a one-phase association nonlinear exponential curve fit (Graphpad Prizm 5.0, San Diego, CA)

1.3.3 Direct binding effects of Rp-cAMPS at the CNB domain of $RI\alpha_A$

Rp-cAMPS binds to $RI\alpha_A$ at the cAMP binding pocket and causes protein-wide changes in dynamics. The most significant differences are observed at a β-barrel and loop region spanning residues 200-212. This region is important in forming multiple direct hydrogen bonds with the cAMP molecule, and all peptides spanning this region show a decrease in deuterium exchange. The decreased exchange seen in this region is consistent with the roles of Glu^{200} and Arg^{209} in coordinating the 2' -OH and

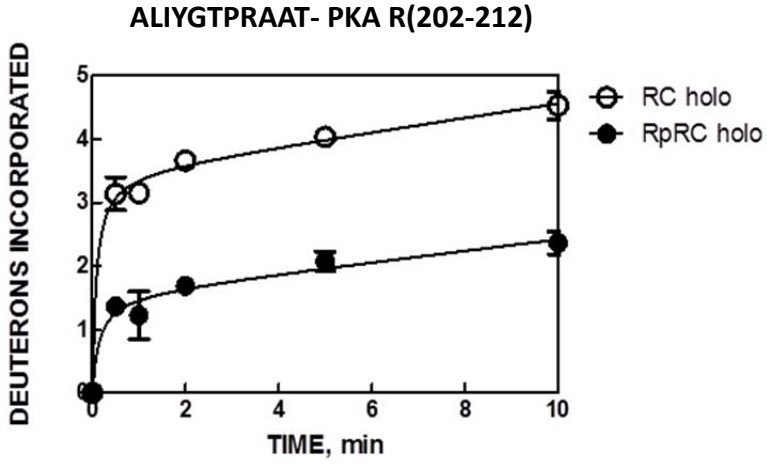

Figure 1.5: Kinetic plot of deuterium exchange for peptide spanning the cAMP binding pocket. Open circle (○) denotes $RI\alpha_A$ in the PKA holoenzyme state, close circle (●) indicates $RI\alpha_A$ in the ternary complex state of $RI\alpha_A$:Rp-cAMPS:PKAC. Deuterium labeling reaction was carried out for 0.5, 1, 2, 5 and 10 min and the data was plotted against time. Data was fit to a one-phase association nonlinear exponential curve fit (Graphpad Prizm 5.0, San Diego, CA)

phosphodiester moieties of cAMP, respectively (Su, Dostmann et al. 1995). In the absence of ligand, this region is partially protected, Rp-cAMPS causes further protection at this loci. Kinetic plot for a peptide lining the PBC is depicted in Figure 1.5. In all overlapping peptides spanning this region, Rp-cAMPS binding to PKA holoenzyme induces ~ 2 Da decrease in deuterium exchange. This is consistent with previous reports, where Rp-cAMPS binding to *apo* $RI\alpha_A$ also showed 2 Da decrease in deuterium exchange (Badireddy, Yunfeng et al. 2011). This proves that the Rp-cAMPS molecule occupies the cAMP binding pocket and forms stable hydrogen bonds with residues lining the pocket.

Cyclic AMP binding to the PBC of PKA is generally considered a phosphorylation event and cAMP can be seen as a soluble phosphate group. This notion stems from the fact that the phosphate group of cAMP makes one key hydrogen bond with the guanidinium nitrogen of an Arginine residue that lines the cAMP binding pocket. While other moieties of the ligand form stable hydrogen bonds with other residues lining the pocket, the key interaction occurs between the cAMP molecule and Arg^{209} in the PBC, and this interaction sets off an allosteric relay that activates the PKA molecule. This is largely similar to a phosphorylation event where a single phosphate group activates the protein/ enzyme.

The Arg^{209} residue is involved in an allosteric relay with Asp^{170} in the presence of cAMP molecule. The equatorial oxygen of cAMP's phosphate group forms direct hydrogen bonds with Arg^{209} and stabilizes this allosteric relay. This relay is disrupted in the PKA holoenzyme state. In the case of Rp-cAMPS, the equatorial oxygen is occupied by a Sulfur group, and due its higher electronegativity, sulfur does not form hydrogen bonds with nitrogen of Arg^{209}. While Rp-cAMPS confers ~2 Da of protection at the binding pocket for both the PKA holoenzyme state and *apo* $RI\alpha_A$, cAMP confers ~4 Da of protection to the *apo* protein. This thus shows that Rp-cAMPS forms a more dynamic interaction with the binding pocket as compared to cAMP.

1.3.4 Allosteric effects in $RI\alpha_A$ caused by Rp-cAMPS binding

Allosteric effects are the ligand induced conformational changes which occur are loci distal to the actual binding site. Allosteric effects of cAMP binding to $RI\alpha_A$ are well documented, with the main locus of allosteric effects to be located around the crucial Arg^{209}-Asp^{170} relay (Anand, Hughes et al.

2002, Das and Melacini 2007, Kim, Cheng et al. 2007). Two important allosteric effects were observed upon Rp-cAMPS binding to $RI\alpha_A$.

A region showing significant differences was a region spanning residues 126-143 which form a 3_{10} helix. Differences in this region were seen on two contiguous peptides one spanning residues 126-135 and the other spanning residues 136-143. Interestingly, this region showed increases in deuterium exchange indicating increased dynamics. While region spanning residues 136-143 showed consistently increased deuterium exchange of ~ 0.7 Da upon ligand binding, the region spanning residues 126-143 shows significantly increased deuterium exchange (1.5 Da) for early time points. But as labeling time increases the difference between ligand free and ligand bound states becomes negligible. Time dependent differences points towards the dynamics nature of the ternary complex. Another peptide spanning the residues 161-172 showed decreased deuterium exchange by ~1 Da, upon Rp-cAMPS binding. This peptide spans the crucial Asp^{170} allosteric relay site. Kinetics plots of these 3 peptides are depicted Figure 1.6.

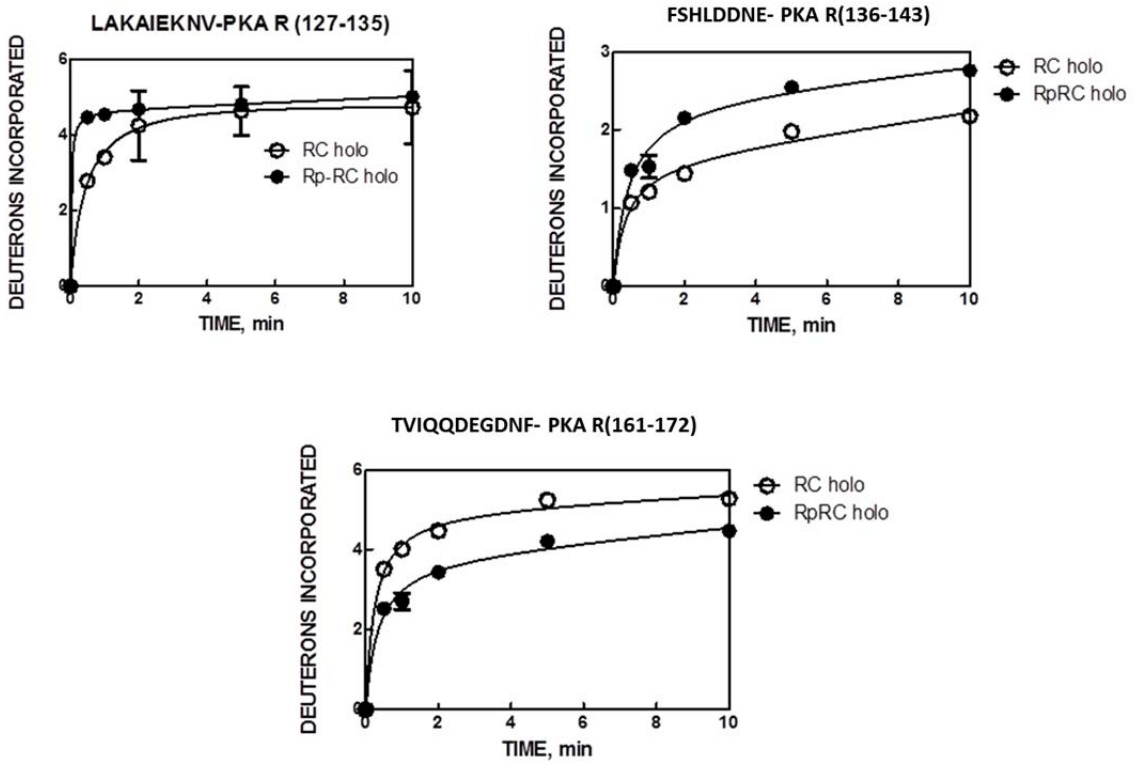

Figure 1.6: Allosteric effects induced on $RI\alpha_A$ by Rp-cAMPS binding to PKA holoenzyme: Kinetic plots of deuterium exchange for peptides that undergo allosteric changes upon Rp-cAMPS binding to PKA holoenzyme. Peptide sequences are indicated and residue numbers are in brackets.

Open circle (○) denotes RIα$_A$ in the PKA holoenzyme state, close circle (●) indicates RIα$_A$ in the ternary complex state of RIα$_A$:Rp-cAMPS:PKAC. Deuterium labeling reaction was carried out for 0.5, 1, 2, 5 and 10 min and the data was plotted against time. Data was fit to a one-phase association nonlinear exponential curve fit (Graphpad Prizm 5.0, San Diego, CA)

The region spanning residues 133-140 of PKA RIα$_A$ is important in forming direct interactions with Site 2 of PKA C (Kim, Xuong et al. 2005) and increased dynamics in this region could indicate that the RIα$_A$ and PKA C interaction at this region is less stable. This provides a model on how ligand cAMP at the binding pocket drives the conformation of RIα$_A$ from PKA C high affinity form to a conformation with low affinity for PKA C by inducing an increase in dynamics at key interaction interfaces.

As discussed in the previous section, the Asp^{170} molecule is involved in an allosteric relay with Arg^{209}. Since Rp-cAMPS does not form stable hydrogen bonds with the Arg^{209} molecule, the Asp^{170} allosteric relay is also not fully stabilized. This should result in a highly dynamic profile at the Asp^{170} loci, but it was seen that Rp-cAMPS binding to the PKA holoenzyme results in protection of 1 Da at this locus. On the other hand, Rp-cAMPS or cAMP binding to *apo* RIα$_A$ causes significantly greater protection of up to 2 Da, thus the protection seen in the Rp-cAMPS:PKA holoenzyme ternary complex, though significant, is significantly less than the protection seen in cAMP: *apo* RIα$_A$. This indicates that though the Arg^{209}-Asp^{170} allosteric relay is the most important relay at this locus, it is also stabilized by other allosteric relays independent of the Arg^{209}-Asp^{170} relay. This points towards a multi-state model for allostery whereby allostery progresses via multiple pathways as opposed to a single allosteric relay (Moorthy and Anand 2012).

A summary of Rp-cAMPS induced effects on $RI\alpha_A$ is mapped onto the crystal structure of PKA holoenzyme in figure 1.7.

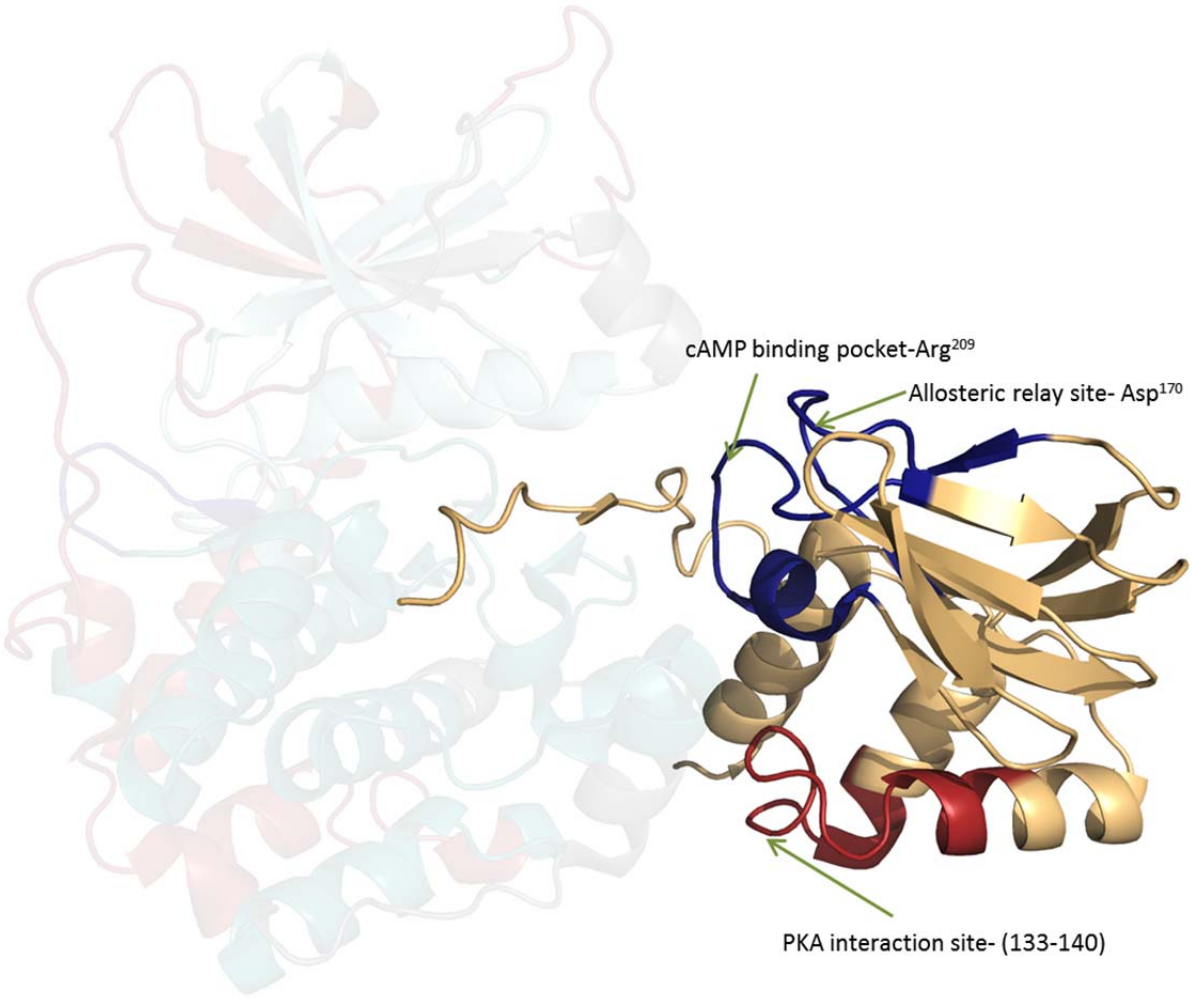

Figure 1.7: Rp-cAMPS induced changes on $RI\alpha_A$: Structure of the PKA holoenzyme (PDB ID:3FHI) with $RI\alpha_A$ in pale green. Regions showing decreases in deuterium exchange upon Rp-cAMPS binding are in blue, and regions showing increased dynamics on ligand binding are in red. The PKA C molecule is transparent for ease of viewing.

1.3.5 Allosteric effects propagate across the interaction interface

Peptides from PKA C were also analyzed and a number of peptides showed significant changes in deuterium exchange upon ligand binding. This was an interesting result as it shows that ligand binding on $RI\alpha_A$ induces allosteric effects to propagate across the protein-protein interaction interface and cause changes in protein dynamics in the interacting protein. Most of the regions showing differences in PKA C showed significant increases in deuterium exchange indicating an overall increase in dynamics in PKA C. The regions showing increased dynamics were mainly seen at the N terminal αA helix, β1-β2 beta strand at the C-terminal tail region. One peptide proximal to the ATP binding site showed decrease in deuterium exchange.

Kinetic plots for peptides showing significant changes in PKA C are depicted in Figure 1.8.

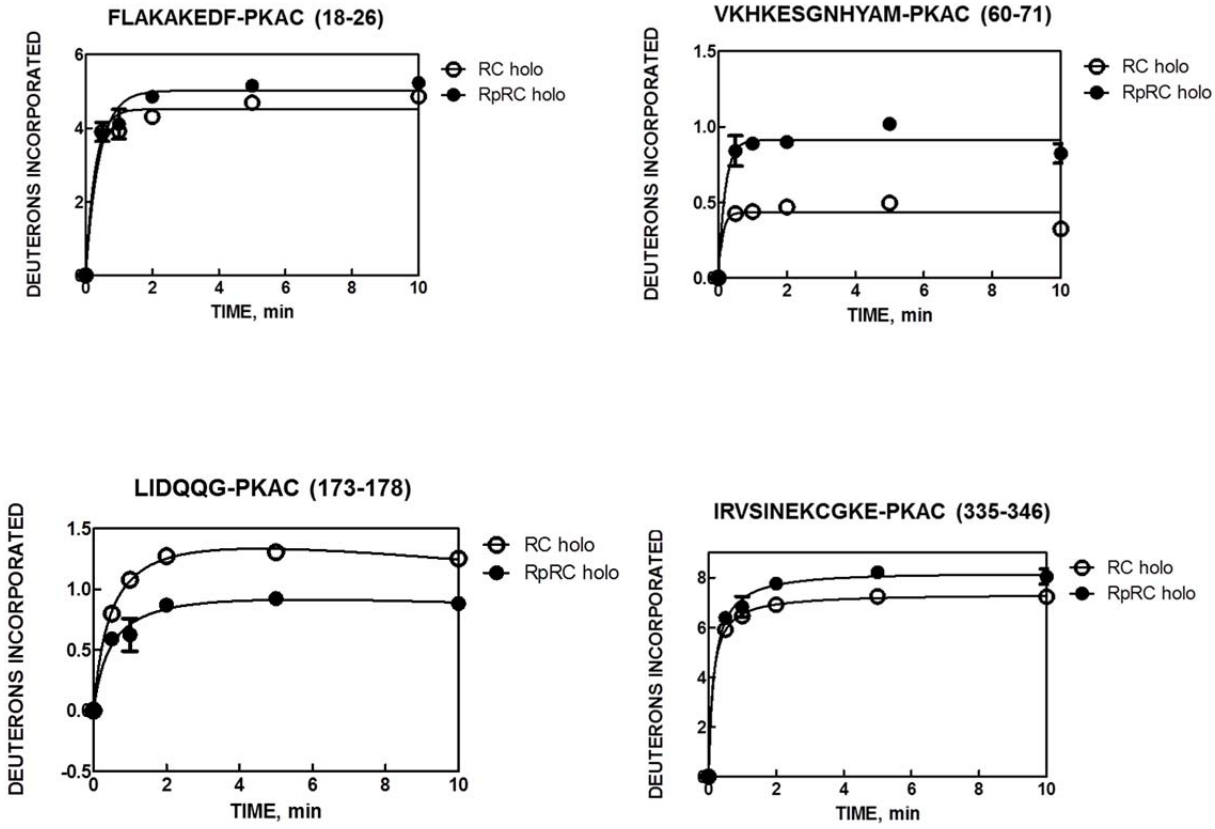

Figure 1.8: Allosteric effects induced on PKA C by Rp-cAMPS binding to PKA holoenzyme: Kinetic plots of deuterium exchange for peptides on PKA C that undergo allosteric changes upon Rp-cAMPS binding to PKA holoenzyme. Peptide sequences are indicated and residue numbers are in brackets. Open circle (○) denotes PKA C in the PKA holoenzyme state, close circle (●) indicates PKA C in the ternary complex state of $RI\alpha_A$:Rp-cAMPS:PKAC. Deuterium labeling reaction was carried out for 0.5, 1, 2, 5 and 10 min and the data was plotted against time. Data was fit to a one-phase association nonlinear exponential curve fit (Graphpad Prizm 5.0, San Diego, CA)

The regions showing changes were mapped onto the structure of PKA holoenzyme as shown in Figure 1.9. Even though changes were mainly seen at the N-terminal and C terminal ends of the protein, from the structure it is evident that these regions form a contiguous surface. Interestingly, these regions which show high dynamics are distal to the $RI\alpha_A$: PKA-C interaction interface. This shows that PKA C, along with $RI\alpha_A$, is also in a highly dynamics state in the ternary complex state.

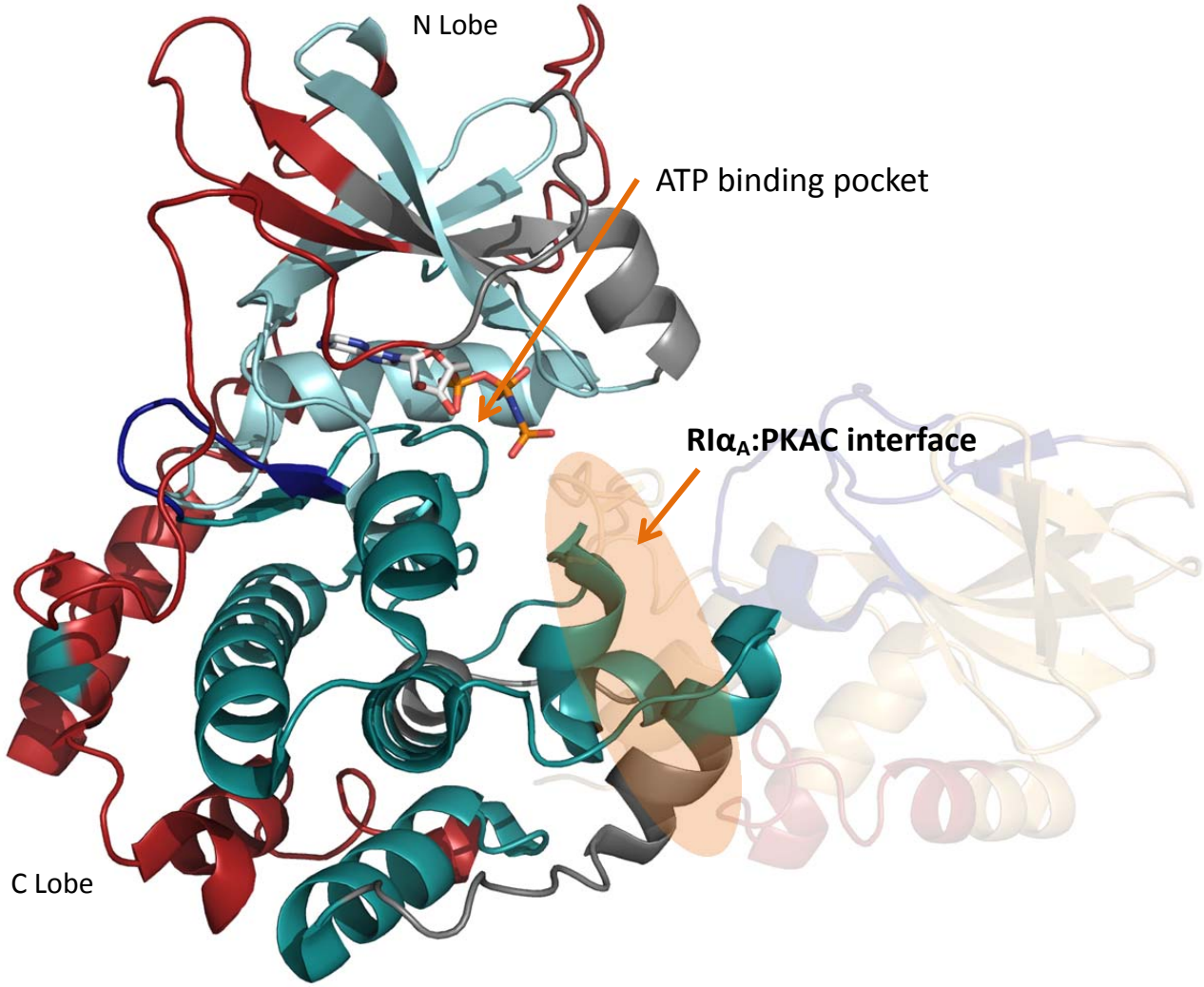

Figure 1.9: Rp-cAMPS induced changes on PKA C: Structure of the PKA holoenzyme (PDB ID:3FHI) with PKA-C N-lobe in cyan and the C-lobe in teal. Regions showing decreases in deuterium exchange upon Rp-cAMPS binding are in blue, and regions showing increased dynamics on ligand binding are in red. The $RI\alpha_A$ molecule is transparent for ease of viewing.

1.3.6 Rp-cAMPS: PKA holoenzyme ternary complex is a 'frustrated' molecule

From previous results it was seen that both $RI\alpha_A$ and PKA C exhibited increased dynamics upon Rp-cAMPS binding. Since ligand binding induces the increased dynamics in the entire protein, we can trace the allosteric path that leads to increased dynamics across the entire PKA holoenzyme molecule, to begin at the PBC of RIαA. The *apo* $RI\alpha_A$ protein is a highly dynamic protein which exists in an ensemble of conformations. $RI\alpha_A$ binds to its target molecules (cAMP/PKAC) by the process of conformation selection, thus, presence of cAMP molecule drives the conformation of $RI\alpha_A$ to the 'B' form (ligand bound), while the PKA C molecule drives the conformation of $RI\alpha_A$ to the 'H' form (Holoenzyme). It was previously shown that Rp-cAMPS is a unique cAMP analog as it drives the conformation of $RI\alpha_A$ to the 'H' form rather than the 'B' form, but it has to be remembered that Rp-cAMPS is almost identical to cAMP expect for a single sulfur substitution (Badireddy, Yunfeng et al. 2011). While it is incapable of activating the Arg^{209}-Asp^{170} relay, thereby causing the dissociation of the PKA holoenzyme, it is still capable of activating other allosteric relays through other interactions it forms at the PBC. In the PKA holoenzyme state, $RI\alpha_A$ already exists in the 'H' conformation as it is bound to PKA C, Rp-cAMPS binding, though largely drives the $RI\alpha_A$ conformation towards the 'H' form, also triggers allosteric relays that destabilize the PKA holoenzyme. These allosteric relays are weaker than the Arg^{209}-Asp^{170} relay that is essential to disrupt the high affinity PKA holoenzyme complex. These weaker allosteric relays destabilize the interaction interface at Site 2 of PKA C, and initiate a cascade of destabilization that traverses across the interaction interface and affects regions distal to the interaction interface. This increased dynamics and, in turn increased entropy, at one end of the protein causes a counter effect of stabilizing the Site 1 of the interaction interface. Rp-cAMPS also drives the conformation of $RI\alpha_A$ towards the 'H' form, the addition of these two effects leads to the increased affinity seen in PKA holoenzyme upon Rp-cAMPS binding.

The adenosine and ribose moieties in Rp-cAMPS induce dissociation of the PKA holoenzyme while the sulfur group, not only prevents dissociation of the holoenzyme, but indirectly increases the affinity of the PKA holoenzyme. Thus the PKA holoenzyme in the Ternary complex state is a 'frustrated'

protein, which exists in a high dynamic state as it cannot attain a stable end point state. Localized frustration has been implicated as the basis of allosteric transitions. The degree of local frustration can define whether the region is a 'hinge' or a 'crack', wherein hinges result in large scale conformational changes and cracks lead to degeneracy in conformations of the protein (Ferreiro, Hegler et al. 2011). The regions of PKA that show higher dynamics upon binding Rp-cAMPS may be correlated to regions that are involved in cAMP dependent dissociation of the PKA holoenzyme. Further studies have to be carried out to accurately characterize the nature of ligand induced frustration in the PKA holoenzyme.

This also provides a model for multiple allosteric pathways that occur upon cAMP binding that leads to the disruption of PKA holoenzyme. These points are summarized in figure 1.10.

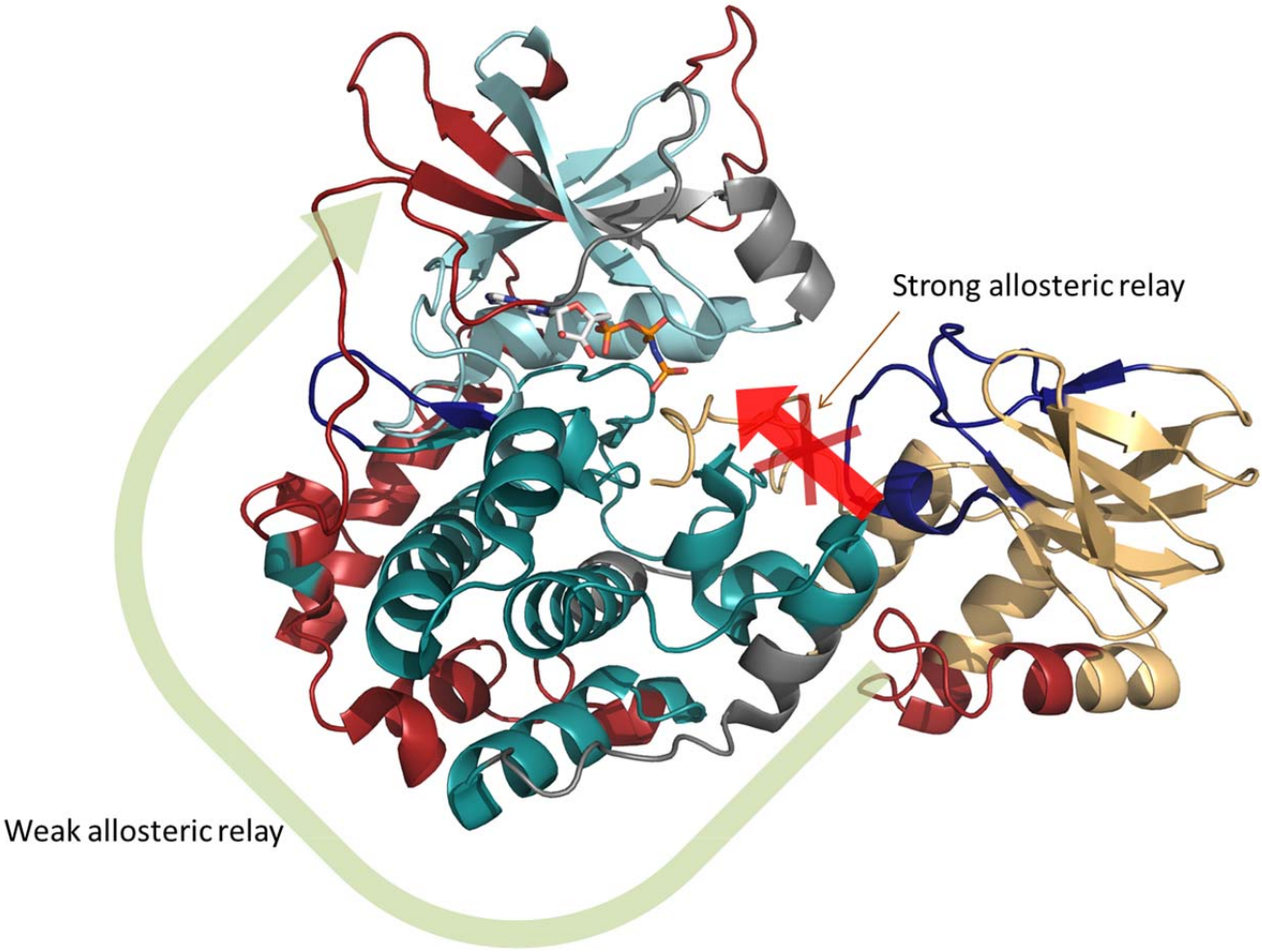

Figure 1.10: Allosteric relays that lead to the PKA dissociation: The weak allosteric relay that induces PKA destabilization is highlight by the green arrow. By tracing the regions showing higher dynamics upon Rp-cAMPS binding (in red), the weak allosteric relay can be determined. The strong allosteric relay (Arg^{209}-Asp^{170} relay) that is essential to fully dissociate PKA is in red. This relay is inactive in the presence of Rp-cAMPS. Structure and color coding for the PKA holoenzyme are the same as for Figure 1.8 and 1.10.

The next two sections, aim to highlight the utility and application of HDXMS in studying protein-ligand interactions with examples obtained from this study.

1.3.7 Using HDXMS to map ligand binding at amino acid resolution

HDXMS has been shown to be a powerful technique to probe and monitor the conformation dynamics of proteins in the influence of a variety of perturbations (Hoofnagle, Resing et al. 2003). In this section I highlight how HDXMS can map subtle effects of ligand binding at amino acid resolution. For this analysis, two peptides close to the PBC of $RI\alpha_A$ were chosen. One peptide spans residues 188-198 while the other peptide has three additional amino acids and spans residues 188-201. The three additional amino acids are highly significant as 2 of the amino acids are known to form highly stable hydrogen bonds with the 2'OH group of the Ribose sugar of cAMP (Su, Dostmann et al. 1995). The ligand free and ligand bound states of the peptides were compared and quantified. While the peptide spanning residues 188-198 shows no significant differences, the peptide containing elements from the PBC, shows a decrease of 2 Da upon ligand binding. The 2 deuterons decrease most likely corresponds to the 2 hydrogen bonds formed by the ligand molecule to the amino acids. This example highlights the sensitivity of HDXMS to accurately identify and localize hydrogen bonding networks. The results are summarized in Figure 1.11

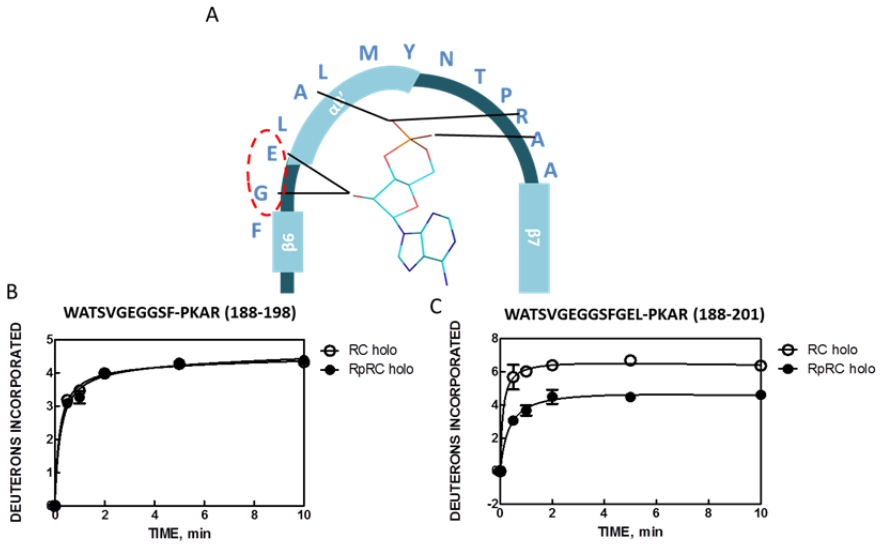

Figure 1.11: Sensitivity of HDXMS in deciphering protein ligand interactions: A) Residues in the PBC of $RI\alpha_A$ are depicted with the key hydrogens bonds formed with cAMP. Residues 199 and 200 which form key hydrogen bonds with 2'OH group on cAMP are circled in red.

B) Kinetic plot for peptide spanning residues just outside the PBC shows no significant difference upon Rp-cAMPS binding, while C) is the kinetic plot of peptide which contains residues 199 and 200 and shows a 2 deuteron protection in the Rp-cAMPS bound state. Open circle (○) denotes PKA C in the PKA holoenzyme state, close circle (●) indicates PKA C in the ternary complex state of $RI\alpha_A$:Rp-cAMPS:PKAC. Deuterium labeling reaction was carried out for 0.5, 1, 2, 5 and 10 min and the data was plotted against time. Data was fit to a one-phase association nonlinear exponential curve fit (Graphpad Prizm 5.0, San Diego, CA)

1.3.8 Differentiating Induced fit from Conformational Selection by HDXMS

$RI\alpha_A$ in its *apo* form is a highly dynamic protein and detects and binds cAMP by the process of conformational selection (Badireddy, Yunfeng et al. 2011). Proteins that undergo conformational selection would by definition be highly dynamic as they are constantly sampling an ensemble of structures (Boehr, Nussinov et al. 2009, Csermely, Palotai et al. 2010). This high degree of dynamics can be evidenced by the hydrogen bonding network, as rigid proteins would have a stable hydrogen bonding network, while more dynamic proteins would have less stable hydrogen bonding networks. To probe these hydrogen bonding networks, HDXMS is a technique of choice as it mainly monitors hydrogen bonding and to a lesser degree solvent accessibility of the protein backbone. (Englander and Kallenbach 1983).

The *apo* $RI\alpha_A$ protein shows an average of 30% to 60% relative deuterium uptake across all peptides, but upon ligand binding shows decreases in deuterium exchange across all regions (Badireddy, Yunfeng et al. 2011). In the *apo* state $RI\alpha_A$ takes up deuterium ions while sampling all conformations, but upon ligand binding, the protein is stabilized. This suggests that the ligand selects, stabilizes and locks $RI\alpha_A$ into one stable conformation. In the case of ligand binding to PKA holoenzyme, both decreases and increases in deuterium exchange are observed. This indicates that in the PKA holoenzyme state, both proteins have reached a stable conformation, and ligand binding induces changes in protein conformation and in some regions increases in dynamics. This implies an 'induced fit' model for ligand binding. The underlying assumption is that proteins that are involved in conformational selection regime are more dynamic as they sample multiple conformations.

It has to be noted that conformational selection and induced fit are just two different pathways of the same thermodynamic cycle. The same protein system may favor conformational selection for one perturbant and induced fit for another perturbant. It is also conceivable that a protein may respond to a

perturbant through the conformational selection regime followed by the induced fit regime or vice versa.

1.4 Conclusions

The activation phase of cAMP pathway is a well-studied pathway but most of the earlier studies have targeted the end state complexes alone. In this study we capture the transient ternary complex of the cAMP activation pathway using the inverse agonist Rp-cAMPS and characterize the conformational dynamics of the ternary complex by HDXMS. It was found that Rp-cAMPS stabilizes $RI\alpha_A$ in the 'H' conformation but simultaneously initiates a weak allosteric relay that serves to dissociate the complex. This weak allosteric relay causes an increase in entropy across the interaction interface in the PKA C molecule. The increased entropy and dynamics indirectly causes greater affinity at Site 1 of the interaction interface. It was seen that Rp-cAMPS is unable to activate the Arg^{209}-Asp^{170} allosteric relay that ultimately leads to the disruption of the complex. This study provides insights into the dynamics involved in ligand mediated complex dissociation. A key conclusion from this study is an example of allosteric effects transmitting across protein-protein interaction interfaces.

HDXMS is a powerful method to monitor conformational changes and allosteric effects. It has proven to be a highly sensitive method to probe ligand binding and elucidate protein-ligand hydrogen bonds with high resolution sequence specific information.

While the activation phase of the cAMP signaling pathway is elucidated in this study, the next two chapters aim to understand the processes involved in the termination phase of the cAMP signaling pathway. The role for HDXMS in monitoring protein-ligand interactions is also explored in great detail in subsequent chapters.

Chapter 2

Conformational Dynamics in Molecular Signaling II: Monitoring Phosphodiesterase-mediated cAMP dissociation from Protein Kinase A in the termination phase of cAMP signaling pathway

2 Conformational Dynamics in Molecular Signaling II: Monitoring Phosphodiesterase-mediated cAMP dissociation from Protein Kinase A in the termination phase of cAMP signaling pathway

2.1 Introduction

The previous chapter detailed allostery and conformational dynamics in the activation phase of the cAMP signaling pathway. In this chapter we attempt to elucidate protein dynamics correlated with enzyme kinetics involved in cAMP termination pathway. While the structural biology (Zheng, Trafny et al. 1993, Su, Dostmann et al. 1995, Wu, Brown et al. 2004, Kim, Xuong et al. 2005, Kim, Vigil et al. 2006), biochemistry and dynamics of cAMP binding to the PKA R-subunit leading to PKA activation have been studied extensively(Herberg, Taylor et al. 1996, Gibson and Taylor 1997, Johnson, Akamine et al. 2001, Esposito, Sjoberg et al. 2006, Abu-Abed, Das et al. 2007, Das, Esposito et al. 2007), very little is known on how 'active' PKA is reset to its 'inactive' state to complete the signaling cycle. The critical step in cAMP signal termination requires cAMP that is tightly bound to the R-subunit to be released (Ogreid and Doskeland 1983) and hydrolyzed by the large family of cAMP phosphodiesterases (PDEs) (Conti and Beavo 2007) (Figure 2.1). This is a critical step as cAMP binds the PKA R-subunit singularly with high affinity (K_D ~ 2-10 nM) (Corbin, Sugden et al. 1978, Doskeland 1978, Moorthy, Gao et al. 2011) and cAMP once bound to the R-subunit does not readily dissociate ($t_{1/2}$ > 5 days) (Corbin, Sugden et al. 1978, Doskeland 1978, Moorthy, Gao et al. 2011).

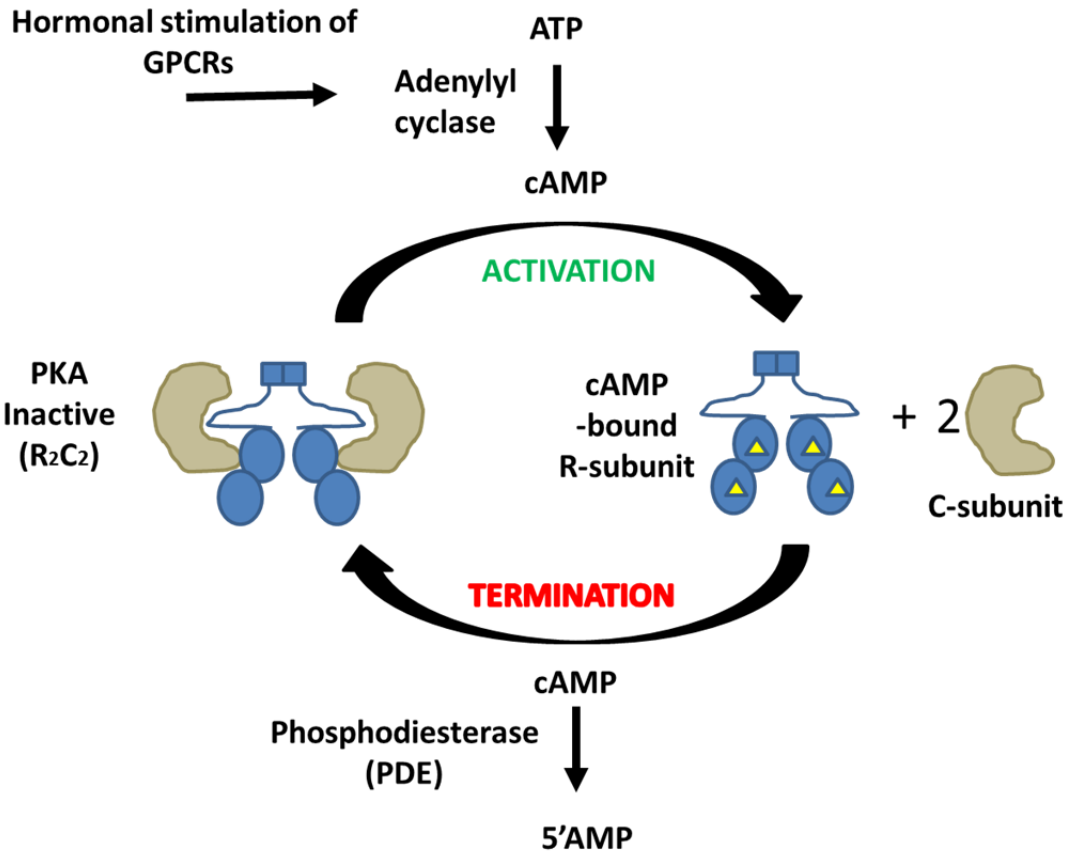

Figure 2.1: Overview of Activation and Termination phases in cAMP signaling. Second messenger cAMP signaling by hormonal stimulation of G-Protein-Coupled Receptors (GPCRs) which activate adenylyl cyclases which in turn catalyze the synthesis of cAMP from ATP. The principal target of cAMP in eukaryotes is Protein Kinase A (PKA) which exists in the absence of cAMP as an inactive complex of Regulatory (R) (blue) and Catalytic (C) subunits (tan). Binding of cAMP to PKA R-subunit results in dissociation of the R-subunit dimer and two C-subunits (activation phase). Phosphodiesterases mediate dissociation and hydrolysis of cAMP bound to the R-subunit to 5'AMP and reassociation with the C-subunit to complete the cAMP signaling cycle (termination phase).

In a recent study, it was reported that PDEs catalyze dissociation of cAMP from the R-subunit and this constitutes the signal termination phase of cAMP signaling (Moorthy, Gao et al. 2011). This occurs through a two-step process involving PDE-induced dissociation of bound cAMP followed by its hydrolysis. The cAMP-free R-subunit then remains bound to the PDE (Figure 2.2). The final step in the process is reassociation of the C-subunit with the cAMP-free R-subunit and dissociation of the PDE to complete the cAMP signaling cycle. For this study, the catalytic domain of RegA, a PDE from *Dictyostelium discoideum* (Moorthy, Gao et al. 2011) was used as a model PDE as it shows high homology to the entire PDE superfamily. Furthermore, it has been known to interact with both *Dictyostelium discoideum* as well as the mammalian PKA R-subunit isoform RIα (Shaulsky, Fuller et al. 1998).

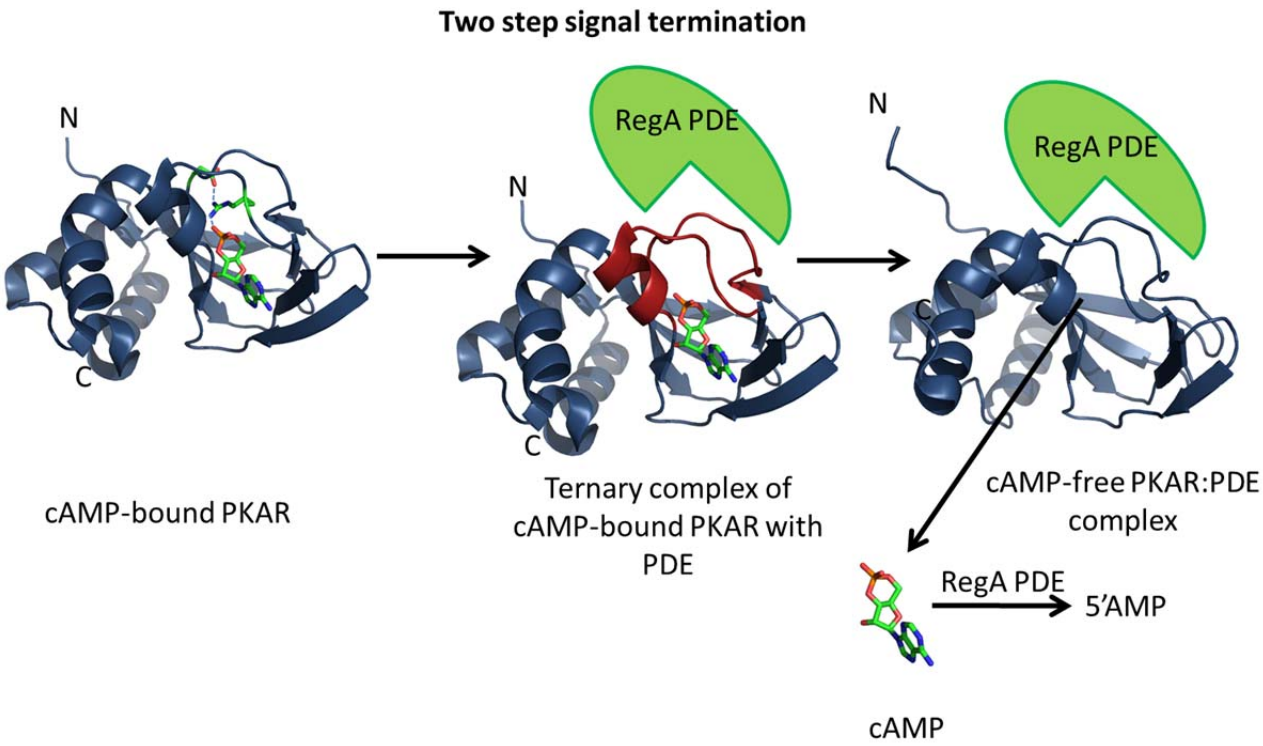

Figure 2.2: Two-state model for PDE-induced dissociation of cAMP from PKA R-subunit: Mechanism of PDE-induced dissociation of bound cAMP from $RI\alpha_A$. Structure of cAMP-bound PKA $RI\alpha_A$ (PDB ID: 3PNA) in blue showing cAMP interacting with two critical anchoring residues, Arg^{209} and Asp^{170}. Interaction of the catalytic domain of RegA PDE (green) with $RI\alpha_A$ by HDXMS (red), leads to formation of a transient ternary complex of RegAc, $RI\alpha_A$ and cAMP. Binding of RegAc facilitates dissociation of cAMP. The cAMP is released from the cAMP binding pocket and is subsequently hydrolyzed by RegAc to 5'AMP.

The RIα isoform is widely prevalent in mammalian cells and exists as a dimer in solution and each monomer consists of two tandem cAMP binding domains (CNB domains). As in the previous chapter, in order to monitor the kinetics of cAMP dissociation, the double deletion mutant, RIα (91-244) (henceforth referred to as $RI\alpha_A$) was used. This deletion mutant still retains full functionality with respect to its ability to inhibit the PKA C-subunit in a cAMP-dependent manner (Anand, Taylor et al. 2007). This deletion mutant was also shown to interact with the catalytic domain of RegA (RegAc) via a distinct interface contributed primarily by the β-sheet containing subdomain (Moorthy, Gao et al. 2011). This together with deletion mutagenesis and fluorescence polarization assays confirmed that RegAc interacted with cAMP-bound RIα, facilitated dissociation of the bound cAMP (k_{off} = 0.5 min^{-1}) followed by hydrolysis, in a two-step reaction (Figure 2.2). Given that we now know structures and dynamics of the *apo* and cAMP-bound R-subunit (Badireddy, Yunfeng et al. 2011) as well as an HDXMS-based interaction map of RegAc-bound to *apo* R-subunit (Moorthy, Gao et al. 2011), we were interested in mapping the ternary complex of RegAc-bound to cAMP-bound R-subunit by HDXMS. We reasoned that this ternary complex would provide important insights into how PDEs mediate dissociation of cAMP bound to PKA R-subunit.

We therefore set out to characterize this ternary complex intermediate formed by the interactions of cAMP-bound $RI\alpha_A$ with RegAc. Since cAMP is readily hydrolyzed by the PDE, it was critical to use a PDE nonhydrolyzable cAMP analog to characterize this intermediate complex. cAMP phosphorothioates have been invaluable for uncovering the mechanism of cAMP action(Schwede, Maronde et al. 2000). Substitution of the equatorial oxygen of cAMP with sulfur (R-enantiomer) generates an antagonist or inverse agonist (Rp-cAMPS) while substitution of the axial oxygen (S-enantiomer), the cAMP agonist generates an agonist (Sp-cAMPS) (Dostmann and Taylor 1991). Comparing the structure and dynamics of agonist and antagonist-bound states of PKA revealed that 'Conformational Selection' best explained the basis for cAMP allostery wherein unliganded $RI\alpha_A$ referred to as the *apo* form in the rest of the text, existed as an ensemble of conformations. Sp-cAMPS 'selected' the cAMP-bound (B) conformation whereas Rp-cAMPS 'selected' the inactive (H) conformation (Badireddy, Yunfeng et al. 2011).

In order to monitor dynamics of the PDE-PKARIα-cAMP ternary complex intermediate, we used amide hydrogen/deuterium exchange mass spectrometry (HDXMS) (Hoofnagle, Resing et al. 2003). This powerful method has been extensively used to map protein-ligand and protein-protein interactions but we wanted to examine its suitability for monitoring dynamics of transient ternary ligand-protein-protein complexes. In this study, we have used HDXMS for monitoring the RegAc-mediated dissociation of the cAMP reaction and map interactions in the ternary complex of RegAc, $RI\alpha_A$ and Sp-cAMPS. Our results indicate that RegA interacts with cAMP-bound R-subunits to generate a ternary complex. This complex is highly dynamic leading to active cAMP dissociation while maintaining the RegA-RIα complex. Our results thus support the two step model for RegA-mediated cAMP dissociation and enable monitoring ternary complex formation at early time points and cAMP dissociation. This study highlights a novel application of HDXMS in capturing the dynamics of transient protein-protein-ligand complexes.

2.2 Materials and Methods

2.2.1 Reagents

Unless otherwise mentioned all reagents were from Sigma Aldrich (St. Louis, MO). CIAP (calf intestinal alkaline phosphatase) was from Fermentas (Burlington, Canada). BL21 (DE3) *E.coli* strains were from Novagen (Madison, WI). Glutathione sepharose 4B and NHS-activated sepharose 4 Fast Flow were obtained from GE (Chicago, IL). 8-AEA-cAMP and 3',5'– cyclic adenosine phosphorothioate, Sp-isomer or Sp-cAMPS, were from Biolog Life Science Institute (Bremen, Germany), cyclic nucleotide phosphodiesterase assay kit was from BIOMOL (Plymouth Meeting, PA), TFA protein sequence analysis grade was from Fluka BioChemika (Buchs, Switzerland), Poroszyme immobilized pepsin cartridges were from Applied Biosystems (Foster city, CA).

2.2.2 Purification of $RI\alpha_A$ and RegAc (RegA (385-780))

$RI\alpha_A$ was purified using cAMP affinity chromatography resin synthesized by coupling 8-AEA-cAMP to NHS-activated sepharose 4 Fast Flow ® beads according to manufacturer specifications (GE Life

Sciences Sing*apo*re) and purified first as a cGMP-eluted protein. *Apo* $RI\alpha_A$ was then obtained by removing weakly bound cGMP by dialysis and size-exclusion chromatography as previously described (Moorthy, Gao et al. 2011). RegAc or RegA (385-780) was expressed as a GST fusion protein in *E. coli* BL21*(DE3). The protein was purified using glutathione sepharose 4B (GE Life Sciences) according to manufacturer specifications followed by size exclusion-gel filtration chromatography as described (Moorthy, Gao et al. 2011). The $RI\alpha_A$:RegAc complex was purified by immobilizing purified GST-tagged RegAc on glutathione beads and incubating with equimolar ratios of $RI\alpha_A$ at concentrations greater than the estimated Kd ~ 1.5 μM, whereby *apo* $RI\alpha_A$ would be fully saturated with RegAc as described previously (Moorthy, Gao et al. 2011). This was concentrated to ~7mg/ml total protein using vivaspin concentrators (Sartorius Stedim Biotech GmbH, Goettingen, Germany). The complex was then incubated with 3 mM (final concentration) Sp-cAMPS.

2.2.3 Amide Hydrogen/Deuterium Exchange Mass Spectrometry (HDXMS)

A 2 μl aliquot of protein samples $RI\alpha_A$ bound to Sp-cAMPS and $RI\alpha_A$: RegAc in the presence of excess Sp-cAMPS (3 mM or 30 mM final concentration) in 20 mM Tris HCl, 50 mM NaCl, 10 mM $MgCl_2$, 5 mM BME, pH 7.5 was mixed with 18 μl of D_2O (99.90%) resulting in a final concentration of 90.0% in D_2O buffer (20 mM Tris HCl, 50 mM NaCl, 5 mM BME, pH_{read} 7.5) to initiate the deuterium exchange reaction. Exchange was carried out at 20ºC for various times (1, 2, 5 and 10 min). The exchange reaction was quenched by adding 40 μl of pre-chilled 0.1% TFA to obtain a final pH_{read} of 2.5. 50 μl (100 pmol protein) of the reaction sample was then injected on to a chilled nano-UPLC sample manager (beta test version, Waters, Milford, MA) as previously described(Wales, Fadgen et al. 2008). Proteolysis of protein samples was achieved by passing the sample through a 2.1 x 30 mm immobilized pepsin column (Porozyme, ABI, Foster City, CA) using 100 μL/min of 0.05% formic acid in water. The digest peptides were trapped on a 2.1 x 5 mm C18 trap (ACQUITY BEH C18 VanGuard Pre-column, 1.7 μm, Waters, Milford, MA). Peptides were eluted using an 8-85% gradient of acetonitrile in 0.1% formic acid at 40 μL/min, supplied by a nanoACQUITY Binary Solvent Manager (Waters, Milford, MA), on to a reverse phase column (ACQUITY UPLC BEH C18 Column, 1.0 x 100 mm, 1.7 μm, Waters, Milford, MA) for resolution. Peptides were detected, mass measured

and sequenced on a SYNAPT HDMS mass spectrometer (Waters, Manchester, UK) acquiring in MS^E mode (Bateman, Carruthers et al. 2002, Silva, Denny et al. 2005).

Peptides were identified by MS^E data of undeuterated samples using Protein Lynx Global Server (PLGS 2.4 (beta test version)) (Waters, Milford, MA) (Li, Vissers et al. 2009). These identifications were mapped on to subsequent deuteration experiments using DynamX HDX software (Version 1.3.0.25(64-bit) (Waters, Milford, MA).

Continuous instrument calibration was carried out with Glu-Fibrinogen peptide (GFP) at 100 fmol/μL. We also visually examined the data to ensure only well-resolved peptide isotopic envelopes were subjected to quantitative analysis. The centroid masses for the isotopic envelopes of all the peptides which reflected the average mass of the peptide were generated by the DynamX software. Deuterium exchange of each pepsin digest fragment was calculated by subtracting the centroid of the undeuterated sample from that of the deuterium exchanged sample. The N-terminal amide of all the peptide fragments exchanges too rapidly to measure and was not included in calculation of average deuterons exchanged (Bai, Milne et al. 1993, Hoofnagle, Resing et al. 2003). All deuterium exchange values reported were corrected for a 32.8% back exchange by multiplying the raw centroid values by a multiplication factor of 1.49 (Anand, Krishnamurthy et al. 2010, Moorthy, Gao et al. 2011).

2.2.4 Phosphodiesterase Assay

GST RegAc was assayed for cAMP hydrolytic activity using a colorimetric cyclic nucleotide phosphodiesterase assay (BIOMOL, Plymouth Meeting, PA) as described previously(Moorthy, Gao et al. 2011).

2.3 Results and Discussion

We have previously used HDXMS in cAMP signaling to map interactions of cAMP and its analogs with $RI\alpha_A$ (Badireddy, Yunfeng et al. 2011) and interactions of *apo* $RI\alpha_A$ with RegAc (Moorthy, Gao et al. 2011). A new method of displaying HDXMS results has been via mirror-plots which plot the relative deuterium exchange for each pepsin digest fragment of interest (Houde, Berkowitz et al. 2011). Even though this plot does not factor in the nonuniform cleavage of the target protein by

pepsin or including the possibility of generating nested peptides by giving an impression of regularly spaced pepsin digest fragments of uniform sizes, it nevertheless allows rapid identification of regions showing altered deuterium exchange within the entire protein. A difference plot highlights the differences in exchange where positive and negative differences indicates greater or less exchange in the sample on top compared to the sample on the bottom of the plot respectively. We set out to map the ternary complex of RegAc and RIα in the presence of molar excess of Sp-cAMPS by HDXMS and used a combination of mirror and difference plots to obtain a protein-wide overview of the differences between the two states and probe the dynamics of the ternary complex. Sp-cAMPS is resistant to PDE hydrolysis according to reagent specifications (Biolog, Bremen, Germany) and this allowed us to use Sp-cAMPS to characterize the ternary RegAc-RIα$_A$-Sp-cAMPS complex.

2.3.1 Dynamics of RegAc-RIα$_A$ interactions in the presence of excess Sp-cAMPS

GST-tagged RegAc was used to pull-down *apo* RIα$_A$ as described in Materials and Methods (Moorthy, Gao et al. 2011) and incubated with an excess of Sp-cAMPS as described in Materials and Methods. While we predicted that RIα would mediate mutually exclusive interactions with Sp-cAMPS and RegAc, we estimated that an excess of Sp-cAMPS (3 mM), significantly greater than the 50 uM protein concentration, would maintain the ternary complex. This was then diluted 10-X fold with buffer prepared in D_2O to initiate the deuterium exchange reaction. Deuterium exchange was carried out for 1, 2, 5 and 10 min and the results are shown in Figure 2.3 in the form of a mirror plot comparing DXMS of Sp-cAMPS –bound RIα$_A$ and the putative ternary complex of RegAc-RIα$_A$ and Sp-cAMPS.

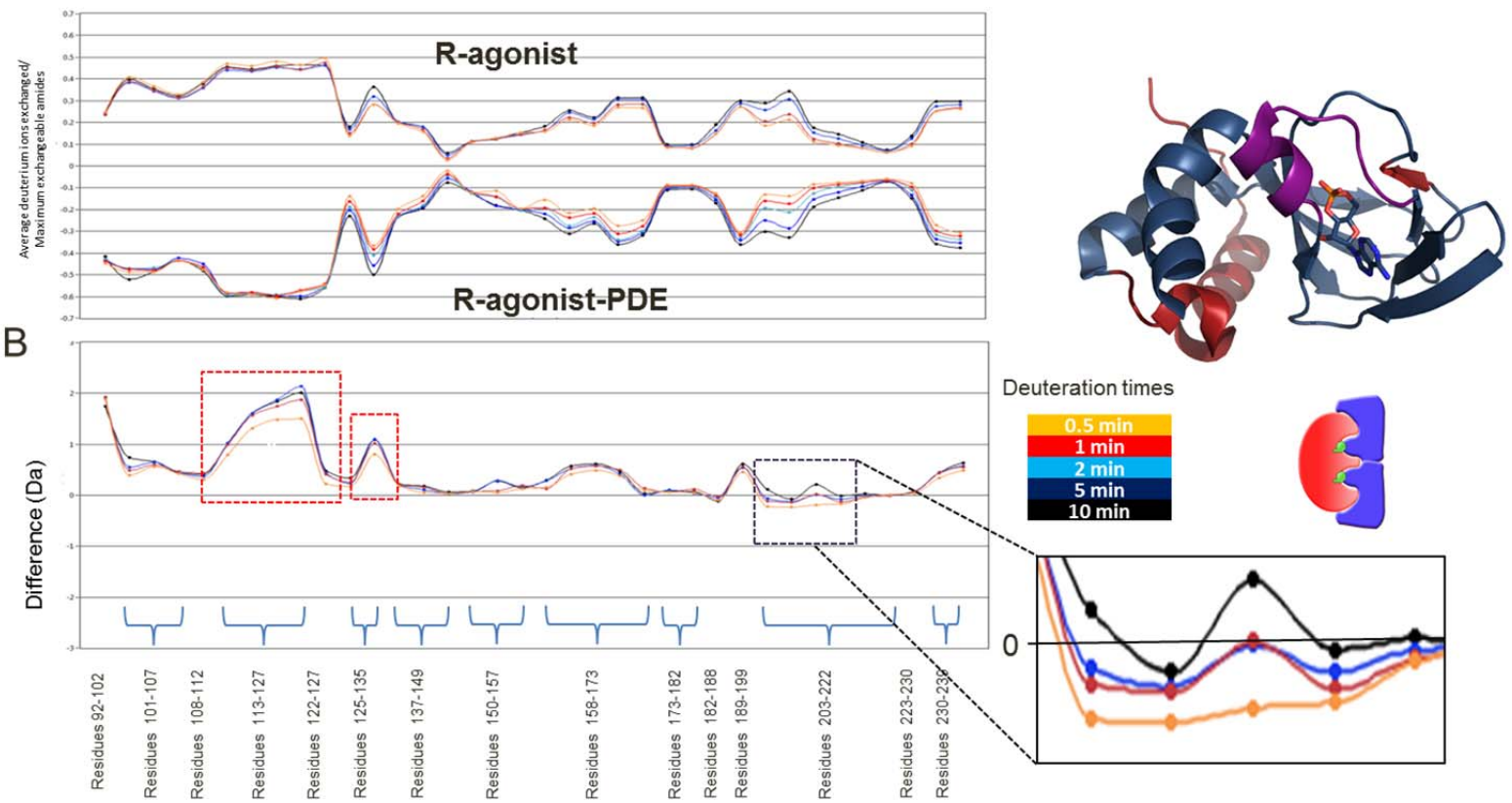

Figure 2.3: HDXMS comparison of Sp-cAMPS RIα$_A$ and RegAc: RIα$_A$: Sp-cAMPS complex : (A) A 'mirror plot', comparing the relative deuterium exchange for each peptide from the N to C terminus of RIα$_A$ for the Sp-cAMPS bound state of RIα$_A$ and in a RegAc: RIα$_A$:Sp-cAMPS complex. (B) A 'difference plot', plotting the difference in absolute deuterium uptake between the Sp-cAMPS bound state of RIα$_A$ and RIα$_A$:RegAc:Sp-cAMPS bound complex state. Two regions of the protein showed significant increases in deuterium exchange difference are boxed in dark red. The residues spanning the cAMP binding pocket (PBC) (Residues 203-222) are boxed in purple. These residues show decrease in deuterium exchange difference for shorter labeling times (<2 min Dex) but this effect is inverted after longer labeling times. Dashed box in red shows an enlarged view of this segment on the difference plot (C) Structure of cAMP-bound RIα$_A$ (PDB ID: 3PNA), with the N-terminal regions (residues 113-127) showing significant increased exchange in the presence of RegAc in dark red. The cAMP binding pocket residues (199-210) are in purple and show decreased deuterium exchange at 1 min and increased exchange at later time points.

The three important loci for conformational dynamics all showed changes in deuterium exchange although the magnitude differences in exchange between the two states were smaller than Sp-cAMPS-bound compared to *apo* RIα$_A$ (Badireddy, Yunfeng et al. 2011), (summarized in Figure 2.4A) and RegAc-bound *apo* RIα$_A$ compared to *apo* RIα$_A$ (Moorthy, Gao et al. 2011), (Figure 2.4B).

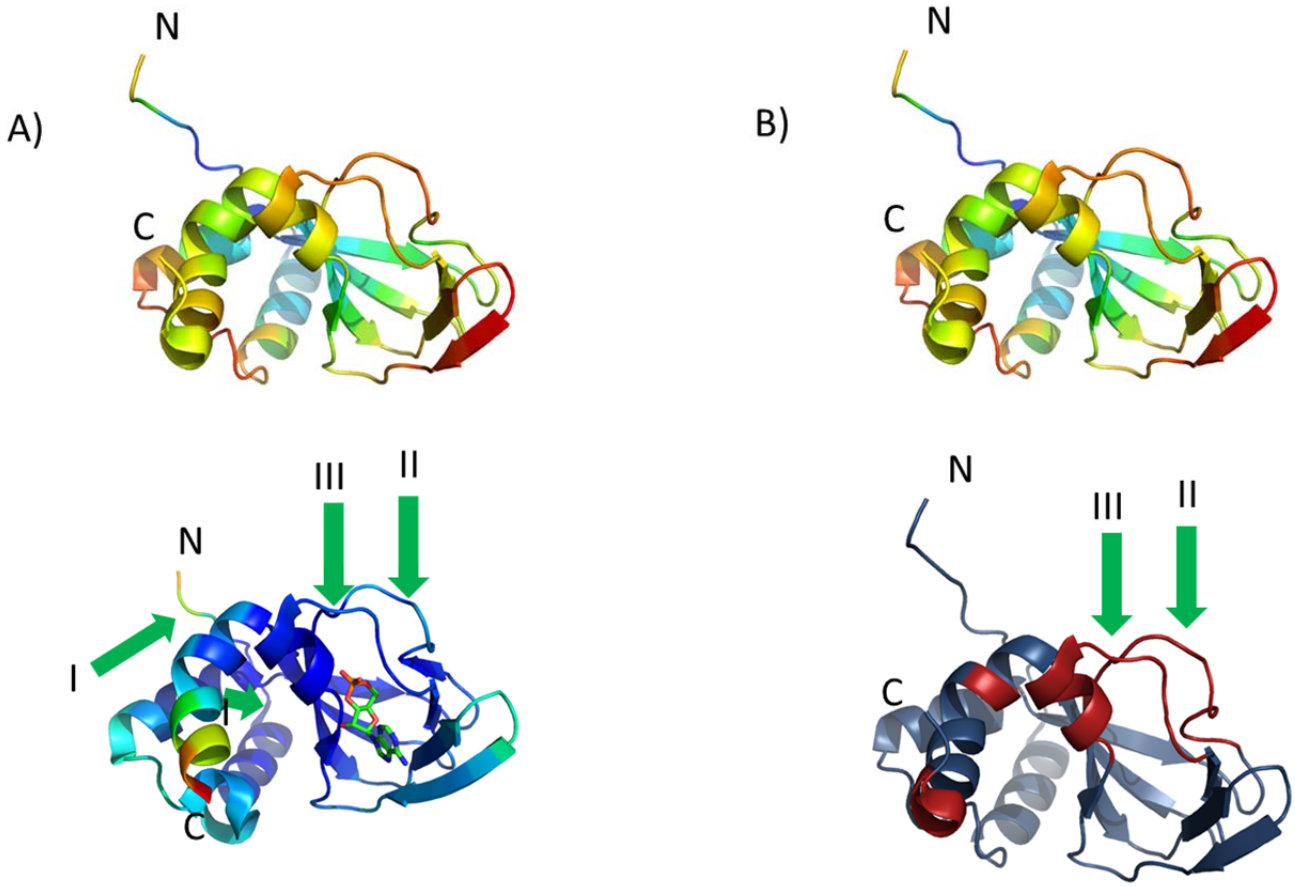

Figure 2.4: Loci showing significant changes upon cAMP/RegA binding on RIα$_A$: Comparative HDXMS analysis of ligand free and Sp-cAMPS bound states of RIα$_A$. Structure of ligand free RIα$_A$ (PDB ID: 3IIA) (top). Structure of RIα$_A$ bound to cAMP (PDB ID: 3PNA). Structures are color coded on the basis of crystallographic B-factor values, with blue and red representing the lowest and highest relative B–factor values. Green arrows highlight the three regions showing the biggest shifts in deuterium exchange upon Sp-cAMPS binding. **(B)** Comparative HDXMS analysis of ligand free and RegAc bound states of RIα$_A$ Structure of ligand free *apo* RIα$_A$ (PDB ID: 3IIA) and color coded on the basis of crystallographic B-factor values (top), structure of ligand free *apo* RIα$_A$ (PDB ID: 3IIA) with regions showing significant changes in deuterium exchange in red. Green arrows highlight the two regions showing the greatest changes upon binding of RegAc (II, III) which also correspond to the regions showing greatest shifts upon binding Sp-cAMPS.

Deuterium exchange (corrected for deuterium back exchange of 32.6%) after 10 min labeling for all 37 pepsin digest fragment peptides of RIα$_A$ are listed in Table 2.1.

Table 2.1. Summary of H/D exchange data for SpcAMPS-bound RIα_A and SpcAMPS-bound RIα_A:RegA

No.	Pepsin digest fragments of RIα_A (m/z)	Charge (z)	Residue Nos.	Maximum Exchangeable amides	Maximum Deuterons Exchanged after 10 min	
					SpcAMPS-bound RIα_A (Mean ± Error)	Sp-cAMPS-bound RIα_A RegA (Mean ± Error)
1	GCRRRGAISAE (588.30)	2	91-101	10	3.6 ± 0.0	6.3 ± 0.4
2	AEVYTEE (840.36)	1	100-106	6	3.6 ± 0.0	4.9 ± 0.1
3	EVYTEE (769.32)	1	101-106	5	2.7 ± 0.0	3.7 ± 0.1
4	VYTEE (640.28)	1	102-106	4	1.9 ± 0.0	2.7 ± 0.0
5	DAASY (526.21)	1	107-111	4	2.4 ± 0.1	3.0 ± 0.0
6	YVRKVIPKD (559.34)	2	111-118	7	4.8 ± 0.0	6.3 ± 0.0
7	YVRKVIPKDYKTM (547.95)	3	111-123	11	7.3 ± 0.0	9.7 ± 0.1
8	YVRKVIPKDYKTMAA (595.31)	3	111-125	13	8.9 ± 0.0	11.6 ± 0.0
9	YVRKVIPKDYKTMAAL (632.33)	3	111-126	14	9.8 ± 0.1	12.8 ± 0.1
10	YKTMAA (684.34)	1	120-125	5	3.4 ± 0.0	4.2 ± 0.1

11	AALAKAIE (394.23)	2	124-131	7	1.9 ± 0.0	2.5 ± 0.1
12	LAKAIEKNV (493.81)	2	126-134	8	4.3 ± 0.1	6.0 ± 0.0
13	FSHLDDNE (976.91)	2	136-143	7	2.1 ± 0.0	2.4 ± 0.0
14	FSHLDDNERSDIF (798.36)	2	136-148	12	3.3 ± 0.0	3.6 ± 0.0
15	RSDIF (880.41)	1	144-148	6	0.3 ± 0.0	0.4 ± 0.0
16	DAMFPVSF (913.41)	1	149-156	6	1.0 ± 0.0	1.2 ± 0.0
17	AMFPVSF (798.39)	1	150-156	5	0.9 ± 0.0	1.6 ± 0.1
18	FPVSF (596.30)	1	152-156	3	0.7 ± 0.0	1.0 ± 0.1
19	IAGETV (589.32)	1	157-162	5	1.5 ± 0.1	1.9 ± 0.1
20	IAGETVIQQGDEGDN (773.35)	2	157-171	14	5.4 ± 0.1	6.3 ± 0.1
21	IAGETVIQQGDEGDNF (846.88)	2	157-172	15	5.1 ± 0.1	6.0 ± 0.0
22	TVIQQGDEGDN (1175.54)	1	161-171	10	4.6 ± 0.0	5.4 ± 0.0
23	VIQQGDEGDNF (1221.58)	1	162-172	10	4.8 ± 0.0	4.8 ± 0.0
24	FYVIDQGEM (1101.50)	1	172-180	8	1.2 ± 0.0	1.3 ± 0.1
25	FYVIDQGEMD (1216.52)	1	172-181	9	1.3 ± 0.0	1.5 ± 0.0
26	DVYVNNE (852.37)	1	181-187	6	1.6 ± 0.0	1.6 ± 0.0
27	WATSVGEGGSF (1097.49)	1	188-198	10	4.5 ± 0.0	5.5 ± 0.1

28	ALIYGTPRAAT (567.31)	2	202-212	9	3.9 ± 0.0	4.0 ± 0.0
29	ALIYGTPRAATVKAKT (554.63)	3	202-217	14	4.8 ± 0.1	5.1 ± 0.1
30	ALIYGTPRAATVKAKTNVKL(705.75)	3	202-221	18	3.2 ± 0.0	3.4 ± 0.0
31	LIYGTPRAATVKAKTNVK (644.00)	3	204-220	16	3.6 ± 0.1	3.4 ± 0.0
32	YGTPRAAT (836.43)	1	205-212	6	3.0 ± 0.0	2.8 ± 0.0
33	VKAKTNVKL (501.33)	2	213-221	8	1.3 ± 0.0	1.3 ± 0.00
34	KTNVKL (351.72)	2	216-221	5	0.6 ± 0.0	0.6 ± 0.0
35	WGIDRDSY (1011.45)	1	222-228	7	1.5 ± 0.0	1.6 ± 0.0
36	RRILMGST (467.26)	2	230-237	7	3.1 ± 0.0	3.7 ± 0.0
37	RRILMGSTL (1046.61)	1	230-238	8	3.6 ± 0.0	4.5 ± 0.00

[a]Mean and errors were calculated with measurements from two independent experiments.

A detailed description of the HDXMS in each of the important loci is provided below:

cAMP-binding site (PBC) shows decreased exchange in the presence of RegAc at early timepoints and increased exchange at later time points of HDXMS:

When we examined deuterium exchange at the phosphate binding cassette (Figure 2.4), which is the most important locus for RegAc and cAMP binding containing the linear motif of invariant residues (residues 199-210) required for high affinity cAMP binding(Canaves and Taylor 2002), we observed a surprising result. After 30s or 1 min HDXMS, we observed decreased exchange in RIα: RegA:Sp-cAMPS compared to RIα:Sp-cAMPS but no differences at the 2 and 5 min time points. Interestingly, this pattern was reversed with the same peptide from RIα:RegA:Sp-cAMPS showing increased exchange after 10 min deuterium exchange (Figure 2.3). Under our experimental conditions, we had expected to capture the ternary complex and this would have translated into decreased exchange in RIα:RegA:Sp-cAMPS relative to RIα:Sp-cAMPS at all time points of exchange, reflecting formation of the ternary complex but instead we observed an inversion in magnitude of relative exchange from the 1 min to 10 min time point of deuterium exchange (Figure 2.5).

These results indicate that in addition to dynamics of the ternary complex, we were also monitoring PDE-dependent dissociation of cAMP from $RI\alpha_A$. It appeared that under conditions prior to deuterium exchange, the ternary complex was indeed maintained under excess Sp-cAMPS conditions (3 mM). However, upon initiation of the deuterium exchange reaction by 10-X dilution of the samples in buffered D_2O, RegA actively mediated dissociation of Sp-cAMPS from the R-subunit and blocked reassociation of excess Sp-cAMPS. This explains the inversion in the difference plot and are consistent with the rates of RegA-mediated active dissociation of cAMP bound to $RI\alpha_A$ ($k_{cAMPdissociation}$ = 0.5 min^{-1}) measured with PDE-resistant 8-Fluorescein-cAMP (Moorthy, Gao et al. 2011). cAMP dissociation from the R-subunit takes a full minute only after which increases in deuterium exchange were observed. This indicates that at all time points less than 1 min under our HDXMS reaction conditions, we were monitoring deuterium exchange in a ternary complex of PDE, RIα and Sp-cAMPS. After 1 min, HDXMS is probing the dynamics of mutually exclusive interactions of the PBC for Sp-cAMPS and RegAc.

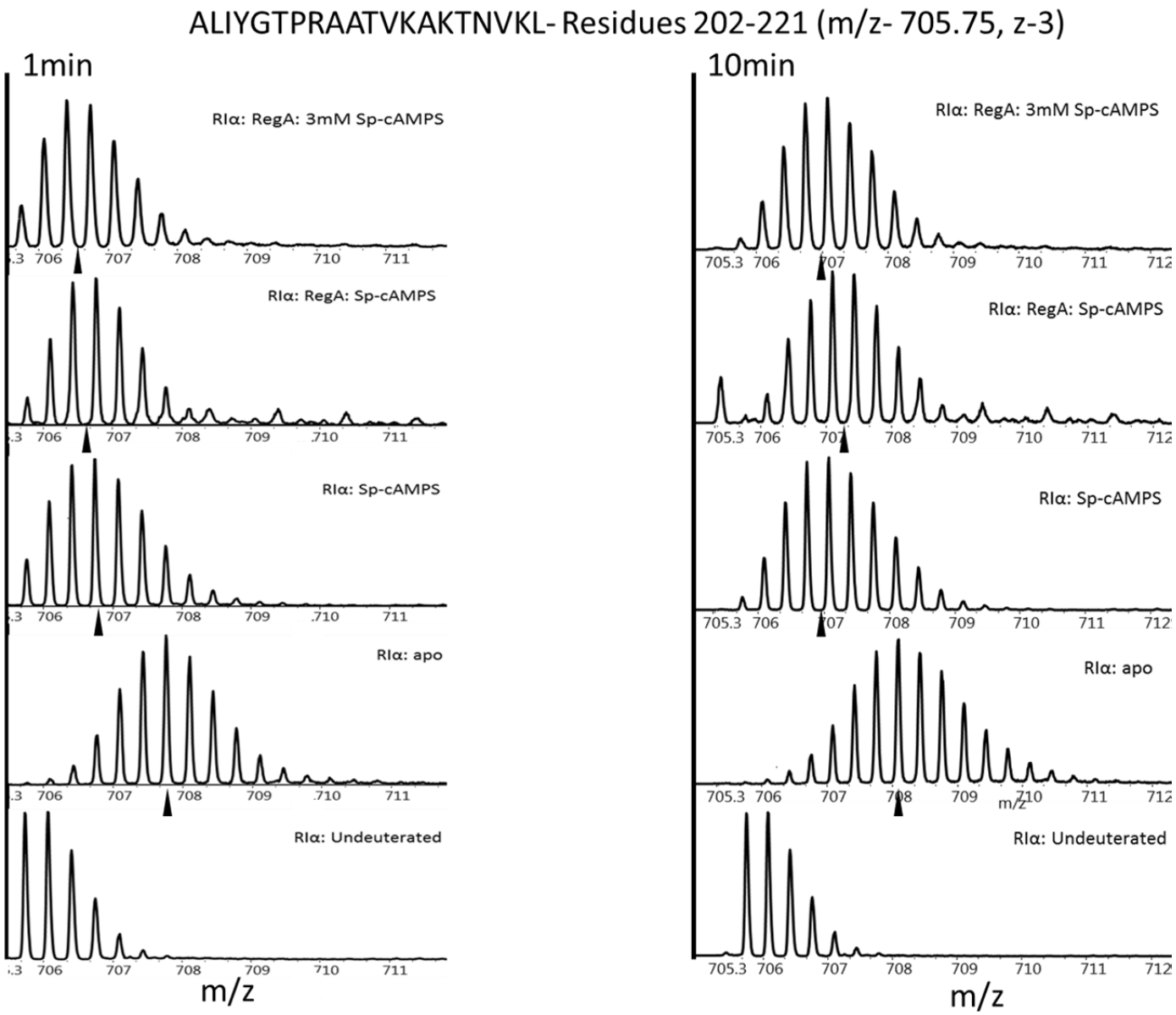

Figure 2.5: Maintaining ternary complex under high ligand concentrations: Left panel: ESI-Q-TOF mass spectra for a peptide spanning residues 202-221 (m/z= 705.75, z=3) for *apo* $RI\alpha_A$, Sp-cAMPS-bound $RI\alpha_A$, Sp-cAMPS-bound $RI\alpha_A$ in the presence of RegAc (300 µM Sp-cAMPS) and Sp-cAMPS-bound $RI\alpha_A$ in the presence of RegAc (3 mM Sp-cAMPS) after 1 min deuterium exchange as indicated. Right panel: isotopic envelope shifts after 10 min deuterium exchange. Centroids for mass spectra are indicated by ▲.

It should be noted that Sp-cAMPS behaves identically to cAMP in kinetic assays and HDXMS and we anticipate that Sp-cAMPS shows the same slow off-rate from RIα as cAMP. In our study this is reflected in a constant magnitude of decreased exchange in Sp-cAMPS-

bound $RI\alpha_A$ for all time points relative to *apo* $RI\alpha_A$. Furthermore, it is clear that under reduced Sp-cAMPS concentrations in our HDXMS experimental conditions (300 μM), RegAc (estimated to be 5 μM) is capable of blocking reassociation of Sp-cAMPS. To unequivocally demonstrate existence of the ternary complex at higher concentrations of Sp-cAMPS, we carried out HDX-MS of $RI\alpha_A$ in the presence of RegAc at a 10-X fold higher starting concentration (30 mM) which upon dilution in deuterated buffer resulted in a concentration of Sp-cAMPS of 3 mM. Under these conditions, the phosphate binding cassette did not show any inversion of deuterium exchange shifts at the 1 min and 10 min time points of deuterium exchange (Figure 2.5), confirming that higher concentrations of Sp-cAMPS maintain the ternary complex. This validated our original assumption for stabilization of the ternary complex at concentrations of Sp-cAMPS (3 mM) and interestingly revealed the time-dependent dissociation under deuterium exchange conditions (300 μM Sp-cAMPS).

Molecular basis for adaptation in cAMP signaling:

The inversion in deuterium exchange differences under a reduced molar excess (300 μM) at early and late time points is highly significant as it explains the basis for adaptation in cAMP-PKA signaling. It has been a mystery why PKA is suited to respond to a flux of cAMP rather than to fixed levels of cAMP (Leiser, Fleischer et al. 1986). Our surprising results from HDXMS, where we ended up monitoring the reaction of PDE-mediated cAMP dissociation, provide insights into adaptation. Once cAMP binding activates the PKA holoenzyme by dissociating the C-subunit, PDEs interact with cAMP-bound R-subunit and mediate the active dissociation and hydrolysis of bound cAMP. It is self-evident that cAMP levels cannot remain constant under these conditions of PDE-mediated active cAMP dissociation and hydrolysis. That RegAc is capable of blocking cAMP reassociation to PKA R-subunit at a specific range of concentrations (300 μM but not 3 mM) further indicates that PDEs block

reassociation of cAMP and function to reset cAMP signaling to prime it for subsequent activation by fluxes of cAMP. This constitutes the basis for adaptation in cAMP signaling.

Changes in RegAc and Sp-cAMPS interaction surface Region II (residues 161-172):

The β-strand proximal to the PBC also shows increased deuterium exchange in the dynamic ternary complex (Figure 2.6). Based on subtractive analysis of overlapping peptides (Table 2.1), the motif consisting of residues 161-163 (Thr-Val-Ile) showed increased exchange in the presence of both RegAc and Sp-cAMPS. This motif is disordered in the structure of *apo* $RI\alpha_A$ (PDB ID:3IIA) but ordered (β-sheet) in the structure of cAMP-bound $RI\alpha_A$ (PDB ID: 3PNA) (Badireddy, Yunfeng et al. 2011). Since this region shows increased exchange in $RI\alpha_A$ bound to Sp-cAMPS and in the presence of RegAc, it resembles *apo* RIα more than Sp-cAMPS-bound RIα. We therefore believe that this increased deuterium exchange in this region in the presence of RegAc reflects RegAc-mediated Sp-cAMPS dissociation.

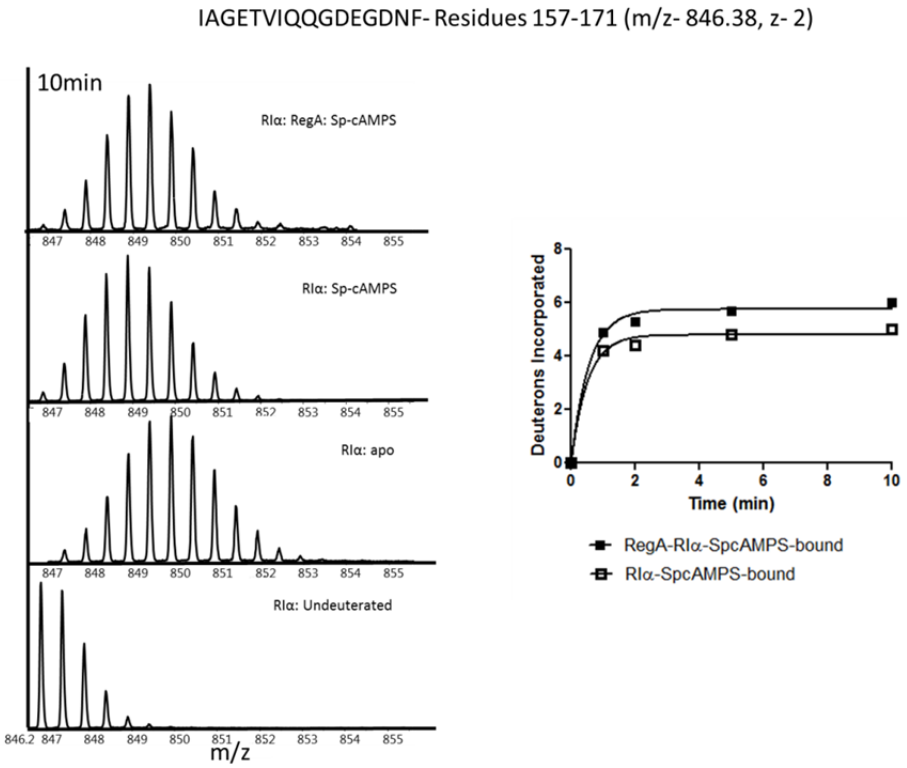

Figure 2.6: Monitoring RegAc mediated Sp-cAMPS dissociation: Left panel: ESI-Q-TOF mass spectra for a peptide spanning residues 157-171 (m/z= 846.38, z=2) of $RI\alpha_A$ for *apo*, Sp-cAMPS-bound and Sp-cAMPS in the presence of RegAc after 10 min Deuterium exchange as indicated. Right panel: Time course of deuterium exchange fit to a single exponential association. (Graphpad Prism 5.0, San Diego, CA)

Increased dynamics in the PKA pseudosubstrate site and N-terminal segments of $RI\alpha_A$:

The N-terminal region including the PKA pseudosubstrate region and residues 113-127 show correlated increases in deuterium exchange in the presence of RegAc and Sp-cAMPS with Region II. These regions are part of the dynamic PKA C-subunit interaction interface and are typically most dynamic in *apo* $RI\alpha_A$ (Figure 2.7 and 2.8). This is part of the allosteric site that couples cAMP binding to PKA regulation and shows a time-dependent increase in exchange and reflects the active RegAc-mediated dissociation of Sp-cAMPS. Together, all the results are consistent with a two-state model for RegA-mediated cAMP dissociation and hydrolysis from $RI\alpha_A$ and provide important insights into signal termination in cAMP signaling.

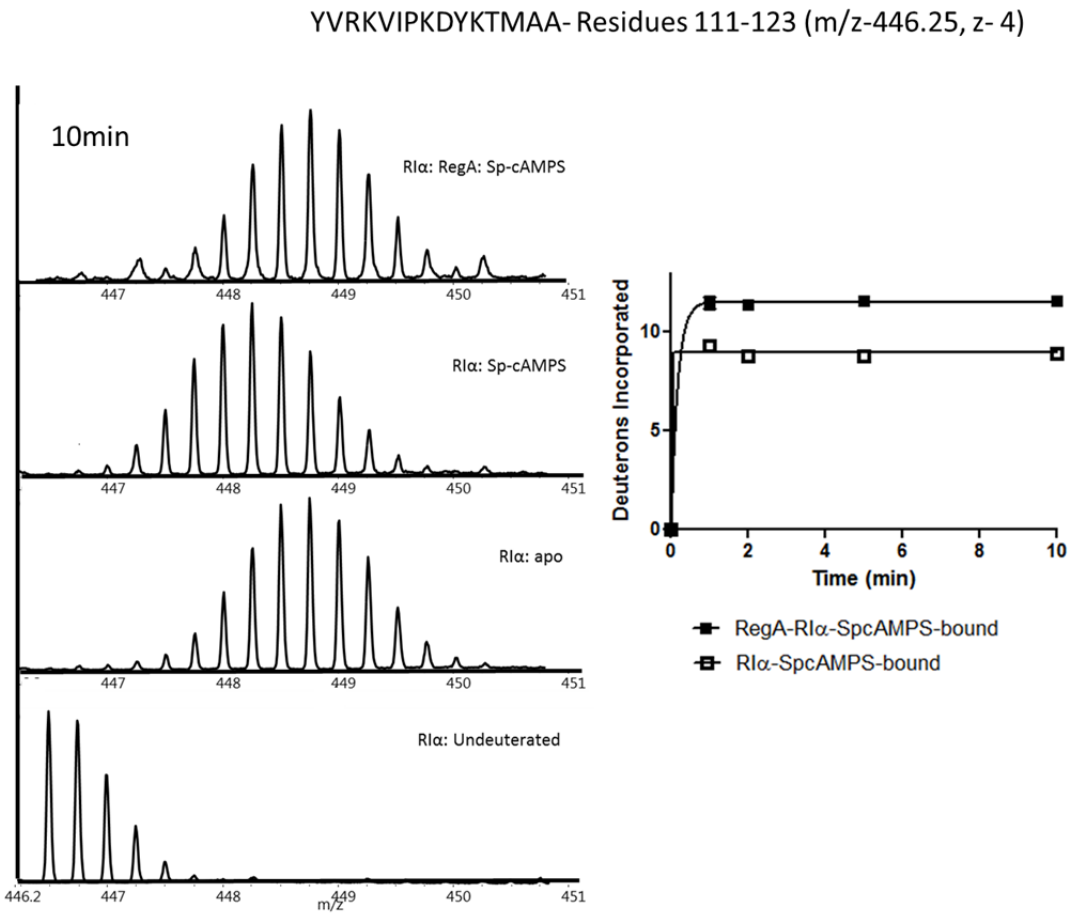

Figure 2.7: Effects of Sp-cAMPS dissociation on allosteric sites: Left panel: ESI-Q-TOF mass spectra for a peptide spanning residues 111-123 (m/z= 446.25, z=4) of $RI\alpha_A$ for *apo*, Sp-cAMPS-bound and Sp-cAMPS in the presence of RegAc after 10 min Deuterium exchange as indicated. Right panel: Time course of deuterium exchange fit to a single exponential association (Graphpad Prism 5.0, San Diego, CA).

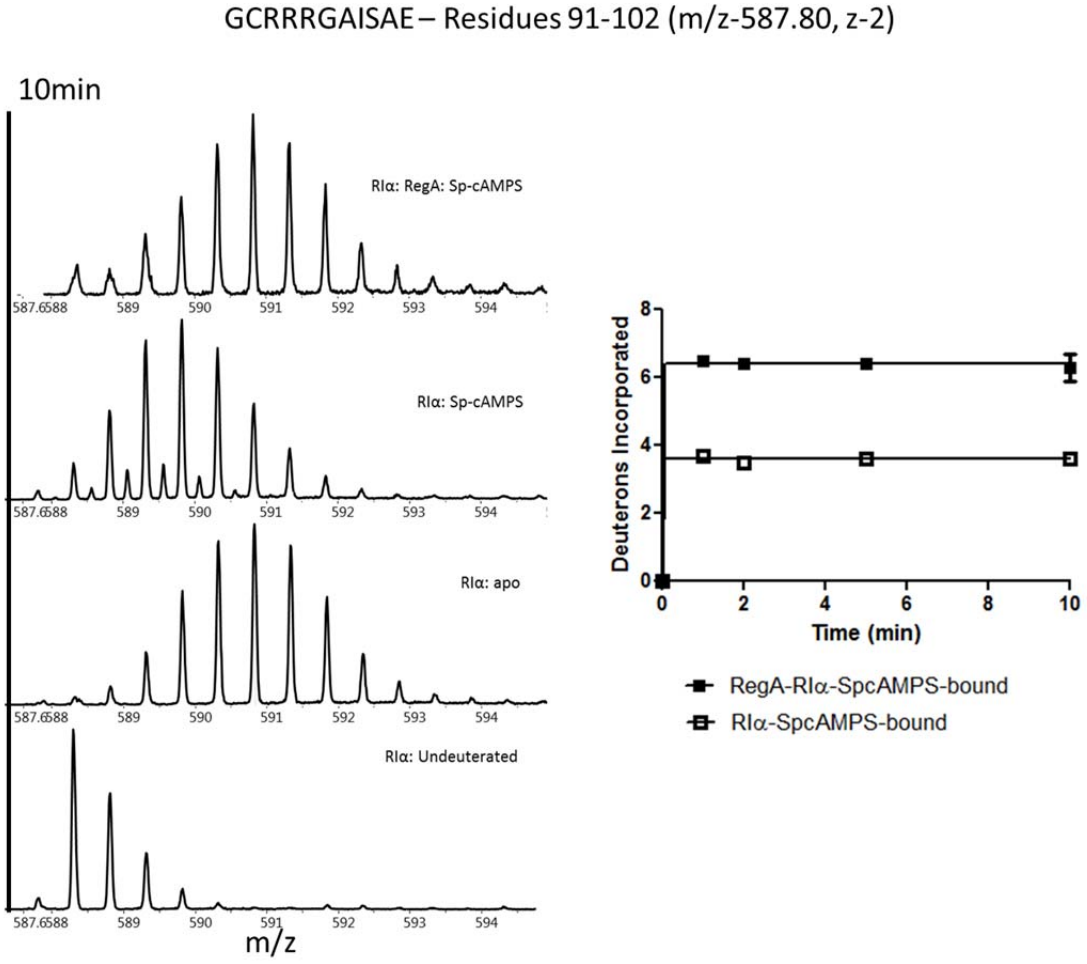

Figure 2.8: Effects of Sp-cAMPS dissociation at PKAC interaction site: Left panel: ESI-Q-TOF mass spectra for a peptide spanning residues 92-102 (m/z= 587.80, z=2) of $RI\alpha_A$for *apo*, Sp-cAMPS-bound and Sp-cAMPS in the presence of RegAc after 10 min Deuterium exchange as indicated. Right panel: Time course of deuterium exchange fit to a single exponential association (Y=Ymax*(1-exp(-K*X) (Graphpad Prism 5.0, San Diego, CA).

2.4 Conclusions:

We have examined dynamics of a transient ternary complex formed by PKA R-subunit, RegA PDE and a nonhydrolyzable cAMP analog, Sp-cAMPS. The R-subunit mediates mutually exclusive interactions with RegAc and Sp-cAMPS. RegAc mediates the active dissociation of bound cAMP by forming direct interactions with the cAMP binding pocket of RIα.

In an experiment using lower concentrations (300 μM final concentration) of Sp-cAMPS it was seen that the ternary complex was observable at earlier time points of the experiements, but as labeling time increased, the Sp-cAMPS was actively dissociated from the pocket. It was interesting to note that even though Sp-cAMPS was at a 100 fold higher concentration to the RegAc: $RI\alpha_A$ complex, reassocation of Sp-cAMPS was not observed. This indicates that under specific concentrations of Sp-cAMPS, RegAc was effective in blocking reassociation. When Sp-cAMPS concentration was increased, the ternary complex was observed for the all labeling times.

This provides a model for adaptation, where the cAMP signaling pathway is reactivated only in the presence of large fluxes of cAMP rather than the basal cAMP levels in the cytoplasm. In addition to mapping the dynamics of the reaction, our results highlight the molecular basis for PDE action in promoting cAMP signal termination.

Our study highlights that with the right conditions, HDXMS can be a powerful tool for reaction monitoring. This is highlighted further in the next chapter.

Chapter 3

Conformational Dynamics in Molecular Signaling III: Active site coupling in PDE-PKA Complexes Promotes cAMP Signal Termination

3 Conformational Dynamics in Molecular Signaling III: Active site coupling in PDE-PKA Complexes Promotes cAMP Signal Termination

3.1 Introduction

While the previous study monitors cAMP dissociation from the cAMP binding pocket of RIα, this study aims to map the interaction interface of PDEs with RIα. Cyclic AMP levels are controlled both by GPCR-mediated activation of adenylyl cyclases, that synthesize cAMP from ATP (Kamenetsky, Middelhaufe et al. 2006), and phosphodiesterases (PDEs) that catalyze hydrolysis of cAMP to 5'AMP (Conti and Beavo 2007). Even though cAMP is synthesized by adenylyl cyclases that are predominantly at the plasma membrane, it does not diffuse uniformly throughout the cell and instead exists in pools or microdomains (Rich, Fagan et al. 2001, Steinberg and Brunton 2001, Conti and Beavo 2007). This has been attributed to diverse PDEs that function to limit cAMP diffusion. An alternative explanation for the limited cAMP diffusion is via 'channeling' of cAMP from cyclases to PDEs through the cAMP receptors in large macromolecular complexes (Davare, Avdonin et al. 2001).

The cAMP signaling pathway can be divided into the activation and termination phase (Figure 3.1). While the activation phase is well studied, how the cAMP-PKA signaling system resets itself by regenerating inactive PKA holoenzyme can be defined as the termination phase and very little is known about this process. cAMP binds the PKA R-subunit with strong affinity (~ 2-10 nM) (Herberg, Dostmann et al. 1994) and a major gap in cAMP signaling is in identifying how the tightly bound cAMP is released from the R-subunit. This is critical to allow reassociation with the C-subunit and resetting of the system through formation of the inactive PKA holoenzyme. A role for PDEs in termination by catalyzing hydrolysis of bound cAMP has come from recent studies with a cAMP PDE from *Dictyostelium discoideum*, RegA (Moorthy, Gao et al. 2011), where RegA is capable of a two-step dissociation and hydrolysis of cAMP bound to PKA R-subunit (Krishnamurthy, Moorthy et al. 2013). The first step in the termination pathway can be defined as the 'Encounter complex' where the PDE first 'encounters' cAMP bound PKA R-subunit (Figure 3.1). PDE-PKA interactions mediate the dissociation and hydrolysis of cAMP from PKA R-subunit leading the 'End-state' complex. This is

critical since cAMP remains tightly bound to the R-subunit and shows negligible dissociation rates (Corbin, Sugden et al. 1978, Doskeland 1978) in the absence of the C-subunit. However the nature of PDE-RIα interactions is completely unknown. Furthermore, no such interactions have been reported in mammalian cAMP signaling whose complexity arises from myriad types/isoforms/splice variants of PDEs (Conti and Beavo 2007) and PKA as well as the presence of diverse scaffold proteins, the A-Kinase Anchoring Proteins (AKAPs) (Dodge, Khouangsathiene et al. 2001).

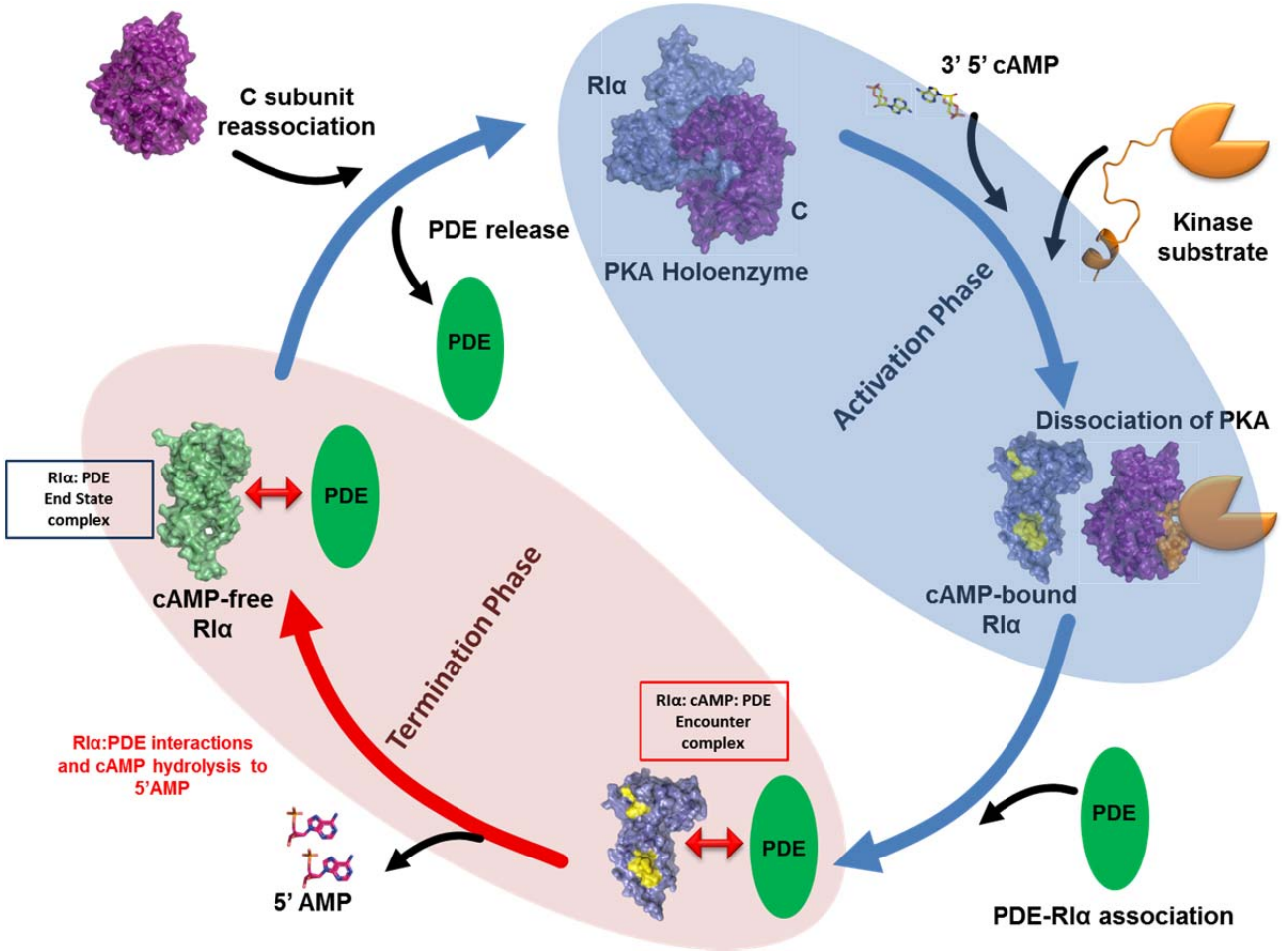

Figure 3.1: ***Role of PDEs in signal termination of PKA mediated cAMP pathway:*** The cAMP-PKA signaling pathway can be divided into Activation and Termination phases. *Activation phase*: In the presence of cAMP (yellow) and a kinase substrate (orange), the inactive PKA holoenzyme dissociates to yield cAMP bound PKA R-subunit (blue) and active PKA C-subunit (purple). *Termination phase:* PDEs in green mediate direct interactions with PKA R-subunit to hydrolyze cAMP bound to both CNB domains of PKAR. The resulting cAMP-free (*apo*) PKAR (green) is primed for reassociation with PKA C-subunit to form the inactive PKA holoenzyme. How PDEs interact with RIα and catalyze hydrolysis of cAMP bound to the R-subunit to 5'AMP is unknown and a focus of this study (highlighted in red). Space filling models based on coordinates of structures of the different proteins are indicated. C-subunit (PDB ID: 1ATP), R-subunit (cAMP-bound PKA RIα(113-379) (PDB ID: 1RGS)), RIα(91-379):C complex (PDB ID:2QCS). Only the monomeric deletion fragment of PKA RIα (residues 113-379) is shown. *Apo* RIα (green) is modeled on the structure of RIα (91-379) bound to PKA C-subunit (PDB ID:2QCS).

In this study we report, a mammalian PDE-PKA RIα complex through an integrated approach combining structural mass spectrometry, fluorescence with computational methods. While localization of PDEs with PKA R-subunits have been observed with specific classes of AKAPs (Dodge, Khouangsathiene et al. 2001), we describe for the first time AKAP-independent interactions between PKA and PDEs in a mammalian system. We also describe a mechanism for PDE-mediated dissociation of cAMP from the two binding sites on the R-subunit. The binding interface residues on RegA mapped by hydrogen/deuterium exchange mass spectrometry (HDXMS) was used to computationally identify and establish PDE8 as a cAMP-PDE interacting partner using cAMP dissociation assays. A combination of HDXMS and computational docking was then used to map and model the PDE8-RIα interface. The power of computational docking has been greatly improved by combination with HDXMS, which provides experimental filters for narrowing the solutions for protein interfaces. This has been used for mapping protein-protein interactions (Anand, Law et al. 2003, Pandit, Tuske et al. 2012) and protein-DNA interactions (Roberts, Pique et al. 2012). The R-subunit is highly modular and is composed of an N-terminal dimerization domain, a pseudosubstrate site and two tandem CNB domains (Johnson, Akamine et al. 2001). The CNB domains are capable of functioning as high affinity binders of both cAMP and C-subunit in the absence of the dimerization domain. This has made it possible to use monomeric deletion mutant constructs of pseudosubstrate region with CNB-A alone (Residues 91-244) or as a construct spanning both CNB domains A and B together with the pseudosubstrate region (Residues 75-379) for detailed mapping of PDE-R-subunit interactions. These are referred to as $RI\alpha_A$ and $RI\alpha_{AB}$ respectively. Of the two PDE8 isoforms, we have used full length PDE8A in this study or a deletion mutant spanning its catalytic domain (residues 472-829), henceforth referred to as $PDE8A_C$.

Our results provide a model which describes a mechanism for how PDE8 catalyzes hydrolysis of cAMP tightly associated with RIα. It also presents a unified explanation for how PDE-cAMP-receptors might form extended macromolecular complexes functioning as regulatory barriers for cAMP diffusion. PDEs are thus an entirely new class of RIα interacting partner proteins involved in a novel mechanism for cAMP signal termination.

3.2 Materials and Methods

3.2.1 Materials

Unless otherwise mentioned all reagents were from Sigma Aldrich (St. Louis, MO). BL21 (DE3) *E.coli* strains were from Novagen (Madison, WI). Glutathione sepharose 4B and NHS-activated sepharose 4 Fast Flow were obtained from GE (Chicago, IL). 8-AEA-cAMP was from Biolog Life Science Institute (Bremen, Germany), TFA protein sequence analysis grade was from Fluka BioChemika (Buchs, Switzerland), Poroszyme immobilized pepsin cartridge was from Applied Biosystems (Foster city, CA). Purified recombinant GST-tagged PDE2A (catalog # 60020), PDE5A(catalog # 60050), PDE8A (catalog # 60080) and PDE9A (catalog # 60090) were purchased from BPS Bioscience (San Diego, CA). Recombinant GST-tagged PDE8A (1mg/ml) was also obtained from Signal Chem (Richmond, Canada) for HDXMS experiments.

3.2.2 Subcloning of PDE8A$_C$ and full length RIα into pETDuet-1 vector

Oligonucleotide primers for PDE8A1 catalytic domain spanning residues 472-829, were designed using codon optimized Human PDE8A1 synthetic gene as a template (DNA 2.0, Menlo Park, CA). The DNA fragments were amplified by PCR and subcloned using BamHI and NotI restriction enzymes into Multiple Cloning Site 1 (MCS1) of pETDuet-1 vector containing a hexahistidine tag, N-terminal to the protein sequence. Full length RIα was cloned into Multiple Cloning Site 2 (MCS2) of pETDuet-1 using NdeI and KpnI restriction enzymes.

3.2.3 Protein expression and purification

We hypothesized that co-expression of full length RIα with PDE8A$_C$ in *E.coli* BL21 (DE3) cells might aid solubility of PDE8A$_C$. Though some of the PDE8A$_C$was found to be soluble, most of it was still present in inclusion bodies. To improve yields of soluble PDE8A$_C$, refolding of inclusion bodies with denaturants was carried out. Thus the pellet with insoluble PDE8A$_C$ was denatured by 6M Guanidinium Hydrochloride and the solubilized PDE8A$_C$ was purified by affinity chromatography

using Cobalt affinity His-Tag resin (Clontech Laboratories, Mountain View, CA). $PDE8A_C$ was refolded by a previously described protocol (Yan, Wang et al. 2009), with the only modification that the Hexahistidine tag was not removed by thrombin cleavage.

cAMP affinity chromatography resin for R-subunit purification was synthesized by coupling 8-AEA-cAMP to the NHS-activated sepharose 4 Fast Flow ® beads according to manufacturer specifications (GE Life Sciences Sing*apo*re) (Diller, Xuong et al. 2000). Both cAMP-bound and cAMP-free $RI\alpha_A$ were expressed and purified as described previously (Anand, Taylor et al. 2007). cAMP-bound $RI\alpha_{AB}$ was expressed and purified by cAMP affinity chromatography resin similar to $RI\alpha_A$. cAMP-free $RI\alpha_{AB}$ was prepared by the dissociation of cAMP by urea stripping and refolding (Buechler and Taylor 1991). RegA (385-780) ($RegA_C$) was expressed as a GST fusion protein in *E. coli* BL21*(DE3). The protein was purified using glutathione sepharose 4B (GE Life Sciences) according to manufacturer specifications followed by size exclusion-gel filtration chromatography on an AKTA system (GE Life Sciences) (Moorthy, Gao et al. 2011).

3.2.4 Fluorescence polarization (FP) assay for cAMP dissociation

To determine if all PDEs were capable of dissociating bound cAMP from RIα, we carried out a fluorescence polarization (FP) assay using 8-(2-[Fluoresceinyl]aminoethylthio)adenosine- 3', 5'-cyclic monophosphate (8-Fluo-cAMP) saturated $RI\alpha_A$ as described (Moorthy, Gao et al. 2011) with PDEs 2A,5A, 8A and 9A. A Biotek Synergy 4 Multi-Detection microplate reader (Winooski, VT) was used in FP mode for the plate reader assays. The excitation and emission wavelengths used were 485 nm and 528 nm, respectively with a bandwidth of 20 nm with an instrument G-factor of 0.87. 96-well black plates were from Greiner (Germany). The FP signals for 0.12 μM of 8-Fluo-cAMP bound $RI\alpha_A$ in buffer A (20 mM Tris-HCl, pH 7.5, 50 mM NaCl, 10 mM $MgCl_2$, 5 mM BME) were monitored in the presence of a 10-X fold molar excess PDE (Figure 3A) and were repeated with equimolar PDE8A (Figure 3B). FP measurements were taken at time intervals of 2 min up to 45 min. In all samples, 0.5 mM cAMP/10 μM cAMP/cGMP was added at 18 min. Data from early time points (0 – 18 min) were fit to a one phase exponential decay equation using Graph Pad Prism software version 5

(San Diego, CA). Fluorescence polarization experiments were carried out together with Dr. B. S. Moorthy, a then senior graduate student in my research group in the Department of Biological Sciences, National University of Singapore.

3.2.5 Amide hydrogen/deuterium exchange mass spectrometry (HDXMS)

To carry out HDXMS experiments of the GST-RegA_C: RIα_A complex, 50 µL of 20 µM GST-RegA_C and 60 µM cAMP free RIα_A (1:3 molar ratio) was incubated at room temperature for 30 min.

HDXMS experiments with the full length PDE8A1: RI$\alpha_A$complex were carried out maintaining sample concentration at 6 µM of PDE8A1 and 42 µM of cAMP-free RIα_A(1:7 molar ratio) in a total reaction volume of 4 µl for each HDXMS experiment.

HDXMS experiments of the PDE8A$_C$RIα_{AB} complex were carried out in two ways. To maintain saturating amounts of RIα_{AB} and maintain all available PDE8A$_C$ in complex form, 30 µM of PDE8A$_C$was incubated with 90 µM cAMP bound RIα_{AB} (1:3 molar ratio) for 1 h on ice. For the inverse experiment, where saturating amounts of PDE8A$_C$ are maintained so all available RIα_{AB} is in complex form, 30 µM of cAMP-bound RIα_{AB} was incubated with 100 µM of PDE8A$_C$(1:3.3 molar ratio) for 1 h on ice. HDXMS of cAMP bound RIα_{AB} was carried out by maintaining a final cAMP concentration of 300 µM. HDXMS of cAMP bound RIα_{AB} without excess cAMP was also carried out to monitor time dependent dissociation of cAMP from RIα_{AB}. All samples were allowed to equilibrate to room temperature prior to deuterium exchange experiments. Deuterium exchange was carried out by diluting the samples in storage buffer (20 mM Tris-HCl, pH 7.5, 50 mM NaCl, 10 mM $MgCl_2$, 5 mM BME) 15X for RegA:PKA R-subunit complex in D_2O (99.90%) resulting in a final concentration of 93.3% deuterated buffer. For full length PDE8A or PDE8A$_C$: RIα_{AB} complexes, samples were diluted 10X in storage buffer resulting in a final concentration of 90% deuterated buffer. . Reaction monitoring experiments, where we monitored PDE-dependent catalytic dissociation of cAMP, were carried out by mixing 90 µM of cAMP bound RIα_{AB} with 30 µM of PDE8A$_C$ (3:1 molar ratio) while simultaneously diluting in D_2O storage buffer (99.9%), obtaining a final D_2O concentration of 90%.

Exchange was carried out at 20ºC for various labeling times (0.5, 1, 2, 5 and 10 min). For initial experiments with full length PDE8A, only a single labeling time of 2 min was carried out. Reaction monitoring experiments were subjected to extended labeling times to allow the catalytic reaction to proceed to completion, thus labeling times for these experiments were 0.5, 1, 2,5, 10, 30 and 60 min. The exchange reaction was quenched by addition of pre-chilled 0.1% TFA to obtain a final pH_{read} of 2.5. 50 µL of the quenched sample was then injected on to a chilled nano-UPLC sample manager (Waters, Milford, MA) as previously described (Wales, Fadgen et al. 2008). The sample was washed through a 2.1 x 30mm immobilized pepsin column (Porozyme, ABI, Foster City, CA) using 100 µL/min 0.05% formic acid in water. The digest peptides were trapped on a 2.1 x 5 mm C18 trap (ACQUITY BEH C18 VanGuard Pre-column, 1.7 µm, Waters, Milford, MA). Peptides were eluted using an 8-40% gradient of acetonitrile in 0.1% formic acid at 40 µL/min, supplied by a nanoACQUITY Binary Solvent Manager (Waters, Milford, MA), on to a reverse phase column (ACQUITY UPLC BEH C18 Column, 1.0 x 100 mm, 1.7 µm, Waters, Milford, MA) for resolution. Peptides were detected and mass measured on a SYNAPT HDMS mass spectrometer (Waters, Manchester, UK) acquiring in MS^E mode (Bateman, Carruthers et al. 2002, Silva, Denny et al. 2005).

Peptides were identified from MS^E data of undeuterated samples using ProteinLynx Global Server (PLGS 2.4, Waters, Milford, MA) (Geromanos, Vissers et al. 2009, Shen, Li et al. 2009). Identifications were only considered if they appeared at least twice out of three replicate runs and had a minimum of 4 digest fragment ions. These identifications were mapped on to subsequent deuteration experiments using prototype custom software (DynamX, Waters, Milford, MA). Data on each individual peptide at every time point was extracted and analyzed using this software. Instrument calibration was carried out as described (Anand, Krishnamurthy et al. 2010, Moorthy, Badireddy et al. 2011).Reported values for all HDXMS experiments are the average of at least two independent deuterium exchange experiments.

3.2.6 Docking

The model of PKA $RI\alpha_{AB}$ bound to $PDE8A_C$ was generated using the HADDOCK web server (Dominguez, Boelens et al. 2003) as a result of our collaboration with Dr. Kavitha Bharatham and Dr. Ivana Mihalek, Bioinformatics Institute, Singapore. The available crystal structures of dimeric $PDE8A_C$ (PDBID: 3ECN) and the cAMP-bound conformation of RIα (PDBID:1RGS) were considered as starting structures for the docking. Since the linker between the two cAMP domains of RIα is highly flexible leading to potentially large conformational changes upon binding PDE8, RIα was split into two CNB domain fragments, RIα_CNB-A (residues 113-235) and RIα _CNB-B (residues 241-379) and docked independently. The active residues that drive the docking calculations were selected based on regions showing decreased deuterium exchange upon complexation with PDE8. Since this region outlined by the experiment was large, and including residues that are buried in the static crystal structure, we only selected a subset of residues that were solvent exposed as the input for docking. The residues around the active residues were considered passive (the default option). The C- and N-termini were kept uncharged as they were not the actual termini. The residues 230-235 in RIα_CNB-A and 241-250 in RIα_CNB-B, were treated as fully flexible. For each run, a total of 1000 structures were calculated by rigid-body minimization of the docking score. Semi flexible simulated annealing followed by refinement in explicit water was performed for the best 200 solutions based on the HADDOCK score. The calculated models were clustered using a 7.5-Å interface RMSD cutoff. The following residues were defined as Ambiguous Interaction Restraints (AIR) to drive the docking:

PDE8 residues: 526, 527, 529, 530, 531, 532, 609, 610, 611, 621, 622, 651, 652, 653, 681, 682, 683, 686, 687, 690, 691, 693, 694, 696, 698, 699, 700, 702, 703, 706, 756, 759, 760, 761, 762, 763.

RIα (CNB-A) residues: 128, 131, 132,133,134, 171,177, 178, 179, 189, 191, 194, 196, 197, 199, 200, 201, 204, 205, 206, 207, 208, 210,216, 217, 218 and

RIα (CNB-B) residues: 268, 269, 270, 271, 272, 273, 274, 275, 276, 277, 278, 322, 323, 324, 325, 328, 329, 330, 331, 332, 333, 334, 335, 336, 354, 355, 356, 358, 359, 361, 362, 363

3.2.7 Selection of the docked pose

The binding models of CNB-A and CNB-B to PDE8A_C dimer from the docked poses of two independent runs were picked based on the following criteria: i) the quality of RIα contacts with the PDE8A_C (using the native HADDOCK score), ii) the accessibility of the RIα bound cAMP to the catalytic site of the PDE8 A_C, and iii) whether the distance and orientation of the two independently docked domains was consistent with the fact that the two are connected by the RIα linker α:C-helix *in vivo*. The criterion (ii) was quantitated in an *ad hoc* way by counting the number of peptide atoms inside the sphere that can be inscribed between the centers of the cAMP binding pockets in PDE and RIα. Namely, if our model is correct, we expect that the cAMP binding pockets in the two proteins should be mutually accessible, allowing the transfer of the substrate between the two. Thus we look for a configuration of the complex in which as few peptide atoms as possible appear in the space between the two pockets. The criterion (iii) was tested by manually modeling back in the central helix.

3.3 Results

*3.3.1 Peptide Array Analysis identifies locus of contiguous RegA:RIα Interactions**

We applied peptide array analysis to independently probe the binding site for full-length RIα on RegA. A library of overlapping peptides of 15-mers from the primary sequence of RegA, each frameshifted by 5 amino acids was synthesized and immobilized on a cellulose membrane (A2 to D8 in Figure 3.2) as described (Burns-Hamuro, Ma et al. 2003). The cellulose membrane was then incubated with cAMP-free full length RIα followed by extensive washing. The bound RIα was then detected with RIα specific antibodies followed by secondary antibodies similar to immunoblotting assays (Sathyanarayana, Houde et al. 2009). Dark spots reflect direct interaction sites with RIα, summarized in the table (Figure 3.2). To minimize false positive results, we only considered

** Peptide array experiments were carried out in collaboration with Prof. Susan Taylor's lab at University of California at San Diego, CA, USA*

overlapping peptides where binding to RIα was detected (Bogacheva, Bogachev et al. 2008). Analysis of the modeled structure of RegA based on that of PDE8A showed that the two overlapping sets of interacting peptides are contiguous. Consecutive peptides showing positive interactions span residues 516-540 important for divalent metal binding and catalysis. A second region included overlapping peptides 556-570, 561-575 and 566-580 that together with the first set highlights the linear loci for interactions with the CNB:A domain of RIα (Figure 3.6B).

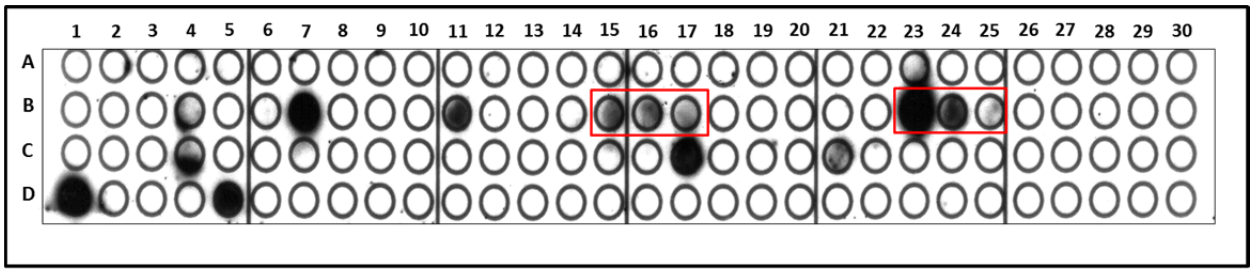

Spot No.	Peptide probe (RegA)	Residue Nos.
B15	DIFALLISCMCHDLN	516-530
B16	LISCMCHDLNHPGFN	521-535
B17	CHDLNHPGFNNTFQV	526-540
B23	LENHHAMLTFKILRN	556-570
B24	AMLTFKILRNSECNI	561-575
B25	KILRNSECNILEGLN	566-580

Figure 3.2: ***Peptide array data shows interaction of RIα with RegA:*** Peptides that interacted with RIα generated dark spots in contrast to non-interacting peptide (blank spots) and peptides interacts specifically with RIα are shown in red box. Spot numbers (A2 to D8) relate to peptides in the scanned array (A2 to D8, spot A2 → 301-315 residues, spot A3 → 306-320 residues and so on to D8→ 781-793) and whose sequence which interacts specifically are listed in the table.

3.3.2 HDXMS analysis of RIα CNB:A-RegAc interaction reveals that the interface encompasses the PDE catalytic active site

To map the interface on RegA that interacted with the CNB:A domain of RIα (Moorthy, Gao et al. 2011), we carried out HDXMS on the $RIα_{A:}$ RegAc complex. Prior to deuterium exchange, undeuterated samples of RegAc were subjected to complete proteolysis by pepsin, followed by peptide sequencing and identification as described in materials and methods (Moorthy, Gao et al. 2011). Overall 32 peptides were detected, which covered ~ 81% of the RegAc sequence. These were

each well resolved with high signal to noise ratios (S/N = 6) and were subsequently analyzed in the deuterium exchange experiments.

Based on the estimated K_D (≤ 1.6 μM) for the RegAc-cAMP free $RI\alpha_A$ complex (Moorthy, Gao et al. 2011), excess cAMP-free $RI\alpha_A$ (60 μM) was incubated with $RegA_C$ (20 μM) to bind RegAc to saturation. Deuterium exchange was then carried out as described in materials and methods. Since the observed rate of exchange, k_{obs} is dependent on an interplay of both the dissociation constant and the intrinsic deuterium exchange rate, we factored in the upper limit of the dissociation constant to optimize the relative and absolute concentrations of both RegAc and $RI\alpha_A$. With a 3X excess of $RI\alpha_A$ (60 μM) for $RegA_C$ (20 μM), we estimated complete saturation of RegAc in complex with $RI\alpha_A$ (Mandell, Baerga-Ortiz et al. 2001), enabling us to monitor the changes in RegAc upon interactions with $RI\alpha_A$. A Difference plot (Houde, Berkowitz et al. 2011) was used to provide a protein-wide overview of the difference in relative deuterium exchange for free and $RI\alpha_A$ bound RegAc (Figure 3.3) for a time course ranging from 0 -10 min. ESI-QTOF spectra for three peptides from $RegA_C$ which show the largest shifts in deuterium exchange (Don=10 min) upon interactions with $RI\alpha_A$ are shown in Figure 3.4. Kinetic plots of deuterium exchange for these peptides (Figure 3.5) reveal significant differences in deuterium exchange that are observable for all of the time points monitored. HDXMS results for the catalytic domain of RegA were mapped onto the homology modeled PDE structure of the closest cAMP PDE homolog of RegA, PDE8 (PDB ID: 3ECM) using SWISS-MODELLER) (Figure 3.6A) (Arnold, Bordoli et al. 2006, Wang, Yan et al. 2008).

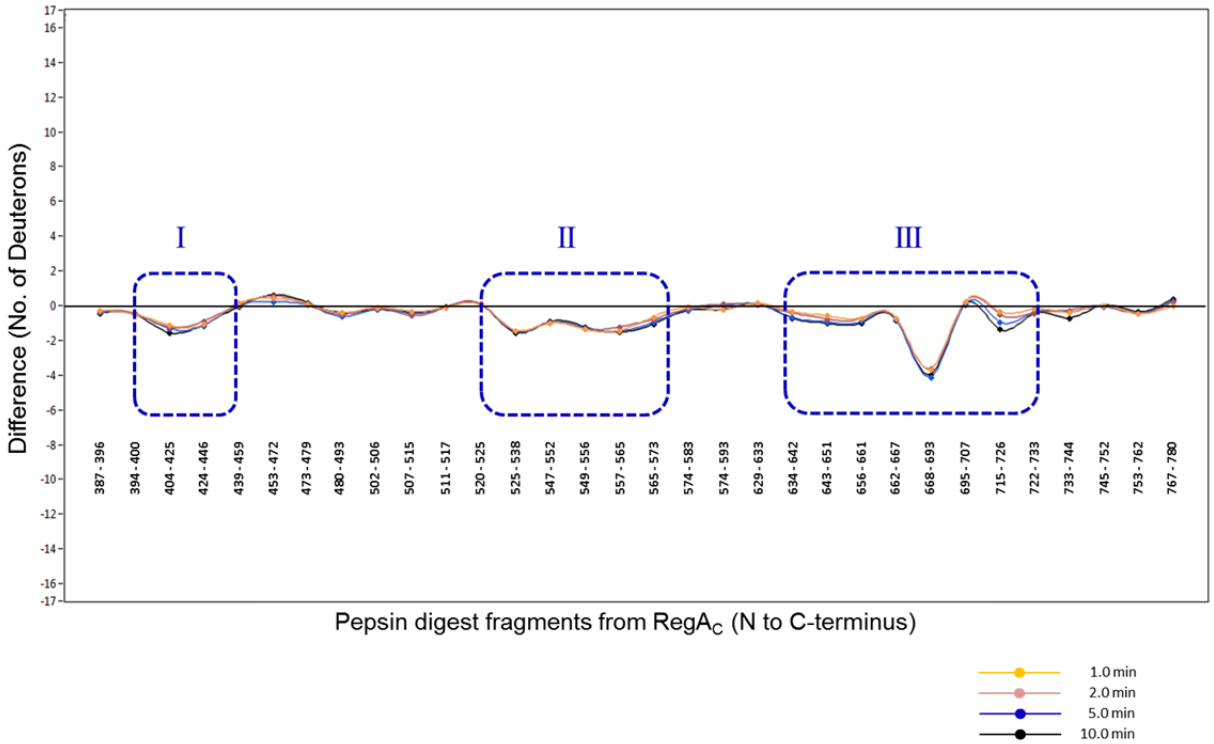

Figure 3.3: Mapping the interaction interface of RIα$_A$ on RegA$_C$ by HDXMS: A) Difference in HDXMS levels (y-axis) between free RegA$_C$ and in complex with RIα$_A$ are plotted for the pepsin digest fragments (x-axis) analyzed in this study. Time points are represented in different colors; orange, brown, blue and black for 1, 2, 5 and 10 min respectively. Blue dotted boxes highlight the three regions (I, II and III) within RegA$_C$ showing decreased deuterium exchange in the PDE-RIα complex. Plots are the average from two independent HDX-MS experiment generated using the DynamX software (Version 2.0, Waters, Milford).

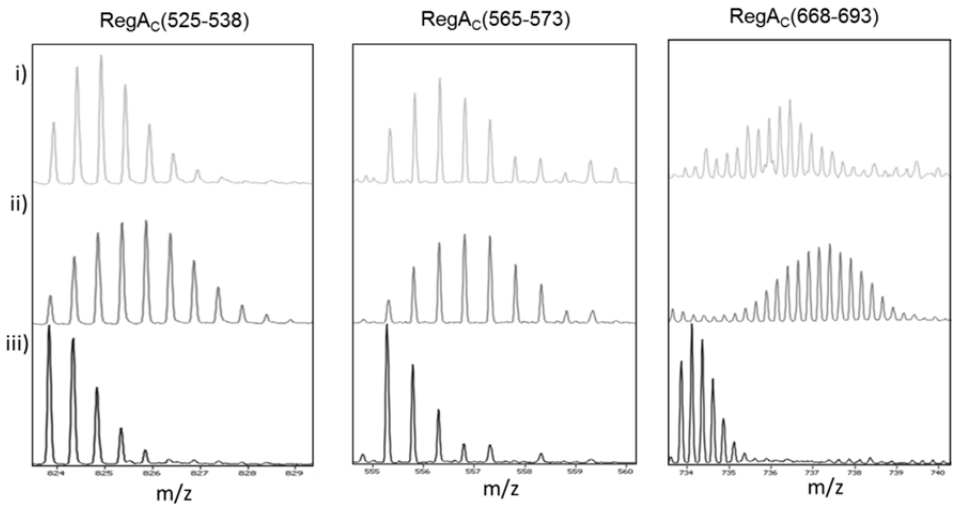

Figure 3.4: ESI-QTOF mass spectra of pepsin digest fragments from different regions of RegA$_C$ that showed significant changes in amide H/D exchange upon interactions with RIα$_A$. (i) The isotopic envelope for the peptides from RegA$_C$ in the presence of RIα$_A$ after 10 min deuteration (ii) The isotopic envelope for the peptides from RegA$_C$ in the absence of RIα$_A$ after 10 min deuteration; (iii) undeuterated isotopic envelope of peptides from RegA$_C$.

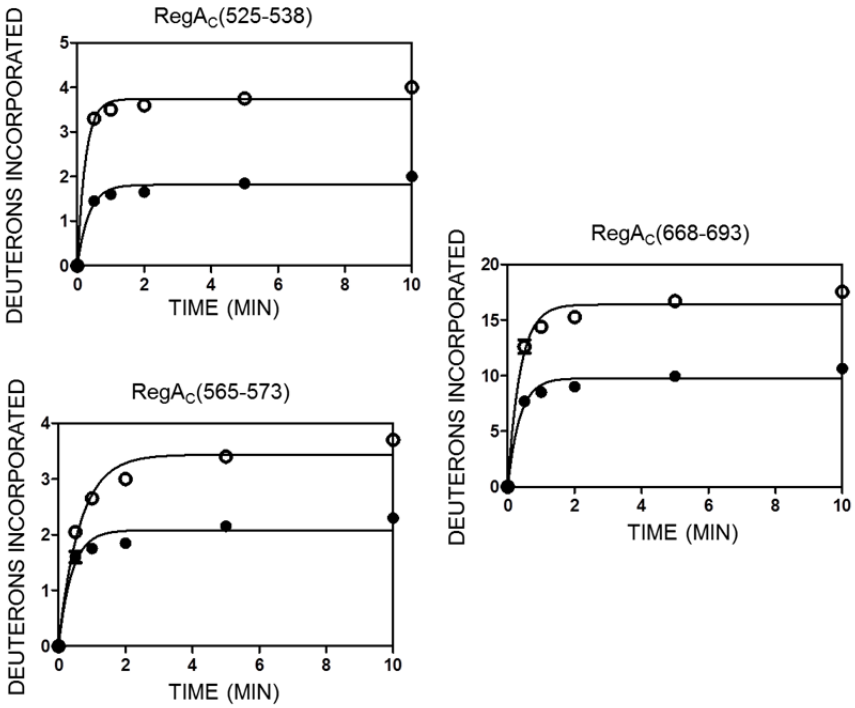

Figure 3.5: Time course (1 - 10 min) of deuterium exchange for peptides from $RegA_C$. Open circle (○), $RegA_C$ in the absence of $RI\alpha_A$; Close circle (●), $RegA_C$ in the presence of RIα (91-244).

Within $RegA_C$, the catalytically important M loop showed decreased exchange upon interactions with $RI\alpha_A$. From multiple sequence analyses, the residues are highly conserved across the PDE superfamily and are critical for the coordination of the two divalent metal ions Zn^{2+} and Mg^{2+} necessary for catalysis. Interestingly HDXMS results showed that pepsin fragment peptides 525-538 and 634-642, which span catalytically important residues H527, D528 and D639 showed significantly reduced exchange upon binding $RI\alpha_A$. Peptides spanning residues also critical for substrate cAMP recognition 525-538, 634-642, 656-661 and 668-693 showed decreased exchange upon interactions with $RI\alpha_A$.

The results enabled a detailed map of the interface which encompassed the PDE active site, when modeled onto the closest cAMP PDE homolog of RegA, PDE8 (PDB ID: 3ECM) using SWISS-MODELLER) (Figure 3.6A, 3.6B, and 2.6C)(Arnold, Bordoli et al. 2006, Wang, Yan et al. 2008).

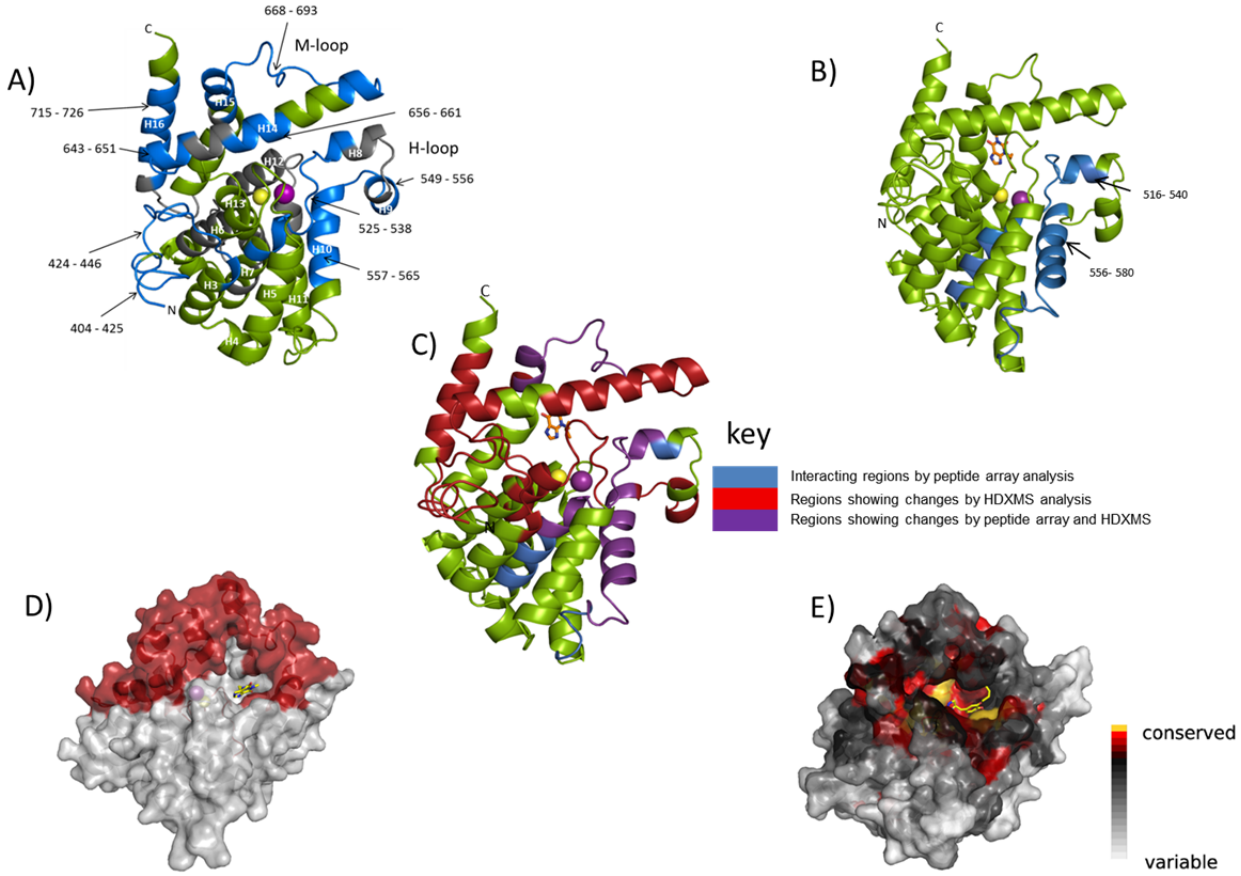

Figure 3.6: Summary of peptide array analysis and HDXMS of RIα-RegAc interactions mapped onto the structure of PDE8A: A) Results from HDXMS for the catalytic domain of RegA mapped onto the homology modeled PDE structure of the closest cAMP PDE homolog of RegA, PDE8 (PDB ID: 3ECN) using SWISS-MODELLER. Peptide fragments showing decreased exchange (after 10 min Deuterium exchange) in the presence of $RI\alpha_A$ are in blue. Regions showing no difference are in green and regions with no pepsin-digest fragment coverage are in grey. B) Results from peptide array analysis for $RegA_C$ mapped onto the homology modeled PDE structure of PDE8 (PDB ID: 3ECN). Peptides showing direct interactions with RIα are blue. C) Composite of HDXMS and peptide array results mapped onto the structure of homology modeled PDE8. Regions showing decreased exchange are red, peptide array fragments are blue, and intersection sites are purple. In addition to Zn^{2+} and Mg^{2+}, the nonspecific PDE inhibitor, 3-isobutyl-1-methylxanthine (IBMX) is shown in B and C (stick representation). D) Results from HDXMS of $RegA_C$:$RI\alpha_A$ interaction are mapped in red onto the surface representation of the modeled RegA structure. The inhibitor IBMX is shown in stick representation in yellow. E) Evolutionary trace analysis of RegA:$RI\alpha_A$ interaction interface mapped onto the structure of the cGMP phosphodiesterase PDE9 (PDB ID: 2HD1).

3.3.3 PDE-RIα interaction interface shows broad conservation across the PDE superfamily

The regions in RegA that interacted with RIα, are regions which show high sequence homology across all PDEs from *Dictystelia* to mammals as these regions are important the catalytic activity of PDE(Conti and Beavo 2007). We nonetheless carried out a comprehensive primary sequence analysis

based on sequence conservation and exon-intron structure, to determine whether any mammalian PDE is an obvious homolog of RegA. Regions on RegA which showed a high sequence homology with other PDEs were the same regions identified by HDXMS and peptide array to form the locus of $RegA_C$-RIα interactions (Figures 3.6D and 3.6E). Broadly the overlap between regions of RIα interaction and the PDE catalytic active site is reflected in high conservation at the PKA-RIα interaction interface within the PDE catalytic domain across vertebrate PDEs, raising the possibility that multiple PDE families interact with PKA RIα. Sequence homology of the catalytic domains alone showed that the closest homolog was the cGMP PDE, PDE9 followed by the cAMP PDE, PDE8. Interestingly, the domain organization of PDE8 shows parallels with RegA, in containing a putative N-terminal response regulator domain (receiver domain) (Shaulsky, Fuller et al. 1998, Thomason, Traynor et al. 1998).

In order to test the broad specificity of PDE interactions with RIα, we used Fluorescence polarization spectroscopy with 8-(2-[Fluoresceinyl]aminoethylthio)adenosine- 3', 5'- cyclic monophosphate (8-fluo-cAMP) as a rapid screen for identifying potential PDEs that are capable of hydrolyzing cAMP bound to the PKA R-subunit. We chose 4 full-length PDEs (2 cGMP PDEs- PDE5A and PDE9A, and 2 cAMP PDEs- PDE2A and PDE8A) to test for dissociation of cAMP bound to CNB-A domain of $RIα_A$. PDE9A and PDE8A were chosen due to the high sequence homology with RegA. Two GAF-domain containing PDEs, PDE2A (dual specificity cAMP/ cGMP PDE) and PDE5A (cGMP-specific PDE) were also examined as controls. Fluorescence polarization assays with 8-fluo-cAMP -labelled $RIα_A$ were carried out as described previously (Moorthy, Gao et al. 2011). 8-fluo-cAMP is resistant to PDE hydrolysis and therefore offered an opportunity for direct monitoring of cAMP dissociation from RIα (Poppe, Rybalkin et al. 2008). No dissociation of 8-fluo-cAMP was observable from CNB-A of RIα in the absence of excess cAMP or upon addition of excess PDE. This is a consequence of a slow kinetic off-rate for cAMP from the R-subunit or fast reassociation rate of released cAMP. This was used as a basis for testing the ability of PDEs to dissociate cAMP bound to CNB-A in $RIα_A$ (Figure 3.7). In these experiments, 8-Fluo-cAMP bound to $RIα_A$ was mixed with excess or equimolar PDEs and FP was measured. In the presence of a 10-X molar excess of full-length PDEs, small increases in

fluorescence polarization (FP) values were observable with time in the presence of PDEs 5,8 and 9. This can be attributed to the ability of PDEs to bind 8-fluo-cAMP despite being incapable of readily hydrolyzing it (Poppe, Rybalkin et al. 2008). Even though equivalent analogs resulting from substitutions at the 8' position of the adenine ring such as 8-Br-cAMP confer resistance to PDE hydrolysis, they nevertheless are capable of binding and functioning as competitive inhibitors of PDEs. Addition of PDE2 resulted in a steady increase in fluorescence polarization with time (Figure 3.7A). This increase is consistent with 8-fluo-cAMP functioning as a cAMP analog and binding the GAF domain of PDE2.

The addition of 0.5 mM cAMP after 18 min showed important differences between the cGMP-specific and cAMP-specific PDEs. Samples containing PDEs 5 and 9 showed a steady drop in FP upto time t=40 min when it reached baseline, upon addition of cAMP. Since cAMP is hydrolyzed poorly by cGMP PDEs, all of the 8-fluo-cAMP bound to RIα is displaced by excess unhydrolyzed cAMP and this is reflected in the drop in FP. The sample containing PDE8 showed a more gradual drop in FP upon addition of cAMP upto time t=28 min after which it increased to a steady intensity at time t=32 min, slightly lower and close to the signal at time t=18 min before the addition of cAMP. PDE8 rapidly hydrolyzes the excess cAMP added to 5'AMP and once the cAMP is depleted, 8-fluo-cAMP reassociates with PDE8 to increase the FP signal. In the sample with PDE2, a further increase in FP was seen upon addition of cAMP (Figure 3.7A).

PDE8 interacts with RIα and facilitates cAMP dissociation:

We next carried out fluorescence polarization assays at lower concentrations of PDE8A (1:1 molar ratios). We observed at these lower concentrations (0.13 μM), PDE8A alone showed no changes in FP suggesting that it did not bind the ligand, 8-fluo-cAMP (Figure 3.7B). These conditions therefore allowed monitoring of cAMP dissociation by PDE8A. Our results showed that PDE8A promotes dissociation of 8-fluo-cAMP both in the presence and absence of the nonspecific PDE inhibitor IBMX. Upon addition of excess cAMP, a larger dip in the FP signal was observed for IBMX-bound PDE8A1. This reflects slower cAMP hydrolysis in the presence of IBMX and consequently a lag in

reassociation of released 8-fluo-cAMP to RIα. This indicates that PDE catalysis and PDE-mediated dissociation of bound cAMP are separate steps (Figure 3.7B). The 8-fluo-cAMP-bound $RI\alpha_A$ showed shifts in fluorescence polarization with all PDEs except PDE9. Thus all the PDEs we tested, with the exception of PDE9A, were capable of interactions with $RI\alpha_A$ resulting in dissociation of cAMP. While these results do not exclude PDEs 2A and 5A as potential $RI\alpha_A$ binders, we chose to explore these PDE8A-$RI\alpha_A$ interactions further given its higher homology with RegA.

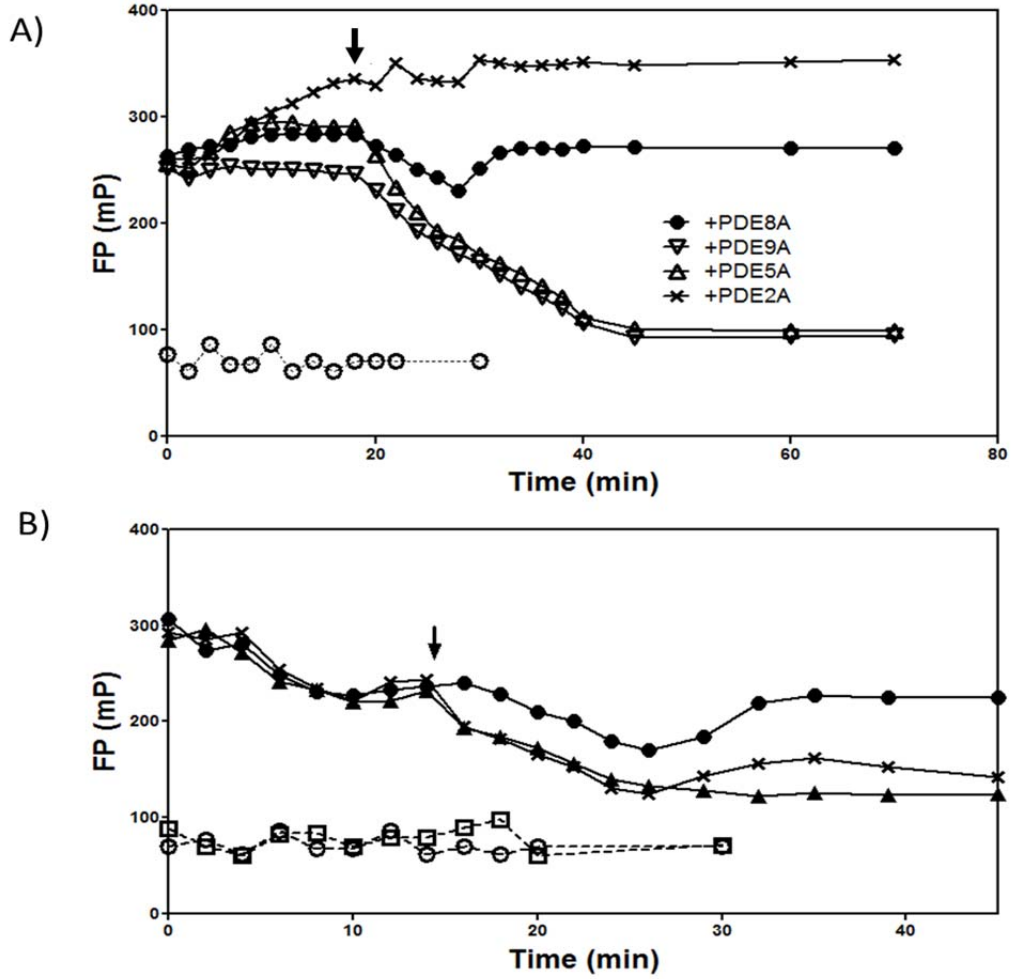

Figure 3.7: ***PDE8A interacts with RIα and blocks cAMP reassociation*****:** A) Dissociation of 8-fluo-cAMP from $RI\alpha_A$(0.12 μM) was monitored by measuring the fluorescence polarization (FP) change in the presence of a molar excess (1.2 μM) of the following phosphodiesterases at (x) PDE2A, (●) PDE8A, (Δ) PDE5A and (∇) PDE9A. Interpolated FP values are plotted vs time; arrow indicates the addition of cAMP (0.5 mM) after 18 min to all reactions. Baseline signal for 8-fluo-cAMP (0.12 μM)(o). B) Dissociation of 8-fluo-cAMP from $RI\alpha_A$(0.12 μM) was monitored by measuring the fluorescence polarization (FP) change in the presence of (0.13 μM) PDE8A (●) and IBMX-saturated PDE8A (x); arrow indicates addition of cAMP (10 μM) or cGMP (10 μM) (▲) after 18 min of the reaction. Baseline signal for 8-fluo-cAMP (0.12 μM)(o) and PDE8A (0.12 μM)(□).

PDE assays showed that PDE8A was capable of hydrolyzing cAMP bound to $RI\alpha_A$ with cAMP-bound $RI\alpha_A$ as the sole substrate (Figure 3.8). This is consistent with previous results obtained with RegA (Moorthy, Gao et al. 2011). We then set out to examine the interactions of the catalytic domain of PDE8A with the CNB domains of PKA R-subunit in greater detail.

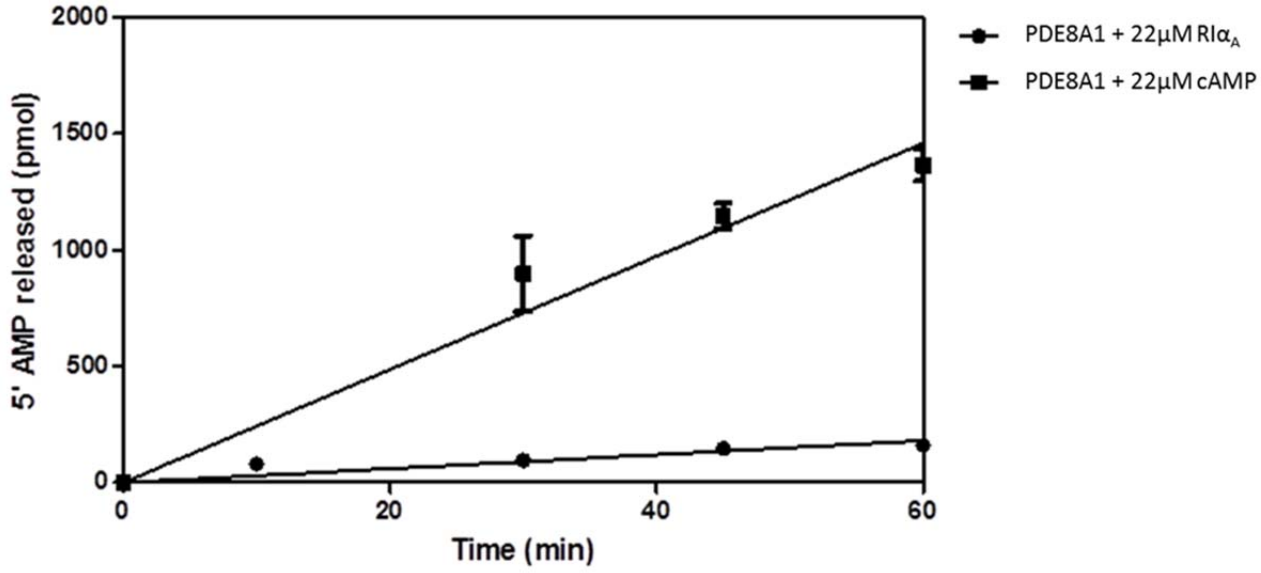

Figure 3.8: ***PDE8A1 is capable of catalyzing hydrolysis of cAMP bound to RIα*****:** Phosphodiesterase activity was calculated using a phosphate coupled colorimetric assay based on hydrolysis of cAMP to AMP by phosphodiesterases coupled to the hydrolysis of AMP to inorganic phosphate by alkaline phosphatase. In this assay, catalytic amounts of PDE8A1 (50 nM) was incubated with 22 μM of cAMP bound $RI\alpha_A$ for different incubation times. Phosphodiesterase activity of PDE8A1 (50 nM) with 22 μM of free cAMP was also carried out for comparison. The plot compares the amount of 5' AMP released (y-axis) with increasing labeling times (x-axis). The plot shows that PDE8A1 is capable of hydrolyzing cAMP bound to $RI\alpha_A$ (■), albeit at a rate 8 times slower than rate of hydrolysis of PDE8A1 for free cAMP (●). The points were fit to a linear equation (Graphpad Prism version 5 (San Diego, CA)).

3.3.4 Expression and purification of Catalytic domain of PDE8A

$PDE8A_C$ was cloned and expressed in Bl21 (DE3) cells as described in materials and methods. $PDE8A_C$ was purified by a refolding procedure as previously described (Yan, Wang et al. 2009). After refolding, Anion exchange chromatography was carried out (MonoQ 5/50 GL, GE healthcare) and protein eluted in 2 peaks at ~ 300 mM salt concentration (Figure 3.9A). Size exclusion chromatography was carried using S200 10/300 size exclusion columns (AKTA columns,GE healthcare). Protein eluted as a monomer-dimer pair, with the dimer peak eluting at ~ 0.54 column

volumes and the monomer eluting at ~0.62 column volumes (Figure 3.9B). SDS- PAGE gels of the fractions revealed protein had a purity of > 95%.

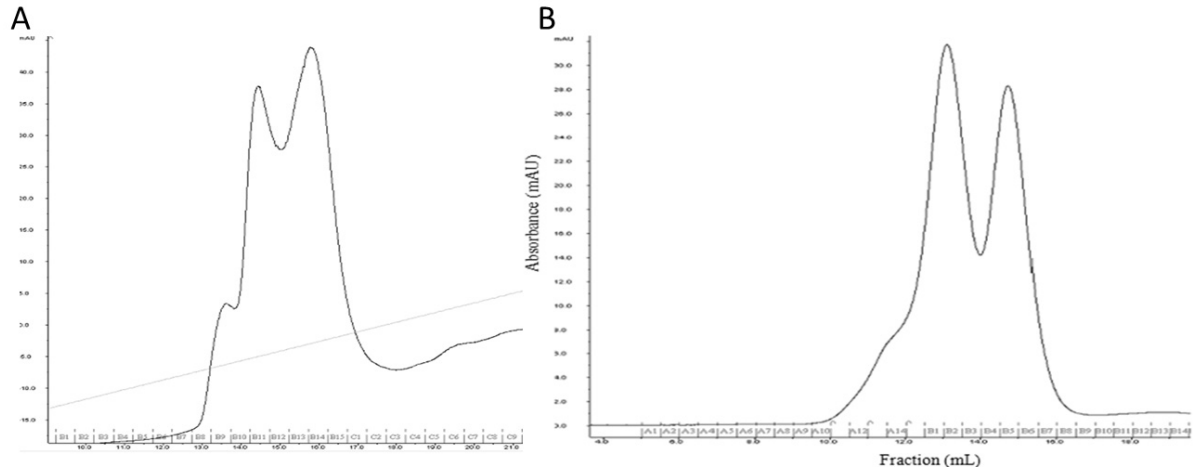

Figure 3.9: Purification of PDE8A$_C$: A) Peak profile of anion-exchange chromatography FPLC of PDE8A$_C$. PDE8A$_C$ was eluted at 300 mM of NaCl. B) Peak profile of FPLC size exclusion chromatography. Dimer-monomer peaks eluted at 0.54 and 0.62 column volumes respectively

3.3.5 Catalytic domain of PDE8A interacts with both cAMP-binding domains of RIα

The model for PDE-mediated dissociation and hydrolysis of cAMP proposed previously (Moorthy, Gao et al. 2011) necessitated interaction of PDE with cAMP-bound RIα ('Encounter' complex) followed by cAMP dissociation resulting in an 'End state' complex of cAMP-free (*apo*) RIα bound to PDE. We first set out to test parallels between the 'End state' complexes of RegA and PDE8A with RIα. This complex was generated as described in materials and methods with PDE8A1 and cAMP-free RIα$_A$ and HDXMS was carried out on the complex. Given that the locus of interactions with RIα in RegA was entirely within the catalytic domain, deuterium exchange analysis for PDE8A1 was restricted to the catalytic domain. A total of 24 peptides were analyzed corresponding to a sequence coverage of 72% for the catalytic domain (residues 480-818). Four regions showed decreased deuterium exchange upon binding to RIα$_A$ (Figure 3.10). The regions span residues 527-547 of H4 and H5, 619-648 of H10, 765-781 of the M-loop, 685-706 on HE1 and HE2. Of these regions, three are proximal to the catalytic site while residues 685-706, represented by two contiguous peptides, are located on a helix loop helix motif (HE1 and HE2) unique to PDE8 (Wang, Yan et al. 2008).

In order to map in greater detail the locus of PDE-PKA interactions, we studied binding of the catalytic domain of PDE8A, $PDE8A_C$, with RIα. Size-exclusion chromatography of $PDE8A_C$ showed two peaks representing a dimer and monomer with a majority of $PDE8A_C$ eluting as a dimer (Figure 3.9). Given that PDE8A and other PDEs exist as dimers in solution (Conti and Beavo 2007), we tested the possibility that a PDE dimer ($PDE8A_C$) interacted with monomeric RIα that included both CNB domains ($RI\alpha_{AB}$).

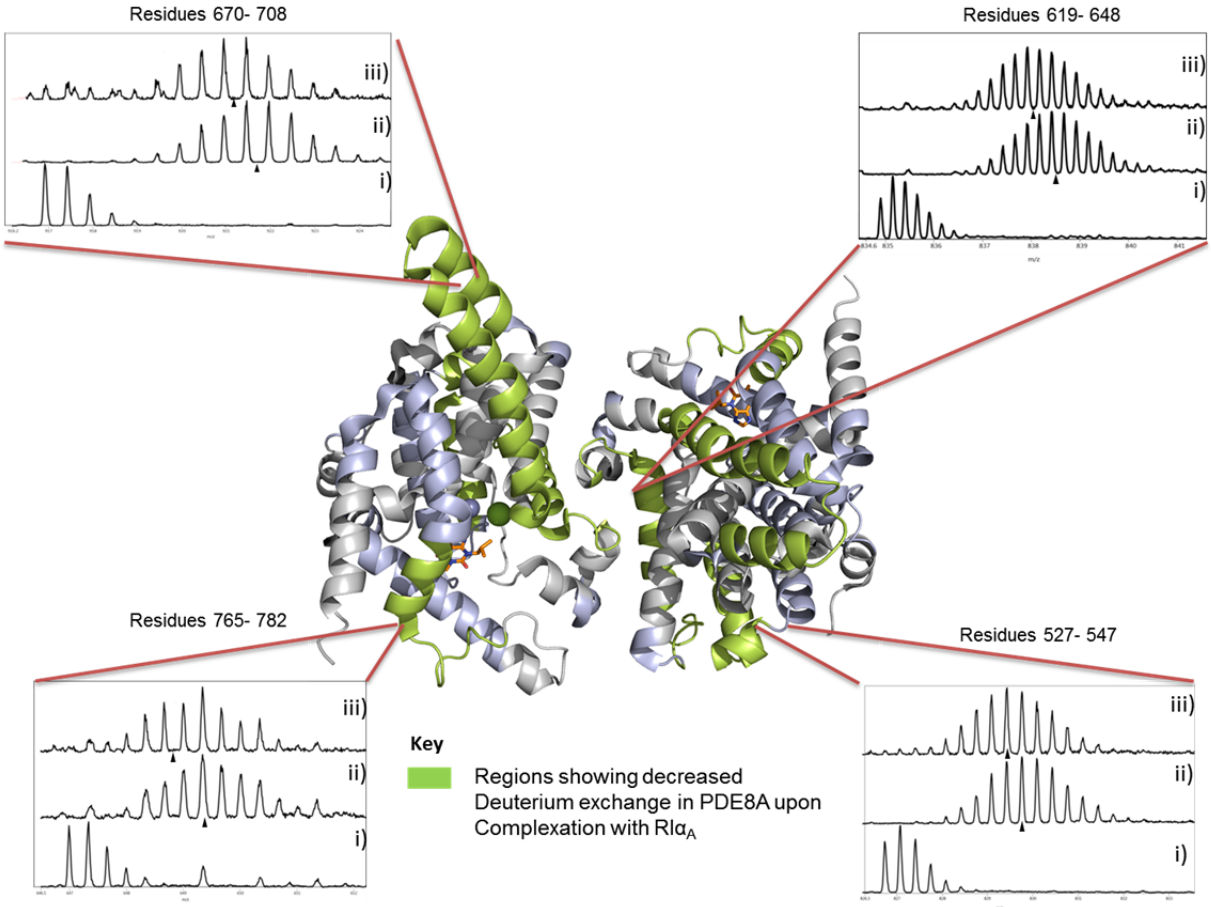

Figure 3.10: ***Map of the RIa_A interaction interface on the catalytic domain of full-length PDE8A:*** Effects of $RI\alpha_A$ interactions with the catalytic PDE domain of full-length PDE8A by HDXMS is mapped onto the dimeric structure of $PDE8A_C$ (PDB ID: 3ECN). Regions of the $PDE8A_C$ that show significant reduction in deuterium exchange upon complex formation are colored green, regions showing no difference in exchange are white. Regions for which no coverage was obtained are in light blue. Mass spectra of peptides showing significant changes upon $RI\alpha_A$ complex formation (Difference>1Da) are shown. The isotopic envelopes of pepsin fragment peptides of i) Undeuterated control of PDE8A ii) free PDE8A after 2 min deuteration iii) PDE8A in a complex with $RI\alpha_A$ after 2 min deuteration are depicted. Centroids are indicated (▲).

We subsequently carried out HDXMS of the $PDE8A_C$: $RI\alpha_{AB}$ complex to map the interface of $RI\alpha_{AB}$ on the surface of $PDE8A_C$. A total of 69 peptides were observed and analyzed by HDXMS, which

corresponds to a coverage of 81% of the primary sequence of $PDE8A_C$. On $PDE8A_C$, regions spanning the conserved catalytic residues showed decreased exchange in the $PDE8A_C$-$RI\alpha_{AB}$ complex (Figure 3.11 and 3.12), and overlapped with the regions that showed decreased exchange in full length PDE8A.

In the inverse HDXMS experiment to map the interaction of $PDE8A_C$ onto the surface of $RI\alpha_{AB}$ in the $RI\alpha_{AB}$:$PDE8A_C$ complex, 49 peptides were observed and quantified, corresponding to a coverage of 80% of the primary sequence of $RI\alpha_{AB}$. The $RI\alpha_{AB}$:$PDE8A_C$ complex was generated by incubating $RI\alpha_{AB}$ with a 3-X molar excess of $PDE8A_C$ for 1 h to ensure all the cAMP bound is fully dissociated from the complex. Interestingly, results for $RI\alpha_{AB}$ showed decreased exchange at both cAMP binding sites (CNB-A and CNB-B) and across regions connecting these two domains (Figure 3.13 and 3.14). Sites showing the greatest shifts in deuterium exchange upon complexation with $PDE8A_C$ thus were not only at the binding sites but also at flanking allosteric sites important for propagation of the effects of cAMP binding. Importantly, N-terminal regions of $RI\alpha_{AB}$ spanning the PKA pseudosubstrate site showed only minor changes in deuterium exchange upon complexation with $PDE8A_C$. A table summarizing deuterium exchange for all the peptides from $PDE8A_C$ and $RI\alpha_{AB}$ across all time points is in Table 3.1 and 3.2.

The effects of cAMP binding on $RI\alpha_{AB}$ (Figure 3.15A, top panel) were different from the effects of PDE complexation (Figure 3.14, bottom panel). This is summarized in Figure 3.15A (bottom panel). cAMP binding results in large decreases in deuterium exchange that are largely within the specific binding pockets in CNB-A and CNB-B. $PDE8A_C$ complexation on the other hand shows smaller magnitude decreases in the cAMP binding sites but shows protein-wide decreases in deuterium exchange (Figure 3.15B) and specifically in the N-terminus and the interdomain α:C helix.

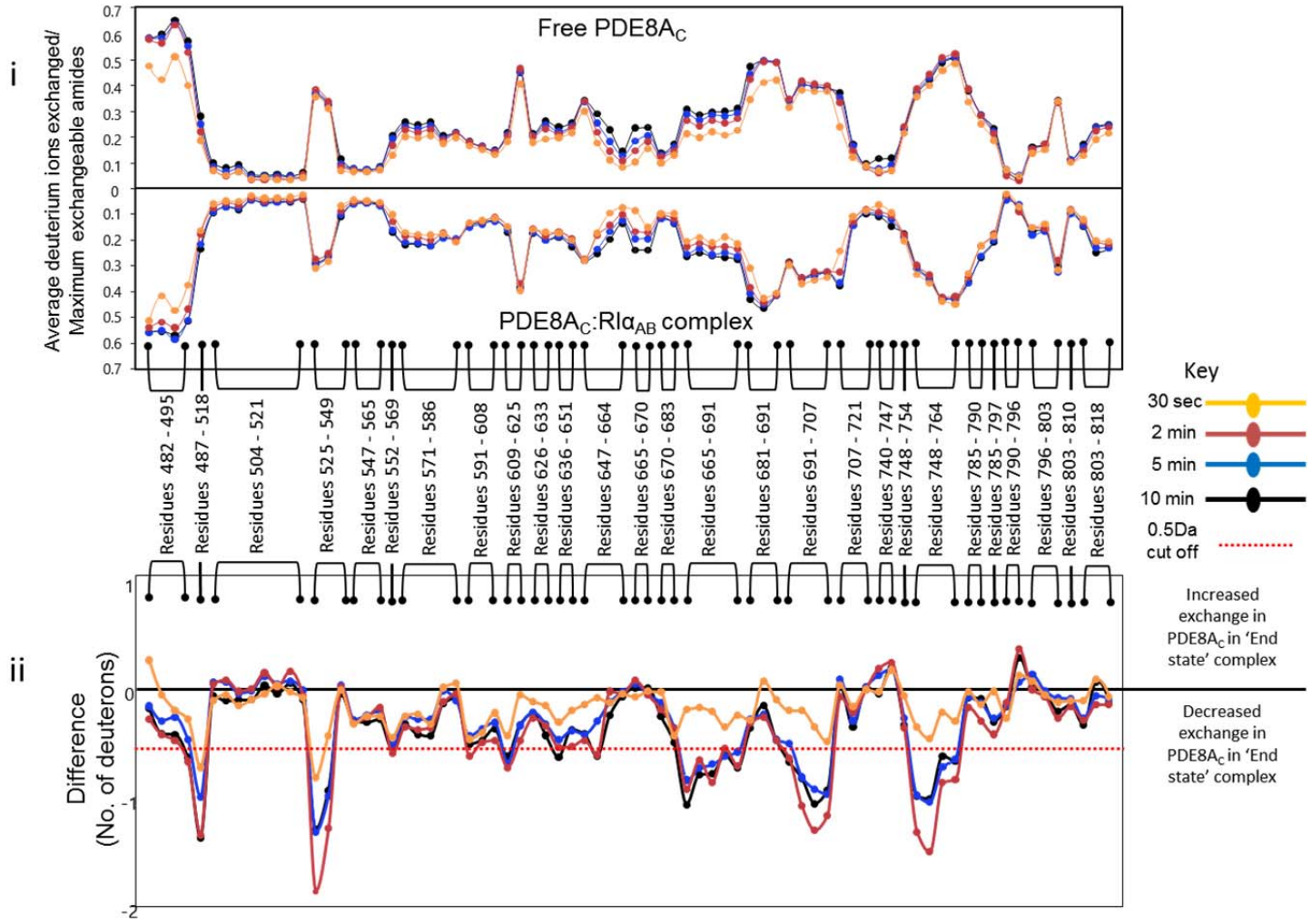

Figure 3.11: ***Protein-wide overview of interaction of RIα$_{AB}$ on PDE8A$_C$***: A) i) 'Mirror' plot representation for comparative analysis of HDXMS of free PDE8A$_C$ (catalytic domain) and in the presence of RIα$_{AB}$. The relative deuterium exchange (y-axis) of each pepsin digest fragment is listed from the N to C terminus (x-axis) of PDE8A$_C$, with deuterium exchange times color coded as per key. In this plot, relative deuterium exchange (y axis) of free PDE8A$_C$ (upper half) is compared with relative deuterium exchange of PDE8A$_C$ in complex with RIα$_{AB}$ (lower half). In the bottom panel the absolute difference in numbers of deuterons (inferred from difference in mass in Daltons (Da)) (y-axis) between the free and complexed state is plotted for each pepsin digest fragment listed from the N to C terminus (x-axis) of PDE8A$_C$ for each Deuterium exchange time point (t= 0.5, 2, 5, 10 min) in a 'difference plot'. Shifts in the positive scale represent increases in deuterium exchange and shifts in the negative scale represent decreases in deuterium exchange. A difference of 0.5 Da is considered significant, and is represented by a dashed red line. Plots were generated using the DynamX software (Version 2.0, Waters, Milford). Each point represents a pepsin digest fragment and brackets group overlapping fragment peptides.

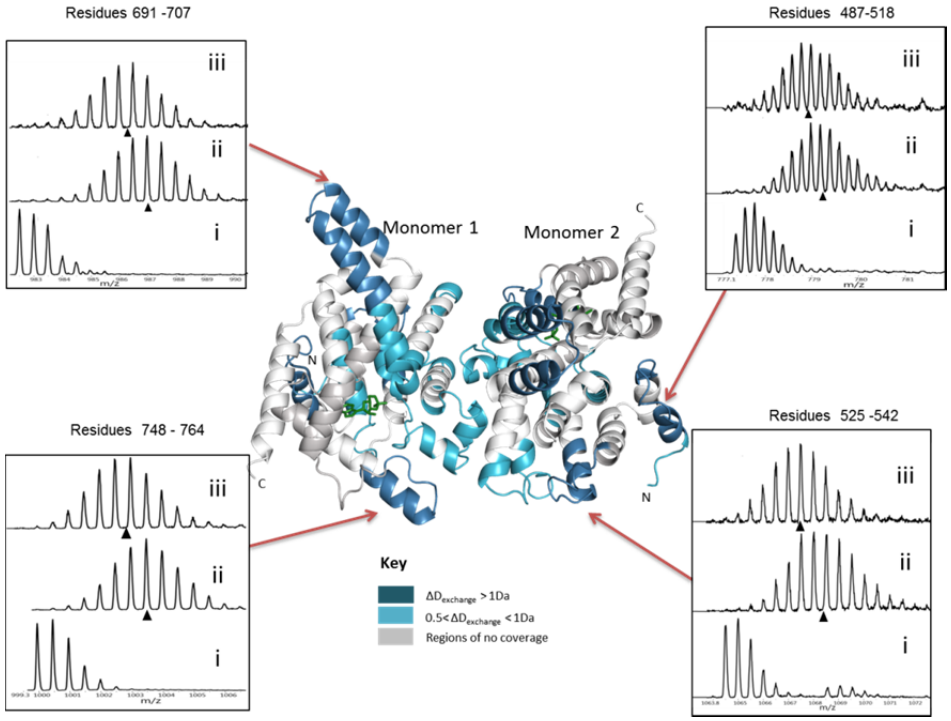

Figure 3.12: Effects of RIα$_{AB}$ interactions from HDXMS analysis mapped onto the dimeric structure of PDE8A$_C$ (PDB ID: 3ECN), IBMX at the active site is in green. Regions of PDE8A$_C$ showing significant decreases in deuterium exchange upon complex formation are colored in shades of blue. Mass spectra of peptides showing significant changes upon RIα $_{AB}$ complex formation (Difference>1 Da) are shown. The isotopic envelopes of pepsin fragment peptides of i) Undeuterated control of PDE8A$_C$ ii) Free PDE8A$_C$ after 2 min deuteration iii) PDE8A$_C$ in a complex with RIα$_{AB}$ after 2 min deuteration are depicted. Centroids are indicated (▲).

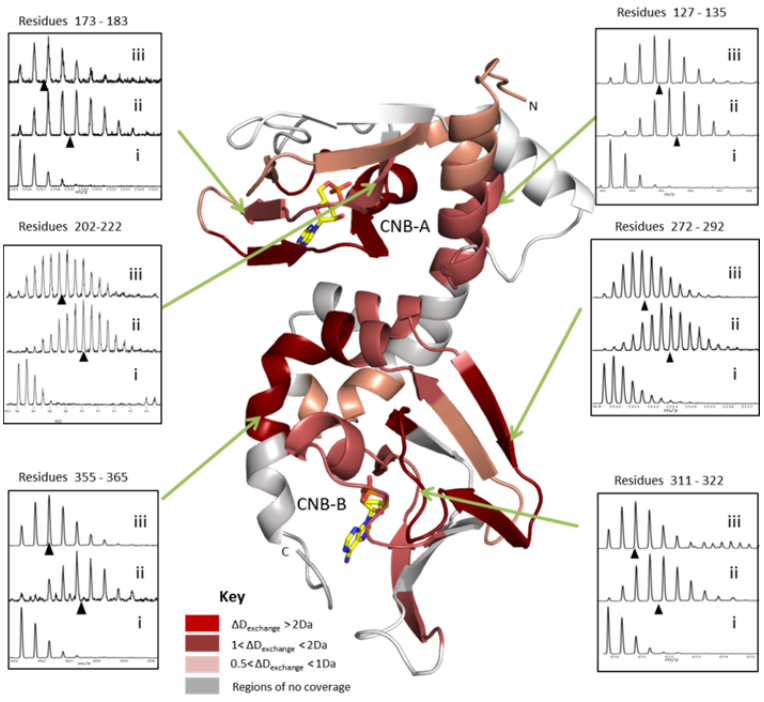

Figure 3.13: A summary of results from HDXMS analysis is mapped onto the structure of cAMP-bound RIα(113-379) (PDB ID: 1RGS). Regions in RIα(113-379) that show significant reduction in deuterium exchange upon complex formation are colored in shades of red. cAMP is shown in stick representation (C: yellow, O: red, N: blue). Mass spectra of peptides showing significant changes upon PDE8A$_C$ complex formation (Difference>1 Da) are shown. The isotopic envelopes of pepsin fragment peptides of i) Undeuterated control of RIα$_{AB}$ ii) Free RIα$_{AB}$ after 2 min deuterium exchange iii) RIα$_{AB}$ in a complex with PDE8A$_C$ after 2 min deuterium exchange are depicted. Centroids are indicated (▲).

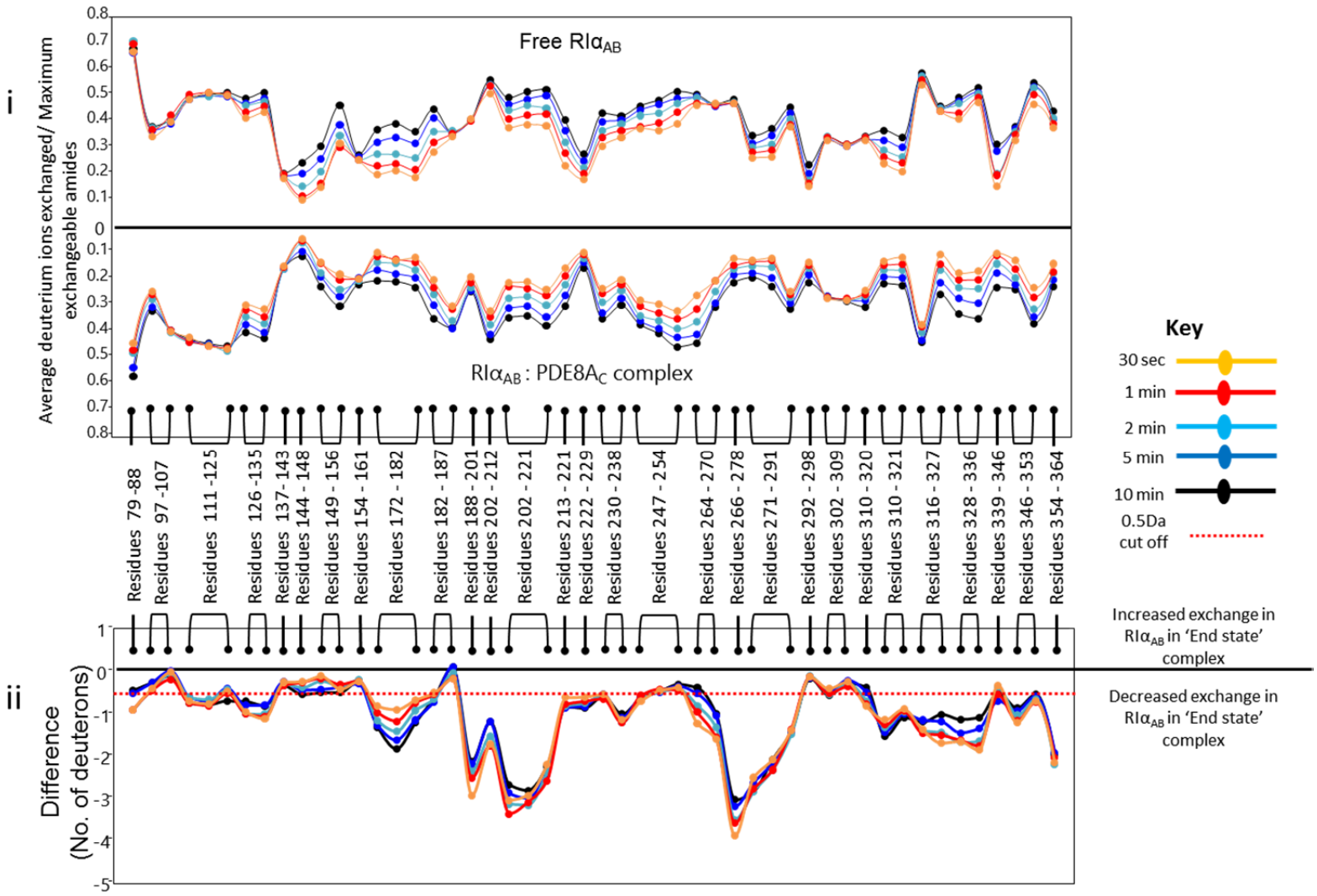

Figure 3.14: ***Protein-wide overview of interaction of PDE8A$_C$ on RIα$_{AB}$:*** A) i)'Mirror' plot representation for comparative analysis of HDXMS of free RIα$_{AB}$ bound to PDE8A$_C$. In this plot, relative deuterium exchange (y axis) of free RIα$_{AB}$ (upper half) is compared with relative deuterium exchange of RIα$_{AB}$ complexed to PDE8A$_C$ (lower half). Difference Plot ii) shows the difference in absolute number of deuterons exchanged between the two states. Negative values indicate decreased exchange upon complexation with PDE8A$_C$. Plots were generated using the DynamX software (Version 2.0, Waters, Milford). Each point represents a pepsin digest fragment and brackets group overlapping fragment peptide

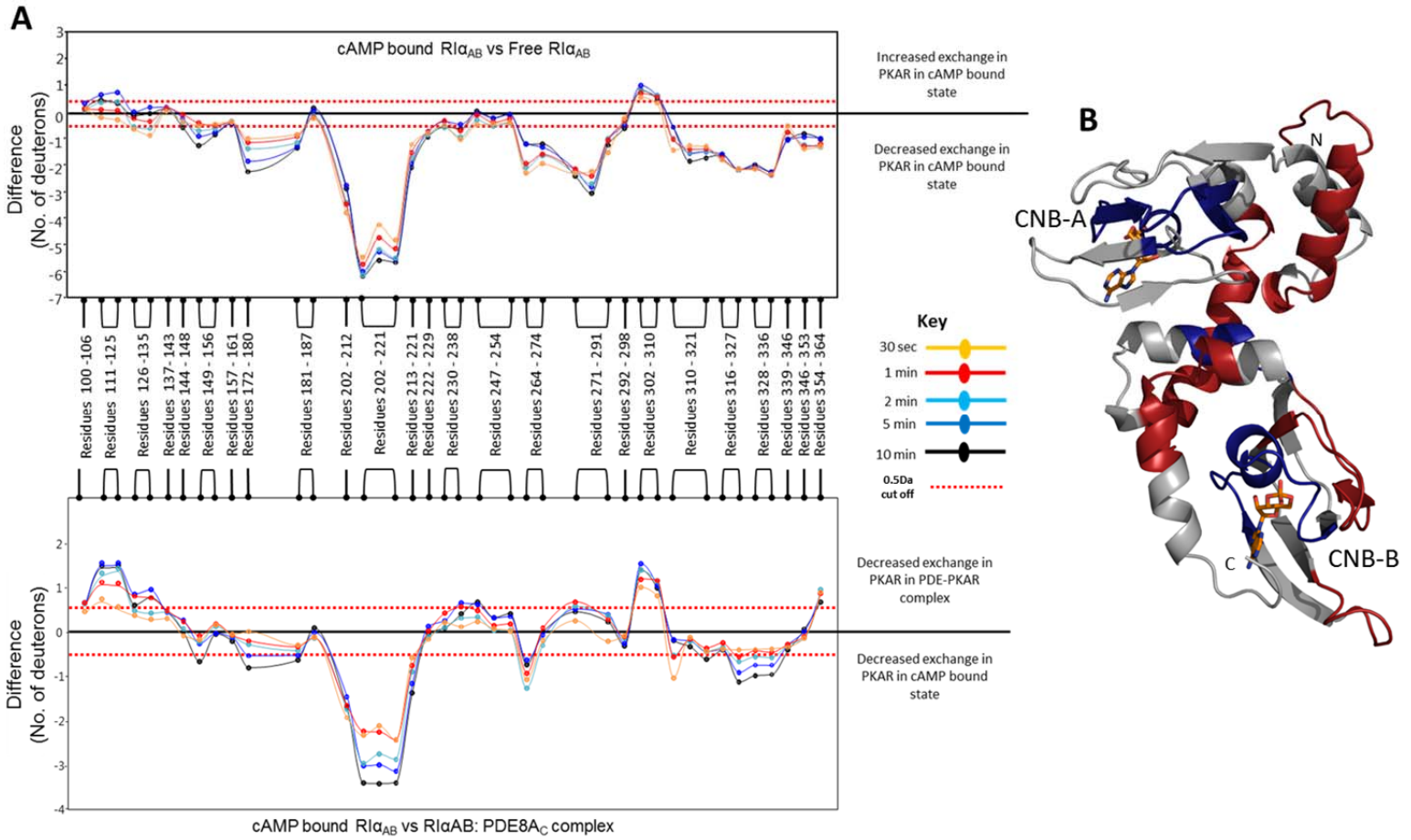

Figure 3.15: ***RIα$_{AB}$ adopts distinct conformations in cAMP bound and 'End state' complex forms:*** A) Top panel; Difference plot comparing RIα$_{AB}$ in the cAMP bound state to the *apo* state (top panel). Peptides in the positive range represent increased deuterium exchange in the cAMP bound state as compared to the *apo* state, while peptides in the negative range represent cAMP induced protection. Bottom panel; Difference plot comparing RIα$_{AB}$ in the cAMP bound state to the 'End state' complex. Peptides in the positive range indicate peptides showing decreased deuterium exchange in the 'End state' complex in comparison to the *apo* state, while peptides in the negative range represent peptides showing decreased deuterium exchange in the cAMP bound state in comparison to the 'End state' complex. Peptide residue numbers, from the N to C terminal of RIα$_{AB}$, are marked along the x-axis; absolute difference in deuterons (Daltons (Da)) is marked along the y-axis. Each point represents a pepsin digest fragment and brackets group overlapping fragment peptides. Deuterium exchange labeling times are colored according to key. B) Results from the cAMP bound state vs 'End state' complex difference plot were plotted onto the structure of RIα (PDB ID: 1RGS). Regions in red show greater protection in 'End state' complex while regions in blue show greater protection in the cAMP bound state. cAMP molecules are depicted as orange sticks bound to CNB-A and CNB-B.

Table 3.1: Summary of H/D exchange data for free PDE8A$_C$ and PDE8A$_C$ bound to RIα$_{AB}$. Peptides showing significant differences (>0.5 Da) are in bold.

No.	Pepsin Digest Fragments of PDE8A$_C$ (m/z)	Charge (z)	Residue nos.	Maximum Exchangeable amides	Maximum deuterons exchanged after 2 min	
					Free PDE8A$_C$ (mean ± SD)	PDE8A$_C$: RIα$_{AB}$ complex (mean±SD)
1	**DDVPPRIARA *(555.303)***	**2**	**482-491**	**7**	**4.06 ± 0.01**	**3.79 ± 0.07**
2	**DDVPPRIARAME *(685.344)***	**2**	**482-493**	**9**	**5.08 ± 0.00**	**4.66 ± 0.02**
3	**DDVPPRIARAMENE *(801.887)***	**2**	**482-495**	**11**	**6.07 ± 0.02**	**5.60 ± 0.10**
4	PPRIARA *(390.741)*	2	485-491	5	3.16 ± 0.02	2.70 ± 0.04
5	**RIARAMENEEYWDFDIFELEAATHNR PLIYLG *(777.378)***	**5**	**487-518**	**30**	**6.72 ± 0.08**	**5.28 ± 0.04**
6	ELEAATHNRPLIY *(763.898)*	2	504-516	11	0.79 ± 0.08	0.84 ± 0.05
7	ELEAATHNRPLIYL *(820.44)*	2	504-517	12	0.60 ± 0.05	0.67 ± 0.05
8	LEAATHNRPLIY *(699.377)*	2	505-516	10	0.67 ± 0.03	0.64 ± 0.04
9	LEAATHNRPLIYLGLKM *(647.359)*	3	505-521	15	0.55 ± 0.08	0.68 ± 0.04
10	EAATHNRPLIYL *(699.377)*	2	506-517	10	0.38 ± 0.06	0.48 ± 0.05
11	ATHNRPLIYL (*599.337)*	2	508-517	8	0.32 ± 0.03	0.34 ± 0.01
12	LGLKM *(561.342)*	1	517-521	4	0.21 ± 0.00	0.16 ± 0.04
13	**FGICEFLHCSESTLRSWL *(1064.499)***	**2**	**525-542**	**17**	**6.55 ± 0.04**	**4.67 ± 0.02**
14	**CSESTLRSWLQIIEAN (*925.455)***	**2**	**533-548**	**15**	**5.10 ± 0.03**	**3.78 ± 0.04**
15	**QIIEANY *(850.430)***	**1**	**543-549**	**6**	**5.10 ± 0.03**	**3.78 ± 0.04**
16	ANYHSSNPYHNSTHSADVL *(705.310)*	3	547-565	17	1.25 ± 0.06	0.90 ± 0.07

17	NYHSSNPYHNSTHSADVL *(681.631)*	3	548-565	16	1.06 ± 0.06	0.80 ± 0.00
18	**SNPYHNSTHSADVLHATA *(641.293)***	**3**	**552-569**	**16**	**2.51 ± 0.09**	**1.68 ± 0.03**
19	FLSKERIKE *(575.331)*	2	571-579	8	1.81 ± 0.03	1.47 ± 0.06
20	FLSKERIKETLDPIDE *(645.009)*	3	571-586	14	3.03 ± 0.10	2.66 ± 0.05
21	LSKERIKETLDPIDE *(595.986)*	3	572-586	13	2.98 ± 0.09	2.62 ± 0.06
22	RIKETLDPIDE *(664.853)*	2	576-586	9	1.68 ± 0.04	1.56 ± 0.00
23	TLDPIDE *(802.382)*	1	580-586	5	1.07 ± 0.00	1.02 ± 0.01
24	**IAATIHDVDHPGRTNS *(568.615)***	**3**	**591-606**	**14**	**2.50 ± 0.01**	**1.90 ± 0.05**
25	**IAATIHDVDHPGRTNSF *(617.633)***	**3**	**591-607**	**15**	**2.37 ± 0.04**	**1.92 ± 0.03**
26	**IAATIHDVDHPGRTNSFL *(655.332)***	**3**	**591-608**	**16**	**2.29 ± 0.03**	**1.81 ± 0.04**
27	**CNAGSELAILYNDT *(742.336)***	**2**	**609-622**	**13**	**2.66 ± 0.04**	**1.91 ± 0.10**
28	ESHHAAL *(373.684)*	2	626-632	6	1.20 ± 0.00	0.94 ± 0.04
29	ESHHAALA *(418.202)*	2	626-633	7	1.62 ± 0.01	1.29 ± 0.02
30	**LTTGDDKCNIFKNM *(800.375)***	**2**	**636-649**	**13**	**2.85 ± 0.01**	**2.05 ± 0.01**
31	**TGDDKCNIFKNMER *(835.881)***	**2**	**638-651**	**13**	**3.06 ± 0.00**	**2.53 ± 0.10**
32	**KNMERNDY *(535.236)***	**2**	**647-654**	**7**	**2.37 ± 0.03**	**1.91 ± 0.07**
33	**KNMERNDYRTLRQGIIDM *(751.707)***	**3**	**647-664**	**17**	**3.76 ± 0.01**	**3.07 ± 0.00**
34	RTLRQGIID *(536.313)*	2	655-663	8	1.16 ± 0.01	1.14 ± 0.06
35	LRQGIID *(814.478)*	1	657-663	6	0.64 ± 0.00	0.60 ± 0.01
36	VLATE *(532.297)*	1	665-669	4	0.59 ± 0.01	0.67 ± 0.04
37	VLATEM *(663.338)*	1	665-670	5	0.94 ± 0.02	0.86 ± 0.04
38	**VLATEMTKHFEHVNKFVNSINKPLAT *(742.892)***	**4**	**665-690**	**24**	**6.31 ± 0.08**	**5.40 ± 0.07**

39	**ATEMTKHFEHVNKFVNSINKPLAT *(689.854)***	**4**	**667-691**	**22**	**5.31 ± 0.10**	**4.67 ± 0.03**
40	**ATEMTKHFEHVNKFVNSINKPLATL *(718.125)***	**4**	**667-692**	**23**	**6.03 ± 0.18**	**5.22 ± 0.16**
41	MTKHFEHVNKF *(473.235)*	3	670-680	10	1.23 ± 0.04	1.05 ± 0.04
42	MTKHFEHVNKFVNS *(573.282)*	3	670-683	13	1.87 ± 0.08	1.50 ± 0.02
43	**MTKHFEHVNKFVNSINKPLAT *(819.097)***	**3**	**670-690**	**19**	**4.84 ± 0.10**	**4.29 ± 0.04**
44	**MTKHFEHVNKFVNSINKPLATL *(856.792)***	**3**	**670-691**	**20**	**5.41 ± 0.07**	**4.72 ± 0.04**
45	VNSINKPLAT (*528.802)*	2	681-690	8	3.38 ± 0.02	3.08 ± 0.02
46	INKPLAT *(756.461)*	1	684-690	5	2.46 ± 0.01	2.21 ± 0.01
47	INKPLATL *(435.272)*	2	684-691	6	2.93 ± 0.01	2.46 ± 0.00
48	**LEENGETDKNQE *(703.304)***	**2**	**691-702**	**11**	**3.85 ± 0.00**	**3.17 ± 0.05**
49	**LEENGETDKNQEVINT *(916.925)***	**2**	**691-707**	**15**	**6.30 ± 0.05**	**5.17 ± 0.00**
50	**LEENGETDKNQEVINTM *(982.445)***	**2**	**691-708**	**16**	**6.49 ± 0.09**	**5.20 ± 0.02**
51	**EENGETDKNQEVINTM *(925.903)***	**2**	**692-708**	**15**	**5.99 ± 0.08**	**4.82 ± 0.01**
52	MLRTPENRTL *(615.831)*	2	707-716	8	2.65 ± 0.05	2.59 ± 0.03
53	LIKRML (*387.253)*	2	716-721	5	0.42 ± 0.01	0.41 ± 0.04
54	WAARISE *(416.715)*	2	740-746	6	0.35 ± 0.00	0.55 ± 0.02
55	WAARISEE *(481.236)*	2	740-747	7	0.49 ± 0.03	0.74 ± 0.03
56	**YFSQTDE *(889.357)***	**1**	**748-754**	**6**	**1.50 ± 0.01**	**1.09 ± 0.01**
57	**YFSQTDEEKQQGLPVVM *(999.974)***	**2**	**748-764**	**15**	**5.79 ± 0.04**	**4.48 ± 0.03**
58	**FSQTDEEKQQGLPVVM *(918.44)***	**2**	**749-764**	**14**	**6.19 ± 0.03**	**4.70 ± 0.02**
59	**DEEKQQGLPVVM *(686.839)***	**2**	**753-764**	**10**	**5.09 ± 0.01**	**4.21 ± 0.12**

60	**EKQQGLPVVM *(564.804)***	**2**	**755-764**	**8**	**4.17 ± 0.03**	**3.34 ± 0.04**
61	FITDM *(626.285)*	1	785-789	4	1.55 ± 0.02	1.38 ± 0.01
62	FITDMF *(773.353)*	1	785-790	5	1.47 ± 0.04	1.12 ± 0.04
63	FITDMFDAWDAFV *(789.349)*	2	785-797	12	2.56 ± 0.03	2.13 ± 0.02
64	FDAWDA *(724.293)*	1	790-795	5	0.25 ± 0.02	0.12 ± 0.04
65	FVDLPDL *(818.429)*	1	796-802	5	0.78 ± 0.03	0.76 ± 0.00
66	VDLPDL *(671.361)*	1	797-802	4	0.68 ± 0.02	0.61 ± 0.02
67	MQHLDNNF *(509.7205)*	2	803-810	7	0.72 ± 0.03	0.57 ± 0.01
68	MQHLDNNFKYWKGLDE *(679.983)*	3	803-818	15	2.15 ± 0.09	1.91 ± 0.01
69	FKYWKGLDE *(593.297)*	3	810-818	8	1.79 ± 0.04	1.65 ± 0.01

Table 3.2: Summary of H/D exchange data for free $RI\alpha_{AB}$ and $RI\alpha_{AB}$ bound to $PDE8A_C$. Peptides showing significant differences (>0.5 Da) are in bold.

No.	**Pepsin Digest Fragments of $RI\alpha_{AB}$ (m/z)**	**Charge (z)**	**Residue nos.**	**Maximum Exchangeable amides**	**Maximum deuterons exchanged after 2 mins**	
					Free $RI\alpha_{AB}$ (mean±SD)	**$RI\alpha_{AB}$: $PDE8A_C$ complex (mean±SD)**
1	**EISPPPPNPV *(523.775)***	**2**	**79-88**	**4**	**2.8 ± 0.15**	**1.9 ± 0.03**
2	AISAE *(490.215)*	1	97-101	4	1.5 ± 0.02	1.1 ± 0.02
3	AEVYTEE *(840.362)*	1	100-106	6	2.5 ± 0.1	2.4 ± 0.04
4	**YVRKVIPKDYKTM *(547.64)***	**3**	**111-123**	**11**	**5.4 ± 0.08**	**4.8 ± 0.09**
5	**YVRKVIPKDYKTMAA *(594.996)***	**3**	**111-125**	**13**	**6.5 ± 0.18**	**5.8 ± 0.09**
6	**VRKVIPKDYKTMAA *(540.643)***	**3**	**112-125**	**12**	**6.1 ± 0.1**	**5.6 ± 0.09**

7	**LAKAIEKNV *(493.604)***	**2**	**126-134**	**8**	**3.7 ± 0.08**	**2.7 ± 0.04**
8	**LAKAIEKNVL *(549.845)***	**2**	**126-135**	**9**	**4.3 ± 0.07**	**3.3 ± 0**
9	FSHLDDNE *(488.700)*	2	136-143	7	1.4 ± 0.01	1.1 ± 0.02
10	RSDIF *(637.33)*	1	144-148	4	0.6 ± 0.04	0.2 ± 0.01
11	DAMFPVSF *(913.412)*	1	149-156	6	1.3 ± 0	1.1 ± 0.04
12	FPVSF *(596.308)*	1	153-156	3	1.1 ± 0	0.7 ± 0
13	IAGET *(490.251)*	1	157-161	4	1 ± 0.02	0.8 ± 0.01
14	**FYVIDQGEM *(1101.49)***	**1**	**172-180**	**8**	**2.2 ± 0.05**	**1.1 ± 0.01**
15	**FYVIDQGEMDV *(1315.59)***	**1**	**172-182**	**10**	**2.8 ± 0.13**	**1.4 ± 0.1**
16	**YVIDQGEMDV *(1168.519)***	**1**	**173-182**	**9**	**2.4 ± 0.06**	**1.5 ± 0.04**
17	**DVYVNNE *(852.3734)***	**1**	**181-187**	**6**	**2.2 ± 0.04**	**1.5 ± 0.02**
18	YVNNE *(638.278)*	1	183-187	4	1.5 ± 0.02	1.4 ± 0.04
19	**WATSVGEGGSFGEL *(698.818)***	**2**	**188-201**	**13**	**5.3 ± 0.10**	**3.0 ± 0.02**
20	**ALIYGTPRAAT *(567.315)***	**2**	**202-212**	**9**	**4.9 ± 0.05**	**3.4 ± 0.04**
21	**ALIYGTPRAATVKAKTNVKL *(705.753)***	**3**	**202-221**	**18**	**8.0 ± 0.16**	**4.9 ± 0.01**
22	**LIYGTPRAATVKAKTNVK *(644.38)***	**3**	**203-220**	**16**	**7.4 ± 0.17**	**4.2 ± 0.08**
23	**YGTPRAATVKAKTNVKL *(606.686)***	**3**	**205-221**	**15**	**6.7 ± 0.20**	**4.4 ± 0.03**
24	**VKAKTNVKL *(500.825)***	**2**	**213-221**	**8**	**2.6 ± 0.04**	**1.8 ± 0.02**
25	**WGIDRDSY *(506.225)***	**2**	**221-229**	**7**	**1.6 ±0.03**	**0.8 ± 0.00**
26	**RRILMGST *(467.265)***	**2**	**230-237**	**7**	**2.6 ± 0.02**	**2.0 ± 0.10**
27	**RRILMGSTL *(523.805)***	**2**	**230-238**	**8**	**3.1 ± 0.04**	**1.9 ± 0.01**
28	**FLSKVSIL *(453.793)***	**2**	**247-254**	**7**	**3.0 ± 0.14**	**2.4 ± 0.01**
29	**LSKVSIL *(759.497)***	**1**	**248-254**	**6**	**2.6 ± 0.06**	**2.1 ± 0**
30	**SKVSIL *(646.413)***	**1**	**249-254**	**5**	**2.4 ± 0.02**	**1.9 ± 0.00**

31	**TVADALE *(718.361)***	**1**	**264-270**	**6**	**3.0 ± 0.09**	**2.2 ± 0.04**
32	**ADALEPVQFEDGQ *(709.82)***	**2**	**266-278**	**11**	**5.3 ± 0.15**	**1.8 ± 0.00**
33	**DALEPVQF *(918.456)***	**1**	**267-274**	**6**	**2.8 ± 0.06**	**1.5 ± 0.00**
34	**PVQFEDGQKIVVQGEPGDEF *(1109.535)***	**2**	**271-290**	**18**	**5.5 ± 0.09**	**2.6 ± 0.04**
35	**EDGQKIVVQGEPGDEF *(873.91)***	**2**	**275-290**	**14**	**4.4 ± 0.07**	**2.1 ± 0.01**
36	**IVVQGEPGDEFF *(668.82)***	**2**	**280-291**	**10**	**4.1 ± 0.08**	**2.7 ± 0.05**
37	IILEGSA *(702.403)*	1	292-298	6	1.1 ± 0.02	0.9 ± 0.00
38	QRRSENEE *(524.24)*	2	302-309	7	2.4 ± 0.06	1.9 ± 0.05
39	QRRSENEEF *(597.775)*	2	302-310	8	2.5 ± 0.05	2.2 ± 0.01
40	**FVEVGRLGPSDY *(669.835)***	**2**	**310-321**	**10**	**3.0 ± 0.06**	**1.6 ± 0.01**
41	**VEVGRLGPSDY *(596.3)***	**2**	**311-321**	**9**	**2.4 ± 0.04**	**1.5 ± 0.07**
42	**LGPSDYFGEI *(549.26)***	**1**	**316-325**	**8**	**4.6 ± 0.05**	**3.2 ± 0.00**
43	**FGEIAL *(649.355)***	**1**	**322-327**	**5**	**2.3 ± 0.04**	**0.8 ± 0.01**
44	**LMNRPRAAT *(1029.562)***	**2**	**328-336**	**7**	**3.3 ± 0.02**	**1.6 ± 0.01**
45	**MNRPRAAT *(458.739)***	**2**	**329-336**	**6**	**3.1 ± 0.04**	**1.4 ± 0.04**
46	ARGPLKCV *(422.243)*	2	339-346	6	1.2 ± 0.07	0.8 ± 0.07
47	**VKLDRPRF *(515.805)***	**2**	**346-353**	**6**	**2.2 ± 0.05**	**1.2 ± 0.02**
48	**LDRPR *(328.692)***	**2**	**348-352**	**3**	**1.6 ± 0.01**	**0.9 ± 0.01**
49	**ERVLGPCSDIL *(601.31)***	**2**	**354-364**	**9**	**3.8 ± 0.01**	**1.6 ± 0.01**

3.3.6 Real time monitoring of PDE8-mediated dissociation of cAMP bound to the PKA R-subunit

We then set out to explore if HDXMS was able to monitor in real time, dissociation of bound cAMP upon complexation with $PDE8A_C$ as has previously been shown with RegA and $RI\alpha_A$

(Krishnamurthy, Moorthy et al. 2013). This would result in progression of PDE-PKAR interactions from an 'Encounter' complex ($RI\alpha_{AB}$: cAMP: $PDE8A_C$) to an 'End state' complex ($RI\alpha_{AB}$: $PDE8A_C$). The PDE-PKAR interactions described in the earlier section represent the 'End state' complex in the reaction. We monitored the effects of cAMP on *Apo* $RI\alpha_{AB}$ dynamics by HDXMS by focusing on a peptide spanning the cAMP binding site (residues 202-221). The peptide in *apo* $RI\alpha_{AB}$ shows the most deuterium exchange (Figure 3.16A), compared to the cAMP-bound state (Figure 2.16B), consistent with cAMP binding the pocket with high affinity (Badireddy, Yunfeng et al. 2011). Even in the absence of excess cAMP, this region shows low levels of deuteration even after 1 h of deuterium exchange. This is interesting as it indicates a stable interaction and reflects the high affinity of cAMP for the R-subunit. Interestingly the 'End state' complex (Figure 3.16C, centroid indicated in blue) exchanges deuterium at a level intermediate to the *apo* (centroid indicated in red) and cAMP-bound states (centroid indicated in green). This further indicates that PDE association and cAMP binding to the *apo* protein alter dynamics in distinct ways.

According to the previously described model (Moorthy, Gao et al. 2011), PDEs would 'encounter' cAMP bound RIα and begin the dissociation-hydrolysis cycle. To probe this dissociation- hydrolysis cycle in real time, we carried out HDXMS of cAMP bound $RI\alpha_{AB}$ in the presence of substoichiometric amounts of $PDE8A_C$. The reaction was initiated by adding $PDE8A_C$ to cAMP bound RIα at a lower 1:3 molar ratio simultaneously with D_2O buffer and the reaction was monitored in a time dependent manner, as described in materials and methods. Peptides from both PKA $RI\alpha_{AB}$ and $PDE8A_C$ were analyzed in parallel to monitor dynamics of the proteins in the 'Encounter' complex.

The global deuterium exchange profile of cAMP bound RIα in the 'Encounter' complex for early time points show a close correlation to cAMP bound RIα (Figure 3.17) top panel). A comparison of $RI\alpha_{AB}$ in the 'Encounter' state complex with the 'End state' complex is summarized in Figure 3.18 bottom panel.

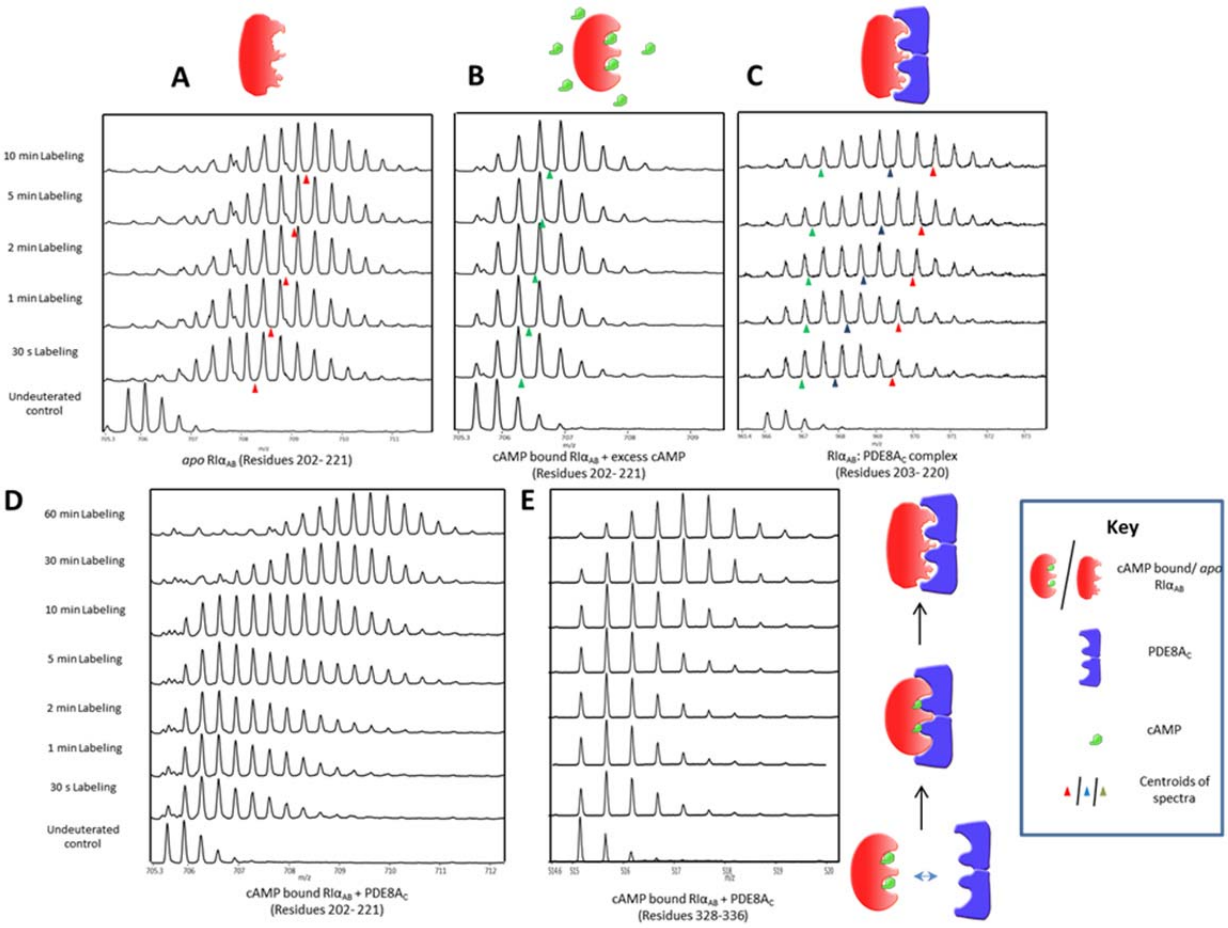

Figure 3.16: ***PDE8A$_C$ mediates dissociation of cAMP bound to both CNB-A and CNB-B of RIα$_{AB}$*****:** Mass spectra of peptide spanning cAMP binding pocket of A) *apo* RIα$_{AB}$ in CNB-A domain at different deuterium labeling times. Red triangle indicates centroid. B) cAMP-bound RIα$_{AB}$ in the presence of excess cAMP. Green triangle indicates centroid. C) PDE8A$_C$-bound *apo* RIα$_{AB}$ ('End state' complex). Blue triangle indicates centroid, red and blue indicate centroid values for *apo* and cAMP-bound states respectively and are shown for comparison. Mass spectra of peptide spanning cAMP binding pockets in CNB-A (D) and CNB-B (E) for cAMP-bound RIα in the presence of substoichiometric amounts of PDE8AC ('Encounter' complex).

Closer inspection of the peptides spanning the cAMP binding regions, residues 202-212 in CNB-A and residues 328-336 in CNB-B, reveals these regions to exhibit a bimodal distribution in deuterium exchange kinetics (Figure 3.16 D and E). Bimodal distributions generally indicate the prevalence of EXI mode of exchange kinetics (Weis, Wales et al. 2006), caused by local unfolding and refolding events at specific loci of the protein. However, in this particular example, cAMP dissociation from the cAMP binding pocket of RIα$_{AB,}$ occurs in a time dependent manner, resulting in the presence of three

distinct forms of $RI\alpha_{AB}$, namely an *apo* form, cAMP bound form and a PDE bound form (as seen in Figure 3.16 A, B and C). These three forms exist in a constantly changing dynamic equilibrium which is dependent on the rate of PDE binding, cAMP dissociation and hydrolysis. At earlier time points the cAMP bound form is most prevalent, but as the reaction proceeds with increasing labeling times, $RI\alpha_{AB}$ tends towards the *apo* form because of increasing dissociation of cAMP. Almost all present $RI\alpha_{AB}$ is in the *apo* form by 30 min. All three forms exist in varying ratios at any given point in time, which results in a time dependent bimodal distribution due to ensemble averaging in HDXMS.

Peptides from $PDE8A_C$ in the 'Encounter' complex were also analyzed to probe the dynamics of $PDE8A_C$ in a catalytically active state. Comparison of $PDE8A_C$ in the 'encounter' state with the *apo* state reveals that regions responsible for cAMP binding show decreased deuterium exchange, while certain regions also show increased deuterium exchange (Figure 3.18, top panel). The presence of both decreased dynamics and increased dynamics within the same protein is indicative of a catalytically active protein. This is in contrast to the consistently decreased dynamics exhibited by $PDE8A_C$ in the 'End state' complex (Figure 3.11). Comparison of the 'Encounter' and 'End state' complexes reveals that the two conformations are distinct from one another, with significant differences in various regions of the protein (Figure 3.18, bottom panel).

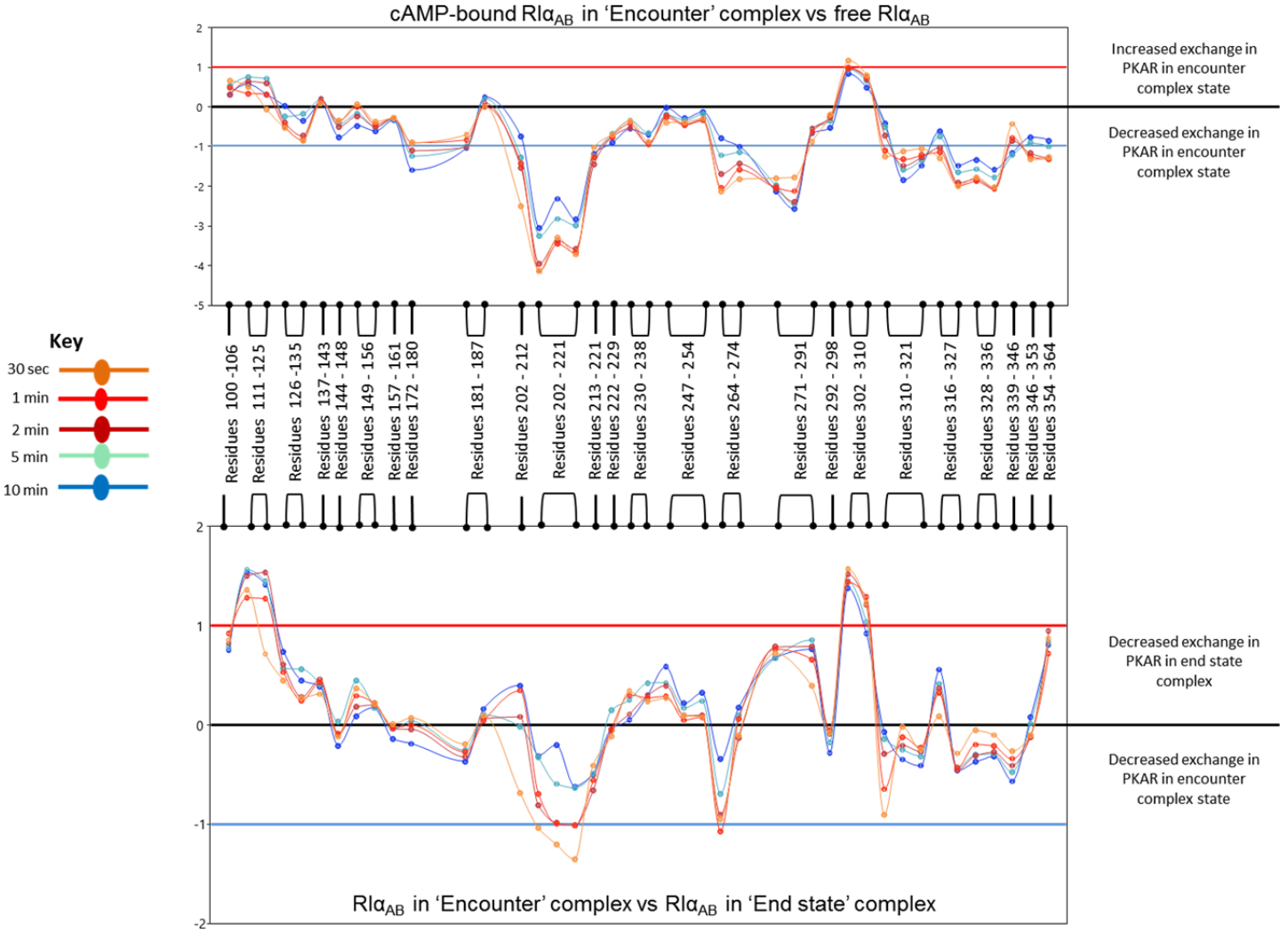

Figure 3.17: ***Comparison of RIα$_{AB}$ in the 'Encounter' complex with the 'End state' complex:*** Top panel; Absolute difference in number of deuterons (inferred from difference in mass in Da, y-axis) between RIα$_{AB}$ in the 'Encounter' complex and the *apo* state are depicted in a difference plot, with pepsin digest peptides labeled along the x-axis. Peptides (points on the graph) in the positive range (red line) undergo increased deuterium exchange in the 'Encounter' complex when compared to the *apo* state, while peptides in the negative range (blue line) undergo decreased exchange in the 'Encounter' complex. Bottom panel; Difference plot comparing RIα$_{AB}$ in the 'Encounter' complex and 'End state' complex. Peptides in the positive range (red line) undergo decreased deuterium exchange in the 'End state' complex in comparison to the 'Encounter' complex, while peptides in the negative range (blue line) undergo decreased exchange in the 'Encounter' complex in comparison to the 'End state' complex. Each colored line in the graph depicts a deuterium labeling time point as explained in the key.

Figure 3.18: ***PDE8A$_C$ exhibits mutually distinct dynamic profiles in the 'Encounter' complex and 'End state' complex:*** Top panel; Difference plot comparing PDE8A$_C$ in the 'Encounter' complex to the *apo* state. Peptides in the positive range (red line) undergo increased deuterium exchange in the 'Encounter' complex, while peptides in the negative range (blue line) undergo decreased deuterium exchange in the 'Encounter complex'. Peptide residue numbers are marked along the x-axis while absolute difference in deuterons (measure in Daltons (Da)) is marked along the y-axis. Bottom panel; Difference plot comparing PDE8A$_C$ in the 'Encounter' complex to PDE8A$_C$ in the 'End state' complex. Peptides in the positive range (red line) undergo decreased deuterium exchange in the 'End state' complex in comparison to the 'Encounter' complex, while peptides in the negative range (blue line) undergo decreased deuterium exchange in the 'Encounter' complex in comparison to the 'End state' complex. Time points are depicted in different colors as explained in the key.

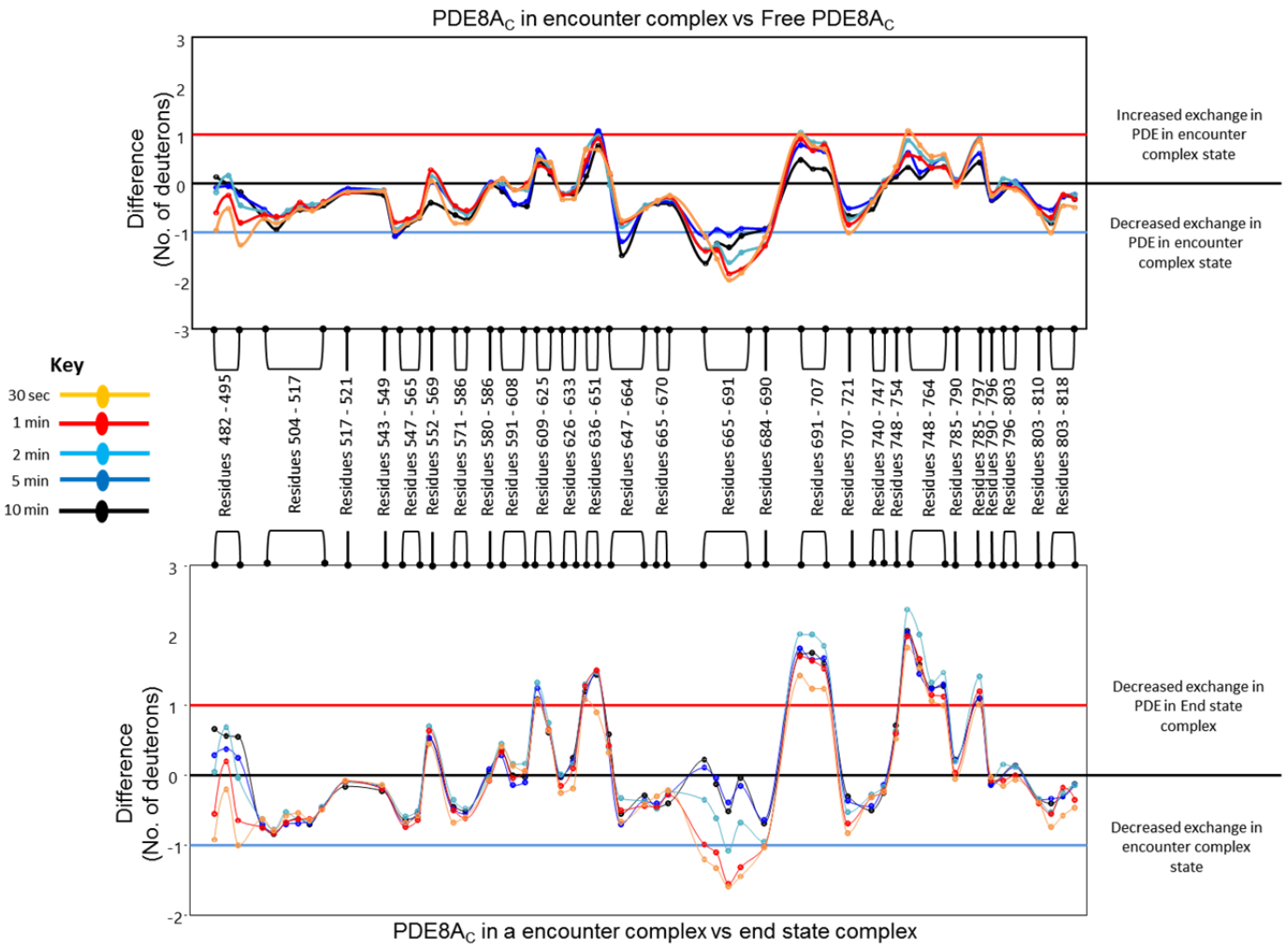

*3.3.7 Model of PDE8A-RIa interface by computational docking suggests substrate channeling in cAMP hydrolysis**

Molecular docking was carried out to model the PDE8-PKA RIα interface based on the HDXMS results. Since size exclusion chromatography of $PDE8A_C$ indicated a majority of $PDE8A_C$ existed as a dimer in solution, and the PDE8 structure (PDB ID: 3ECN) crystallized as a dimer, the dimeric structure of the catalytic domain of PDE8, was used for docking with monomeric RIα(113-379) ((PDB ID:1RGS)). Such a complex would show a stoichiometry of one PDE dimer interacting with one monomer of RIα(113-379).

RIα exists in two distinct conformations, bound to PKA catalytic subunit (H-form) and bound to cAMP (B-form). We hypothesize that the B-form of RIα must interact with PDEs (Encounter complex) for hydrolysis of the tightly bound cAMP, leading to cAMP signal termination (Figure 3.1). These can occur through a simultaneous interaction of the two cAMP-bound CNB-domains or via tandem binding of each cAMP-bound CNB domain to individual PDE units in the dimer. Since it is known that the two cAMP binding domains in RIα are connected by a dynamic C-helix (Kornev, Taylor et al. 2008, Moorthy, Badireddy et al. 2011), we reasoned that the central helix undergoes dynamic rearrangements, making equally plausible, accommodation of both CNB domains binding simultaneously or in tandem. Furthermore, mapping of PDE8-RIα interactions by HDXMS suggests that the PDE8 binding interface is symmetric, while differential exchange across the two CNB domains of RIα is nonuniform. These are suggestive of an asymmetric interaction surface across the individual CNB domains of RIα. To factor in dynamics of the interdomain linker, HADDOCK runs were set up in two different ways: The cAMP-bound conformation of RIα (PDB ID: 1RGS chain B) was modeled i) as one whole unit with a rigid helix linker, and ii) as two separate cAMP binding domains sans the linker. In the latter runs, to circumvent the limitation of docking programs in modeling large conformational changes, each CNB domain was independently docked to mimic the freedom that a flexible linker would provide. It is well established that the solutions generated by

** Molecular Docking experiments were carried out in collaboration with Dr. Ivana Mihalek, Bioinformatics Institute, A*Star laboratories, Biopolis, Singapore*

HADDOCK, are closer to native complexes if the docking is driven by restraints based on experimental data. In our case, these constraints were provided by results from HDXMS. The changes in deuterium exchange upon complexation in $PDE8A_C$ and $RI\alpha_{AB}$ are rendered in surface representation in Figure 3.19 A and B respectively.

In our computational experiment, we first docked RIα as a rigid unit. Upon inspection of the solutions, it was clear that the two cAMP binding domains cannot be made simultaneously accessible to the catalytic sites of PDEs. It is conceivable that one of the RIα cAMP binding domains acts first; after it extracts the cAMP, it is released, which enables the other cAMP binding domain to bind to PDE. However, since the cAMP binding domains in RIα are highly homologous, and the linker C-helix is highly dynamic (Kornev, Taylor et al. 2008), we proceeded to investigate whether the geometry of the two proteins, aided with some flexibility in the central helix of RIα, could allow simultaneous docking of the two domains. Thus in subsequent docking experiments, the two domains of RIα were docked onto the PDE8 dimer individually. The high structural similarity of the two domains suggests that they could also bind to each of the PDE8 catalytic sites in a quasi-symmetrical way.

It should be kept in mind that the scoring, and even more so the ranking, in the computational reconstruction of protein complexes remains problematic (Lensink and Wodak 2010). Thus we use docking to generate geometrically feasible models of the interaction proposed in this study, and use the HADDOCK's native score as guidance, but also as only one of the constraints that the model should satisfy. The chosen pose for CNB-B domain has the best HADDOCK score of -37.55 while CNB-A with a HADDOCK score of 43.29 belongs to the top 8% in its class (Figure 3.19 C). The number of intervening atoms, criterion (ii), for CNB-B was among the top 3%, smallest in the 200 chosen poses, and for CNB-A among the top 30%, suggesting that the degree of the conformational change might be still larger than indicated by the model.

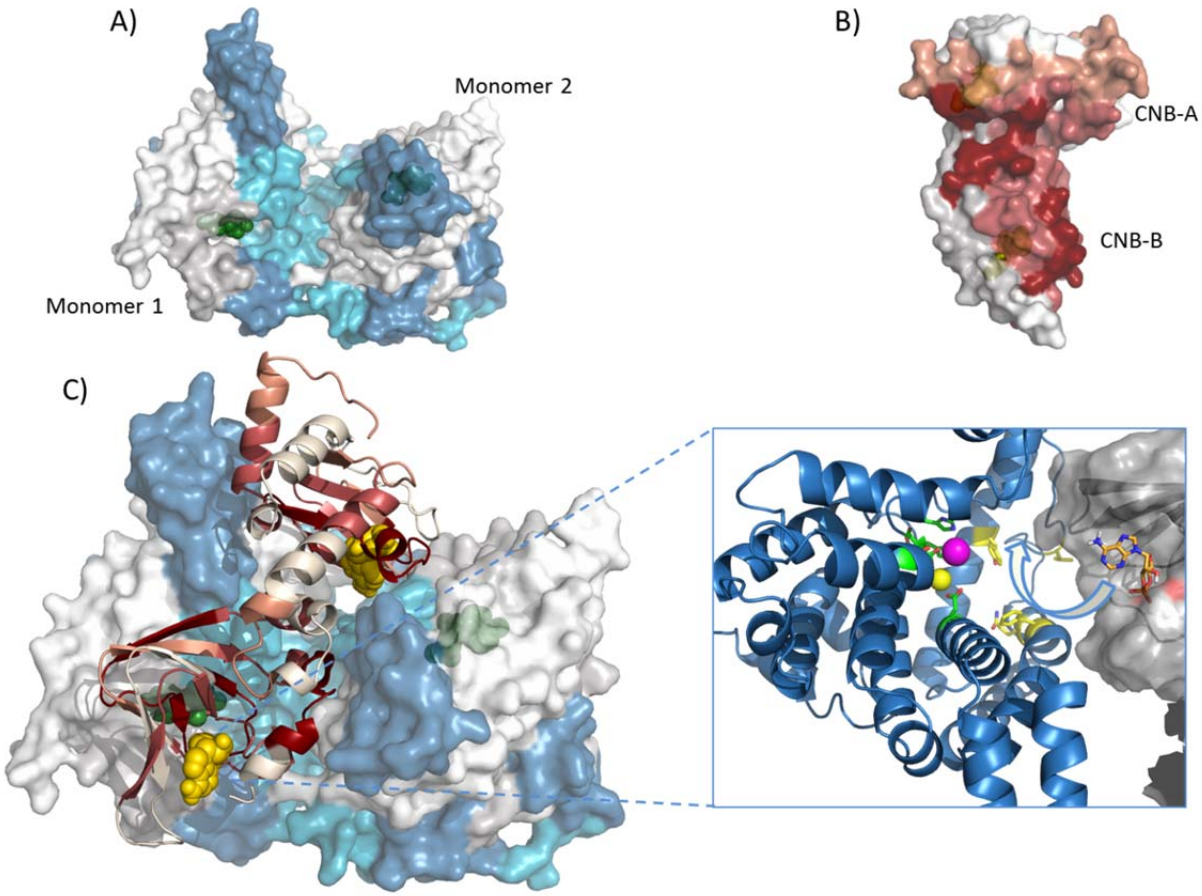

Figure 3.19: ***Evidence for cAMP channeling between CNB binding site and PDE active site from interaction interface***: A) HDXMS results of $RI\alpha_{AB}$ interaction mapped onto a surface representation of the structure of dimeric $PDE8A_C$ and color coded as per Figure 3.12. B) HDXMS results of $PDE8A_C$ interaction mapped onto a surface representation of the structure of $RI\alpha_{AB}$ and color coded as per Figure 3.13. C) Docking model of the $PDE8A_C$:$RI\alpha_{AB}$ complex highlighting proximity of the cAMP-binding sites on the R-subunit to the PDE active site. Proposed mechanism for channeling in dissociation and hydrolysis of cAMP bound to RIα. Inset: Close-up of the PDE active site in the model of the PDE8-RIα complex with the PDE8 (PDB ID: 3ECN) in blue and RIα (113-379)(PDB ID: 1RGS) in grey surface representation. cAMP is shown in yellow stick representation. Catalytic metal ions: Zn^{2+} (yellow sphere) and Mg^{2+} (magenta sphere) atoms are part of the hydrolytic core. Conserved residues important for substrate recognition are yellow, metal ion anchoring and hydrolytic center are green. RIα in surface representation (only cAMP:A domain (residues 113-244) shown for clarity). A single chain of PDE8A (chain A) alone shown for clarity. Residues 662-679 have been hidden to enable clear view of the active site. PDE binding mediates dissociation of the phosphate of cAMP from RIα (indicated by arrow).

3.4 Discussion

In this study we report the description of a signaling complex of PDEs with PKA RIα through a combination of orthogonal experimental and computational approaches. This constitutes a fundamental signaling complex in the termination phase of cAMP signaling. Our results support a universal model for how PDEs bind both CNB domains of RIα and catalyze hydrolysis of bound

cAMP leading to signal termination. This complex shows broad conservation from dictyostelia to mammalian systems.

HDXMS studies of PDE:PKAR complexes localized the interactions to span the cAMP binding pockets of PKA RIα and the regions lining the catalytic site of PDEs. This has been observed in evolutionarily distant PDEs tested, namely RegA and the full length and catalytic domain fragment of mammalian PDE8. On the PDEs, residues that showed decreased deuterium exchange were mostly located proximal to the catalytic pocket or were residues involved in dimerization (Figure 3.6A, Figure 3.19A). RIα on the other hand showed protein-wide decreases in deuterium exchange across several regions upon complexation with $PDE8A_C$ as seen in Figure 3.19B. These include the cAMP binding pockets in both CNB-A and CNB-B, the N-terminal helical subdomain and interdomain helical connector regions. However in the cAMP bound state, large decreases in exchange are seen mainly at the cAMP binding pockets at CNB-A and CNB-B with little effects at other regions. These two states would thus represent two distinct end point conformations of RIα consistent with our results from docking.

Computational docking guided by results from HDXMS provides a model for the PKA RIα-PDE8 interface. This solution was readily generated through docking with minimal rearrangements in the interdomain linker of RIα. Given the intrinsic ability of RIα to toggle between multiple conformational states (Badireddy, Yunfeng et al. 2011), and the high dynamics of the interdomain C-helix, such a rearrangement is likely through conformational selection. Together, this work highlights how computational docking with HDXMS and fluorescence spectroscopy can enable rapid mapping of the dynamics of transient interactions into multi-protein signaling complexes.

Analysis of HDXMS data and the docking model, reveal that highly conserved residues responsible for substrate recognition, are at a close proximal distance to the cAMP that is bound to RIα. This provides a model for mechanism of action, whereby active site coupling between the PDE and RIα engages residues important for cAMP binding and allostery, thereby weakening key hydrogen bonds between RIα and cAMP. The cAMP released from RIα is subsequently captured by substrate

recognition residues on PDE and is channeled into the active site to be hydrolyzed into 5'AMP (Figure 3.19C inset). The model shown here is that of monomeric $RI\alpha_{AB}$ in complex with $PDE8A_C$ dimer. We believe this can be extended to model dimeric full-length RIα in complex with 2 dimers of full-length PDE.

Real time monitoring of $PDE8A_C$-mediated cAMP dissociation by HDXMS allowed detailed examination of the changes to the cAMP binding pockets in both CNB domains. These provided powerful insights that experimentally complemented the docking model. The results of computational docking shown in Figure 3.19C shows PDE8A interacting with cAMP-bound $RI\alpha_{AB}$ in the 'Encounter state' complex. Comparison of HDXMS of 'Encounter' state complex with the 'End state' complex showed important differences highlighting the time-bound dissociation of cAMP. Most importantly we were able to directly monitor $PDE8A_C$-dependent cAMP dissociation simultaneously from both CNB domains in a time-dependent manner. This additionally highlights an important application of HDXMS in monitoring dynamics of transient interactions in real time at peptide resolution and complements traditional fluorescence spectroscopy approaches (Figure 3.7).

An important question that is relevant to cAMP signaling is in understanding how cAMP bound to the PKA R-subunit is hydrolyzed to reset PKA. Our results demonstrate how PDE8 binds RIα and facilitates dissociation of cAMP from both CNB domains. This further highlights how RIα might serve to buffer intracellular cAMP and 'channel' it to the active site of PDE8. Substrate channeling is characteristic of metabolic enzymes (Huang, Holden et al. 2001) but is being proposed here for the first time in cAMP signaling. Sequestering of cAMP-bound RIα by PDEs has important implications. This allows for localized pools of cAMP to activate PKA in microdomains. It also facilitates adaptation to steady state levels of cAMP by completing the cAMP cycle through regeneration of the inactive holoenzyme. This also ensures that reactivation of PKA would occur preferentially upon large fluxes of cAMP levels in the cell (Leiser, Fleischer et al. 1986). PDE-PKA RIα interactions described are only likely to be enhanced further by AKAPs.

3.5 Conclusion

In the previous chapter, RegA mediated cAMP dissociation from the PBC of RIα was monitored by HDXMS. In this chapter we have mapped the interaction interface between PDEs and RIα, and it was seen that the main interaction interface is on the catalytic pocket of RegA and the cAMP binding pocket of RIα. It was further seen that the interaction interface is conserved across all PDEs. Fluorescence polarization experiments were carried out to rapidly screen for PDEs capable of mediating dissociation of cAMP from RIα. PDE8A was found to be a likely candidate, and HDXMS was used to map the interaction interface. HDXMS was also used for Real time monitoring of cAMP release from RIα. It was seen that cAMP dissociation and ultimately cAMP pathway signal termination is mediated by active site coupling between PDEs and RIα.

This study has broad implications in the field of cAMP signaling. This study is the first report on PDE-PKAR interactions in mammalian systems and provides a model for how cAMP signal termination occurs. This study also highlights how HDXMS can be used to monitor reactions in real time by monitoring certain 'marker' peptides that are directly involved in the reaction mechanism.

In the previous 3 chapters, Structural mass spectrometry was used as a tool to elucidate conformational dynamics in signaling pathways, particularly to map out dynamics of transient states in the cAMP pathway. The following two chapters aim to establish a role for structural mass spectrometry in drug discovery screening (Chapter 4) and to apply structural mass spectrometry to increasingly complex biological systems (Chapter 5). The next chapter derives from previous work on protein ligand interactions and applies HDXMS as a screening tool in Fragment based ligand discovery.

Chapter 4

Detecting low affinity binders by hydrogen/deuterium exchange mass spectrometry: An application for Fragment based ligand discovery

4 Detecting low affinity binders by hydrogen/deuterium exchange mass spectrometry: An application for Fragment based ligand discovery

4.1 Introduction

Over the past decade, our understanding of cellular functions and processes, especially in the field of cell signaling has progressed at a great pace. This has been accompanied by the discovery of a large number of proteins that are postulated to be high value targets for drug discovery approaches (Schreiber 2005). These proteins are of high interest to the field of chemical biology and the pharmaceutical industry as targets for drug design. Recent advances in combinatorial chemistry and high throughput screening (HTS) have enabled rapid screening of large compound libraries against important drug targets. This is often dependent on structural information obtained by virtual ligand screening techniques and structure based drug design. These techniques require screening of millions of compounds and are dependent on the presence of large compound library and crystal structures of the target proteins (Shoichet 2004, Scapin 2006, Hajduk and Greer 2007).

Fragment based ligand design (FBLD) has in recent years proven to be an attractive alternative approach to the traditional HTS techniques to develop inhibitors against therapeutically important target proteins. Fragments are small, hydrophilic molecules that are derived from the breakdown of large ligand molecules. Fragments constitute the active moieties of these large ligand molecules and serve as the building blocks to form larger tighter binding molecules. They typically form very weak interactions with target proteins, and only after multiple rounds of combinatorial design does a fragment give an inhibitor molecule with improved affinity and specificity. The major advantage in FBLD is that the design of the ligand and its active moieties can closely be monitored and controlled thereby ensuring success in later stages of the drug discovery pipeline.

A major challenge in FBLD is detecting very weak affinity interactions, and the screening methods available to measure these interactions have been limited (Hajduk and Greer 2007). The most

commonly used biophysical methods for screening are: thermal melting, surface plasmon resonance, crystallography, nuclear magnetic resonance, and isothermal calorimetry. The limitations include poor dynamics range for the low affinity screening, high demand on protein and throughput of analysis. Crystallography has been mainly used as a methodology to validate fragment hits found by other techniques (Schmidt and Rademann 2009). X-ray crystallography has a clear advantage over other techniques as it gives a detailed three-dimensional picture of the binding interaction. However, atomic structures do not give a detailed map of the dynamics of protein-ligand interactions. This technique also has the inherent limitations in that, crystals with good diffractibility are essential. FBLD by crystallography generally involves soaking the crystals in fragment solutions which might further damage the crystals. Structure activity relationships by NMR (SAR by NMR) has proven to be the gold standard for mapping fragment-protein interactions and gives high resolution data on protein structure and dynamics (Shuker, Hajduk et al. 1996). This method has been used to successfully develop drug molecules against numerous targets (Meyer and Peters 2003).

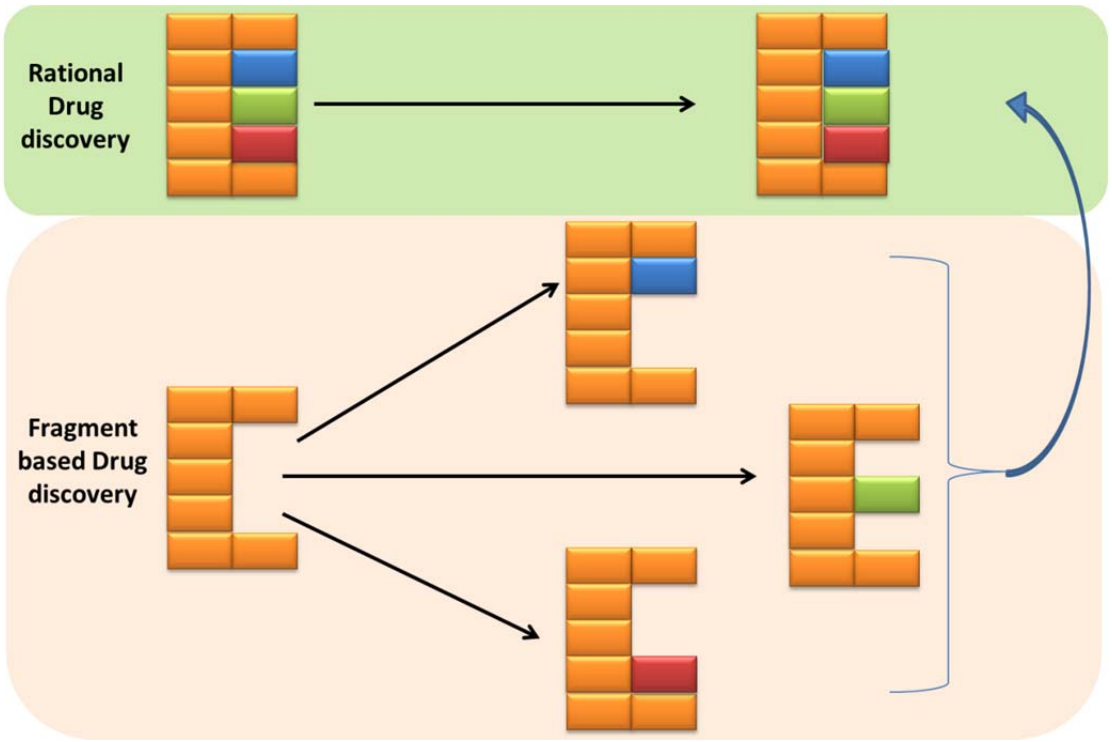

Figure 4.1: Drug discovery strategies: Rational drug discovery is the process by which millions of ligands screened by high throughput screening techniques to find a molecule that has a high affinity to the drug target. In fragment based drug discovery, small fragments are tested which may bind only a portion of the ligand binding pocket. Multiple fragments are screened and linked by combinatorial chemistry to arrive at a high affinity ligand molecule.

From previous chapters it was seen that Hydrogen/Deuterium Exchange Mass Spectrometry (HDXMS) is a powerful tool to monitor a variety of perturbations. It was seen that HDXMS is a highly sensitive and rapid approach to characterize the effect of perturbations on the conformational dynamics of proteins (Hoofnagle, Resing et al. 2003, Kaveti and Engen 2006). This technique has rapidly emerged as an invaluable tool for biophysicists, structural biologists and protein chemists to correlate protein structure to its function. The main advantages of HDXMS is that each experiment requires small amounts of protein, there is no size limit and high resolution structural information is not necessary to decipher ligand binding regions. Recent advances in instrumentation for HDXMS experiments include an automated robotic system coupled to an Electrospray mass spectrometer. This enables rapid amide exchange measurements with high reproducibility and low back exchange effects (Wales, Fadgen et al. 2008).

Hsp90 (heat shock protein 90) is an important member of the chaperone class of proteins and is involved in protein folding pathways, stabilizing various proteins such as steroid receptors, and is also involved in protein degradation pathways (Schneider, Sepp-Lorenzino et al. 1996). It also stabilizes a number of proteins involved in tumor growth, and hence is the target of numerous anti-cancer drugs (Solit and Rosen 2006). Inhibitors of Hsp90 have been identified and isolated from natural sources, namely Geldanamycin and Radicicol. Structural biology of these molecules reveals that they bind to the N-terminal ATPase domain and inhibit the entire molecule. It was thus seen that the N-terminal domain alone was sufficient to guide the design of inhibitors to inhibit the entire molecule. In this study we use two high affinity ligands, Radicicol and a Geldanamycin derivative 17-N-Allylamino-17-demethoxygeldanamycin (17-AAG). Their binding affinities for Hsp90 are 19 nM and 33 nM respectively. Hsp90 has also been the subject of numerous FBLD approaches (Huth, Park et al. 2007, Brough, Barril et al. 2009, Murray, Carr et al. 2010) and in this study we test whether HDXMS is sensitive to weak affinity fragments by selecting three fragments that were previously found to bind to Hsp90 and lead to the development of molecules which are currently in clinical trials against Hsp90. Of the three fragments, two fragments are phenolic compounds (Murray, Carr et al. 2010) with binding affinities ~500 μM and an aminopyrimidine class molecule (Brough, Barril et al. 2009) with a binding affinity of 20 μM.

We have for the first time demonstrated that HDXMS is sensitive enough to detect weak affinity inhibitors. Our approach provides a method not only for screening low affinity fragments that bind to a target protein but also to combine ligand binding information with structural and conformational dynamics information as well.

Our results show that all three fragments showed evidence for binding to Hsp90. We also observed the ligand binding and resultant allosteric effects can be differentiated by monitoring time dependence of the effects observed. Finally we propose a workflow for how HDXMS can carve a niche for itself into the current FBLD pipeline.

4.2 Materials and Methods

4.2.1 Materials

Unless otherwise mentioned all ligands/compounds were purchased from Sigma Aldrich (St. Louis, MO).

*4.2.2 Protein Expression and Purification**

The gene coding for M1-E236, the ATP binding domain of human hsp90 isoform 1, were subcloned into the pNIC28-Bsa4 vector (GenBank^{TM} accession number EF198106), yielding an expression construct with an N-terminal hexahistidine tag and a TEV protease recognition site. The positive recombinant clone was retransformed and expressed in T1 phage-resistant BL21(DE3) *E. coli* strain (Merck). For expression, the cells were grown at 37°C in a LEX system using 0.75 L of Terrific Broth medium supplemented with 8 g/L glycerol, 50 µg/mL of kanamycin, and 34 µg/mL of chloramphenicol. When OD_{600} reached ca. 2, the temperature was reduced to 18°C. After 30–60 min, the expression of the target protein was induced by addition of 0.5 mm isopropyl β-d-thiogalactopyranoside (IPTG) and incubated for 17–20 h. The cells were harvested by centrifugation and resuspended in lysis buffer (100 mM HEPES, 500 mM NaCl, 10 mM imidazole, 10% (v/v) glycerol, 0.5 mM TCEP, pH 8.0) supplemented with Protease Inhibitor Mixture Set III, EDTA free (Merck) and 2000 units of benzonase (Merck), and stored at −80 °C. Cells were disrupted by

** Hsp90 expression and purification was carried out in collaboration with Dr. Anna Jansson and Dr. Andreas Larsson, Structural biology consortium, Nanyang Technological University, Biopolis, Singapore*

sonication on ice using Vibra-Cell processor (Sonics & Materials Inc., Newtown, CT, USA). The lysate was clarified by centrifugation at 47,000 × *g* for 25 min at 4 °C, and the supernatant was filtered through a 1.2-µm syringe filter. Filtered lysates were loaded onto 1 mL of nickel-nitrilotriacetic acid Superflow resin (Qiagen Inc., Valencia, CA, USA) in IMAC wash buffer 1 (20 mM HEPES, 500 mM NaCl, 10 mM imidazole, 10% (v/v) glycerol, 0.5 mM TCEP, pH 7.5) and washed with IMAC wash buffer 2 (20 mM HEPES, 500 mM NaCl, 25 mM imidazole, 10% (v/v) glycerol, 0.5 mM TCEP, pH 7.5). Bound proteins were eluted with 500 mM imidazole and loaded onto a HiLoad 16/60 Superdex-200 column (GE Healthcare, Waukesha, WI, USA) pre-equilibrated with equilibration buffer (20 mM HEPES, 300 mM NaCl, 10% (v/v) glycerol, 0.5 mM TCEP, pH 7.5). Fractions containing the protein of interest were pooled. TCEP was added to a final concentration of 2 mM, and the sample was concentrated using Vivaspin 20 filter concentrators (15-kDa MW cutoff) (GE Healthcare) at 15 °C. The final protein concentration and yield was 16.5 mg/mL, 6 mg.

4.2.3 Amide Hydrogen/Deuterium Exchange Mass Spectrometry

Amide exchange reaction for ligand free protein was initiated by diluting 1 µL of 100 µM stock Hsp90 protein in 99.9% D_2O buffer (20 mM HEPES, 300 mM NaCl, 10% (v/v) glycerol, 0.5 mM TCEP, pH 7.5) to obtain a final D_2O concentration of 90%. For experiments monitoring ligand binding to Hsp90, concentrated ligands in DMSO were diluted into 99.9% D_2O buffer. Hsp90 was subsequently added to the D_2O buffer to initiate deuterium exchange reaction. This is carried out so that Hsp90 is not denatured by the high DMSO concentration in the ligand solution. Radicicol and 17-AAG were maintained at a final concentration of 20 µM and EA1 and EA4 were maintained at a final concentration of 5 mM. A list of all ligands tested along with their molecular weight and K_D values are given in Table 4.1. It has to be noted that, the amino pyrimidine fragment was only tested for 2 timepoints (1 min and 10 min) due to non-availability of the compound as it is no longer commercially available.

HDXMS was carried out as described in the materials and methods section of Chapter 3.

Compound	Structure	K_D	MW
17-*N*-Allylamino-17-demethoxygeldanamycin (AAG)	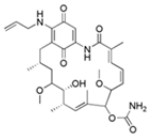	33nM	585.7
Radicicol	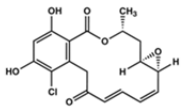	19nM	364.78
Methyl 3,5-Dihydroxyphenylacetate (EA4) (Phenolic class)	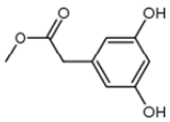	490µM	182.17
2,4 dihydroxypropiophenone (EA1) (Phenolic class)	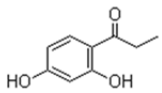	570µM	166.17
2-Amino-4-Methyl-6-(Trifluoromethyl)Pyrimidine (2A-4M-6TMP) (Aminopyrimidine class)	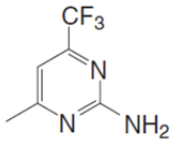	20µM	177.13

Murray *et al*. (2010), *J. Med. Chem*. 53: 5942-5955
Brough *et al*. (2009), *J. Med. Chem*. 52: 4794-4809

Table 4.1: Table lists all ligands tested for binding to Hsp90 by HDXMS along with their molecular weights and binding affinities. High affinity ligands are boxed in black and low affinity ligands boxed in grey.

4.3 Results and Discussion

4.3.1 Dynamic regions of Hsp90 are proximal to the substrate binding pocket

HDXMS experiments of *apo* Hsp90 were carried out as described in materials and methods. A total of 42 peptides were obtained corresponding to a sequence coverage of 95% of the primary of Hsp90. All peptides were quantified and each peptide was plotted against the relative deuterium uptake value (Figure 4.2 A). Relative deuterium uptake is the ratio of average number of deuterium ions incorporated to the maximum exchangeable amides. This is a parameter to define the dynamics of regions of the protein. Relative deuterium uptake (RDU) plot of Hsp90 indicates many regions of the protein show >0.6 relative deuterium uptake values. It was important to classify regions of the

proteins showing increased dynamics as compared to the rest of the protein. Thus the following criterion was used to identify highly dynamic regions vs regions which are more ordered.

$$Dynamic\ region\ if\ RDU > 0.5 \times maximum\ RDU\ for\ the\ protein$$

Equation 1

For Hsp90, the maximum RDU value was seen to be 0.67, thus regions showing RDU values greater than 0.335 were considered dynamic regions (highlighted by blue boxes in figure 4.2 A). Regions showing high dynamics were mapped onto the surface representation of Hsp90 and interestingly it was seen that all these regions were proximal to the ligand binding pocket (figure 4.2 B). This was consistent with the notion that ligand binding pockets tend to be dynamic loci and respond to ligands via conformational selection (Boehr, Nussinov et al. 2009, Badireddy, Yunfeng et al. 2011). This suggests that the dynamic regions proximal to the ligand binding pocket, are sampling multiple conformations to effectively respond to ligands.

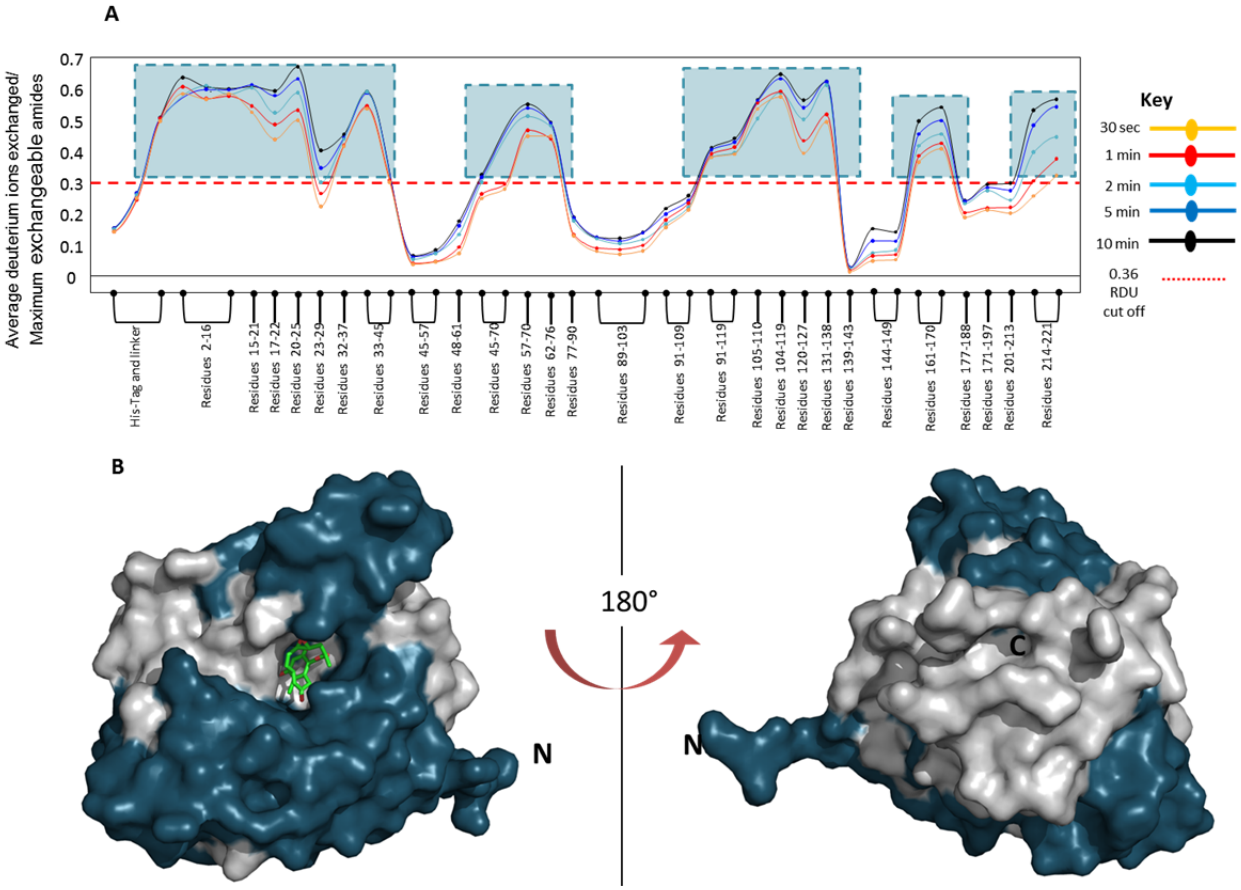

Figure 4.2: Dynamic regions line the ligand binding pocket: A) Relative deuterium uptake values (y-axis) is plotted for each peptide from the N to C terminus (x-axis) of Hsp90. Various time points were quantified and colored according to key. Dynamic regions were determined according to Eqn. 1 and boxed in blue. B) Regions showing high dynamics were plotted onto the surface representation of Hsp90 (PDB Id: 4EGK) in blue. Radicicol present in the ligand binding pocket is shows as green sticks.

4.3.2 Mapping high affinity ligand binding sites on Hsp90 by HDXMS

HDXMS was used to determine the regions of Hsp90 involved in ligand binding. To this end two high affinity ligands, namely Radicicol, a natural antibiotic, and 17-AAG, a Geldanamycin derivative were tested by HDXMS (Table 4.1). These ligands have very high affinities for Hsp90 with K_D in the low nanomolar range.

A difference plot summarizing results from HDXMS is shown in Figure 4.3A, regions which show decreased deuterium exchange are depicted by points in the positive scale and regions showing increased exchange are depicted in the negative scale. Both high affinity ligands tested showed decreased deuterium exchange across the entire protein indicating that the dynamic *apo* Hsp90 adopts

a stable structure upon ligand binding (Figure 4.3). Interestingly, both Radicicol and 17-AAG caused decreased deuterium exchange at the same regions of the proteins. These regions were mainly centered around a helix-loop-helix region spanning residues 91-119. Other regions showing significant decreases in deuterium exchange are at the N-terminal linker region spanning residues 2-16, the long helix-loop motif spanning residues 45-76 and a β strand-loop motif part of a β sheet spanning residues 171-197. All these regions are proximal to the ligand binding site except the N-terminal linker region. Previous structural characterization of the Hsp90-ATP interaction has shown that all these regions form important interactions with the ligand (Prodromou, Roe et al. 1997, Ali, Roe et al. 2006). These high affinity ligands are known to bind at the ligand binding pocket, (Schulte, Akinaga et al. 1998, Murray, Carr et al. 2010) and thus serve as a good template to define the regions of the protein that directly interact with the ligand (Figure 4.4 A). Subtractive analysis of all peptides lining the binding pocket reveals a minimal ligand binding region, highlighted in blue in Figure 4.4 A. This minimal binding region is the shortest stretch of amino acids (4 residues) that shows a clear reduction in deuterium exchange upon ligand binding. It spans residues 104 to 107. Regions that showed high dynamics in the *apo* state along with decreased deuterium exchange in the ligand bound state were mapped onto the structure of Hsp90 (Figure 4.4 B). It was observed that these regions perfectly line the outer edge of the binding pocket, further establishing the importance of these regions for ligand recognition and binding.

In HDXMS experiments, regions that exchange readily with solvent are highly important especially when monitoring exchange in the fast dynamics regime (<10 min of deuterium labeling). These regions are the regions that will respond to perturbations for two reasons, firstly they rapidly exchange with the label and hence would also be the regions where changes in deuterium exchange are readily monitored. Secondly, regions that rapidly exchange with solvent are dynamic in nature, and as seen earlier, and are important for ligand sensing and binding. Defining these dynamic regions is important, as they are the regions which are most responsive to ligand binding. Once we have a detailed knowledge of these dynamic regions, we can easily carry out rapid screening of weakly binding ligands by monitoring changes at the dynamic regions.

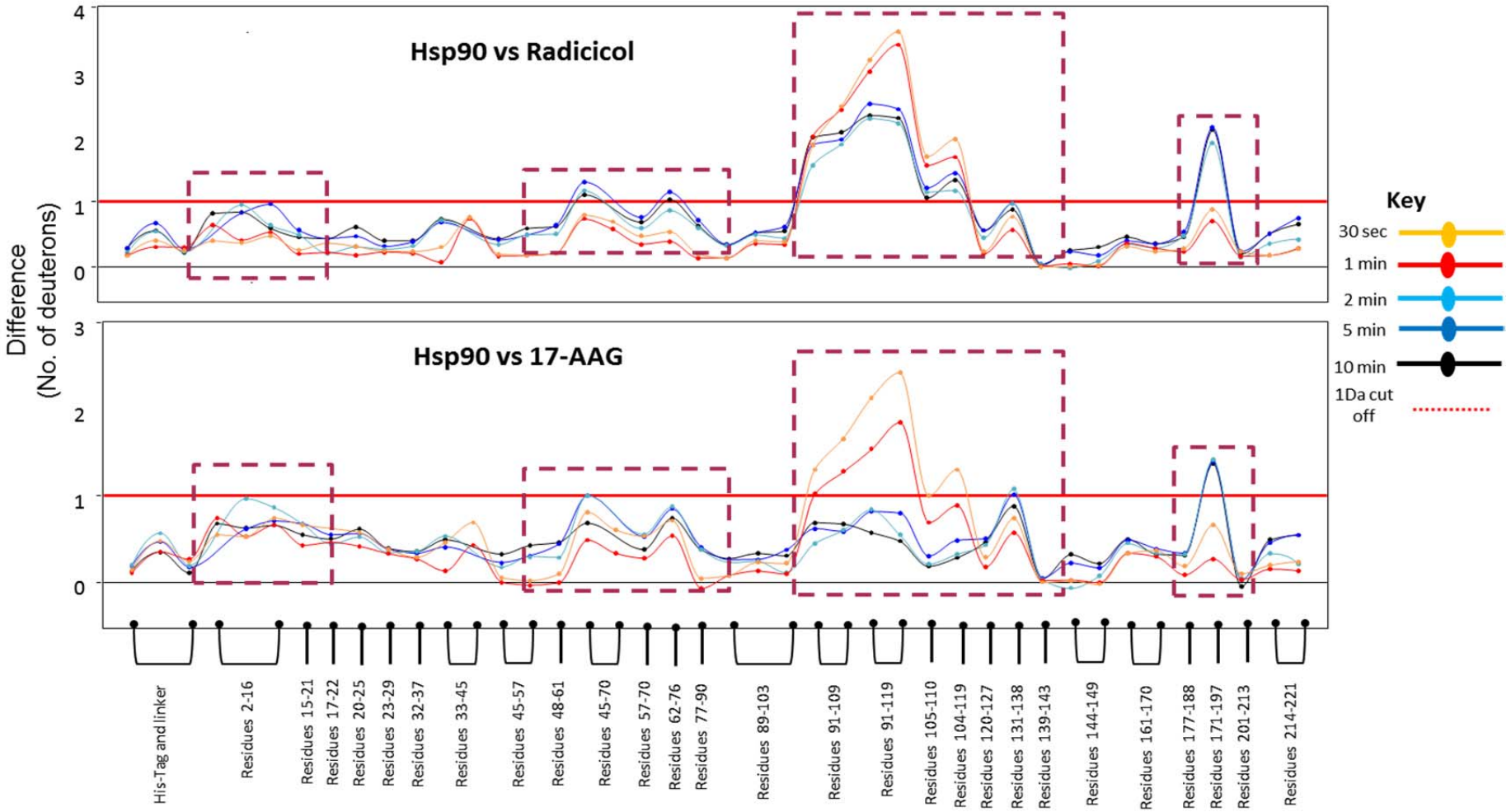

Figure 4.3 : Summary of Hsp90- high affinity ligand interactions by HDXMS: The absolute difference in numbers of deuterons (inferred from difference in mass in Daltons (Da) (y-axis) between the free and ligand bound state is plotted for each pepsin digest fragment listed from the N to C terminus (x-axis) of Hsp90 for each Deuterium exchange time point (t= 0.5, 2, 5, 10 min) in a 'difference plot'. Shifts in the positive scale represent decreases in deuterium exchange and shifts in the negative scale represent increases in deuterium exchange when compared to the *apo* Hsp90. The top panel shows regions showing differences upon Radicicol binding and the bottom panel shows differences upon 17-AAG binding. Regions showing significant differences (>1 Da) are boxed in red. Time points are colored according to key.

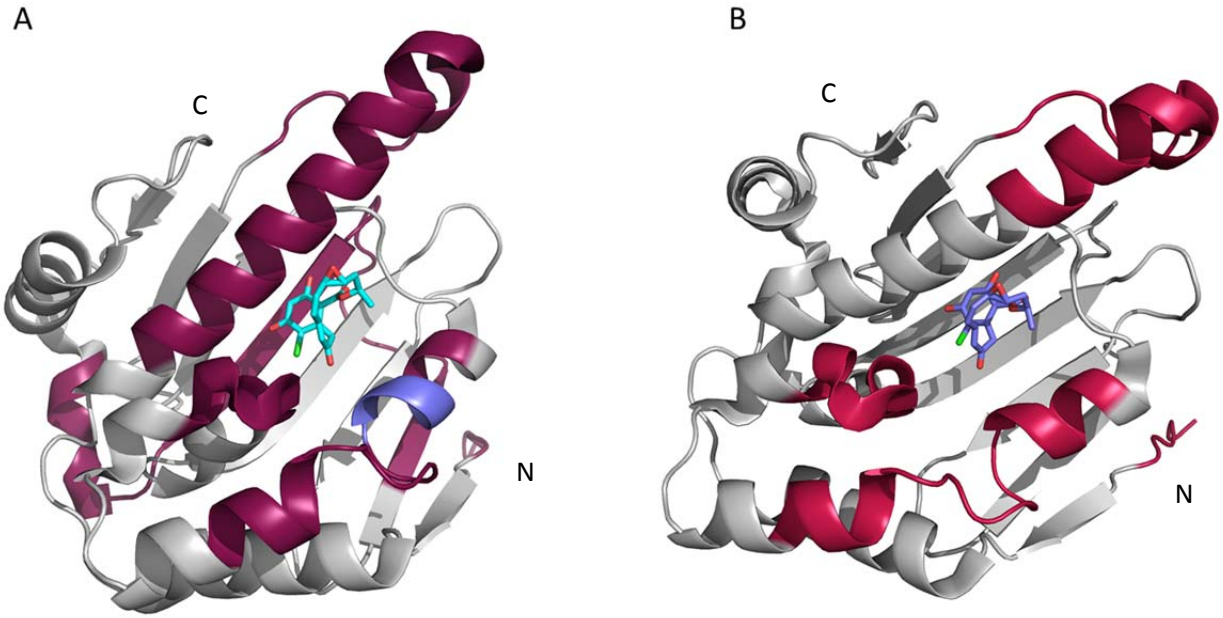

Figure 4.4: High affinity ligands bind at the ATP binding pocket of Hsp90: A) Regions showing decreased exchange upon ligand binding (either Radicicol or 17-AAG) are depicted in purple onto the structure of Hsp90. The minimal binding region is in blue. B) Regions that showed high dynamics in the *apo* state as well as decreases upon ligand binding are mapped onto the structure of Hsp90 in red. For both structures, Radicicol bound at the ligand binding pocket is depicted as cyan sticks. PDB ID: 4EGK.

4.3.3 Low affinity fragments EA4 and EA1 bind at the same loci as the high affinity ligand

To test whether HDXMS is capable of detecting binding interactions between proteins and low affinity fragments, three fragment molecules were used to test for binding with Hsp90 (grey box, Table 4.1). Two of the fragments were phenolic compounds while the third fragment was an aminopyrimidine class molecule. By definition, fragments are small molecules with very low binding affinities and all three fragment compounds tested were >200 Da and had K_Ds in the micromolar range. The phenolic compounds had binding affinities ~0.5mM (Murray, Carr et al. 2010) and the aminopyrimidine (2,4,6 AMP) molecule had a K_D of ~20 μM (Brough, Barril et al. 2009). HDXMS experiments of Hsp90 interaction with fragment molecules revealed interesting results.

Results show that, though the phenolic compounds are the same class of molecule and similar in reactive species, they showed significantly different effects on binding to Hsp90. It was seen that EA4 seemed to form more stable interactions at the binding pocket (residues 109-119) and showed decreased deuterium exchange pattern similar to the high affinity ligands. EA1 on the other hand caused increased dynamics at the binding pocket but showed decreased deuterium exchange at the other important loci (regions showing significant differences are boxed in blue in Figure 4.5). The aminopyrimidine molecule, 2,4,6 AMP, showed similar deuterium exchange effects to EA4 molecule.

While the regions which showed decreased deuterium exchange for the fragment molecules were the same as seen for the high affinity ligands, the magnitude of difference was significantly less than those seen for the high affinity molecules. This effect was mainly observed at the ligand binding site, centered at residues 109-119. Radicicol and 17-AAG caused decreased deuterium exchange of upto 3 Da (Figure 4.3), EA4 binding lead to a decrease in deuterium exchange of ~1 Da. EA1binding on the other hand leads to an increase in deuterium exchange of upto 0.75 Da. Mass spectral envelopes for a peptide spanning the ligand binding pocket upon binding all ligands tested is shown in figure 4.6A. Other regions of the ligand binding pocket showed decreased exchange upon fragment binding, equivalent to decreased deuterium exchange seen upon high affinity ligand binding. The changes upon ligand binding were seen to be time-dependent and the significance of this is discussed in detail in the next section.

At almost all loci, the fragment molecules accessed the same regions that the high affinity ligands accessed. This is expected as the high affinity ligands are large molecules that can access the entire conformational space of the binding pocket. The fragments being smaller molecules should only be able to access a subset of the regions available to the high affinity. While it was remarkable that the fragments tested showed effects at all loci that the high affinity ligands bind, what was unexpected was the EA4 molecule causing long range conformational stabilization effects at a region unchanged by both high affinity ligands. This region is boxed in red in Figure 4.5 (top panel). This peptide is part of a helix region that is distal to the binding site and spans residues 201 to 213 (Figure 4.6B).

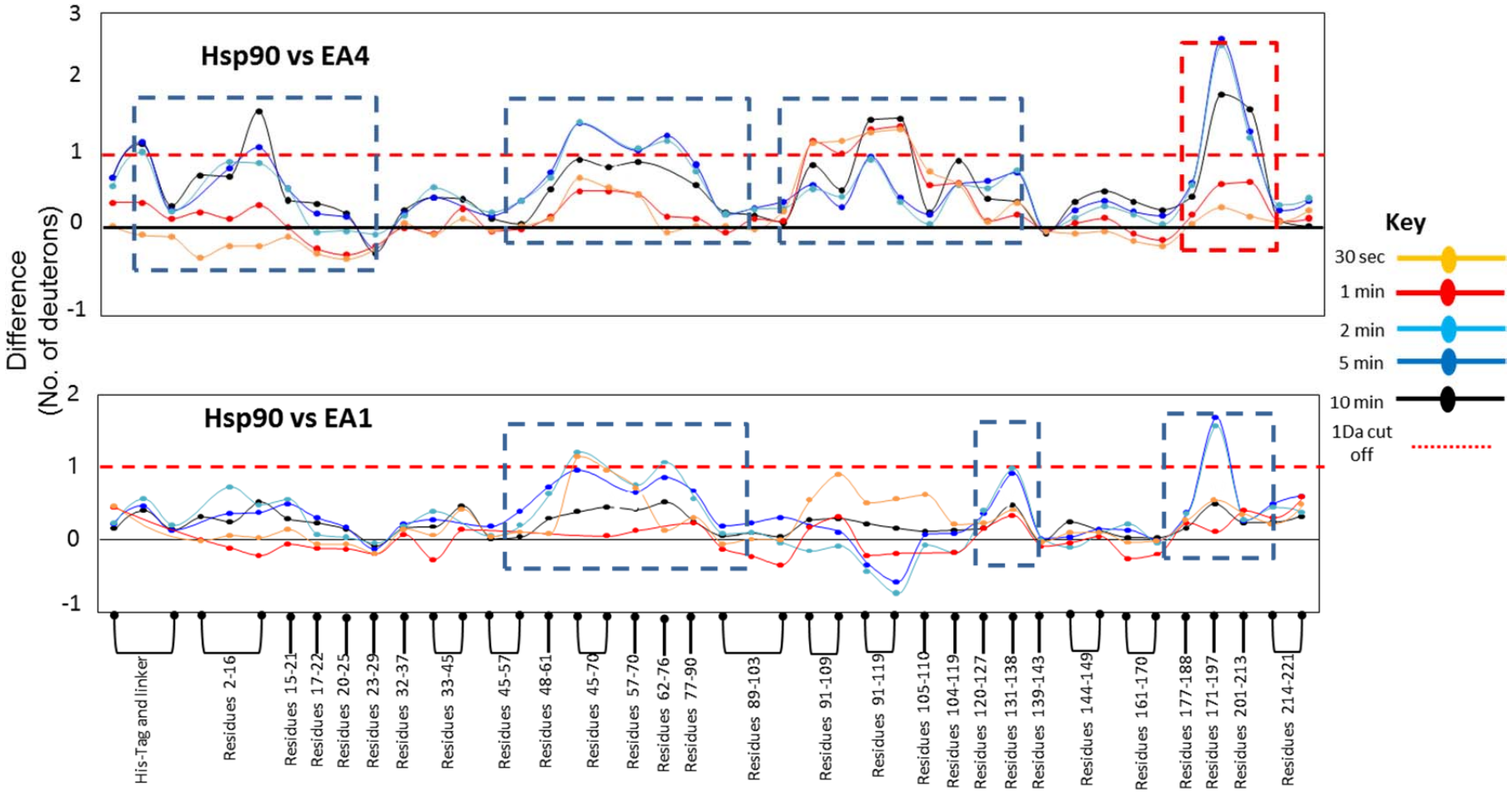

Figure 4.5: Summary of Hsp90-low affinity ligand interaction by HDXMS: The absolute difference in numbers of deuterons (inferred from difference in mass in Daltons (Da) (y-axis) between the free and ligand bound state is plotted for each pepsin digest fragment listed from the N to C terminus (x-axis) of HSp90 for each Deuterium exchange time point (t= 0.5, 2, 5, 10 min) in a 'difference plot'. Shifts in the positive scale represent decreases in deuterium exchange and shifts in the negative scale represent increases in deuterium exchange when compared to *apo* form of Hsp90. The top panel shows regions showing differences upon EA4 binding and the bottom panel shows differences upon EA1 binding. Regions showing significant differences (>1 Da) are boxed in red. Time points are colored according to key.

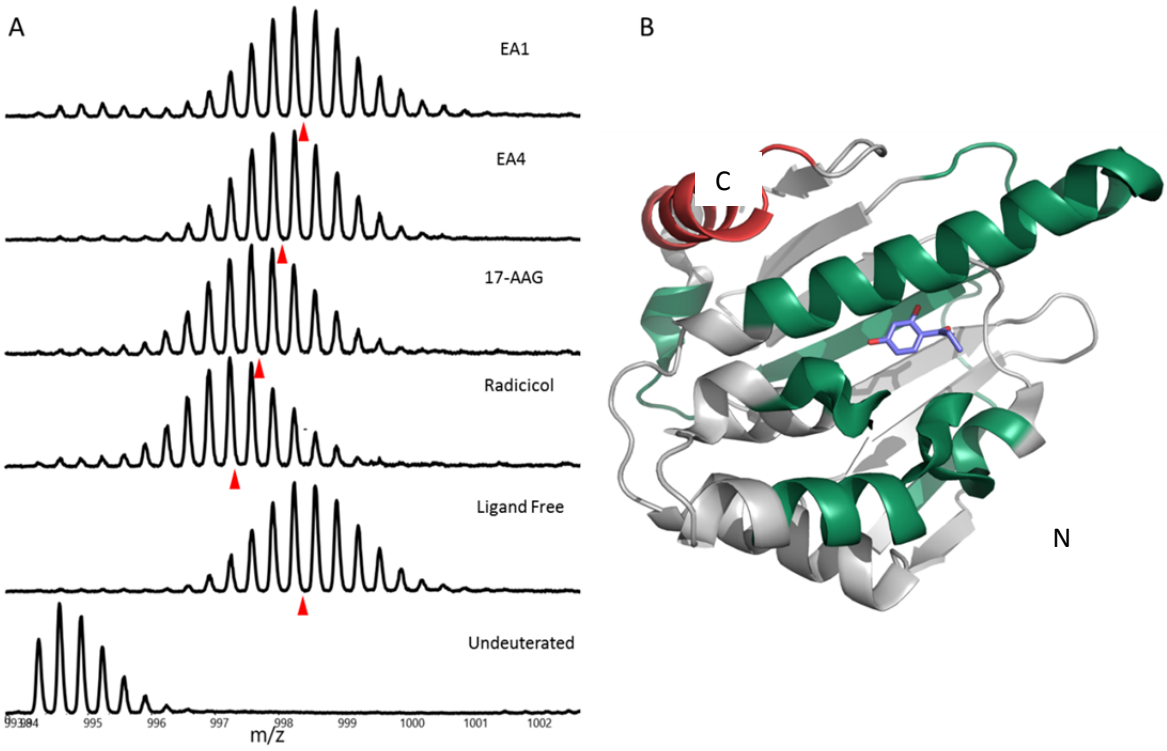

Figure 4.6: Low affinity ligand EA4 binds at the ATP binding pocket of Hsp90: A) Mass spectral isotopic envelopes of a peptic peptide fragment spanning residues 91-119 of Hsp90. Isotopic envelopes are shown for the *apo* protein and compared with ligand bound states. Red triangles indicate centroids of the envelope. B) Regions showing decreased deuterium exchange in Hsp90 upon EA4 binding are mapped onto the structure of Hsp90 in green. The region showing decreased deuterium exchange unique to EA4 binding is labeled in red. The EA4 molecule in the binding pocket is in blue sticks. PDB ID: 2YE4.

4.3.4 Differentiating ligand binding and ligand mediated conformational changes

One of the most important conclusions from this study was the prevalence of a time dependence on observed differences in deuterium exchange seen upon ligand binding. Radicicol being the highest affinity ligand tested showed decreased deuterium exchange across all time points at all loci (Figure 4.7 A). 17-AAG, the next highest affinity ligand showed decreased deuterium exchange across all time points at almost all loci except the ligand binding pocket spanning residues 91-119 (Figure 4.7 B). At this loci, it was seen that ligand induced decreases in deuterium exchange were greatest at earlier time points. As labeling time increased it was seen that the difference between the *apo* form and ligand bound form diminished. The greatest time-dependent effects were observed upon EA4 binding to Hsp90. It was seen that at the binding site peptide, earlier time points showed the greatest decreases in deuterium exchange and as labeling time increases these differences decreased to be almost negligible. At other loci, the opposite effect was observed; earlier time points showed no

significant differences but as labeling time increases the differences increased (Figure 4.7 C). These results are summarized in figure 4.7, where regions showing decreased deuterium exchange after 30 s of deuterium labeling are in orange and regions showing decreased exchange after 5 min of deuterium labeling are in blue.

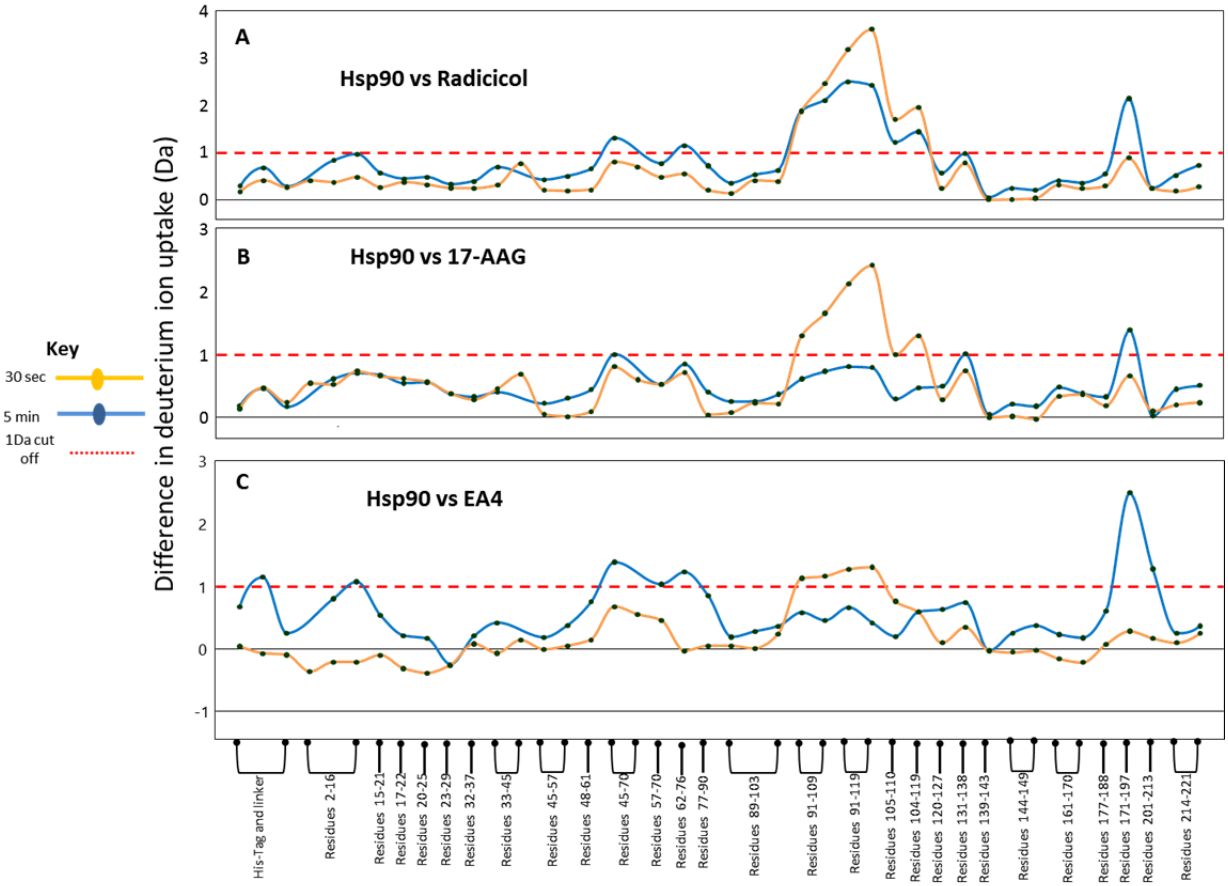

Figure 4.7: Time dependent differences in deuterium exchange upon ligand binding: A) Difference plot of Radicicol binding to Hsp90 comparing 30 sec and 5 min time points. B) Difference plot of 17-AAG binding to Hsp90 comparing 30 s and 5 min time points. C) Difference plot of EA4 binding to Hsp90 comparing 30 s and 5 min timepoints.

The dissociation constant K_D is the ratio of the dissociation rate (k_d) by the association rate (k_a), and for small molecules, association rates are generally diffusion rate controlled. A high K_D value implies that the dissociation rate is also a high value. Thus the lower deuterium exchange values observed at the binding site are most likely the result of the fragment having a high on/off rate at the binding pocket. As mentioned in section 4.3.1, the regions lining the ligand binding pocket are highly dynamic regions thus they exchange deuterium ions rapidly. Due to the ligands intrinsic on/off rate, deuterium exchange occurs rapidly in the time span the pocket is not occupied by a ligand. In earlier time points,

the probability of ligand not occupying the pocket is low, so the pocket is protected from deuterium exchange. As labeling time increases, the probability of ligand occupancy in the pocket also decreases thereby allowing deuterium exchange at the pocket. This effect leads to diminishing differences between *apo* state and ligand bound as labeling time increases. This is defined by the following equation

$$kobs = \frac{kd \times kex}{ka[ligand] + kex}$$ **Equation 2 (**Mandell, Baerga-Ortiz et al. 2001)

Where k_{obs} is the observed deuterium exchange rate, k_a is the association rate and k_d is the dissociation rate, k_{ex} is the inherent deuterium exchange rate for a given amide and [ligand] is the concentration of ligand used. Thus the observed deuterium exchange rate is inversely proportional to the ligand concentration and directly proportional to the K_D. Thus as the K_D (k_d/ka)increases the observed deuterium exchange rate at a particular amide also increases, this is offset by the addition of excess ligand. If ligand is added at a considerable excess then equation 2 condenses to equation 3.

$$kobs = \frac{kd \times kex}{ka[ligand]}$$ **Equation 3**

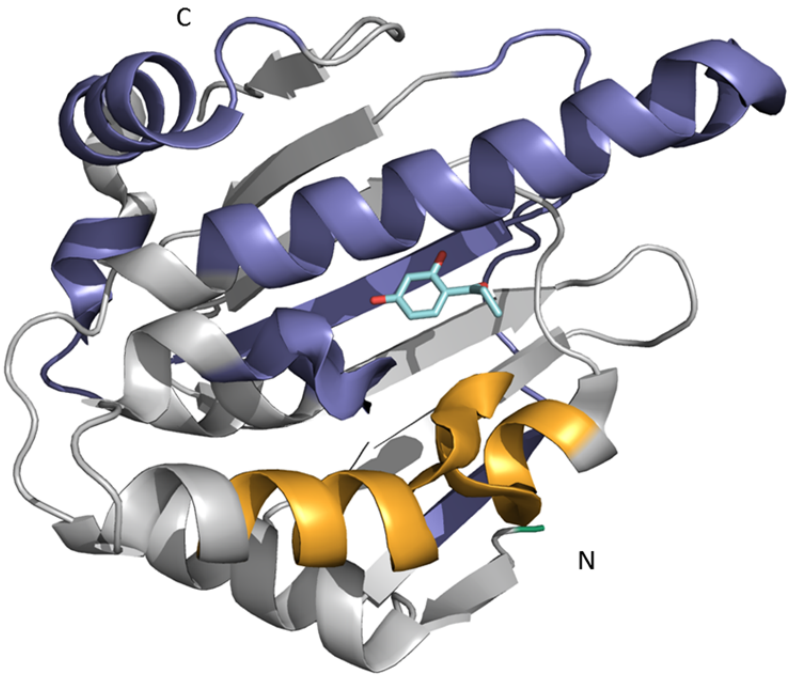

Figure 4.8: Time dependent differences caused by EA4 binding to Hsp90: Regions showing differences at early time points are labeled in orange and regions differences at later time points are labeled in blue onto structure of Hsp90. EA4 molecule is in cyan stick representation at the ligand binding pocket. PDB ID: 2YE4

In most experiments, the ligand concentration is maintained high enough such that observed deuterium exchange rate is governed by equation 3. But in the case of fragments, the K_D value is very high and ligand added at a very high concentration is still not enough to offset deuterium exchange to occur at an amide at the binding site. On the other hand it has to be remembered that, even though the ligand has a fast on/off rate inside the binding pocket, the pocket would on average always be occupied by a ligand. This is ensured by maintaining a high ligand concentration. Thus regions of the protein that indirectly respond to ligand binding (i.e. allosteric regions) are activated by the continued presence of ligand in the pocket. As time increases, the differences from conformational stabilization would incrementally add up to be reflected in significant differences at later time points.

It has to be noted that differences between binding effects and conformational stabilization effects would only be observed in systems with a fast on/fast off rate. Also the slowest ligand off rate that can be probed by this approach is yet to be described and at present would need to be tested empirically. This observation is of a qualitative nature and would be useful to possibly differentiate what is likely to be the binding sites from other regions that respond to ligand binding outside of the ligand-binding pocket. Allosteric effects and other conformational stabilization effects theoretically occur in the μs to ms time regime and hence the observations described at later time points do not directly relate to allosteric effects.

4.3.5 Workflow for fragment based ligand discovery by HDXMS

HDXMS is thus proven to be sensitive to weak affinity fragment binding to target proteins. A workflow for how HDXMS can aid current efforts in fragment based ligand discovery is proposed here (Figure 4.9).

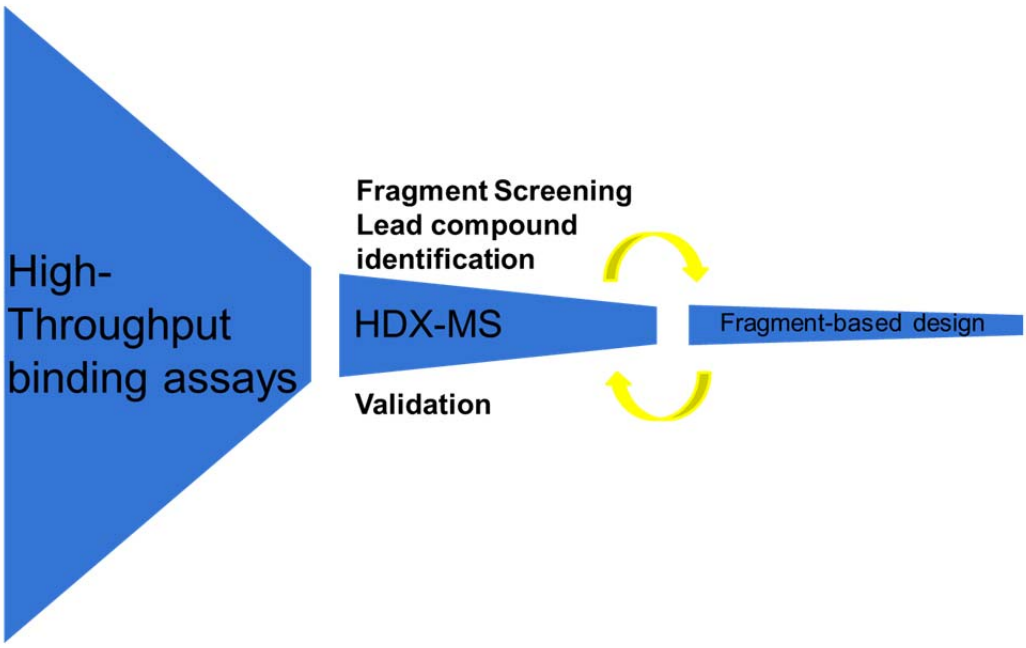

Figure 4.9: Workflow for HDXMS in fragment based ligand design: High throughput assays serve as a funnel to reduce the number of ligands tested from >2000 to ~200. HDXMS based lead compound identification is followed by combinatorial chemistry. The resulting products are iteratively screened and validated by HDXMS to obtain a tight binding ligand that is further validated by structural biology.

Most fragment libraries contain more than 2000 fragment molecules, and thus it is not feasible to test every fragment for binding to target protein by HDXMS. This would be a time consuming process and also consume large amounts of target protein. An alternative is to use high throughput binding assays to coarsely screen for fragments that potentially bind to the target protein. The top 200 hits are taken for further testing by HDXMS.

HDXMS experiments are first carried out using a high affinity ligand to define the regions that show the greatest exchange upon ligand binding as seen in section 4.3.1. Shorter labeling times were more sensitive to weak affinity ligand binding at the binding pocket; hence all ligands are subjected to HDXMS with the target protein for a short labeling time of < 2 min.

To increase efficiency of the data analysis process only the peptides showing decreased exchange upon high affinity ligand binding are tested for fragment ligand binding. Ligands showing positive hits are chosen for lead compound design by fragment based ligand discovery. Combinatorial chemistry is used to modify the ligands or link two ligands together. The resulting molecules are

iteratively screened by HDXMS and modified by combinatorial chemistry to obtain a tight binding ligand. This high affinity ligand is further validated by structural means. Thus HDXMS can be used as a highly sensitive screening tool which provides both ligand binding and associated protein dynamics information.

4.4 Conclusions

In this study it HDXMS was used map out regions that are highly dynamic based on deuterium ions incorporation. These highly dynamics regions were the same regions that also showed decreases in deuterium exchange upon high affinity ligand binding. Weak affinity fragment molecules were tested and showed that HDXMS is sensitive enough to detect very weak binders. A workflow is proposed for how HDXMS can be used in the fragment based ligand discovery pipeline.

In recent years, with advances in mass spectrometry and separation science, HDXMS has proven to be a powerful technique to map protein-ligand interactions. In this study, an important application for HDXMS in drug discovery is postulated.

In the first part of the next chapter, HDXMS is used to map interactions between an partially disordered protein and a DNA fragment. In the second part, HDXMS is used to monitor interactions between a viral capsid and its maturation protease.

Chapter 5

Role of conformational dynamics in complex biological systems

5 Role of conformational dynamics in complex biological systems

In this chapter, I highlight the role of HDXMS in elucidating conformation dynamics in complex biological systems. I also attempt to relate the existing structural data to the known functional data by understanding the dynamics of the system. This chapter is split into two parts, Part I is on the conformational dynamics of a partially disordered DNA binding protein. Part II is on the interactions between a virus and its maturation protease.

5.1 Part I- DNA-dependent Conformational Switching and H-NS-mediated Gene Silencing

5.1.1 Introduction

In various pathogenic bacteria, a locus of foreign acquired genes are responsible for expression of pathogenicity-specific genes (Hacker and Kaper 2000). In *Salmonella*, these are referred to as Salmonella Pathogenicity Islands (SPI) which play a central role in infection propagation through transepithelial migration survival. *Salmonella* tightly regulate the expression of these acquired gene clusters in order to minimize the negative effects of these genes and to express them only during infection and under conditions of stress. Genes encoded by the SPI-2 gene locus comprise a specialized type three secretory system to resist host immune cells. Specific environmental cues in response to infection stimulate SPI-2 expression and tight regulation of this process is critical for the survival of *Salmonella*. In the absence of these environmental signals, SPI-2 is kept silenced by an important nucleoid protein called H-NS (Heat-stable nucleoid protein). H-NS is an important bulwark against unregulated SPI-2 gene expression in the absence of specific environmental signals and is found in most gram negative bacteria. Silencing prevents foreign genes from being deleterious to the host, thus H-NS serves as an "immune sentinel" to repress newly acquired genes. H-NS thus plays a critical role in regulating numerous genes in response to the external environmental changes of bacteria such as temperature and osmolarity (Atlung and Ingmer 1997).

Despite the fundamental nature of H-NS-DNA interactions, the molecular details of how H-NS interacts with DNA are lacking, which in turn precludes an understanding of the molecular basis for gene silencing and regulation. Recently, two modes of H-NS binding to DNA using magnetic tweezers and atomic force microscopy (AFM) was described (Liu, Chen et al. 2010). A bridging mode describes H-NS binding to DNA and promoting looping accompanied by putative oligomerization of H-NS. The other, polymerization mode leads to stiffening of target DNA with no alteration in DNA secondary structure. These two binding modes possibly underlie the two H-NS activities *in vivo*, compaction of the nucleoid and repression of gene expression. This study also revealed a magnesium-dependent (Mg) ionic switch between the two modes of H-NS binding and highlighted Mg-induced alteration of H-NS binding to DNA from polymerization to bridging mode. We hypothesize that the large differences in binding modes must reflect alternate conformations of H-NS in the two modes (Esposito, Petrovic et al. 2002, Arold, Leonard et al. 2010) (Figure 5.1.1)

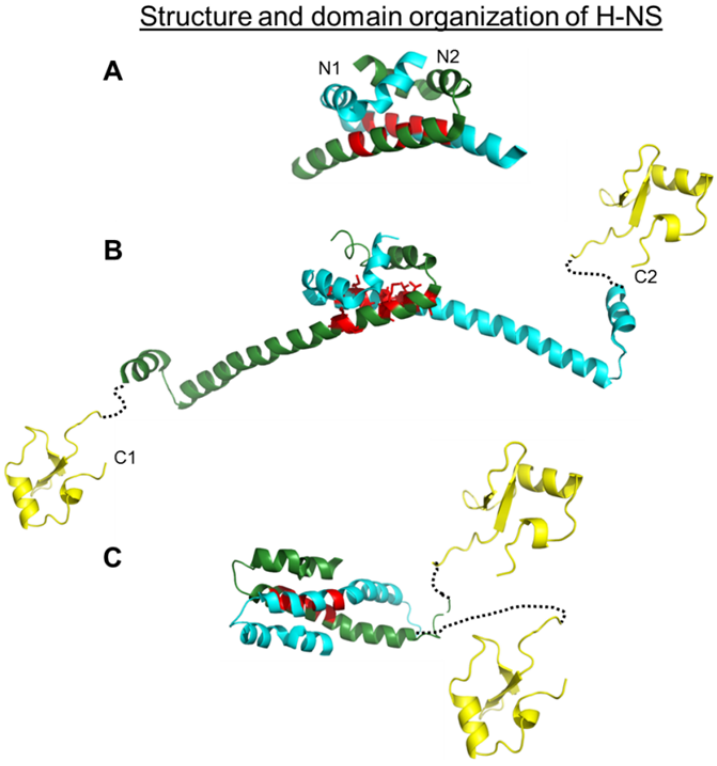

Figure 5.1.1: Spatial representation of full length H-NS using solution structures of the N-terminal dimerization domain dimer(in blue/green) and C terminal DNA binding domain (PDB ID: 1HNR) (in yellow) connected by a disordered linker region (green dashed line). The N-terminal domain has been observed to dimerize either in an antiparallel configuration (A) (PDB ID: 1NI8), B) (PDB ID:3NR7) or (C) parallel configuration (PDB ID:1LR1). N1, C1 and N2, C2 are the N and C termini of each H-NS monomer in the dimer. The core of the dimerization domain is contributed by two amphipathic helices generating a hydrophobic core (red).

Two techniques in structural mass spectrometry:- i) Ion mobility mass spectrometry (IMS)(Sharon and Robinson 2007) and ii) Amide hydrogen/deuterium exchange mass spectrometry (HDXMS)(Hoofnagle, Resing et al. 2003) represent powerful approaches to map conformational dynamics of proteins in solution . We have used IMS to

interrogate the putative multiple conformations in solution. To map the changes in H-NS between the two binding modes, we have used HDXMS of H-NS under polymerization and bridging mode conditions. Additionally, a major gap in understanding H-NS-mediated gene silencing is its apparent ability to bind nonspecifically to stretches of genomic DNA, even though it has been shown to have a preference for A-T rich and curved DNA, preferentially found within gene promoter regions (Spassky, Rimsky et al. 1984, Tupper, Owen-Hughes et al. 1994) (Liu, Chen et al. 2010). We additionally hypothesize that the basis for the dual nature of H-NS-binding to both A-T rich motifs, henceforth referred to as nucleation-motif DNA (N-motif DNA) and nonspecifically to genomic DNA (GDF) is through distinct conformations of H-NS stabilized through interactions with both classes of target DNA. In this study, we have used HDXMS to interrogate the conformations of H-NS in H-NS-Genomic DNA and H-NS-Promoter DNA complexes. Our IMS results show that H-NS is a highly dynamic protein that is a mixture of monomeric and dimeric states in the gas phase and exists as an ensemble of multiple conformations. HDXMS results also reflect the ensemble property of *apo* H-NS in solution and highlight the distinct conformations adopted by H-NS in H-NS-Genomic DNA and H-NS-Promoter DNA complexes and under Polymerization and Stiffening modes of binding DNA. Based on these results, a model for H-NS mediated gene silencing based on Conformational Silencing is proposed.

5.1.2 Materials and methods

5.1.2.1 DNA fragments

A 145 bp N-motif DNA Fragment containing part of the gene promoter and some coding regions of capsid protein (protein F) with a single AT-rich motif 'AGGATAAATT' in front of the start codon, was amplified from PhiX174 by PCR using two primers: '5-CGTCTTTGGTATGTAGGTGGTCA-3'and'5-CAATCTGACCAGCAAGGAAGCCA-3' (Sigma-Aldrich). The overall A-T content was calculated to be ~53%. A second 141 bp Genomic DNA Fragment (GDF) was amplified from the coding region for the gene encoding the PhiX174 minor spike protein (protein H) by PCR using primers '5-CACGCCAGAATACGAAAGAC-3' and '5- GGCGCATAATCTCGGAAACCT-3'

(Sigma-Aldrich Pte Ltd, Sing*apo*re). Its overall AT content was calculated to be ~54.6% and this fragment lacked any A-T rich motifs.

5.1.2.2 H-NS over-expression and purification

An H-NS expression clone pBAD-HNS was transformed into *E. coli* strain BL21* and protein was expressed with a 6X-His tag at the C-terminus. Cells were grown until OD600 to 0.6 and induced overnight with arabinose (0.1%) in 18 °C. Cells were pelleted and store in -20°C until required. For protein purification, cell pellets were resuspended in lysis buffer (20 mM Tris-HCl pH 7.4, 20 mM NaH2PO4, 500 mM NaCl, 10 mM imidazole) containing protease inhibitor (cOmplete, Roche) and sonicated for 3 min (2 sec. on, 4 sec. off, 30% amplitude on a Sonics Vibra-Cell sonicator. To lyse cells. The sample was centrifuged at 17000×g for 30 min at 4 °C (Sigma 3-18K). The supernant was then incubated with Talon cobalt His-tag resin (Clontech) for 1 h at 4°C. The resin was washed with 5 ml wash buffer A (20 mM Tris-HCl pH 7.4, 20 mM NaH_2PO_4, 500 mM NaCl, 10 mM imidazole, 3 mM BME), followed by wash buffer B (20 mM Tris-HCl pH 7.4, 20 mM NaH_2PO_4, 500 mM NaCl, 10 mM imidazole, 500 mM KCl and 20 mM Tris-HCl pH 7.4, 20 mM NaH_2PO_4, 500 mM NaCl, 10 mM imidazole and 3 mM BME), wash buffer C (20 mM Tris-HCl pH 7.4, 20 mM NaH_2PO_4, 1 M KCl, 10 mM imidazole and 3 mM BME), and wash buffer D (20 mM Tris-HCl pH 7.4, 20 mM NaH_2PO_4, 500 mM NaCl, 20 mM imidazole, 3 mM BME). H-NS protein was then eluted in 300 µl of elution buffer (20 mM Tris-HCl, 50 mM NaH_2PO_4, 500 mM NaCl, 250 mM imidazole and 20 mM Tris-HCl pH 7.4, 20 mM NaH_2PO_4, 500 mM NaCl, 10 mM imidazole, 3 mM BME). The purity of protein was evaluated by SDS PAGE and the protein concentration was measured using Coomassie (Bradford) Protein Assay Kit (Thermo Fisher Scientific) according to manufacturer protocol.

5.1.2.3 Amide Hydrogen/Deuterium Exchange Mass Spectrometry

HDXMS experiments on H-NS were carried out together with Dr. Gao Yunfeng, a then research fellow at Department of Biological Sciences, National University of Singapore. H-NS protein was changed into binding buffer A using Bio-Gel P6 micro bio-spin column (Bio-Rad) according to manufacturer's recommendations. The protein concentration was determined by Bradford assay (Thermo Fisher Scientific). The H-NS was incubated with DNA fragment in 100:1 molar ration in

binding buffer A at room temperature for 1 hour. Deuterium exchange was carried out by mixing 2 µl of 100-150µl of H-NS with 28 µl of D_2O (99.90%) buffer resulting in a final concentration of 93.3% deuterated buffer A (20 mM TrisCl, pH 8.0, 50 mM NaCl, 5 mM BME). Exchange was carried out at 20ºC for various times (0.5, 1, 2, 5 and 10min). The exchange reaction was quenched by adding 30 µL of pre-chilled 0.1% TFA to adjust pH to 2.5. 50 µl of the quenched sample was then injected on to a nano-UPLC sample manager at 4 °C (beta test version, Waters, Milford, MA). HPLC based separation and mass spectrometry along with peptide identification and data analysis were carried out as mentioned in chapter 3

5.1.3 Results

5.1.3.1 Ion mobility mass spectrometry of apo H-NS

We set out to determine the preferred oligomeric state of H-NS using Ion mobility mass spectrometry (IMS), a powerful technique (Sharon and Robinson 2007)that is well suited to report on the shape morphology of proteins in the gas solution phase. Results showed that H-NS existed in a mixture of monomers and dimeric states with the monomeric state being the preferred state (Figure 5.1.2).

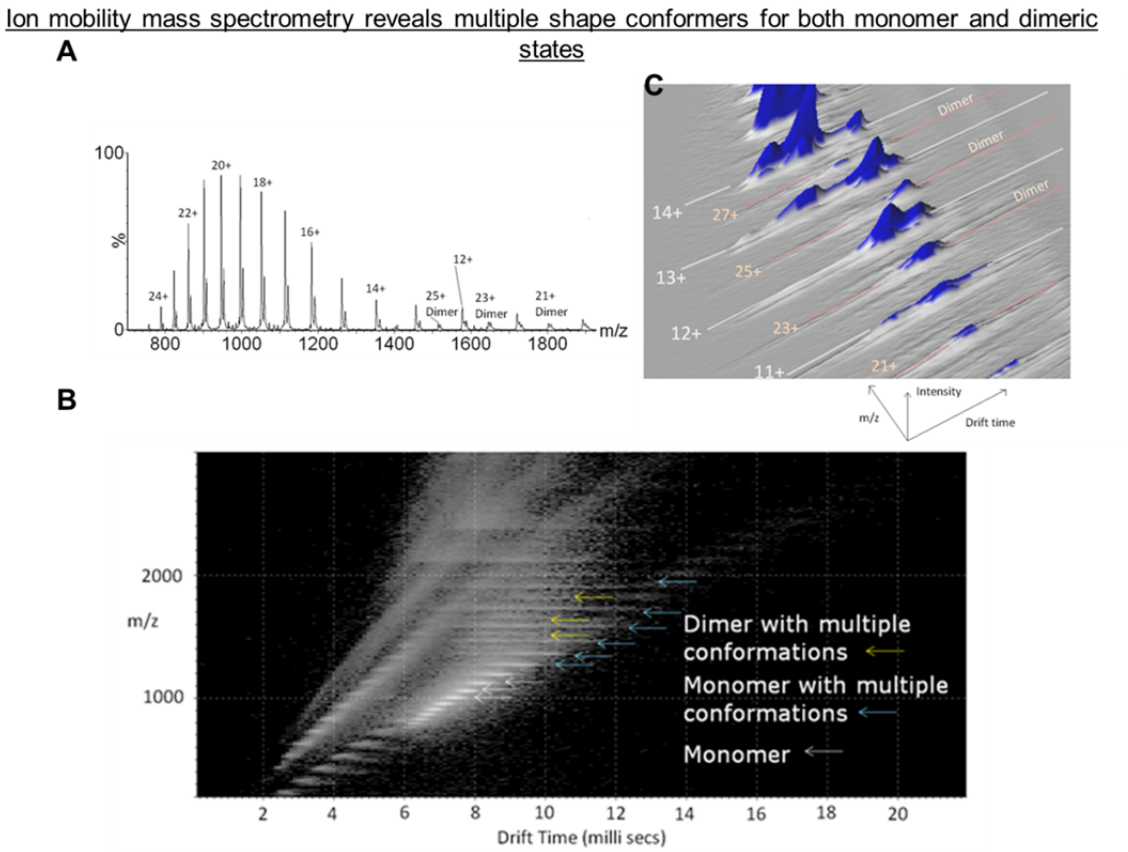

Figure 5.1.2: A. Mass spectrum of native H-NS in 200 mM Ammonium Acetate pH 8.0 data. The broad range of charge states reflects conformational heterogeneity at the low m/z values, while the higher m/z species (m/z~1400 and above) represent the H-NS dimer. At every charge state, the peak doublets are reflective of the intact protein with and without the N-terminal Methionine processed. B. Driftscope 2.1 plot of IMS-ToF analysis of HNS in 200mM Ammonium acetate pH 8.0 data, showing unstructured monomers (white arrows), multiply structured monomers (blue arrows) and multiply structured dimers (yellow arrows). C. 3D Driftscope 2.1 plot of IMS-ToF analysis of HNS in 200 mM Ammonium acetate pH 8.0, shows multiple conformations for the monomer and dimer, each with the same mass/charge but distinct drift times, reflective of heterogeneous shape morphologies in solution.

Interestingly, both the monomeric and dimeric species showed two distinct drift time profiles for the same mass-to-charge ratio of the ions examined. This provided clear evidence for conformational heterogeneity with at least two shape morphologies and suggested that H-NS existed as an ensemble of two or more distinct conformations in solution.

The mass spectra for the pH 7.0 and pH 8.0 buffered experiments show a wide range of charge states (11+ to 25+) and tending towards a relatively low m/z range, usually indicative of a denatured protein, however as HNS is believed to be have a high degree of disorder this observation is expected. Dimer peaks were also observed in the mass spectrum (Figure 5.1.2 A) among the lower charge states.

** Ion Mobility Mass spectrometry was carried out in collaboration with Mark Ritchie, Waters Asia-Pacific, Singapore*

Collisional Cross Sections for each of the monomers were compared to establish the number of potential structures in the ensemble. It is postulated that 4 distinct monomer structures exist.

5.1.3.2 Effects of DNA binding on H/D exchange in H-NS

To probe the conformational changes occurring in H-NS upon DNA binding, HDXMS experiments were carried out on *apo* H-NS and H-NS bound to DNA using both 140 bp DNA fragments, N-motif and GDF, as described earlier. Thirty peptides were obtained which corresponded to ~90% of the primary sequence of H-NS full length protein (Listed in Table 5.1.1). Analysis of deuteration exchange of *apo* H-NS protein revealed that many peptides show complete exchange in all the available backbone amide positions in 2 min, indicating that H-NS is a highly dynamic protein. The results are shown in table 5.1.1. Three peptides which spanned the residues 29-39 were of specific interest as they exhibited bimodal profiles for deuterium exchange as shown in Figure 5.1.3 A. These peptides span the N-Terminal dimerization domain of H-NS. The corresponding regions in the 3D structure of H-NS dimer are depicted in Figure 5.1.3 B.

Bimodal distributions indicate either that the protein exists in quasi-equivalent states or exhibits EX1 deuteration kinetics (Weis, Wales et al. 2006, Gertsman, Fu et al. 2010). Analysis of the isotopic profiles of the three peptides revealed that the peak width increased sharply after 2 min deuterium exchange and decreased after 30 min indicating EX1 kinetics (Weis, Wales et al. 2006).Also it was seen that while the intensities of the higher exchanging peak increased with deuteration times, the overall number of deuterons incorporated did not change. This is again consistent with EX1 hydrogen exchange kinetics

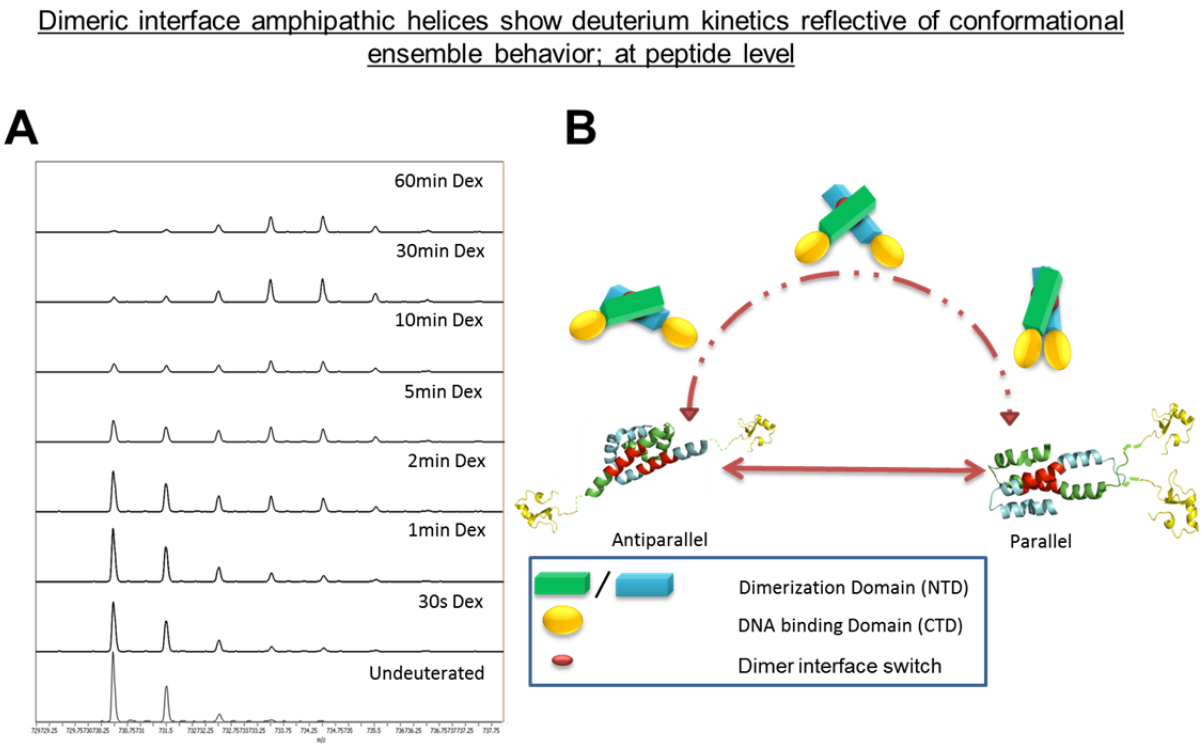

Figure 5.1.3: A)Electrospray ionization quadrupole time-of-flight (ESI-Q-TOF) mass spectra (A) for a peptide (m/z =730.4, z = 1), spanning residues 30-35, upon deuterium exchange (Dex). Two distinct exchange envelopes representative of a low exchanging conformation and a higher exchanging conformation were observed after 2 min Dex with a bimodal distribution characteristic of EX1 deuterium exchange kinetics and reflecting conformational heterogeneity within the region. B) Peptides exhibiting EX1 kinetics of deuterium exchange are highlighted in red in solution structures of the N terminal dimerization domain of H-NS in both (B) parallel (PDB:1NI8) and (C) antiparallel (PDB:1LR1) configurations. All peptides showing this pattern span the dimerization interface.

HDXMS analyses of both H-NS: DNA complexes were carried out using concentrations of protein and DNA optimized to ensure all the target DNA was fully saturated with H-NS. Amide H/D exchange analysis of the H-NS-N-motif complex revealed two regions of reduced deuterium exchange (Figure 5.1.4). A region spanning residues 80-99 is part of the linker region and N-terminal region of the C-terminal DNA binding region of the protein. The region exhibited reduced deuterium exchange only upon binding to N-motif but not GDF.

The region spanning residues 30-35 of *apo* H-NS which showed a bimodal distribution showed an altered profile when the N-motif DNA was complexed to H-NS with a shift favoring the low exchanging population. Interestingly, only very slight differences were observed in the GDF-H-NS complex (Figure 5.1.4 B). Furthermore, the bimodal distribution showed an even distribution of the higher and lower exchanging conformation. This suggested that H-NS conformational equilibria were

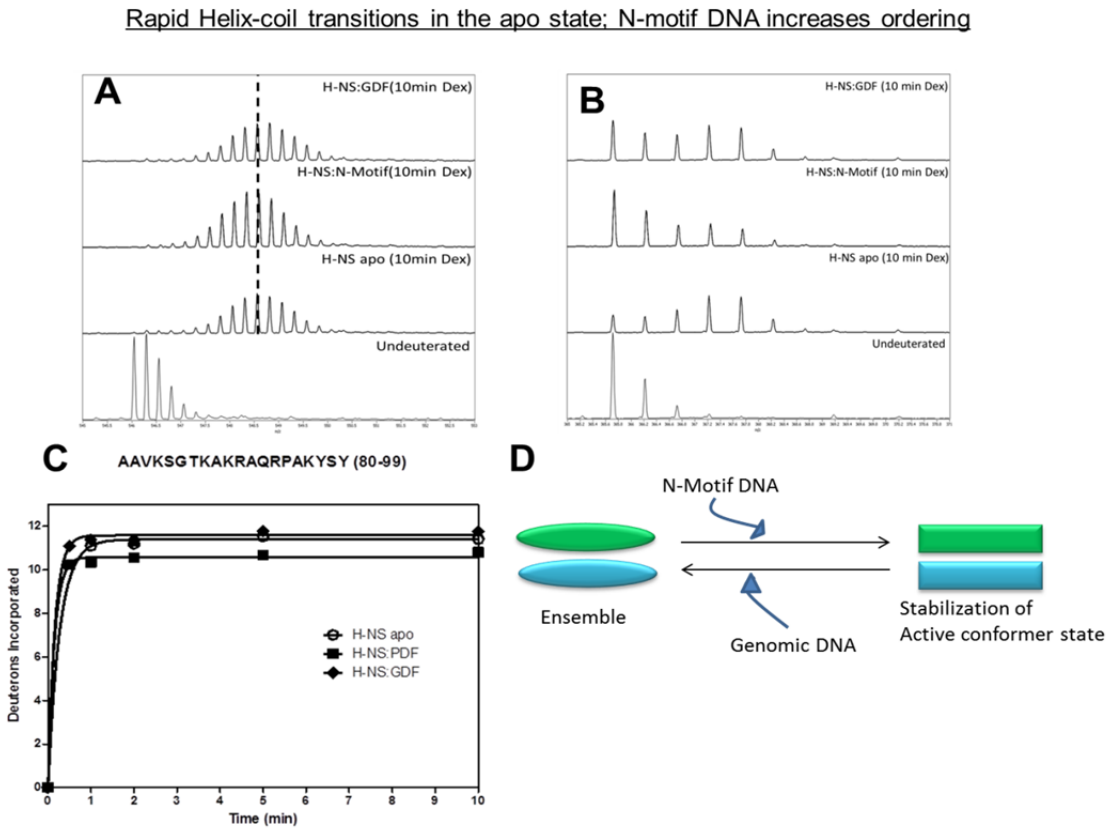

sensitive to DNA binding.

Figure 5.1.4: (A) Electrospray ionization quadrupole time-of-flight (ESI-Q-TOF) mass spectra of a peptide (m/z = 546.1, z =4) spanning H-NS residues 80-99 The isotopic envelope for (i) Undeuterated sample, (ii) *apo* H-NS (10 min Dex) , (iii) H-NS:N-motif DNA complex (10 min Dex) and (iv) H-NS: Genomic DNA complex (10 min Dex). Dashed line highlights the approximate centroid of *apo* H-NS and is provided as a reference point for comparison with the other two samples (B) Mass spectrum of H-NS N –Terminal peptide spanning residues 30-35, after 10 min of deuterium exchange, exhibiting bimodal distribution with the higher exchanging population being more predominant in the *apo* condition. On addition of N-motif DNA , the bimodal distribution shifts with majority of the population tending towards the lower exchanging population. On addition of Genomic DNA, the bimodal distribution shows a greater separation of higher and lower exchanging envelopes. (C). Kinetics of deuterium exchange in residues (80-99) of H-NS binding to DNA with and without N-Motif DBA. (o) *apo* H-NS (▲) H-NS:N-motif DNA complex and (▼)H-NS: Genomic DNA complex. D). In the unbound state, H-NS exists as an ensemble. Mg2+ or Nucleation-motif DNA alone selectively stabilize the dimer. This ability forms the basis for selectivity of H-NS function.

5.1.3.3 Effects of Mg^{2+} binding on H-NS conformational equilibria

Previous studies revealed that in the presence of Mg^{2+} ions, H-NS, which normally carries out gene silencing in the 'Stiffening mode', shifts to the 'Bridging mode' of Gene silencing (Liu, Chen et al. 2010). Analysis of deuterium exchange revealed that the most significant effect of Mg^{2+} was seen in the region spanning residues 30-35. The bimodal distribution that was observed in *apo* H-NS protein (Figure 5.1.3) was shifted in the presence of Mg^{2+}, to the same extent as seen in the H-NS-N-motif complex (Figure 5.14). This indicated that Mg^{2+} locked the H-NS protein into one conformation or preferentially 'selected' a particular conformation. H-NS-N-motif complex in the presence of Mg^{2+} had similar deuterium exchange profile compared to *apo* H-NS with Mg^{2+}. H-NS-GDF complex in the presence of Mg^{2+} had two important effects observed in the deuterium exchange profile. Firstly, in the C-terminal DNA binding domain, it was seen that the region exhibited increased dynamics (Fig. 5.1.5 A). In the N terminal dimerization domain, the region spanning residues 30-35 there is evidence for a bimodal distribution (Figure 5.1.5 B). These results show that in the presence of Mg^{2+}, N-motif with 'AT rich' motif has no effects on the conformational dynamics of H-NS. GDF DNA containing the 'random' DNA sequence, on the other hand, increases the dynamics of both the N terminal dimerization domain and the C terminal DNA binding domain.

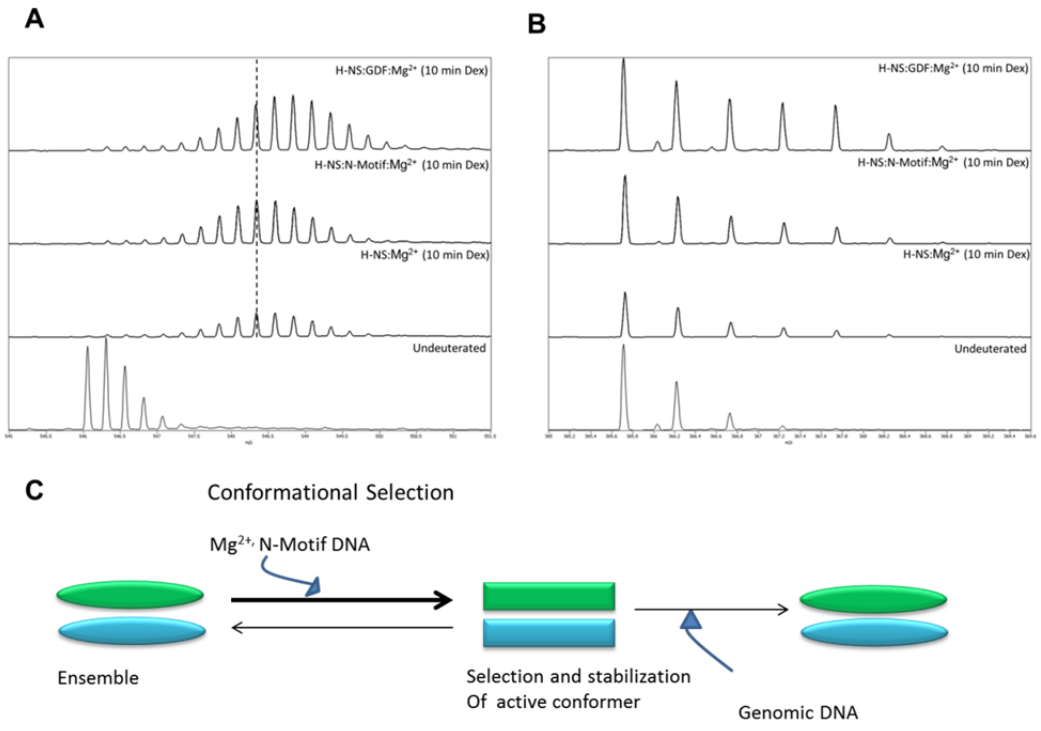

Figure 5.1.5: (A) Electrospray ionization quadrupole time-of-flight (ESI-Q-TOF) mass spectra of a peptide (m/z = 546.1, z =4) spanning H-NS residues 80-99 The isotopic envelope for (i) Undeuterated sample, (ii) *apo* H-NS (10 min Dex) , (iii) H-NS:N-motif DNA complex (10 min Dex) and (iv) H-NS: Genomic DNA complex (10 min Dex). Dashed line highlights the approximate centroid of *apo* H-NS and is provided as a reference point for comparison with the other two samples (B) Mass spectrum of H-NS N –Terminal peptide spanning residues 30-35, after 10 min of deuterium exchange, exhibiting bimodal distribution with the higher exchanging population being more predominant in the *apo* condition. On addition of N-motif DNA , the bimodal distribution shifts to a unimodal form. On addition of Genomic DNA, the bimodal distribution is more pronounced. C). In the unbound state, H-NS exists as an ensemble. Mg2+ or N-motif DNA alone selectively stabilize the dimer. While GDF drives H-NS conformation to a dynamic form.

5.1.3.4 Deuterium exchange tables

Table 5.1.1: Summary of Deuterium exchange (10 min Dex) for *Apo* H-NS, N-motif-H-NS and GDF-H-NS complexes

Peptide	No. of exchangeable amides	m/z	Z	H-NS *apo*	H-NS:PDF	H-NS:GDF
SEALKILNNIRTLRAQARE (2-20)	18	549.8	4	17.2 ± 0.0	17.3 ± 0.0	17.2 ± 0.1
ALKILNN (4-10)	6	785.5	1	4.7 ± 0.1	4.7±0.0	4.7 ± 0.0
KILNNIRT (6-13)	7	486.3	2	5.5 ± 0.1	5.6 ± 0.1	5.6 ± 0.0
IRTLRA (11-16)	5	365.238	2	3.4 ± 0.0	3.5 ± 0.0	3.4 ± 0.0
IRTLRAQARE (11-20)	9	405.241	3	7.7 ± 0.0	7.6 ± 0.0	7.7 ± 0.1
MLEKLEV (29-35)	6	431.2	2	ND	ND	ND
LEKLEV (30-35)	5	730.44	1	ND	ND	ND
EVVVNE (34-39)	5	688.3	1	ND	ND	ND
EVVVNERREEESAA (34-47) *	**13**	**808.9**	**2**	**9.2 ± 0.2**	**7.9 ± 0.0**	**8.6 ± 0.1**
VVNERREEESAA (36-47) *	**11**	**694.8**	**2**	**7.5**	**6.8 ± 0.0**	**7.1 ± 0.0**
VEERTRKLQQ (51-60)	9	643.8	2	6.2 ±0.2	6.5 ± 0.0	6.6 ± 0.1
YREML (61-65)	4	711.35	1	2.3 ± 0.0	2.5	2.5 ± 0.0
MLIADGID (58-71)	7	847.422	1	5.0 ± 0.1	5.0 ± 0.0	5.1 ± 0.05
IADGID (66-71)	5	603.3	1	3.2 ± 0.05	3.2 ± 0.1	3.2 ± 0.0
IADGIDPNE (66- 74)	7	943.431	1	4.4 ± 0.7	4.5 ± 0.0	4.5 ± 0.0
IADGIDPNEL (66- 75)	8	1056.51	1	5.1 ± 0.1	5.3 ± 0.0	5.2 ± 0.0
IADGIDPNELL (66-76)	9	1169.6	1	6.0 ± 0.3	6.4 ± 0.0	6.2 ± 0.0
LNSLAAVKSGTKAKRAQR (76-93)	17	475.536	4	8.7 ± 0.2	8.7 ± 0.1	8.8 ± 0.1

AAVKSGTKAKRAQRPAKYSY (80-99) *	**18**	**546.1**	**4**	**11.4 ± 0.1**	**10.8 ± 0.1**	**11.8 ± 0.2**
KSGTKAKRAQRPAKYSYV (83-100)*	**16**	**510.545**	**4**	**11.2 ± 0.1**	**11.0 ± 0.1**	**11.4 ± 0.1**
VDENGETKTWTGQGRTPAV (100-118)	17	682.669	3	12.1 ± 0.3	12.5 ± 0.0	12.1 ± 0.1
VDENGETKTWTGQGRTPAVI (100-119)	18	720.367	3	12.7 ± 0.3	13.2 ± 0.0	12.9 ± 0.1
VDENGETKTWTGQGRTPAVIKKAMDEQGKS (100-129)	28	653.135	5	20.1± 0.3	20.2 ± 0.1	20.5 ± 0.1
ETKTWTGQGRTPAVI (105-119)	13	822.9	2	9.4 ± 0.3	9.7 ± 0.05	9.5 ± 0.1
WTGQGRTPAVIKKAMDEQGKSLDDF (109-133)	23	695.357	4	17.5 ± 0.3	16.7 ± 0.0	17.2 ± 0.0
IKKAMDEQGKSLDD (119-132)	13	526.6	3	8.1 ± 0.10	8.0 ± 0.0	8.2 ± 0.0
IKKAMDEQGKSLDDF (119-133)	14	575.6	3	8.5 ± 0.1	8.3 ± 0.0	8.5 ± 0.0
KKAMDEQGKSLDD (120-132)	13	488.906	3	7.8 ± 0.15	7.9 ± 0.0	8.0 ± 0.0

*ND: Centroids could not be determined due to EX1 kinetics governing deuterium exchange. *Highlighted peptides showing reduce deuterium exchange upon binding to N-motif DNA. [a]Average number of deuterons exchanged determined from the mean and standard values after 10 min Dex. All deuterium exchange values reported were corrected for a 17% back exchange by multiplying the centroid values by a multiplication factor of 1.3.*

Table 5.1.2: Summary of Deuterium exchange (10 min Deuterium exchange) for H-NS, Nmotif-H-NS and GDF-H-NS complexes in the presence of 10 mM Mg^{2+} (Bridging mode conditions).

Peptide	**No. of exchangeable amides**	**m/z**	**Z**	**H-NS:Mg^{2+}**	**H-NS:PDF:Mg^{2+}**	**H-NS:GDF:Mg^{2+}**
SEALKILNNIRTLRAQARE (2-20)	18	549.8	4	17.3 ± 0.1	17.2 ± 0.1	17.5 ± 0.1
ALKILNN (4-10)	6	785.5	1	4.7 ± 0.0	4.7 ± 0.0	4.7 ± 0.01
KILNNIRT (6-13)	7	486.3	2	5.6 ± 0.1	5.5 ± 0.0	5.8 ± 0.0
IRTLRA (11-16)	5	365.2	2	3.5 ± 0.0	3.5 ± 0.0	3.6 ± 0.0
IRTLRAQARE (11-20)	9	405.2	3	7.7 ± 0.0	7.5 ± 0.13	7.9 ± 0.0
MLEKLEV (29-35)	6	431.2	2	ND	ND	ND
LEKLEV (30-35)	5	730.4	1	ND	ND	ND
EVVVNE (34-39)	5	688.3	1	ND	ND	ND
EVVVNERREEESAA (34-47) *	**13**	**808.9**	**2**	**7.4 ± 0.0**	**7.2 ± 0.1**	**8.1 ± 0.1**
VVNERREEESAA (36-47) *	**11**	**694.8**	**2**	**6.8 ± 0.0**	**6.5 ± 0.1**	**7.2 ± 0.0**
VEERTRKLQQ (51-60)	9	643.9	2	6.5 ± 0.0	6.5 ± 0.1	6.8 ± 0.0
YREML (61-65)	4	711.3	1	2.0 ± 0.0	2.1 ± 0.01	2.1 ± 0.0
MLIADGID (58-71)	7	847.4	1	4.8 ± 0.1	5.0 ± 0.1	5.0 ± 0.1

IADGID (66-71)	5	603.3	1	3.2 ± 0.0	3.2 ± 0.0	3.2 ± 0.0
IADGIDPNE (66- 74)	7	943.4	1	4.7 ± 0.0	4.6 ± 0.0	4.7 ± 0.0
IADGIDPNEL (66- 75)	8	1056.5	1	5.5 ± 0.2	5.3 ± 0.0	5.4 ± 0.0
IADGIDPNELL (66-76)	9	1169.6	1	6.4 ± 0.1	6.4 ± 0.0	6.4 ± 0.0
LNSLAAVKSGTKAKRAQR (76-93)	**17**	**475.5**	**4**	**8.9 ± 0.2**	**8.9 ± 0.1**	**9.4 ± 0.1**
AAVKSGTKAKRAQRPAKYSY (80-99) *	**18**	**546.1**	**4**	**11.3 ± 0.0**	**10.9 ± 0.1**	**12.4 ± 0.1**
KSGTKAKRAQRPAKYSYV (83-100)	**16**	**510.5**	**4**	**11.0 ± 0.0**	**10.1 ± 0.1**	**12.3 ± 0.1**
VDENGETKTWTGQGRTPAV (100-118)	17	682.7	3	12.5 ± 0.1	12.5 ± 0.0	12.7 ± 0.0
VDENGETKTWTGQGRTPAVI (100-119)	18	720.4	3	13.3 ± 0.1	13.3 ± 0.0	13.5 ± 0.1
VDENGETKTWTGQGRTPAVIKKAMDEQGKS (100-129)	**28**	**653.1**	**5**	**20.1 ± 0.5**	**20.2 ± 0.2**	**21.7 ± 0.1**
ETKTWTGQGRTPAVI (105-119)	13	822.9	2	9.6 ± 0.2	9.7 ± 0.0	10.1 ± 0.1
WTGQGRTPAVIKKAMDEQGKSLDDF (109-133)	**23**	**695.4**	**4**	**17.0 ± 0.2**	**16.8 ± 0.2**	**18.4 ± 0.0**
IKKAMDEQGKSLDD (119-132)	**13**	**526.6**	**3**	**8.0 ± 0.1**	**7.8 ± 0.1**	**8.7 ± 0.0**
IKKAMDEQGKSLDDF (119-133)	**14**	**575.6**	**3**	**8.4 ± 0.1**	**8.3 ± 0.1**	**9.0 ± 0.0**
KKAMDEQGKSLDD (120-132)	**13**	**488.9**	**3**	**7.5 ± 0.0**	**7.5 ± 0.1**	**8.0 ± 0.0**

*ND: Centroids could not be determined due to EX1 kinetics governing deuterium exchange. *Peptides showed increased deuterium exchanges upon binding to GDF in the presence of 10 mM Mg^{2+}. [a]Average number of deuterons exchanged determined from the mean and standard values for a 2-min.*

Table 5.1.3: Summary of Deuterium exchange (10 min Deuterium exchange) for *Apo* H-NS and H-NS (+Mg^{2+})

Peptide	**No. of exchangeable amides**	**m/z**	**Z**	**H-NS *apo***	**H-NS:Mg^{2+}**
SEALKILNNIRTLRAQARE (2-20)	18	549.8	4	17.2±0.05	17.31±0.09
ALKILNN (4-10)	6	785.5	1	4.66±0.07	4.69±0.04
KILNNIRT (6-13)	7	486.3	2	5.5±0.13	5.62±0.12
IRTLRA (11-16)	5	365.238	2	3.41±0.04	3.47±0.03
IRTLRAQARE (11-20)	9	405.241	3	7.66±0.02	7.69±0.0
MLEKLEV (29-35)	6	431.2	2	ND	ND
LEKLEV (30-35)	5	730.44	1	ND	ND
EVVVNE (34-39)	5	688.3	1	ND	ND
EVVVNERREEESAA (34-47)	**13**	**808.9**	**2**	**9.20±0.22**	**7.39±0.03**
VVNERREEESAA (36-47)	**11**	**694.8**	**2**	**7.46**	**6.83±0.01**

VEERTRKLQQ (51-60)	9	643.867	2	6.25±0.2	6.53±0.0
YREML (61-65)	4	711.35	1	2.34±0.01	1.96±0.0
MLIADGID (58-71)	7	847.422	1	4.99±0.13	4.80±0.15
IADGID (66-71)	5	603.3	1	3.17±0.05	3.22±0.02
IADGIDPNE (66- 74)	7	943.431	1	4.42±0.7	4.70±0.02
IADGIDPNEL (66- 75)	8	1056.51 1	1	5.14±0.14	5.50±0.16
IADGIDPNELL (66-76)	9	1169.6	1	5.97±0.26	6.45±0.07
LNSLAAVKSGTKAKRAQR (76-93)	17	475.536	4	8.71±0.25	8.95±0.18
AAVKSGTKAKRAQRPAKYSY (80-99)	18	546.1	4	11.42±0.14	11.26±0.0
KSGTKAKRAQRPAKYSYV (83-100)	16	510.545	4	11.22±0.14	11.04±0.0
VDENGETKTWTGQGRTPAV (100-118)	17	682.669	3	12.07±0=.35	12.51±0.15
VDENGETKTWTGQGRTPAVI (100-119)	18	720.367	3	12.75±0.34	13.27±0.1
VDENGETKTWTGQGRTPAVIKKAMDEQGKS (100-129)	28	653.135	5	20.11±0.299	20.14±0.5
ETKTWTGQGRTPAVI (105-119)	13	822.9	2	9.44±0.27	9.62±0.19
WTGQGRTPAVIKKAMDEQGKSLDDF (109-133)	23	695.357	4	17.51±0.26	17.05±0.16
IKKAMDEQGKSLDD (119-132)	13	526.6	3	8.14±0.13	7.99±0.1
IKKAMDEQGKSLDDF (119-133)	14	575.6	3	8.49±0.09	8.42±0.11
KKAMDEQGKSLDD (120-132)	13	488.906	3	7.82±0.15	7.52±0.05

*ND: Centroids could not be determined due to EX1 kinetics governing deuterium exchange. *Peptides showed reduce deuterium exchanges with 10 mM Mg^{2+} (Bridging mode conditions).[a]Average number of deuterons exchanged (2 min deuterium exchange). All deuterium exchange values reported were corrected for a 17% back exchange by multiplying the centroid values by a multiplication factor of 1.3.*

5.1.4 Discussion

Ion mobility experiments provided compelling evidence that H-NS exists in an ensemble of conformations. It is known that H-NS is a partially disordered protein, but interestingly, IMS revealed that H-NS preferentially populates a subset of 4 populations as opposed to a continuum of conformations. This suggests that the anti-parallel and parallel forms of H-NS would be quasi-stable forms of H-NS. HDXMS studies of H-NS with N-motif DNA and GDF revealed that N-motif DNA drives H-NS to a stable conformation while GDF does not alter the stability of H-NS. Mg^{2+} was

previously shown to influence H-NS to switch from the 'sitffening' form to the 'bridging' form (Liu, Chen et al. 2010). Experiments with H-NS in the presence of Mg^{2+} provided interesting results when DNA fragments were introduced. In the presence of Mg^{2+}, N-motif DNA had no further stabilization effect on H-NS but GDF was seen to cause local unfolding of existing Mg^{2+} mediated stable conformation. These results provide an explanation for how DNA and Mg^{2+} influence conformational switching in H-NS. These results are summarized in Figure 5.1.6

This study highlights the role of H-NS in understanding the interplay between dynamics and function in disordered proteins. While the availability of a three-dimensional structure would greatly aid data analysis, it is not essential to tease out a correlation between dynamics and function of proteins with a high degree of disorder.

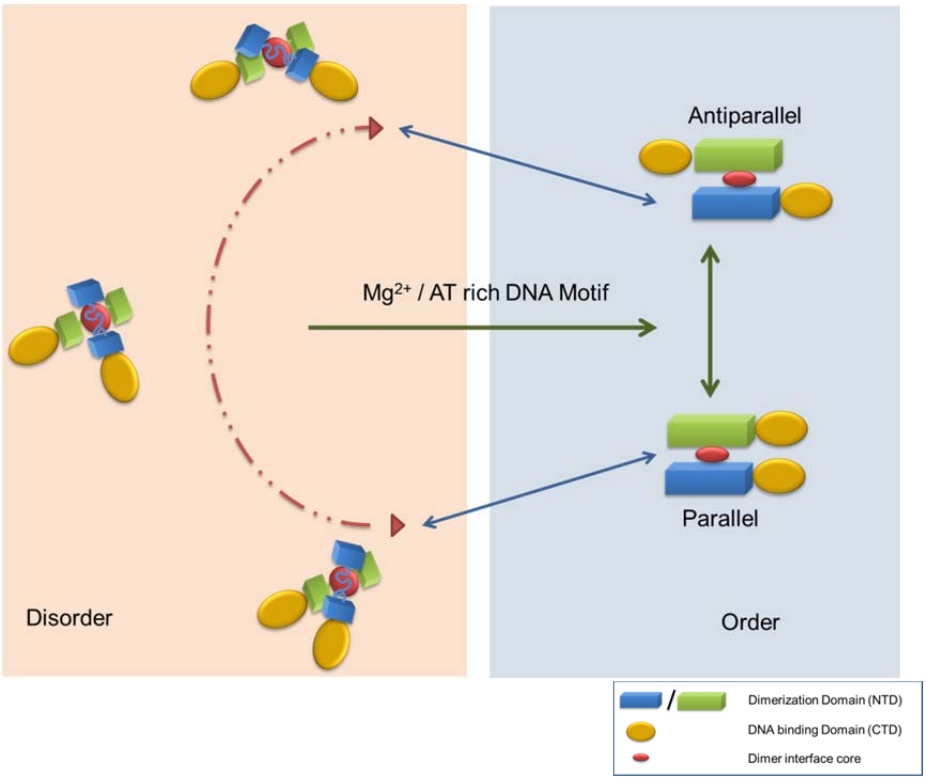

Figure 5.1.6: Figure 5. Model for H-NS Dynamics and function: H-NS exists as an ensemble of interconverting parallel and antiparallel conformations with a hydrophobic core at the dimer interface formed by two amphipathic helices maintaining the dimer. Mg2+ or N-motif DNA alone stabilize one conformation associated with gene silencing while DNA increases conformational dynamics of H-NS.

5.2 Part II- Monitoring transient virus capsid-maturation protease interactions by HDXMS in the maturation pathway of HK97 bacteriophage

5.2.1 Introduction

Virus maturation is an integral part of the lifecycle of the virus and it corresponds to a transition from an initial non-infectious to an infectious and robust virion. Viruses are maturation begins with the production of large amounts of the individual subunit proteins. The virus maturation pathway begins by the spontaneous association of these subunit proteins driven by an association energy that favors assembly over disassembly. But there are provisions for self-correction to correct mismatched interactions.(Caspar 1980, Katen and Zlotnick 2009). In this study, a lambdoid dsDNA phage HK97 is studied as a model system to understand virus maturation dynamics. It constitutes an accessible model system for studying maturation of such viruses due to its well characterized genetics and ease of handling (Veesler and Johnson 2012). Its capsid maturation pathway is mediated by intermediate particle forms (Figure 5.2.1) which constitute discrete steps in the maturation pathway and each step can be isolated using a combination of molecular biology and biochemical techniques. The HK97 capsid precursor protein is composed of two main regions, the scaffolding protein (δ-domain, residues 2-103) and the coat subunit (residues 104-385) which spontaneously forms a mixture of hexamers and pentamers upon association. *In vivo*, 415 coat subunits (60 hexamers and 11 pentamers) assemble with a dodecameric portal along with an unknown number of protease molecules in an icosahedral configuration called Prohead-1 (Figure 5.2.1). This is a reversible state and it is possible to revert back to the individual subunit molecules by maintaining the right conditions. Activation of the viral protease, which occurs after particle assembly, is initiated by the protease mediated digestion of the scaffolding domains and autodigestion of the aforementioned protease to produce small peptide fragments that diffuse out of the particle to yield Prohead-2. This step is in an irreversible step and constitutes a key step in the activation of the virus maturation pathway (Gertsman, Gan et al. 2009,

Huang, Khayat et al. 2011). The Prohead-2 state is a meta-stable local free-energy minimum state and is primed to fold to a lower energy conformation constituting the expansion and cross linking segment of the virus maturation pathway. Native mass spectrometry based quantification of the number of protease molecules in each Prohead 1 capsid particle revealed, ~120 copies of protease molecules exist in each viral capsid (Veesler, Khayat et al. 2013).

In this study HDXMS is used to map the interactions that the protease makes with viral capsid protein. A catalytically dead protease is used, so the virus is trapped in a transient state. The scaffolding domain is present in the first 100 amino acids of the viral capsid protein, thus the protease interactions were expected to occur at N-terminal region of the protein. Interestingly conformational stabilization effects distal to the interaction site were also observed. A distinction between binding and conformational stabilization could be made based on the time dependent changes observed.

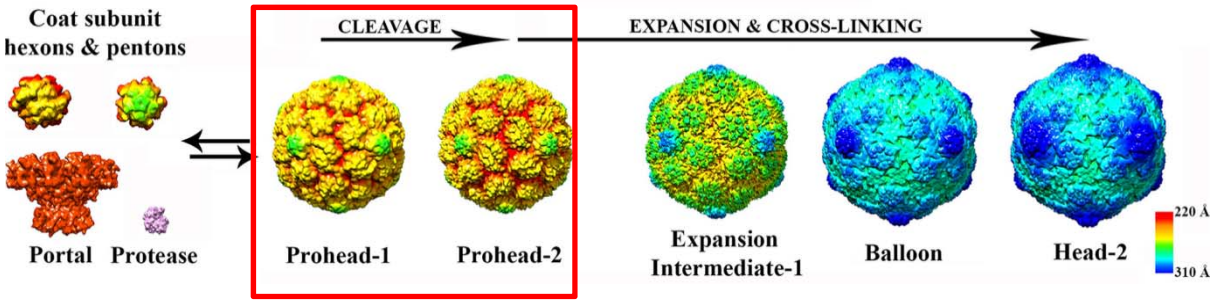

Adapted from (Gertsman, Gan et al. 2009)

Figure 5.2.1: HK97 maturation pathway involves three main steps, the reversible association of hexons and pentons of the coat protein to form Prohead-1 state, the irreversible protease mediated cleavage of the scaffolding domain and the spontaneous expansion and cross-linking steps.

5.2.2 Experimental procedures

5.2.2.1 Viral capsid expression and purification

Intact HK97 bacteriophage Prohead 1 particle with inactive protease was expressed and purified by previously described methods in (Gertsman, Gan et al. 2009) . Intact Prohead 1 particle was obtained from our collaborator, Prof. John E. Johnson's lab at Scripps Research Institute at La Jolla, California.

5.2.2.2 Amide hydrogen/deuterium exchange mass spectrometry

Prohead 1 with and without maturation protease was maintained at 5 mg/ml concentration to get adequate signal in the mass spectrometric analysis. All deuterium exchange experiments were carried out in a 99.9% D_2O buffer containing 20mM Tris-HCl, 50mM NaCl, maintained at pH 7.5. HDXMS experiments were carried out as described in materials and methods of chapter 3.

5.2.3 Results and Discussions

5.2.3.1 The maturation protease binds at the N terminal scaffolding domain

HDXMS experiments were carried out comparing Prohead 1 state in presence and absence of the maturation protease. A total of 81 peptides were obtained which corresponded to 93% coverage of the primary sequence. It was seen that the protease molecules interact mainly at the N terminal scaffolding domain. Protease binding at the N terminal caused stabilization of the entire scaffolding domain. These effects were observed almost exactly until the end of the 100 amino acid scaffolding domain (Figure 5.2.2).

These stabilization effects were observed as a decrease in deuterium exchange across almost all peptides across the first 100 residues. The main decreases in deuterium exchange were seen at residues 5-21 and 22-44 with deuterium exchange protection of almost 2 Da observed. As mentioned earlier, only 120 protease molecules exist in each viral capsid protein while each capsid has more than 400 capsid protein molecules. There is a vast excess of capsid protein to protease molecules. These results are remarkable as 1:4 molar ratio of protease of capsid protein gives almost 2 Da of protection at the binding site. It can be postulated that if equimolar ratios of protease to capsid protein exist, the deuterium exchange decrease would only be greater.

5.2.3.2 Conformational stabilization effects caused by protease binding affect distal regions of the capsid protein

While protease binding showed significant decreases at the scaffolding domain, all other regions of the protein showed decreased deuterium exchange indicating, protease binding stabilizes the capsid.

Certain regions of the protein showed significant (>0.5 Da) decreases in deuteration greater and these regions represent the conformational stabilization effects seen upon protease binding.

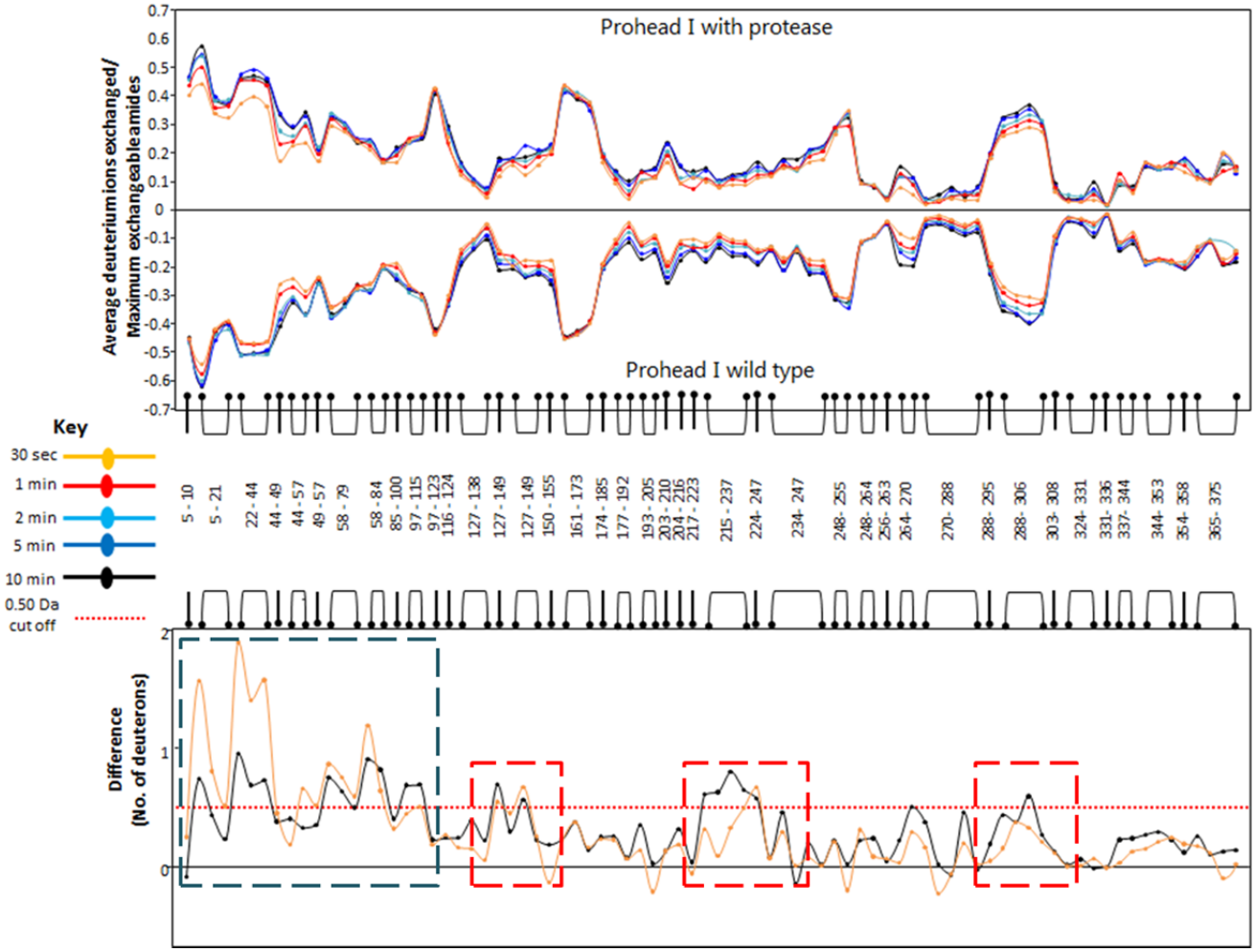

Figure 5.2.2: Summary of HDXMS results from HK97 interactions with processing protease: Top panel: Mirror plot of the relative deuterium exchange across pepsin digest fragments from N to C-terminus. Each plot represents a time point of deuterium labeling (t=30s, 1min, 2min, 5min, 10min), color coded as indicated. Bottom panel: Difference plot showing the average mass difference resulting from deuterium exchange between the two Prohead-1 forms, i.e. protease-free minus protease-containing procapsids. Positive differences represent regions that are protected from deuterium exchange in presence of the protease. Regions showing direct binding effects at the scaffolding domain are boxed in blue. Regions showing conformational stabilization effects are boxed in red.

(Adapted and reprinted with permission from Veesler.D et al, 2013)

Stabilization effects were mainly observed in regions distal to the protease binding site. These regions were mostly seen at residues spanning residues 127-149, 215-247, 264-270 and 288-306 (Figure 5.2.2). These regions are plotted onto, the structure of the hexameric capsid protein in Figure 5.2.3. These regions may be distal to each other on the monomeric form of the capsid protein but in the hexamer, structure these regions form a contiguous surface. There is the existence of two rings of stabilization effects, one ring follows the outer edge of the hexamer and the other effect is concentrated at the center of the hexamer.

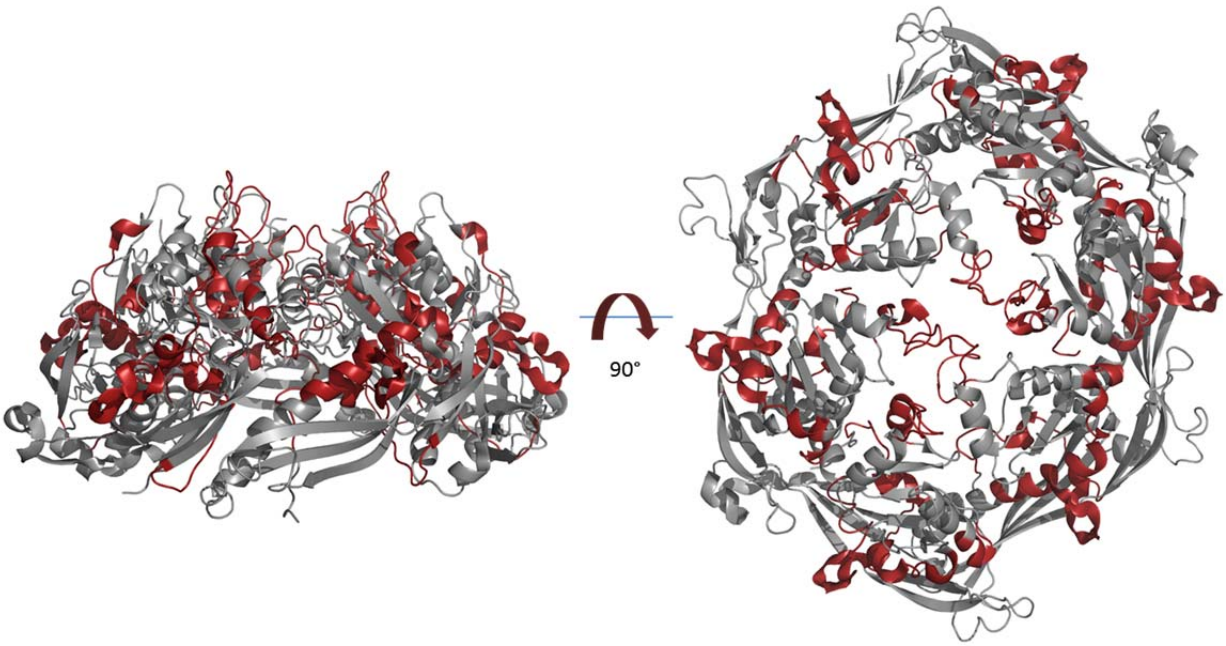

Figure 5.2.3: HDXMS results mapped onto HK97 structures: Structure of the hexameric HK97 subunit molecule (PDB ID: 3QPR), looking at the hexamer side on (left) and front on (right). This structure does not contain the N terminal scaffolding domain. Regions showing significant stabilization effects are mapped in red.

An important observation was of time dependence in deuterium exchange differences. As seen in the previous chapter, the binding site shows large differences in deuterium exchange at early time points while the allosteric effects show greater changes at later time points. This is an indication that the protease molecule follows an fast association/dissociation pattern. The protease molecule is an enzymatic molecule which cleaves the scaffolding domain before binding and cleaving its next target. In our experiment, the protease molecule is inactive, but it is still capable of binding target domains.

The molecule shuttles between the scaffolding domains of the capsid protein, without cleaving the scaffolding domains, thus it leads to increased exchange over time at the binding interface, but conformational stabilization effects take place at a slower timescale and hence are observed upon protease binding.

5.3 Conclusions

This chapter focused on deciphering protein dynamics of an partially disordered protein and a viral maturation pathway. In both examples, it was seen that a thorough understand of the dynamics of the system provided deep insights into the function of the protein. The complexity of the systems studied made analysis of the results that much more challenging. But it was seen that parallels could be drawn from studies carried out on soluble proteins (explained in earlier chapters) and applied to understand these complex biological systems better.

6 Concluding Remarks and Future directions

The aim of my research has been to use protein dynamics information obtained from structural mass spectrometry and correlate it with its function. I describe how dynamics plays a key role in the activation phase of the cAMP signaling pathway. The dissociation of the PKA holoenzyme is brought about by cAMP binding and induces increased dynamics in the regulatory subunit of PKA, this causes allosteric effects across the interaction interface to cause increased dynamics at the catalytic subunit. In the termination phase of the cAMP signaling pathway, the formation of a transient ternary complex was monitored along with ligand release, providing insights into how PDEs mediate release and hydrolysis of cAMP from PKA. PDE8A was found to be a mammalian homolog of RegA and found to cause the dissociation of cAMP bound to PKA. The interaction interface between PDE8 and PKA regulatory domain was also described for the first time and a model for how cAMP termination progresses, was provided. HDXMS was subsequently applied to fragment screening and deciphering dynamics and function of complex biological systems.

These results pave the way for future directions to further understand how transient states play a role in biological regulation.

1. Monitoring cAMP mediated dissociation of PKA holoenzyme

In this study we had used Rp-cAMPS, a cAMP analog which captures the ternary complex in a metastable state. HDXMS of the PKA holoenzyme interaction with cAMP can be monitored by starting the deuterium exchange reaction along with the addition of cAMP. Real time monitoring of cAMP binding and PKA holoenzyme dissociation can provide interesting insights into the processes involved in the dissociation of the complex.

2. Interactions between RegA and the PKA regulatory subunit from *Dictyostelium*

Previously described RegA-PKA, were between a *Dictyostelium* RegA and a mammalian PKA. In this study, a model was described for PDE-PKA interactions in a mammalian system. Similar experiments can be carried out in proteins from *Dictyostelium* to confirm whether the proposed model is evolutionarily conserved.

3. Deciphering stoichiometry of the PDE-PKA complex

In this study we propose a model where the PDE8 dimer binds to the tandem CNB domains of PKAR. To experimentally prove the actual stoichiometry of the complex, native mass spectrometry techniques can be employed to calculate the overall mass of the complex and its constituent components. This will provide detailed insight into the intact complex and confirm our model on PDE-PKA interactions.

4. PDE-PKA interactions occur only in the presence of cAMP

The sequence of events in the cAMP signaling pathway dictates that PDE-PKA interactions can only occur when PKA R is bound to cAMP. As it is the termination phase of the cAMP pathway, PDE would only recognize the cAMP bound form of PKA R. While this seems logical, to prove this concept, ion mobility mass spectrometry of the complex can be carried out. Ion mobility mass spectrometry describes the cross section of a molecule in the microsecond regime, thus complex formation and dissociation can be monitored in the presence and absence of cAMP.

5. HDXMS in fragment screening of membrane proteins

The sensitivity and robustness of HDXMS, makes this technique ideally suited to be included in the fragment screening pipeline. This screening technique can be applied to challenging drug targets which are currently inaccessible to traditional structure based fragment screening techniques. While membrane proteins are high value drug targets that influence entire signaling pathway, they are difficult targets for structural characterization. Recent work on me

7 References

- Abu-Abed, M., R. Das, L. Wang and G. Melacini (2007). "Definition of an electrostatic relay switch critical for the cAMP-dependent activation of protein kinase A as revealed by the D170A mutant of RIalpha." Proteins **69**(1): 112-124.
- Akimoto, M., R. Selvaratnam, E. T. McNicholl, G. Verma, S. S. Taylor and G. Melacini (2013). "Signaling through dynamic linkers as revealed by PKA." Proc Natl Acad Sci U S A **110**(35): 14231-14236.
- Ali, M. M., S. M. Roe, C. K. Vaughan, P. Meyer, B. Panaretou, P. W. Piper, C. Prodromou and L. H. Pearl (2006). "Crystal structure of an Hsp90-nucleotide-p23/Sba1 closed chaperone complex." Nature **440**(7087): 1013-1017.
- Amieux, P. S. and G. S. McKnight (2002). "The essential role of RI alpha in the maintenance of regulated PKA activity." Ann N Y Acad Sci **968**: 75-95.
- Anand, G., S. S. Taylor and D. A. Johnson (2007). "Cyclic-AMP and Pseudosubstrate Effects on Type-I A-Kinase Regulatory and Catalytic Subunit Binding Kinetics." Biochemistry **46**(32): 9283-9291.
- Anand, G. S., C. A. Hughes, J. M. Jones, S. S. Taylor and E. A. Komives (2002). "Amide H/2H exchange reveals communication between the cAMP and catalytic subunit-binding sites in the R(I)alpha subunit of protein kinase A." J Mol Biol **323**(2): 377-386.
- Anand, G. S., S. Krishnamurthy, T. Bishnoi, A. Kornev, S. S. Taylor and D. A. Johnson (2010). "Cyclic-AMP and Rp-cAMPS induced conformational changes in a complex of the catalytic and regulatory (RIa) subunits of PKA." Mol Cell Proteomics.
- Anand, G. S., S. Krishnamurthy, T. Bishnoi, A. Kornev, S. S. Taylor and D. A. Johnson (2010). "Cyclic AMP- and (Rp)-cAMPS-induced conformational changes in a complex of the catalytic and regulatory (RI{alpha}) subunits of cyclic AMP-dependent protein kinase." Mol Cell Proteomics **9**(10): 2225-2237.
- Anand, G. S., D. Law, J. G. Mandell, A. N. Snead, I. Tsigelny, S. S. Taylor, L. F. Ten Eyck and E. A. Komives (2003). "Identification of the protein kinase A regulatory RIalpha-

catalytic subunit interface by amide H/2H exchange and protein docking." Proc Natl Acad Sci U S A **100**(23): 13264-13269.

- Anfinsen, C. B. (1973). "Principles that govern the folding of protein chains." Science **181**(4096): 223-230.
- Anfinsen, C. B., D. Steinberg and M. Vaughan (1956). "Kinetic aspects of assembly and degradation of proteins." Science **124**(3218): 389-395.
- Arnold, K., L. Bordoli, J. Kopp and T. Schwede (2006). "The SWISS-MODEL workspace: a web-based environment for protein structure homology modelling." Bioinformatics **22**(2): 195-201.
- Arold, S. T., P. G. Leonard, G. N. Parkinson and J. E. Ladbury (2010). "H-NS forms a superhelical protein scaffold for DNA condensation." Proc Natl Acad Sci U S A **107**(36): 15728-15732.
- Atlung, T. and H. Ingmer (1997). "H-NS: a modulator of environmentally regulated gene expression." Mol Microbiol **24**(1): 7-17.
- Badireddy, S., G. Yunfeng, M. Ritchie, P. Akamine, J. Wu, C. W. Kim, S. S. Taylor, L. Qingsong, K. Swaminathan and G. S. Anand (2011). "Cyclic AMP analog blocks kinase activation by stabilizing inactive conformation: conformational selection highlights a new concept in allosteric inhibitor design." Mol Cell Proteomics **10**(3): M110 004390.
- Bai, Y., J. S. Milne, L. Mayne and S. W. Englander (1993). "Primary structure effects on peptide group hydrogen exchange." Proteins **17**(1): 75-86.
- Bateman, R. H., R. Carruthers, J. B. Hoyes, C. Jones, J. I. Langridge, A. Millar and J. P. Vissers (2002). "A novel precursor ion discovery method on a hybrid quadrupole orthogonal acceleration time-of-flight (Q-TOF) mass spectrometer for studying protein phosphorylation." J Am Soc Mass Spectrom **13**(7): 792-803.
- Beebe, S. J. (1994). "The cAMP-dependent protein kinases and cAMP signal transduction." Semin Cancer Biol **5**(4): 285-294.
- Beebe, S. J. a. C., J.D. (1986). Cyclic nucleotide-dependent protein kinase.

- Benson, E. E. and K. Linderstrom-Lang (1959). "Deuterium exchange between myoglobin and water." Biochim Biophys Acta **32**: 579-581.
- Berendsen, H. J. and S. Hayward (2000). "Collective protein dynamics in relation to function." Curr Opin Struct Biol **10**(2): 165-169.
- Berman, H. M., L. F. Ten Eyck, D. S. Goodsell, N. M. Haste, A. Kornev and S. S. Taylor (2005). "The cAMP binding domain: an ancient signaling module." Proc Natl Acad Sci U S A **102**(1): 45-50.
- Boehr, D. D., R. Nussinov and P. E. Wright (2009). "The role of dynamic conformational ensembles in biomolecular recognition." Nat Chem Biol **5**(11): 789-796.
- Bogacheva, O., O. Bogachev, M. Menon, A. Dev, E. Houde, E. I. Valoret, H. M. Prosser, C. L. Creasy, S. J. Pickering, E. Grau, K. Rance, G. P. Livi, V. Karur, C. L. Erickson-Miller and D. M. Wojchowski (2008). "DYRK3 dual-specificity kinase attenuates erythropoiesis during anemia." J Biol Chem **283**(52): 36665-36675.
- Brough, P. A., X. Barril, J. Borgognoni, P. Chene, N. G. Davies, B. Davis, M. J. Drysdale, B. Dymock, S. A. Eccles, C. Garcia-Echeverria, C. Fromont, A. Hayes, R. E. Hubbard, A. M. Jordan, M. R. Jensen, A. Massey, A. Merrett, A. Padfield, R. Parsons, T. Radimerski, F. I. Raynaud, A. Robertson, S. D. Roughley, J. Schoepfer, H. Simmonite, S. Y. Sharp, A. Surgenor, M. Valenti, S. Walls, P. Webb, M. Wood, P. Workman and L. Wright (2009). "Combining hit identification strategies: fragment-based and in silico approaches to orally active 2-aminothieno[2,3-d]pyrimidine inhibitors of the Hsp90 molecular chaperone." J Med Chem **52**(15): 4794-4809.
- Buechler, Y. J. and S. S. Taylor (1991). "Mutations in the autoinhibitor site of the regulatory subunit of cAMP-dependent protein kinase I. Replacement of Ala-97 and Ser-99 interferes with reassociation with the catalytic subunit." J Biol Chem **266**(6): 3491-3497.
- Burgin, A. B., O. T. Magnusson, J. Singh, P. Witte, B. L. Staker, J. M. Bjornsson, M. Thorsteinsdottir, S. Hrafnsdottir, T. Hagen, A. S. Kiselyov, L. J. Stewart and M. E. Gurney

(2010). "Design of phosphodiesterase 4D (PDE4D) allosteric modulators for enhancing cognition with improved safety." Nat Biotechnol **28**(1): 63-70.

- Burns-Hamuro, L. L., Y. Ma, S. Kammerer, U. Reineke, C. Self, C. Cook, G. L. Olson, C. R. Cantor, A. Braun and S. S. Taylor (2003). "Designing isoform-specific peptide disruptors of protein kinase A localization." Proc Natl Acad Sci U S A **100**(7): 4072-4077.
- Canaves, J. M. and S. S. Taylor (2002). "Classification and phylogenetic analysis of the cAMP-dependent protein kinase regulatory subunit family." J Mol Evol **54**(1): 17-29.
- Caspar, D. L. (1980). "Movement and self-control in protein assemblies. Quasi-equivalence revisited." Biophys J **32**(1): 103-138.
- Changeux, J. P. and S. Edelstein (2011). "Conformational selection or induced fit? 50 years of debate resolved." F1000 Biol Rep **3**: 19.
- Conti, M. and J. Beavo (2007). "Biochemistry and physiology of cyclic nucleotide phosphodiesterases: essential components in cyclic nucleotide signaling." Annu Rev Biochem **76**: 481-511.
- Corbin, J. D., C. E. Cobb, S. J. Beebe, D. K. Granner, S. R. Koch, T. W. Gettys, P. F. Blackmore, S. H. Francis and J. N. Wells (1988). "Mechanism and function of cAMP- and cGMP-dependent protein kinases." Adv Second Messenger Phosphoprotein Res **21**: 75-86.
- Corbin, J. D., P. H. Sugden, L. West, D. A. Flockhart, T. M. Lincoln and D. McCarthy (1978). "Studies on the properties and mode of action of the purified regulatory subunit of bovine heart adenosine 3':5'-monophosphate-dependent protein kinase." J Biol Chem **253**(11): 3997-4003.
- Csermely, P., R. Palotai and R. Nussinov (2010). "Induced fit, conformational selection and independent dynamic segments: an extended view of binding events." Trends Biochem Sci **35**(10): 539-546.
- Das, R., V. Esposito, M. Abu-Abed, G. S. Anand, S. S. Taylor and G. Melacini (2007). "cAMP activation of PKA defines an ancient signaling mechanism." Proc Natl Acad Sci U S A **104**(1): 93-98.

- Das, R. and G. Melacini (2007). "A model for agonism and antagonism in an ancient and ubiquitous cAMP-binding domain." J Biol Chem **282**(1): 581-593.
- Davare, M. A., V. Avdonin, D. D. Hall, E. M. Peden, A. Burette, R. J. Weinberg, M. C. Horne, T. Hoshi and J. W. Hell (2001). "A beta2 adrenergic receptor signaling complex assembled with the Ca2+ channel Cav1.2." Science **293**(5527): 98-101.
- Diller, T. C., N. H. Xuong and S. S. Taylor (2000). "Type II beta regulatory subunit of cAMP-dependent protein kinase: purification strategies to optimize crystallization." Protein Expr Purif **20**(3): 357-364.
- Dodge, K. L., S. Khouangsathiene, M. S. Kapiloff, R. Mouton, E. V. Hill, M. D. Houslay, L. K. Langeberg and J. D. Scott (2001). "mAKAP assembles a protein kinase A/PDE4 phosphodiesterase cAMP signaling module." Embo J **20**(8): 1921-1930.
- Dominguez, C., R. Boelens and A. M. Bonvin (2003). "HADDOCK: a protein-protein docking approach based on biochemical or biophysical information." J Am Chem Soc **125**(7): 1731-1737.
- Doskeland, S. O. (1978). "Evidence that rabbit muscle protein kinase has two kinetically distinct binding sites for adenosine 3' ; 5'-cyclic monophosphate." Biochem Biophys Res Commun **83**(2): 542-549.
- Dostmann, W. R. (1995). "(RP)-cAMPS inhibits the cAMP-dependent protein kinase by blocking the cAMP-induced conformational transition." FEBS Lett **375**(3): 231-234.
- Dostmann, W. R. and S. S. Taylor (1991). "Identifying the molecular switches that determine whether (Rp)-cAMPS functions as an antagonist or an agonist in the activation of cAMP-dependent protein kinase I." Biochemistry **30**(35): 8710-8716.
- Engen, J. R. (2009). "Analysis of protein conformation and dynamics by hydrogen/deuterium exchange MS." Anal Chem **81**(19): 7870-7875.
- Englander, S. W. and N. R. Kallenbach (1983). "Hydrogen exchange and structural dynamics of proteins and nucleic acids." Q Rev Biophys **16**(4): 521-655.

- Esposito, D., A. Petrovic, R. Harris, S. Ono, J. F. Eccleston, A. Mbabaali, I. Haq, C. F. Higgins, J. C. Hinton, P. C. Driscoll and J. E. Ladbury (2002). "H-NS oligomerization domain structure reveals the mechanism for high order self-association of the intact protein." J Mol Biol **324**(4): 841-850.
- Esposito, V., T. Sjoberg, R. Das, S. Brown, S. S. Taylor and G. Melacini (2006). "NMR assignment of the cAMP-binding domain A of the PKA regulatory subunit." J Biomol NMR **36 Suppl 5**: 64.
- Ferreiro, D. U., J. A. Hegler, E. A. Komives and P. G. Wolynes (2011). "On the role of frustration in the energy landscapes of allosteric proteins." Proc Natl Acad Sci U S A **108**(9): 3499-3503.
- Francis, S. H., M. A. Blount and J. D. Corbin (2011). "Mammalian cyclic nucleotide phosphodiesterases: molecular mechanisms and physiological functions." Physiol Rev **91**(2): 651-690.
- Francis, S. H. and J. D. Corbin (1994). "Structure and function of cyclic nucleotide-dependent protein kinases." Annu Rev Physiol **56**: 237-272.
- Frauenfelder, H., S. G. Sligar and P. G. Wolynes (1991). "The energy landscapes and motions of proteins." Science **254**(5038): 1598-1603.
- Geromanos, S. J., J. P. Vissers, J. C. Silva, C. A. Dorschel, G. Z. Li, M. V. Gorenstein, R. H. Bateman and J. I. Langridge (2009). "The detection, correlation, and comparison of peptide precursor and product ions from data independent LC-MS with data dependant LC-MS/MS." Proteomics **9**(6): 1683-1695.
- Gertsman, I., C. Y. Fu, R. Huang, E. A. Komives and J. E. Johnson (2010). "Critical salt bridges guide capsid assembly, stability, and maturation behavior in bacteriophage HK97." Mol Cell Proteomics **9**(8): 1752-1763.
- Gertsman, I., L. Gan, M. Guttman, K. Lee, J. A. Speir, R. L. Duda, R. W. Hendrix, E. A. Komives and J. E. Johnson (2009). "An unexpected twist in viral capsid maturation." Nature **458**(7238): 646-650.

- Gesellchen, F., A. Prinz, B. Zimmermann and F. W. Herberg (2006). "Quantification of cAMP antagonist action in vitro and in living cells." Eur J Cell Biol **85**(7): 663-672.
- Gibson, R. M. and S. S. Taylor (1997). "Dissecting the cooperative reassociation of the regulatory and catalytic subunits of cAMP-dependent protein kinase. Role of Trp-196 in the catalytic subunit." J Biol Chem **272**(51): 31998-32005.
- Gurrath, M. (2001). "Peptide-binding G protein-coupled receptors: new opportunities for drug design." Curr Med Chem **8**(13): 1605-1648.
- Hacker, J. and J. B. Kaper (2000). "Pathogenicity islands and the evolution of microbes." Annu Rev Microbiol **54**: 641-679.
- Hajduk, P. J. and J. Greer (2007). "A decade of fragment-based drug design: strategic advances and lessons learned." Nat Rev Drug Discov **6**(3): 211-219.
- Henzler-Wildman, K. and D. Kern (2007). "Dynamic personalities of proteins." Nature **450**(7172): 964-972.
- Herberg, F. W., W. R. Dostmann, M. Zorn, S. J. Davis and S. S. Taylor (1994). "Crosstalk between domains in the regulatory subunit of cAMP-dependent protein kinase: influence of amino terminus on cAMP binding and holoenzyme formation." Biochemistry **33**(23): 7485-7494.
- Herberg, F. W., S. S. Taylor and W. R. Dostmann (1996). "Active site mutations define the pathway for the cooperative activation of cAMP-dependent protein kinase." Biochemistry **35**(9): 2934-2942.
- Hoofnagle, A. N., K. A. Resing and N. G. Ahn (2003). "Protein analysis by hydrogen exchange mass spectrometry." Annu Rev Biophys Biomol Struct **32**: 1-25.
- Houde, D., S. A. Berkowitz and J. R. Engen (2011). "The utility of hydrogen/deuterium exchange mass spectrometry in biopharmaceutical comparability studies." J Pharm Sci **100**(6): 2071-2086.

- Huang, L. J. and S. S. Taylor (1998). "Dissecting cAMP binding domain A in the RIalpha subunit of cAMP-dependent protein kinase. Distinct subsites for recognition of cAMP and the catalytic subunit." J Biol Chem **273**(41): 26739-26746.
- Huang, R. K., R. Khayat, K. K. Lee, I. Gertsman, R. L. Duda, R. W. Hendrix and J. E. Johnson (2011). "The Prohead-I structure of bacteriophage HK97: implications for scaffold-mediated control of particle assembly and maturation." J Mol Biol **408**(3): 541-554.
- Huang, X., H. M. Holden and F. M. Raushel (2001). "Channeling of substrates and intermediates in enzyme-catalyzed reactions." Annu Rev Biochem **70**: 149-180.
- Huth, J. R., C. Park, A. M. Petros, A. R. Kunzer, M. D. Wendt, X. Wang, C. L. Lynch, J. C. Mack, K. M. Swift, R. A. Judge, J. Chen, P. L. Richardson, S. Jin, S. K. Tahir, E. D. Matayoshi, S. A. Dorwin, U. S. Ladror, J. M. Severin, K. A. Walter, D. M. Bartley, S. W. Fesik, S. W. Elmore and P. J. Hajduk (2007). "Discovery and design of novel HSP90 inhibitors using multiple fragment-based design strategies." Chem Biol Drug Des **70**(1): 1-12.
- Jeon, Y. H., Y. S. Heo, C. M. Kim, Y. L. Hyun, T. G. Lee, S. Ro and J. M. Cho (2005). "Phosphodiesterase: overview of protein structures, potential therapeutic applications and recent progress in drug development." Cell Mol Life Sci **62**(11): 1198-1220.
- Johnson, D. A., P. Akamine, E. Radzio-Andzelm, M. Madhusudan and S. S. Taylor (2001). "Dynamics of cAMP-dependent protein kinase." Chem Rev **101**(8): 2243-2270.
- Kamenetsky, M., S. Middelhaufe, E. M. Bank, L. R. Levin, J. Buck and C. Steegborn (2006). "Molecular details of cAMP generation in mammalian cells: a tale of two systems." J Mol Biol **362**(4): 623-639.
- Katen, S. and A. Zlotnick (2009). "The thermodynamics of virus capsid assembly." Methods Enzymol **455**: 395-417.
- Katta, V. and B. T. Chait (1991). "Conformational changes in proteins probed by hydrogen-exchange electrospray-ionization mass spectrometry." Rapid Commun Mass Spectrom **5**(4): 214-217.

- Kaveti, S. and J. R. Engen (2006). "Protein interactions probed with mass spectrometry." Methods Mol Biol **316**: 179-197.
- Kim, C., C. Y. Cheng, S. A. Saldanha and S. S. Taylor (2007). "PKA-I holoenzyme structure reveals a mechanism for cAMP-dependent activation." Cell **130**(6): 1032-1043.
- Kim, C., D. Vigil, G. Anand and S. S. Taylor (2006). "Structure and dynamics of PKA signaling proteins." Eur J Cell Biol **85**(7): 651-654.
- Kim, C., N. H. Xuong and S. S. Taylor (2005). "Crystal structure of a complex between the catalytic and regulatory (RIalpha) subunits of PKA." Science **307**(5710): 690-696.
- Kim, E., S. Lee, A. Jeon, J. M. Choi, H. S. Lee, S. Hohng and H. S. Kim (2013). "A single-molecule dissection of ligand binding to a protein with intrinsic dynamics." Nat Chem Biol **9**(5): 313-318.
- Kornev, A. P., S. S. Taylor and L. F. Ten Eyck (2008). "A generalized allosteric mechanism for cis-regulated cyclic nucleotide binding domains." PLoS Comput Biol **4**(4): e1000056.
- Koshland, D. E. (1958). "Application of a Theory of Enzyme Specificity to Protein Synthesis." Proc Natl Acad Sci U S A **44**(2): 98-104.
- Krishnamurthy, S., B. S. Moorthy, L. Liqin and G. S. Anand (2013). "Dynamics of phosphodiesterase-induced cAMP dissociation from protein kinase A: capturing transient ternary complexes by HDXMS." Biochim Biophys Acta **1834**(6): 1215-1221.
- Leiser, M., N. Fleischer and J. Erlichman (1986). "Enhanced activation of cAMP-dependent protein kinase by rapid synthesis and degradation of cAMP." J Biol Chem **261**(33): 15486-15490.
- Lensink, M. F. and S. J. Wodak (2010). "Docking and scoring protein interactions: CAPRI 2009." Proteins **78**(15): 3073-3084.
- Li, G. Z., J. P. Vissers, J. C. Silva, D. Golick, M. V. Gorenstein and S. J. Geromanos (2009). "Database searching and accounting of multiplexed precursor and product ion spectra from the data independent analysis of simple and complex peptide mixtures." Proteomics **9**(6): 1696-1719.

- Liu, Y., H. Chen, L. J. Kenney and J. Yan (2010). "A divalent switch drives H-NS/DNA-binding conformations between stiffening and bridging modes." Genes Dev **24**(4): 339-344.
- Mandell, J. G., A. Baerga-Ortiz, S. Akashi, K. Takio and E. A. Komives (2001). "Solvent accessibility of the thrombin-thrombomodulin interface." J Mol Biol **306**(3): 575-589.
- Mandell, J. G., A. M. Falick and E. A. Komives (1998). "Identification of protein-protein interfaces by decreased amide proton solvent accessibility." Proc Natl Acad Sci U S A **95**(25): 14705-14710.
- Meyer, B. and T. Peters (2003). "NMR spectroscopy techniques for screening and identifying ligand binding to protein receptors." Angew Chem Int Ed Engl **42**(8): 864-890.
- Monod, J., J. Wyman and J. P. Changeux (1965). "On the Nature of Allosteric Transitions: A Plausible Model." J Mol Biol **12**: 88-118.
- Moorthy, B. S. and G. S. Anand (2012). "Multistate allostery in response regulators: phosphorylation and mutagenesis activate RegA via alternate modes." J Mol Biol **417**(5): 468-487.
- Moorthy, B. S., S. Badireddy and G. S. Anand (2011). "Cooperativity and allostery in cAMP-dependent activation of Protein Kinase A: Monitoring conformations of intermediates by amide hydrogen/deuterium exchange." International Journal of Mass Spectrometry **302**(1-3): 157-166.
- Moorthy, B. S., Y. Gao and G. S. Anand (2011). "Phosphodiesterases catalyze hydrolysis of cAMP-bound to regulatory subunit of protein kinase A and mediate signal termination." Mol Cell Proteomics **10**(2): M110 002295.
- Murray, C. W., M. G. Carr, O. Callaghan, G. Chessari, M. Congreve, S. Cowan, J. E. Coyle, R. Downham, E. Figueroa, M. Frederickson, B. Graham, R. McMenamin, M. A. O'Brien, S. Patel, T. R. Phillips, G. Williams, A. J. Woodhead and A. J. Woolford (2010). "Fragment-based drug discovery applied to Hsp90. Discovery of two lead series with high ligand efficiency." J Med Chem **53**(16): 5942-5955.

- Ogreid, D. and S. O. Doskeland (1983). "Cyclic nucleotides modulate the release of [3H] adenosine cyclic 3',5'-phosphate bound to the regulatory moiety of protein kinase I by the catalytic subunit of the kinase." Biochemistry **22**(7): 1686-1696.
- Pandit, D., S. J. Tuske, S. J. Coales, S. Y. E, A. Liu, J. E. Lee, J. A. Morrow, J. F. Nemeth and Y. Hamuro (2012). "Mapping of discontinuous conformational epitopes by amide hydrogen/deuterium exchange mass spectrometry and computational docking." J Mol Recognit **25**(3): 114-124.
- Poppe, H., S. D. Rybalkin, H. Rehmann, T. R. Hinds, X. B. Tang, A. E. Christensen, F. Schwede, H. G. Genieser, J. L. Bos, S. O. Doskeland, J. A. Beavo and E. Butt (2008). "Cyclic nucleotide analogs as probes of signaling pathways." Nat Methods **5**(4): 277-278.
- Prodromou, C., S. M. Roe, R. O'Brien, J. E. Ladbury, P. W. Piper and L. H. Pearl (1997). "Identification and structural characterization of the ATP/ADP-binding site in the Hsp90 molecular chaperone." Cell **90**(1): 65-75.
- Rich, T. C., K. A. Fagan, T. E. Tse, J. Schaack, D. M. Cooper and J. W. Karpen (2001). "A uniform extracellular stimulus triggers distinct cAMP signals in different compartments of a simple cell." Proc Natl Acad Sci U S A **98**(23): 13049-13054.
- Roberts, V. A., M. E. Pique, S. Hsu, S. Li, G. Slupphaug, R. P. Rambo, J. W. Jamison, T. Liu, J. H. Lee, J. A. Tainer, L. F. Ten Eyck and V. L. Woods, Jr. (2012). "Combining H/D exchange mass spectroscopy and computational docking reveals extended DNA-binding surface on uracil-DNA glycosylase." Nucleic Acids Res **40**(13): 6070-6081.
- Sathyanarayana, P., E. Houde, D. Marshall, A. Volk, D. Makropoulos, C. Emerson, A. Pradeep, P. J. Bugelski and D. M. Wojchowski (2009). "CNTO 530 functions as a potent EPO mimetic via unique sustained effects on bone marrow proerythroblast pools." Blood **113**(20): 4955-4962.
- Scapin, G. (2006). "Structural biology and drug discovery." Curr Pharm Des **12**(17): 2087-2097.

- Schmidt, M. F. and J. Rademann (2009). "Dynamic template-assisted strategies in fragment-based drug discovery." Trends Biotechnol **27**(9): 512-521.
- Schneider, C., L. Sepp-Lorenzino, E. Nimmesgern, O. Ouerfelli, S. Danishefsky, N. Rosen and F. U. Hartl (1996). "Pharmacologic shifting of a balance between protein refolding and degradation mediated by Hsp90." Proc Natl Acad Sci U S A **93**(25): 14536-14541.
- Schreiber, S. L. (2005). "Small molecules: the missing link in the central dogma." Nat Chem Biol **1**(2): 64-66.
- Schulte, T. W., S. Akinaga, S. Soga, W. Sullivan, B. Stensgard, D. Toft and L. M. Neckers (1998). "Antibiotic radicicol binds to the N-terminal domain of Hsp90 and shares important biologic activities with geldanamycin." Cell Stress Chaperones **3**(2): 100-108.
- Schwede, F., E. Maronde, H. Genieser and B. Jastorff (2000). "Cyclic nucleotide analogs as biochemical tools and prospective drugs." Pharmacol Ther **87**(2-3): 199-226.
- Shabb, J. B. (2001). "Physiological substrates of cAMP-dependent protein kinase." Chem Rev **101**(8): 2381-2411.
- Sharon, M. and C. V. Robinson (2007). "The role of mass spectrometry in structure elucidation of dynamic protein complexes." Annu Rev Biochem **76**: 167-193.
- Shaulsky, G., D. Fuller and W. F. Loomis (1998). "A cAMP-phosphodiesterase controls PKA-dependent differentiation." Development **125**(4): 691-699.
- Shen, Z., P. Li, R. J. Ni, M. Ritchie, C. P. Yang, G. F. Liu, W. Ma, G. J. Liu, L. Ma, S. J. Li, Z. G. Wei, H. X. Wang and B. C. Wang (2009). "Label-free quantitative proteomics analysis of etiolated maize seedling leaves during greening." Mol Cell Proteomics **8**(11): 2443-2460.
- Shoichet, B. K. (2004). "Virtual screening of chemical libraries." Nature **432**(7019): 862-865.
- Shuker, S. B., P. J. Hajduk, R. P. Meadows and S. W. Fesik (1996). "Discovering high-affinity ligands for proteins: SAR by NMR." Science **274**(5292): 1531-1534.
- Silva, J. C., R. Denny, C. A. Dorschel, M. Gorenstein, I. J. Kass, G. Z. Li, T. McKenna, M. J. Nold, K. Richardson, P. Young and S. Geromanos (2005). "Quantitative proteomic analysis by accurate mass retention time pairs." Anal Chem **77**(7): 2187-2200.

- Solit, D. B. and N. Rosen (2006). "Hsp90: a novel target for cancer therapy." Curr Top Med Chem **6**(11): 1205-1214.
- Spassky, A., S. Rimsky, H. Garreau and H. Buc (1984). "H1a, an E. coli DNA-binding protein which accumulates in stationary phase, strongly compacts DNA in vitro." Nucleic Acids Res **12**(13): 5321-5340.
- Steinberg, S. F. and L. L. Brunton (2001). "Compartmentation of G protein-coupled signaling pathways in cardiac myocytes." Annu Rev Pharmacol Toxicol **41**: 751-773.
- Su, Y., W. R. Dostmann, F. W. Herberg, K. Durick, N. H. Xuong, L. Ten Eyck, S. S. Taylor and K. I. Varughese (1995). "Regulatory subunit of protein kinase A: structure of deletion mutant with cAMP binding domains." Science **269**(5225): 807-813.
- Thomason, P. A., D. Traynor, G. Cavet, W. T. Chang, A. J. Harwood and R. R. Kay (1998). "An intersection of the cAMP/PKA and two-component signal transduction systems in Dictyostelium." Embo J **17**(10): 2838-2845.
- Tupper, A. E., T. A. Owen-Hughes, D. W. Ussery, D. S. Santos, D. J. Ferguson, J. M. Sidebotham, J. C. Hinton and C. F. Higgins (1994). "The chromatin-associated protein H-NS alters DNA topology in vitro." EMBO J **13**(1): 258-268.
- Veesler, D. and J. E. Johnson (2012). "Virus maturation." Annu Rev Biophys **41**: 473-496.
- Veesler, D., R. Khayat, S. Krishnamurthy, J. Snijder, R. K. Huang, A. J. Heck, G. S. Anand and J. E. Johnson (2013). "Architecture of a dsDNA Viral Capsid in Complex with Its Maturation Protease." Structure.
- Viste, K., R. K. Kopperud, A. E. Christensen and S. O. Doskeland (2005). "Substrate enhances the sensitivity of type I protein kinase a to cAMP." J Biol Chem **280**(14): 13279-13284.
- Wales, T. E., K. E. Fadgen, G. C. Gerhardt and J. R. Engen (2008). "High-speed and high-resolution UPLC separation at zero degrees Celsius." Anal Chem **80**(17): 6815-6820.

- Wang, H., Z. Yan, S. Yang, J. Cai, H. Robinson and H. Ke (2008). "Kinetic and structural studies of phosphodiesterase-8A and implication on the inhibitor selectivity." Biochemistry **47**(48): 12760-12768.
- Weis, D. D., J. R. Engen and I. J. Kass (2006). "Semi-automated data processing of hydrogen exchange mass spectra using HX-Express." J Am Soc Mass Spectrom **17**(12): 1700-1703.
- Weis, D. D., T. E. Wales, J. R. Engen, M. Hotchko and L. F. Ten Eyck (2006). "Identification and characterization of EX1 kinetics in H/D exchange mass spectrometry by peak width analysis." J Am Soc Mass Spectrom **17**(11): 1498-1509.
- Wess, J. (1997). "G-protein-coupled receptors: molecular mechanisms involved in receptor activation and selectivity of G-protein recognition." FASEB J **11**(5): 346-354.
- Wu, J., S. Brown, N. H. Xuong and S. S. Taylor (2004). "RIalpha subunit of PKA: a cAMP-free structure reveals a hydrophobic capping mechanism for docking cAMP into site B." Structure **12**(6): 1057-1065.
- Wu, Y., J. R. Engen and W. B. Hobbins (2006). "Ultra performance liquid chromatography (UPLC) further improves hydrogen/deuterium exchange mass spectrometry." J Am Soc Mass Spectrom **17**(2): 163-167.
- Yan, Z., H. Wang, J. Cai and H. Ke (2009). "Refolding and kinetic characterization of the phosphodiesterase-8A catalytic domain." Protein Expr Purif **64**(1): 82-88.
- Zaccolo, M. (2006). "Phosphodiesterases and compartmentalized cAMP signalling in the heart." Eur J Cell Biol **85**(7): 693-697.
- Zheng, J., E. A. Trafny, D. R. Knighton, N. H. Xuong, S. S. Taylor, L. F. Ten Eyck and J. M. Sowadski (1993). "2.2 A refined crystal structure of the catalytic subunit of cAMP-dependent protein kinase complexed with MnATP and a peptide inhibitor." Acta Crystallogr D Biol Crystallogr **49**(Pt 3): 362-365.